Control of Crystallisation through the Use of Microemulsions

COOK, OLIVER,JAMES

Control of Crystallisation through the Use of Microemulsions

Oliver James Cook

St Cuthbert's Society

Department of Chemistry

University of Durham

September 2012

Thesis submitted to the University of Durham in partial fulfilment of the regulations for the Degree of Doctor of Philosophy.

Declaration and Statement of Copyright

The work reported in this thesis was carried out in the laboratories of the Department of Chemistry, Durham University and at the Ogden Centre for Fundamental Physics, Durham University between October 2008 and September 2012. This work is the original work of the author. No part of this work has previously been submitted for a degree at this or any other university.

Abstract

Control of crystallisation is hugely important in many areas of science and technology. The size of crystals can often be crucial in how they perform. In addition the polymorphism of crystals is just as important, especially for the pharmaceutical sciences, where unexpected changes in polymorphism can spell disaster for certain drugs. With these requirements in mind, we have demonstrated that microemulsions can be used to offer thermodynamic control of crystallisation, not just with regards to polymorphism of organic crystals, but also to the synthesis of certain inorganic compounds.

The polymorphism of glycine was first investigated in an attempt to grow all three polymorphs (α-, β- and γ-) at room temperature and pressure. The most stable of these, γ-glycine grows ~ 500 times more slowly than the next most stable form, α-glycine. Using microemulsions made up with the surfactant AOT, the continuous oil phase heptane and a nanoconfined aqueous glycine solution, all three polymorphs of glycine were crystallised by adding methanol dropwise under varying conditions. Non-ionic surfactant systems were also investigated, using combinations of the surfactants Span 80/Tween 80 and Span 80/Brij 30. Using the Span 80/Brij 30 system, the most stable form, γ-glycine, could be formed predominantly by mixing an aqueous glycine microemulsion with an aqueous methanol microemulsion. This proved that Ostwald's Rule of Stages could be circumvented in order to obtain the most stable polymorph.

Following this, microemulsions were used to demonstrate that inorganic crystalline materials could be synthesised in microemulsion droplets- again at room temperature and pressure. Hydroxyapatite, known as a component of natural bone, was made using Triton X-100/1-hexanol/cyclohexane microemulsions via two methods, firstly via direct addition of reactants, then again via mixed microemulsion methods. Subsequent analysis showed that the final product showed excellent correlation with bought-in hydroxyapatite (reagent grade), with regards to purity and crystallinity.

Finally the synthesis of titanium dioxide nanoparticles was reported. These set of experiments brought both challenges of controlling polymorphism and synthesising materials together. Rutile – the most stable of polymorph of titanium dioxide – was synthesised as the predominant polymorph from the microemulsions. Electron

microscopy studies were able to track the particle size growth between 2 and 13 nm at various times up to 18 hours after mixing the reactant microemulsions.

Acknowledgements

Firstly, huge thanks to Dr Sharon Cooper for the last four years – not just for all the introductions to new areas of research, but for helping out with constant suggestions as to how I should further my work, and especially helping me to understand all the background and theory that goes with the chemistry.

Many thanks to Helen Riggs and Dr. Budhika Mendis for manning all the analysis machines I had to use. They additionally provided invaluable help when teaching me to use the apparatus, as well as stepping in to help when things went wrong or problems were found.

My next group of thank-yous go to the my fellow PhD students and Postdoctoral Research Fellows who were present in the lab – namely Kate Nicholson, Chris Herron, Cen Chen and Natasha Loines. All of your advice and the "tips and tricks" of the trade was very helpful, informative and occasionally amusing, and you can rest assured that I took it all to heart. More thanks as well to the many Masters' students I've known pass through the lab, namely Emma, Linda, Kirsty, Stephanie, Helen and Mike. You contributed much support and understanding to the cause.

Thanks also go to my parents – I know you may not understand what I'm working on most of the time, but you both continue to express great enthusiasm for what I do and have done – and that has been a great help.

Finally, thank you to everyone who I've known who has studied chemistry with me – you've all contributed in some way to the position that I'm in today, and I am eternally grateful for that.

List of Publications

1. C. Chen, O. Cook, C.E. Nicholson, S.J. Cooper, "Leapfrogging Ostwald's Rule of Stages: Crystallization of Stable γ-glycine Directly from Microemulsions", *Crystal Growth & Design*, 2011, **11 (6)**, 2228-2237.
2. S.J. Cooper, O. Cook, N.J. Loines, "Crystallisation in Microemulsions: A Generic Route to Thermodynamic Control and the Estimation of Critical Nucleus Size", *Crystallization / Book 1*, ed. M.R.B. Andreeta, Intech, 2012, pp. 121-148.

Conferences Attended

BACG 40th Anniversary Conference 2009: Wills Hall, University of Bristol, 6th – 8th September 2009. *Poster*: "Thermodynamic Control of Crystallisation Through the Use of Microemulsions".

BACG Annual Conference 2010: University of Manchester, 5th – 7th September 2010.

BACG Annual Conference 2011 (jointly with the DACG): University College London, 10th – 12th July 2011. *Poster:* "Synthesis of Hydroxyapatite Nanoparticles through the Use of Microemulsions".

Contents

List of Figures

List of Tables

1. Introduction and Theory

1.1 The kinetics and thermodynamics of crystallisation

Crystallisation can be defined as the creation of a crystalline phase from a parent phase via a condensation process. Classically, it is seen as a two-step process – nucleation, followed by crystal growth. For materials to crystallise, aggregates of material need to be of at least a certain size and/or larger before it is favourable for them to grow further and become a condensed phase. All aggregates of this volume are known as critical nuclei.

Nucleation is described as "The process of random generation of nanoscopically small formations of a new phase that have the ability for irreversible growth to macroscopically large sizes".[1] Nucleation can be classed as homogeneous, where the crystallising species nucleates from within a single component phase, or heterogeneous, where the nucleation process takes place on a substrate, usually a surface of some kind. The homogeneous mechanism was postulated in 1927, and is known as the Szilard-Farkas model (see Figure 1):[2]

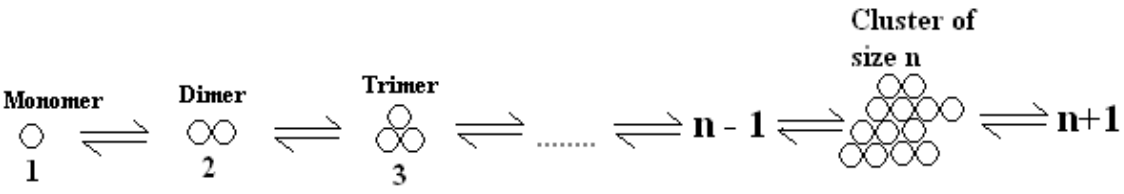

Figure 1: Diagram showing a simple version of the Szilard-Farkas model.

Each step between the formation of a combination of monomers has a rate of frequency attached to it (see Figure 2):

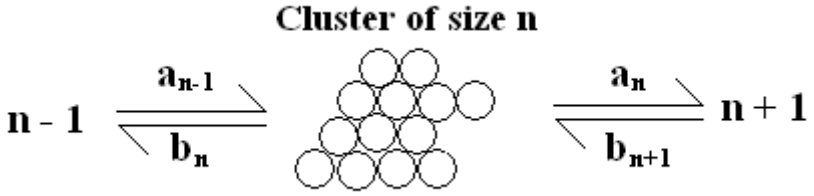

Figure 2: Part of Figure 1 showing the respective rates of frequency. a_n = attachment frequency of monomers to cluster of size n and b_n = detachment frequency of monomers to cluster of size n.

The overall process can be described as a series of 'reactions' between 'monomers' and 'clusters' (where a monomer can be termed as either an atom, a molecule or a building unit of any sort, and a cluster as a group of monomers). The model itself is still used today, with just three assumptions:

1. Clusters of size n = 1,2,3,..., all exist.
2. Attachment and detachment of monomers is present throughout.
3. All clusters of size n have the same shape.

In 1935, Richard Becker and Werner Döring, built upon these original theories for their own treatment of nucleation.[3-6] The cluster is designated as the letter C with size r by the term C_r. The mechanism remains the addition or detachment of a single monomer, therefore the equation is:

$$C_r + C_1 \Leftrightarrow C_{r+1} \qquad (1)$$

The concentration of C_r is denoted as c_r, and the concentration of C_1 is given as c_1. The rates of addition and detachment remain a_r and b_{r+1}. The total mass of material q is given as:

$$q = \sum_{r=1}^{\infty} r c_r \qquad (2)$$

q is kept constant. The resultant rate equations are:

$$c_r = J_{r-1} - J_r \qquad (3)$$

$$J_r = a_r c_r c_1 - b_{r+1} c_{r+1} \qquad (4)$$

$$c_1 = -J_1 - \sum_{r=1}^{\infty} J_r \qquad (5)$$

The entity J_r refers to the flux of clusters from r to $r + 1$. It includes both a_r and b_{r+1}, and is therefore a useful term to simplify the equations.

It is these first equations and hypotheses that would lead to the development of the ideas of Classical Nucleation Theory.

1.1.1 Classical Nucleation Theory

Classical Nucleation Theory (abbreviated to CNT) was an early attempt to model and calculate a mathematical expression for the overall process of nucleation. Though initially used to describe liquid condensation from a vapour, it is frequently used to model nucleation of a crystal from a melt or solution.[7] The rate of nucleation is taken to be *J*, and is itself a two-step process. Firstly, a concentration of critical nuclei *n(i*)* must be established at equilibrium. Secondly, a rate constant is assigned to the rate of impingement onto the critical nuclei to form the bulk condensed phase. This rate is given the symbol *W**. As a result, the overall rate of nucleation can be termed as:

$$J = W^* n(i^*) \qquad (6)$$

The entity *n(i*)* can be defined as:

$$n(i^*) = n \exp\left[\frac{-\Delta G^*}{k_B T}\right] \qquad (7)$$

Where n is concentration of the crystallising compound and ΔG^* is the Gibbs' free energy of formation of a critical nucleus. The overall term $\exp(-\Delta G^*/k_B T)$ describes the probability of forming a critical nucleus.

The Gibbs' free energy of formation ΔG^* can be derived as follows. To start with, the free energy of formation of a cluster needs to be defined. If the cluster has *i* monomers:

$$\Delta G_i = -i(\Delta\mu) + \sum_n \gamma_n A_n \qquad (8)$$

where γ_n = the surface tension of the nth phase, A_n = the area of the nth phase and $\Delta\mu$ = supersaturation, which is the difference in chemical potential between the parent (i.e. solution or melt) and daughter (i.e. crystal) phases. The second term therefore refers to the work required to form the surface tension of the cluster. To further derive the expression, it can be assumed that the cluster is spherical.[8] Equation (8) therefore becomes:

$$\Delta G_i = -\frac{4\pi r^3}{3v_c}(\Delta\mu) + (4\pi r^2)\gamma \quad (9)$$

In this equation, r = the radius of the cluster and v_c is the molecular volume of the cluster i.e. the volume of a molecule in the cluster, not the overall volume of the cluster). With the radius becoming the only variable in the equation, a graph of ΔG_i against r can be drawn (see Figure 3 – blue line).

When a crystal grows, the supersaturation of the solid phase (i.e. the crystallising phase) eventually becomes less than the supersaturation of the liquid phase (i.e. the solution or melt). As a result, the magnitude of the radius of the crystal becomes important. If r is small, $4\pi r^2\gamma > 4(\pi r^3\Delta\mu/3v_c)$ and therefore the value of ΔG_i is greater than zero. As the radius increases, the r^3 term dominates. Consequently, a maximum value appears on the graph (see Figure 3 – red line):

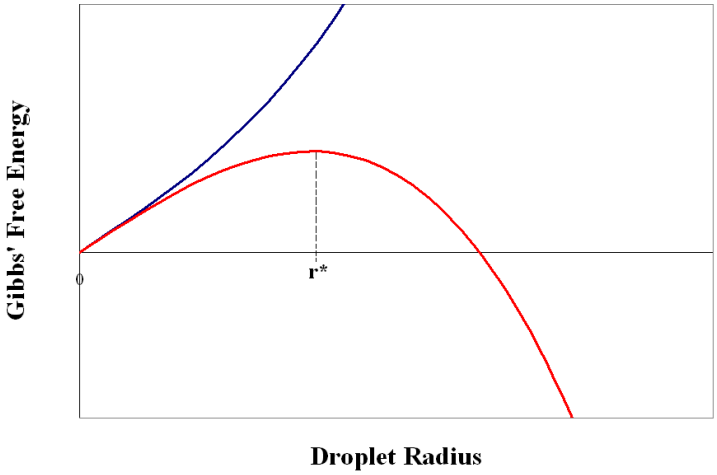

Figure 3: Graph showing the change in graph shape when the radius increases and the chemical potential of the bulk crystalline phase is less than that of the melt or solution (red line). The blue line shows the variation of Gibbs' free energy with droplet radius

The maximum is termed r^* - this is the radius of the critical nucleus. Upon reaching the critical nucleus size, the nucleus will have an equal chance of growing or melting or dissolving. To find the r^* value, equation (9) needs to be differentiated:

$$\frac{d\Delta G_i}{dr} = -\frac{4\pi r^2}{v_c}\Delta\mu + 8\pi r\gamma = 0 \quad (10)$$

And when setting the value to equal zero, the critical nucleus radius is found to be:

$$r^* = \frac{2\gamma v_c}{\Delta\mu} \quad (11)$$

This is analogous to the Gibbs-Thomson equation for a liquid droplet:

$$\Delta\mu = \frac{2\gamma\nu}{r} \qquad (12)$$

Substituting equation (11) into equation (9) now gives the Gibbs' free energy of formation of the critical nucleus in terms of the supersaturation:

$$\Delta G^* = \frac{16\pi\gamma^3\nu_c^2}{3\Delta\mu^2} \qquad (13)$$

Therefore the overall equation for homogeneous nucleation rate becomes:

$$J = \Omega\exp\left[-\frac{\Delta G^*}{k_B T}\right] = \Omega\exp\left[\frac{-16\pi\gamma^3\nu_c^2}{3\Delta\mu^2 k_B T}\right] \qquad (14)$$

Ω is the pre-exponential factor and is related to a volume diffusion step – it denotes the energy barrier which needs to be overcome for molecules from the bulk solution to be incorporated into the critical nucleus

.[9] Typical values for it are usually in the region of $10^{25} – 10^{35}$ cm^{-3} s^{-1}.

Once the radius of the particles increases past r^*, the value of ΔG^* decreases and becomes negative, meaning that further crystal growth becomes favourable and the crystals themselves will eventually become bulk-phase solid.

At low values for the supersaturation, J also remains close to zero. At a certain point, known as the Ostwald metastable limit, the value of J rises dramatically (see Figure 4). The advantage of the dramatic increase is that the onset of nucleation can be detected fairly accurately, and that at low to moderate supersaturation values, the metastable limit can be more easily found.[8]

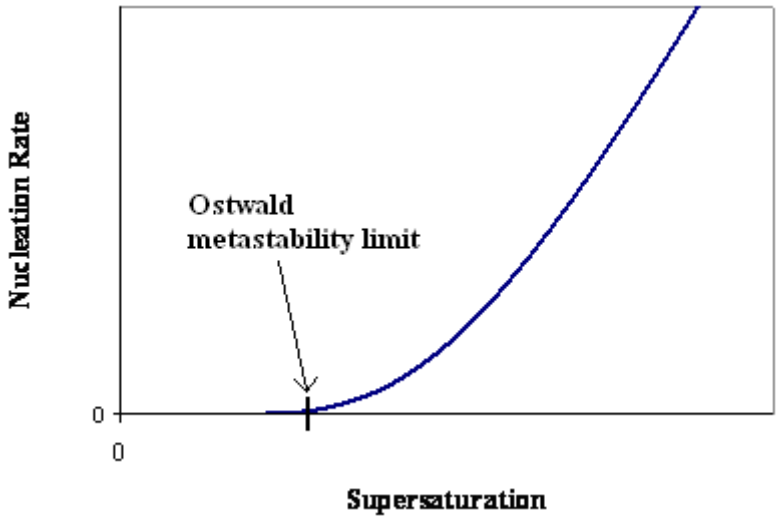

Figure 4: Graph showing the change in nucleation rate upon increasing the supersaturation.

1.2 Polymorphism

1.2.1 Introduction

Polymorphism is defined as the ability of a solid material to exist in one or more forms or crystal structures, and it can happen in many different types of compounds, including polymers and metals. There are many ways in which polymorphism can occur – the most common is through different packing of the material's molecules. In larger molecules, the term polymorphism can be applied to molecules which have different conformers. It is generally believed that polymorphism was first seen by Friedrich Wöhler and Justus von Liebig in 1832 when they found that cooling a solution of benzamide produced crystals which varied in shape: a needle-type crystal and a rhombic type.[10]

Today, it is of great importance to the pharmaceutical industry, where many of the drugs synthesised have more than one polymorph. In a similar vein to the problems with chirality and enantiomers, failure to obtain the correct polymorph of a compound can lead to extensive damage. One of the most famous cases concerned the drug Ritonavir, marketed as Norvir, which was seen as one of the few effective drugs against AIDS.[11, 12] It was administered as a liquid and a semi-solid capsule, and went on sale in 1996. Two years later, numerous reports came in that the capsules were failing dissolution requirements. X-Ray diffraction and microscopy

studies showed the presence of a new polymorph, termed form II, which was far less soluble than form I. Solubility studies which involved dissolving the forms in an ethanol/water mixture found that the difference in solubility was even greater when the proportion of water was increased. In the preparation, Ritonavir was dissolved in a solution of ethanol that was unsaturated with respect to form I, but 400 % supersaturated with respect to form II. Form II also crystallised faster at a lower temperature, especially in the region of 2-8 °C – a temperature range at which much of the stock was stored.[13] Furthermore, if a batch of Form I Ritonavir was contaminated with Form II polymorph of any amount, the rate of conversion from Form I → II increased greatly. The whole batch of drugs had to be recalled, and a re-formulation of Ritonavir had to be found. The laboratories at the centre of the problem, Abbott Laboratories, had to invest $300 million in developing a new and fully stable preparation to put on the market.

After comprehensive study of both forms of Ritonavir, it was found that one of the factors affecting the solubility difference was the presence and type of hydrogen bonds in each polymorph, which also determined the structure of each form. Form I has two patterns of hydrogen bonding - the molecules in stacks with hydrogen bonds forming between carboxyl- and amide groups only, and bonds between the alcohol groups and the thiazole groups on other molecules (see Figures 5 and 6):

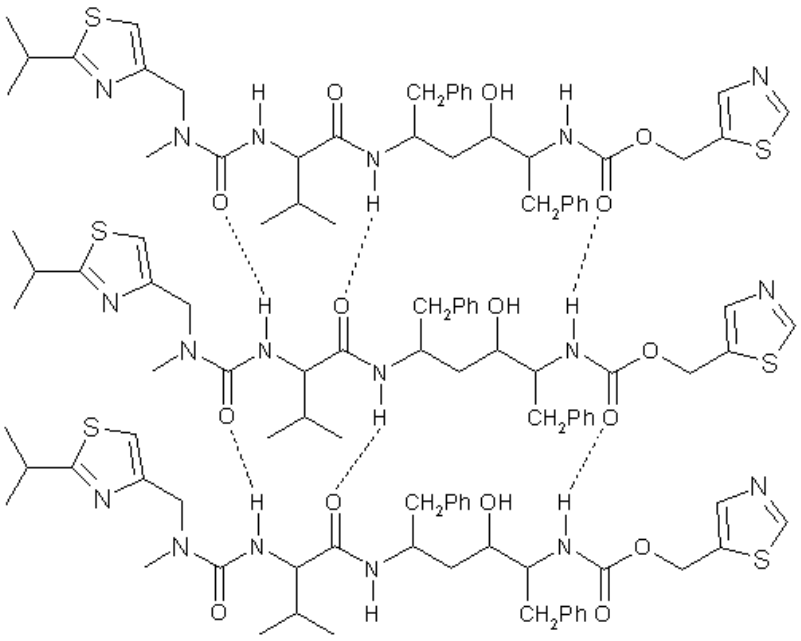

Figure 5: Diagram showing the arrangement of molecules and hydrogen bonding in Form I Ritonavir.

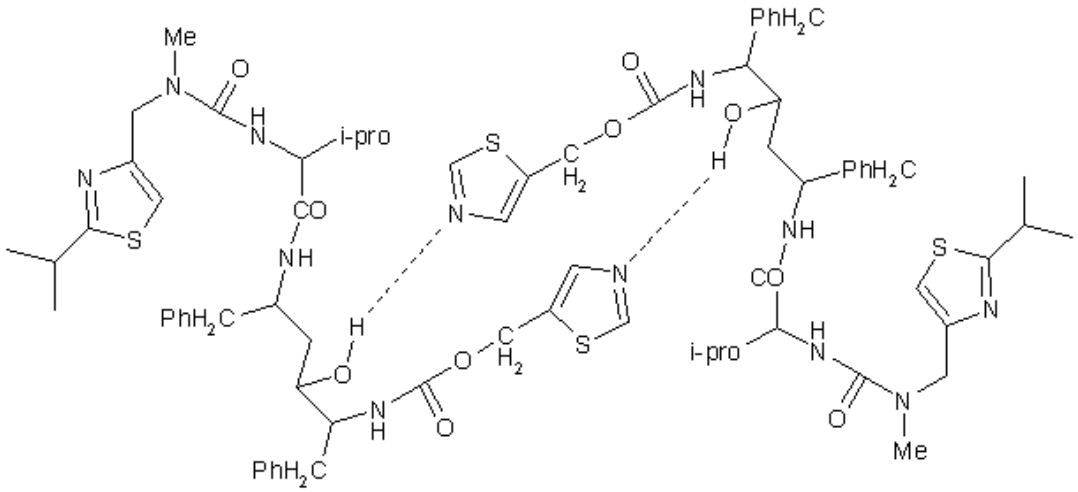

Figure 6: Diagram showing the other set of hydrogen bonds between the alcohol and the thiazole groups in Form I Ritonavir.

In form II, there is only one basic pattern of hydrogen bonding (see Figure 7). Both forms of Ritonavir have the same number of hydrogen bonds, but in Form I, the hydrogen bond between the alcohol group and the thiazole group is weaker. In Form II, an alcohol group is involved in two hydrogen bonds as a hydrogen donor and acceptor. This results in a synergistic effect, making both hydrogen bonds stronger.[13]

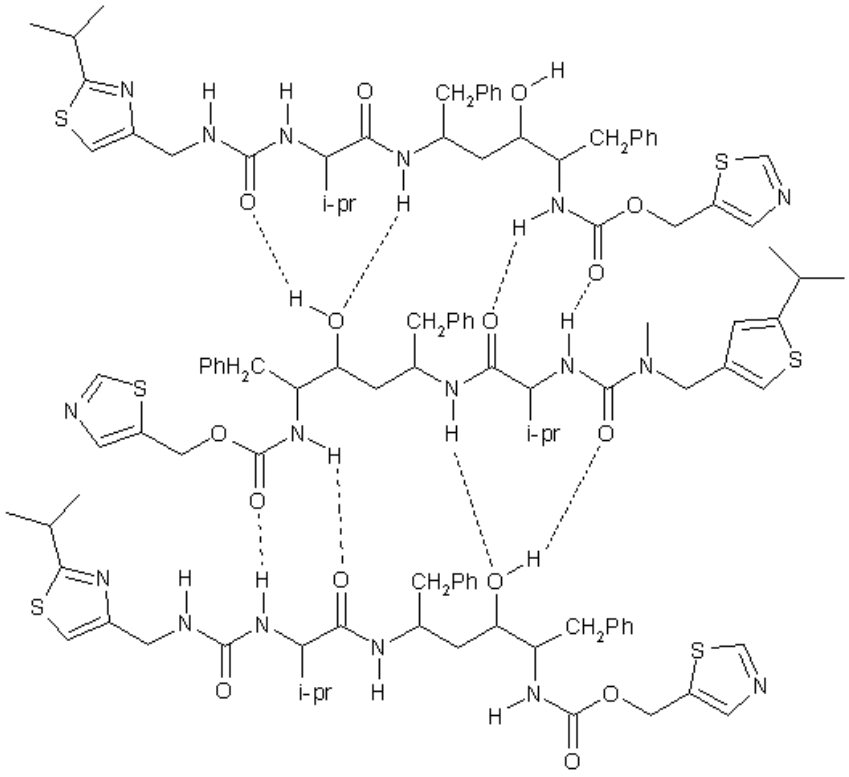

Figure 7: Diagram showing the hydrogen bonds and packing arrangement of Form II Ritonavir.

In addition to the difference in hydrogen bonding, the crystals in Form I have more of their crystal faces exposed. Because of this, more of the hydrogen-bonding groups are exposed, meaning that the crystallisation and dissolution rates – and subsequently the solubility – are much greater in Form I than in Form II.

As a direct result of the case study, much more time has been put into screening potential new drug molecules, and the solubility of polymorphs has been noted as an important area to test. Simple dissolution tests cannot be used only, since both particle size and wettability (the ability of a liquid to remain in contact with a solid surface) can affect values.[14] Equilibrium solubility tests – where the drug molecules are in chemical equilibrium with a solution of the same compound) have been found to be the most effective technique, since results from the tests are affected by polymorphic form. They have also been championed as an essential step in determining whether new polymorphs can still retain bioavailability.[12, 15]

Amongst the most well-known drugs, paracetamol is another example of a polymorphic material. It has three polymorphs, of which there have been very few sightings of the third form.[16] Amino acids are also known to exhibit polymorphism e.g. L-glutamic acid, which has two polymorphs and has been thoroughly studied.[17, 18] It is therefore of great importance to deduce all the polymorphs of a crystal and determine their stabilities. It is hoped that the use of confined phases can bring about an unprecedented level of control to crystallisation.

1.2.2 Beating Ostwald's Rule of Stages

The main problem with attempting to control crystallisation is that the rate of crystallisation in a system is often governed by the nucleation energy barrier. It was Wilhelm Ostwald who postulated a theory in 1897, known as Ostwald's Rule of Stages, stating that the least stable polymorph of a crystal will often crystallise first, before changing over time into more stable forms.[19] Complicating matters is the fact that not all systems and compounds follow this rule. For example, calcium carbonate has been found to first crystallise its amorphous form, before transforming into the more stable polymorphs and calcite.[20, 21] By contrast, the amino acids L-glutamic acid and L-histamine crystallise in the most stable polymorph immediately, without

first crystallising the metastable polymorphs.[22] These examples show that Ostwald's Rule of Stages should be treated as a guiding principle, and not as a factual statement.[21]

To illustrate Ostwald's Rule of Stages, a crystal with polymorphs a) and b) is taken. Polymorph a) is stable, while polymorph b) is metastable (it can exist, but is prone to change with a relatively small energy input or change in conditions). A graph of Helmholtz free energy ΔF (which is used because it is not affected by isobaric restrictions, and can therefore apply to these systems which are held at constant temperature and volume) versus particle size is shown in Figure 8:

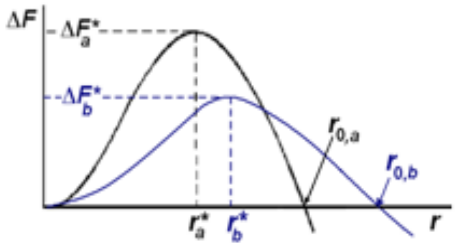

Figure 8: Graph showing the energy barriers (ΔF_a^* and ΔF_b^*) for polymorphs a) and b). Polymorph b) is the least stable. r_a and r_b are the critical nucleus sizes of polymorphs a) and b).[23]

Because polymorph b) has a lower energy barrier, that will be the polymorph that crystallises quickest, and it could be assumed that polymorph b) is the only stable polymorph, something known to be untrue because polymorph a) exists. Theoretically, this problem can be solved if, when crystallisation occurs, it happens in a confined volume. Using this method, the amount of material available in a confined volume is reduced, and so polymorph a) will form if the confining radius r is given by $r_{0,a} \leq r < r_{0,b}$. Therefore, theoretically, polymorphic control of the system is achieved.

This argument assumes that crystallisation is occurring from the melt. It can be modified for crystallisation occurring from a nanoconfined solution. If the polymorphic material is nanoconfined, the supersaturation of the material decreases rapidly as crystal growth progresses (because the amount of material remaining in the nanoconfined solution decreases rapidly). This leads to a minimum in the free energy curve where essentially, the nucleus is surrounded by saturated solution. The size of this nucleus is termed r^*_{min}. The solubility of the more stable polymorph is

less than that of the metastable polymorph, meaning that the nuclei of the stable polymorph can grow to larger sizes before the supersaturation is relieved, thereby increasing the value of r_{min} and decreasing its ΔF value. The challenge is now to confine the volume such that $\Delta F_{min,A}^{*} \leq kT$ for polymorph a), but not for polymorph b), meaning that polymorph a) will be formed only. This can be done by ensuring that the system is at the point where crystallisation is only just possible. In particular, the starting point is a nanoconfined solution in which neither polymorph will crystallise, because both polymorphs have a minimum well above kT in energy (see Figure 9):

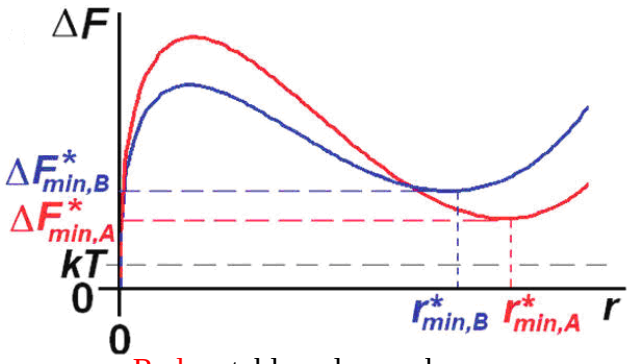

Figure 9: Graph showing free energy change ΔF versus the nucleus size r.

Such a solution is said to be stabilised due to nanoconfinement. It is highly supersaturated, but will not crystallise. The supersaturation of this nanoconfined solution is then incrementally increased (typically by cooling or adding antisolvent) until crystallisation is first possible (see Figure 10):

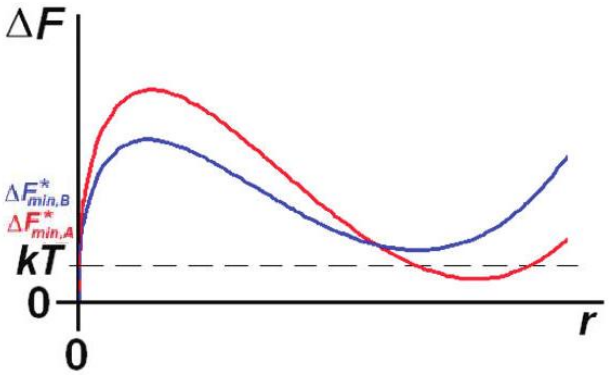

Figure 10: Graph showing the ideal setup for obtaining polymorph a) from solution. The maxima are now at a similar r-value, meaning that from the melt, polymorph a) should form more easily. From solution in a confined volume, polymorph a) has a negative minimum in the free energy, meaning that it should be the only polymorph formed.[23, 24]

1.3 Surfactants

Surfactants (an abbreviation for "surface active agents") are compounds designed to lower the surface tension of a liquid, or to reduce the interfacial tension between either two liquids or a liquid and a solid. This has made them essential for making emulsions and microemulsions. They are amphiphilic compounds – meaning that they contain both hydrophilic and hydrophobic parts in their molecular structure.

All surfactants can be placed in two categories – ionic and non-ionic. Ionic surfactants contain a charged head group, and can themselves be sub-divided into three groups. Anionic and cationic surfactants have a negatively-charged and positively-charged head group respectively, while zwitterionic surfactants contain both charges. Zwitterionic surfactants can act as ampholytes – they can react with, and contain characteristics of both acids and bases. Non-ionic surfactants contain no charges – but they do contain highly polar functional groups which can interact with water via hydrogen bonding. An example of each type of surfactant is shown in Figure 11:

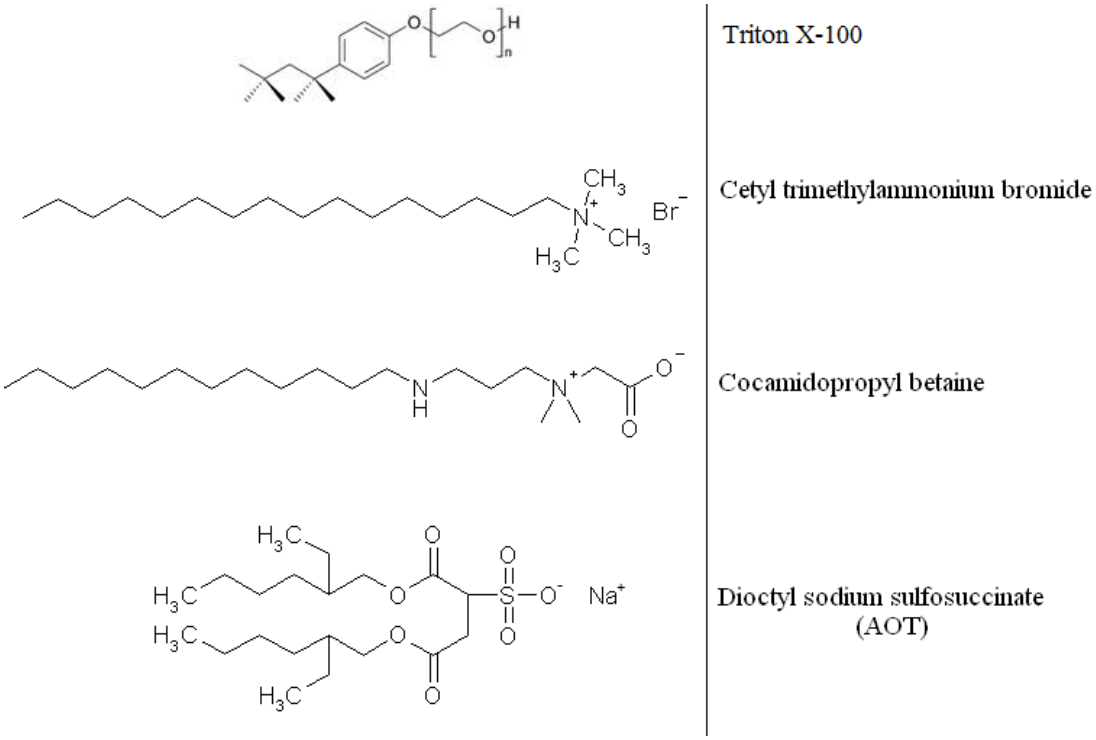

Figure 11: Examples of different types of surfactants. From top to bottom, the types are non-ionic, cationic, zwitterionic and anionic.

Another difference between ionic and non-ionic surfactants is that they show differences in performance when the temperature is increased or decreased. In the case of non-ionic surfactants, clouding phenomena is observed.[25, 26] When the temperature of a solution containing a non-ionic surfactant is raised, a phase separation occurs to form a two-phase fluid. This has an opaque appearance, due to initial formation of droplets, which are large enough to scatter light. The relevant temperature is referred to as the cloud point (T_c). This temperature is very dependent on the surfactant concentration, and the water solubility of the surfactant is inversely proportional to the temperature. Therefore, if the temperature is below the cloud point, micelles form and it becomes likely that a microemulsion will form.[27] The value of T_c may change if other components are present. For example, addition of salts to a poly(ethylene oxide) solution will reduce the cloud point by up to 60 °C.[28]

Ionic surfactants, instead of a cloud point, have an assigned Krafft temperature / Krafft point (T_{Krafft}). This is defined as being a certain temperature where the solubility of a surfactant in water increases abruptly, and the surfactant molecules are able to form micelles. The Krafft point has therefore also been defined as the melting point of a hydrated solid surfactant.[29] Figure 12 shows an example graph of what happens to surfactant molecules in solution when the temperature rises:

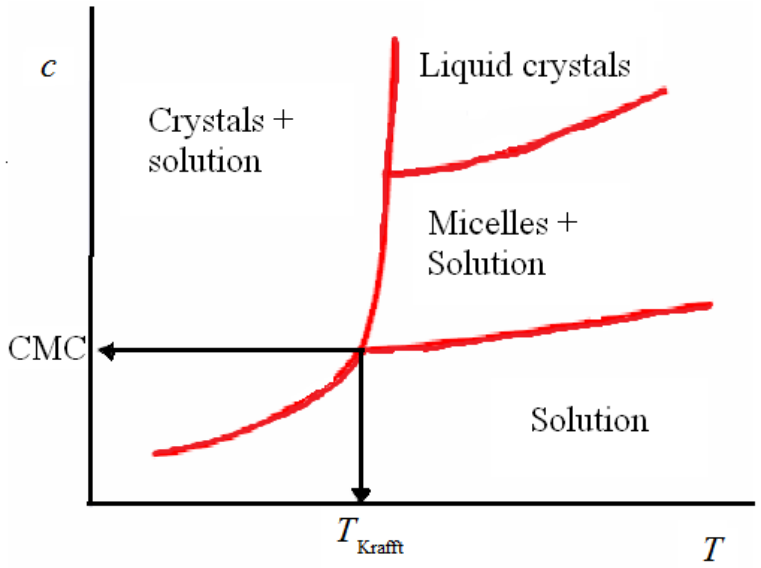

Figure 12: Hypothetical graph showing the relationship between surfactant concentration and temperature with respect to the Krafft temperature.

Kuneida *et al.* showed that for surfactants containing long carbon chains, the chain length is directly proportional to T_{Krafft}.[29] The nature of the surface active ion can

also affect T_{Krafft}, in that the steepness of the slope of Krafft point v chain length increases with the extent of hydration of the counterion.

The choice of surfactant for a particular microemulsion is an important factor. In making water-in-oil microemulsions, which will be used for most experiments, double-tail surfactants with hydrophobic functional groups are best. One of the most useful is AOT (see Figure 11). Probably its most well-known use is in the oil dispersant Corexit, which was used in the cleanup of the *Deepwater Horizon* oil spill in 2010 in the Gulf of Mexico.[30] But in addition, this surfactant has been used many times for making microemulsions.[31, 32]

1.4 Microemulsions and nanoemulsions

The definition of the term microemulsion has changed many times over the last century. Microemulsions, like normal emulsions, can be described as a homogeneous mixture of oil, water and surfactant when mixed (since most emulsions need to be stabilised, surfactant is almost always used in emulsions). At a microscopic level, it is found that both emulsions and microemulsions contain individual domains of water and oil. The main difference, from the point of view of the human eye, is that microemulsions are transparent in appearance, though not necessarily colourless. This is due to the droplets in the main mixture being far smaller (nanometres in size) than those found in an emulsion, where droplet sizes are in the order of micrometres. However this was not seen as being a fundamental difference between emulsions and microemulsions, and in 1958, the definition was changed. Emulsions (sometimes known as macroemulsions), are unstable by nature, and if left without agitation for some time, the droplets in the emulsion would coalesce, forming a two layer, two phase system. Microemulsions on the other hand are thermodynamically stable, and so can be left indefinitely without any phase separation, provided the temperature remains essentially constant. This notion of stability is now the crucial point when defining the type of emulsion.[33]

Nanoemulsions are similar systems, where the droplet diameter is between 20-500 nm.[34] They can also be used as confining solutions like microemulsions and have many of the same properties. However, they are metastable, not thermodynamically stable like microemulsions, and cannot be formed spontaneously. In many cases the

preparation and even the order in which the nanoemulsion components are added determine the success of whether a nanoemulsion is formed and the properties it has, in addition to the thermodynamic conditions which are required for forming both microemulsions and nanoemulsions.[35, 36]

Often in microemulsions and multi-phase systems with a low surfactant concentration, certain equilibria can be defined – these are known as Winsor phases. A microemulsion in equilibrium with excess oil is defined as a Winsor I system. When in equilibrium with excess water, the microemulsion is defined as a Winsor II system. Both excess water and oil can be present in a system as well, giving rise to a Winsor III system. This has a bicontinuous structure, rather than a droplet structure. Despite there being a microemulsion phase present, these systems (Winsor I, II and III) are still classed as emulsions, because there has been phase separation in forming them, thereby defining them as unstable. The systems can interchange with one another if the temperature is varied. A Winsor type IV system may be formed as well. This is defined as a thermodynamically stable, single-phase microemulsion.[37] Winsor type IV microemulsions have become increasingly important, as the excess phase is often a hindrance whilst experiments are carried out on the microemulsion phase. Generic diagrams of each Winsor type are show in Figure 13:

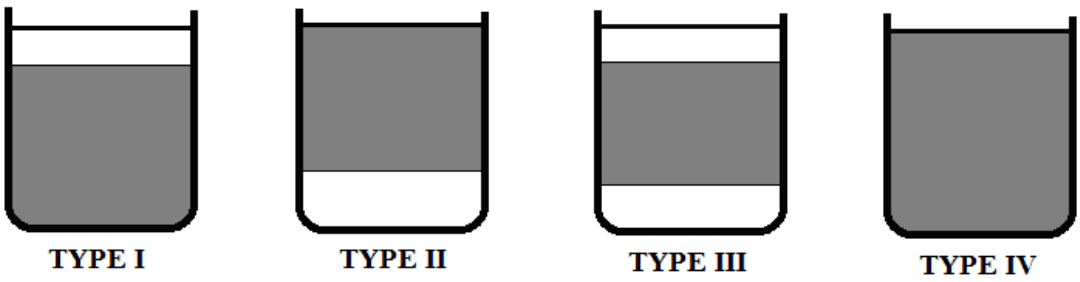

Figure 13: Diagrams showing the four types of Winsor system. Blank space above shaded area = oil phase, blank space below shaded area = water phase, dark grey area = microemulsion phase.[38]

Original theories suggested that four components were needed to make a stable microemulsion – a surfactant, water phase, oil phase and a cosurfactant to enhance stability.[37] But now, recent studies have found that in some cases, just three components are needed (the co-surfactant may no longer be needed in certain cases).[37, 39] This has often been due to an increase in surfactant used to make a

Winsor Type IV system, but this is not always the correct solution. For instance, the surfactant AOT is able to form Winsor IV systems at relatively low concentrations

1.4.1 Microemulsions in synthesis

One of the most notable uses of microemulsions is the ability to perform chemical reactions within the microemulsion droplets. Due to its confined volume, very specific compounds can be made in the 'minireactor', and regioselectivity can be enforced very well. Synthesis in the dispersed phase of microemulsions has been thoroughly studied in the last 30 years. Many areas of chemistry can be covered through these syntheses, including polymer and organic synthesis:

Polymer synthesis – Size and weight distribution of polymers can be a major factor in certain reactions and in certain cases, a single weight of polymer chain is desired. The synthesis of polyacrylamide is a successful example where the technique of using microemulsions was used.[40] Conventional latex polymerisation leads to rather uncontrolled growth, with a polydispersity index (expressed as d_w/d_n where d_w is the weight average molecular weight and d_n is the number average molecular weight) of about 2. Using microemulsions, the droplets are small enough to contain a very few particles, just the same result as with the polymorph control principle used in microemulsions. This means that the molecular weight of the polymers remains high, but the polydispersity index is significantly reduced, down to ~ 1.15.

Organic synthesis – One type of synthesis in which microemulsions have proved to be adept at driving are regioselective reactions. One of the earliest experiments carried out was the improvement of regioselectivity in the nitration of phenol. It is a simple process for the synthesis, where aqueous nitric acid is added to phenol to obtain the product. However, three different products could be formed – the *ortho*, *meta* and *para* products (otherwise known as 2, 3 and 4-nitrophenol respectively – 4-nitrophenol itself has two polymorphs). In reality, only the *ortho* and *para* forms are synthesised in the proportion 35:65, one of the main reasons being that the *ortho* product is far more sterically hindered. Therefore, the *para* product is favoured kinetically and thermodynamically. Chhatre et al. performed the reaction in an oil-in-water microemulsion.[41] Phenol was dissolved in benzene, which became the oil

phase, and the nitric acid was in the aqueous solution as before. This led to the setup shown in Figure 14:

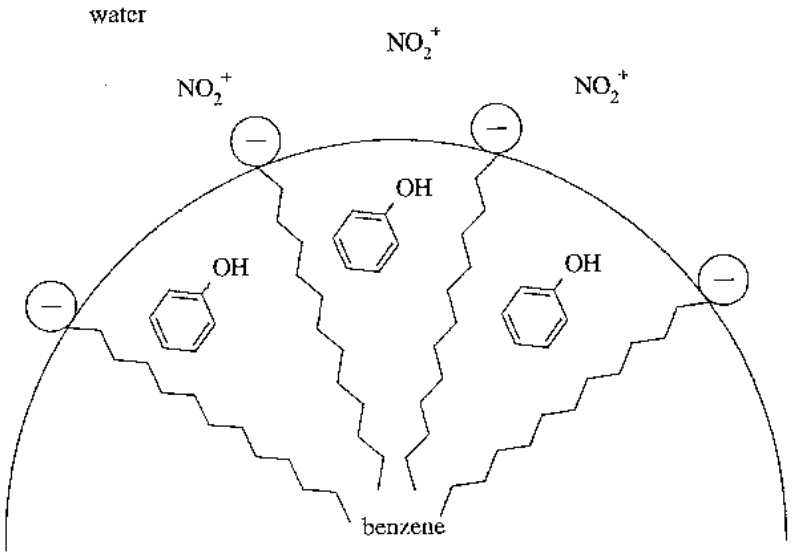

Figure 14: Diagram showing the reactants just after addition of the microemulsion.[33, 41]

Considering that phenol contains a hydroxide group, it will naturally wish to be in an aqueous environment, as it is also the polar end of the molecule. This gives the orientation of the molecules shown in Figure 15:

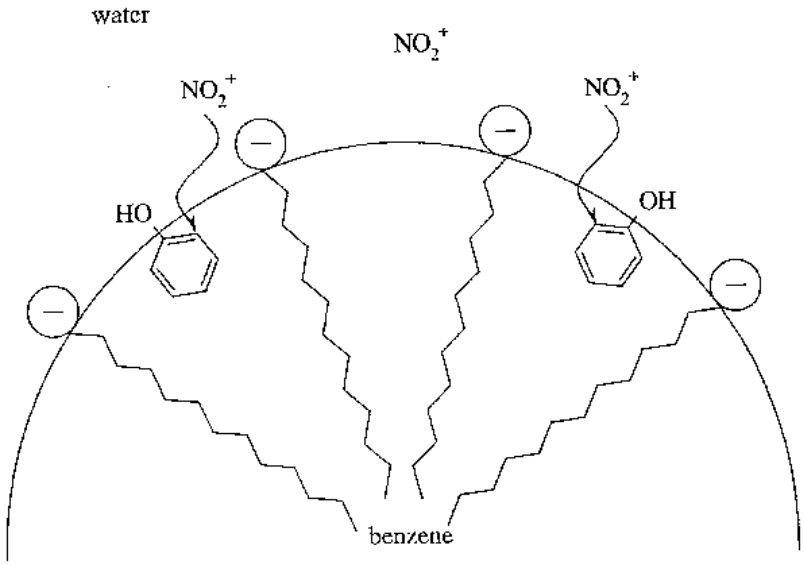

Figure 15: Diagram showing the orientation of the phenol reactants when placed in a microemulsion and the subsequent reaction that takes place with the nitronium ions.[33, 41]

Since the nitronium ion can only reside in the aqueous phase, then it is most likely to attack the *ortho* position on the phenol. The results obtained from using microemulsions are shown in Figure 16:

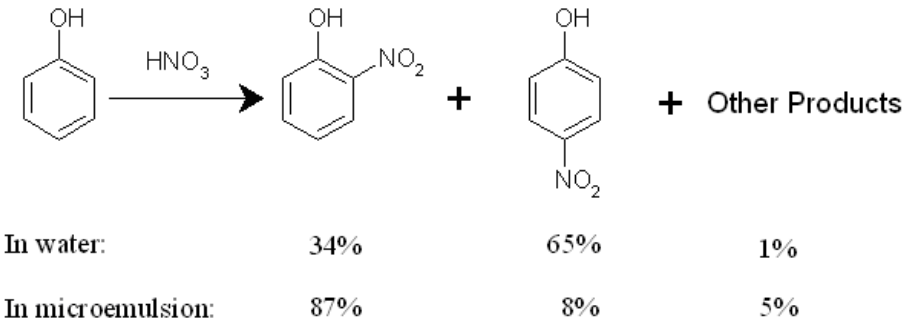

Figure 16: Comparison of the reaction products obtained when reaction is performed in water and a microemulsion.[43]

Use of microemulsions has enabled the proportion of σ-nitrophenol synthesised to increase by a full 52 %, while eight times less ρ-nitrophenol is produced. The other products include m-nitrochlorobenzene, which is the dominant waste product.

Microemulsions can also help overcome problems with the non-compatibility of reagents. Many organic chemistry syntheses suffer from slow rates of reaction due to the incompatibility of the reagents. Examples include the hydrolysis of esters with alkalis and the addition of hydrogen sulphite to aldehydes. The most important factor to discuss is the fact that in these reactions, there is poor phase contact between the reagent and the solvent, which in both cases is a large, organic, non-polar molecule. One method for solving this is by substituting the solvent for a polar, aprotic one, or adding said solvent in addition to all the other reagents. The major problem is that this solution cannot be used for large-scale work, due to the possible toxicity of the extra solvent and the fact that the extra solvent is difficult to remove via low temperature evaporation methods, thereby decreasing the purity of the final product.

Microemulsions are ideally suited to this type of work. The key point which works in their favour is that on a macroscopic level, microemulsions are homogeneous mixtures, whilst on a microscopic level they appear as a dispersed and localised two-phase system. An important example of using microemulsions in this way was the detoxification of mustard carried out by Menger et al.[42]

Mustard (Cl-CH_2-CH_2-S-CH_2-CH_2-Cl, or bis(2-chloroethyl)sulphide) and its derivatives carry an infamous reputation, with mustard having become one of the most well-known chemical warfare agents. The danger it poses is that it can bond very quickly with DNA (see Figure 17):

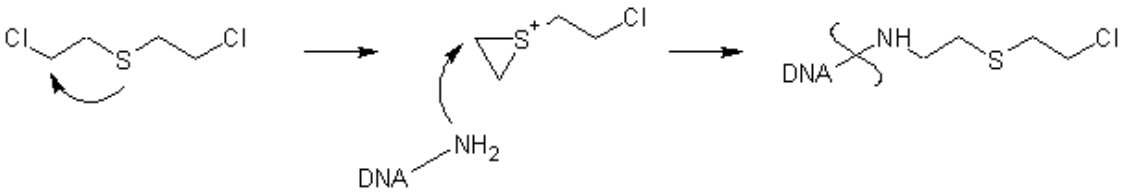

Figure 17: Reaction scheme for the reaction of mustard with DNA

Because of the bifunctionality of the molecule, mustard can bind to two guanine molecules in DNA. This now has the effect of cross-linking the double helix, and stopping the strands from separating during DNA replication.[43]

An additional danger with the mustard is that it is very insoluble in water, making dilution and removal tricky. Instead of dissolving, mustard will stay on the surface of water for many months. In the laboratory, removal by water is possible, but only with low substrate concentrations, and even the addition of caustic soda does not increase the rate by an appreciable amount.[33]

Though the question of removing mustard has not yet been solved, microemulsions have been used to oxidise and hydrolyse half-mustard ($CH_3CH_2SCH_2CH_2Cl$) to less volatile compounds. The oxidation process, using the hypochlorite ion in the aqueous phase was far faster when carried out in both oil-in-water and water-in-oil microemulsions. The reaction itself took roughly 15 seconds, compared to 20 minutes when carried out in a two-phase system. The possible scheme for the reaction is shown in Figure 18:

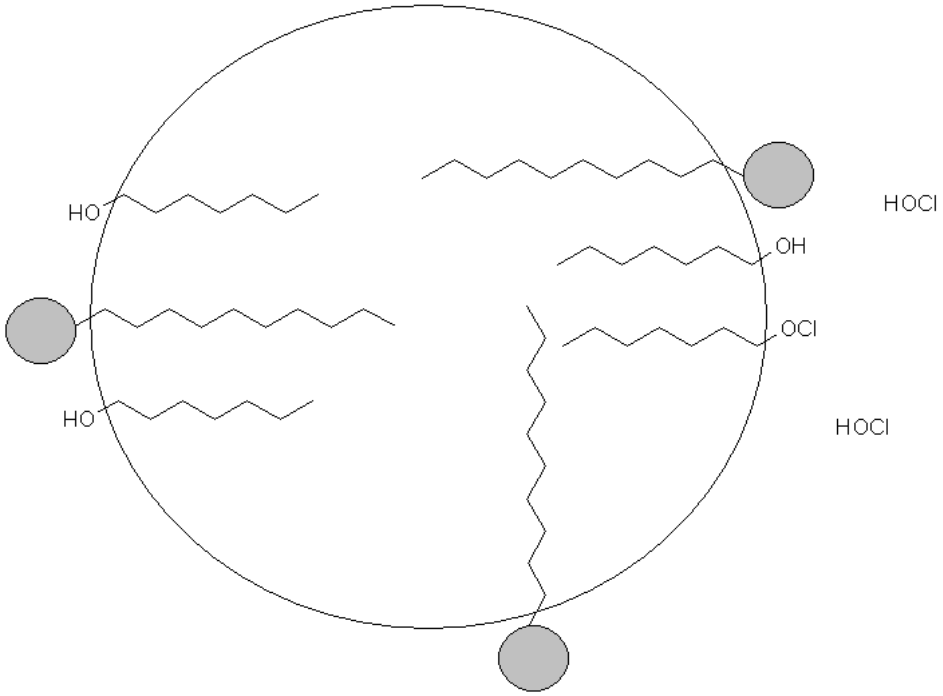

Figure 18: Hypothetical scheme for the oxidation of the chemical mustard while it is contained in an oil-in-water microemulsion.[42] The molecules with grey circles are surfactant molecules. An oil-in-water microemulsion is depicted.

In a microemulsion, the contact area between hydrocarbon and water phases (the 'oil' and water environments) is much larger than in a normal two-phase system. This allows for greater interaction between the mustard molecules and the hypochlorite ions. Despite them being in different phases themselves, reactions can occur due to the proximity of the hypochlorite ions to the oil/water interface. Hypochlorite functional groups are formed from the long chain alcohols. They subsequently react with mustard molecules with the equation $R_2S \rightarrow R_2SO$. Other uses of microemulsions in synthesis include:

Bioorganic synthesis – Using surfactant/water/oil systems, enzymes can be trapped within the droplets of microemulsion systems. This makes the whole system somewhat analogous to biomembrane fragments in terms of structure and content.[44] This has given more information into the properties of biomembranes in biocatalysis. Microemulsions have also shown their usefulness in enzyme modification.[45]

Inorganic synthesis – Performing chemical reactions in microemulsions is not just limited to organic chemistry. Many inorganic reactions have been performed in microemulsions, specifically the creation of nanoparticles. The principles of stability are the same, though the overall method is different. It often involves making two

microemulsion mixtures, which contain the reactants A and B. The microemulsions are then mixed thoroughly. The droplets containing the reactants move via Brownian motion, and doing so means that the droplets will inevitably collide with each other. The most energetic collisions will cause the droplets involved to coalesce and form transient 'dimers' or larger aggregates. These though are short-lived, and if the interacting droplets happen to be the same (i.e. (A + A) or (B + B) collision), they will decoalesce and separate essentially without change, unless the solute concentrations are different. However if different reactants interact, due to the coalescence forcing them together, the reactants can mix, thus causing the reaction to occur. Since the interaction and coalescence of identical compounds in droplets never lasts for long, the distribution of reactants A and B is equilibrated throughout the system, with a Poisson distribution often assumed. Pillai et al. were able to create the ferrite $BaFe_{12}O_{19}$ using this type of method.[46] Chen et al. used similar methods to make nickel nanoparticles.[47] Microemulsions containing aqueous $NiCl_2$ and N_2H_4 were mixed together, with the subsequent reaction taking place:

$$2Ni^{2+} + N_2H_4 + 4OH^- \rightarrow 2Ni + N_2 + 4H_2O$$

It is interesting to note that there were no nickel-containing products other than the pure nanoparticles obtained from this reaction. Originally this was attributed to the nitrogen atmosphere used in the reaction, but when the experiment was performed in a normal atmosphere, the results were the same. The only problem was that the reaction only worked at temperatures of above 40 ºC, and even then the reaction was slow.

It has been noted that most of these reactions can already be carried out using other means of confinement, mainly through the use of supramolecular chemistry. Crown ethers, cyclodextrins and carcerands can all trap molecules very effectively and be hosts to chemical reactions. However, the molecules themselves are very expensive, due to their synthesis costs. Microemulsions generally use materials which are far cheaper and abundant.

2. Experimental and Analytical Techniques

2.1 Preparation of Microemulsions

A stock solution was made, consisting of the surfactant, co-surfactant (if applicable) and the continuous phase. The mixture was shaken by hand for a few seconds to ensure mixing. From the stock solution, various volumes could be drawn out for the experiments. The disperse phase was then added using a pipette or micro-pipette to the desired weight/volume. The phases were mixed again by hand and by vortex mixing for ~ 15 seconds to form a microemulsion. A quick check of the solution by eye was carried out to ensure a microemulsion had formed – if the solution was cloudy or showed any other opaqueness, an emulsion had been formed. If the solution was clear, but retained a slight blue colouration, a nanoemulsion had formed. In both cases, the solution was re-made unless an emulsion or nanoemulsion was specifically required. Anti-solvent could then be added to induce crystallisation.

For mixed microemulsion experiments, each microemulsion was made up as before, but the disperse phases and/or anti-solvents were added to separate stock solutions to form separate microemulsions. These microemulsions were then mixed to form a single, stable microemulsion.

All microemulsions were kept at a constant temperature, except where temperature changes were necessary.

2.2 Analytical Techniques

2.2.1 Fourier Transform Infra-Red Spectroscopy (FTIR)

The theory behind FTIR comes from the fact that molecules can sometimes absorb radiation of frequencies – namely resonant frequencies, which correspond to the frequency at which certain bonds in molecules vibrate. However, only certain vibrations will be detected by IR analytical instruments, namely those that cause a change in the dipole moment of the molecule. If a CH_2 group within a molecule is taken as an example, 3 of its 6 possible vibrations are not IR-active (see Figure 19):

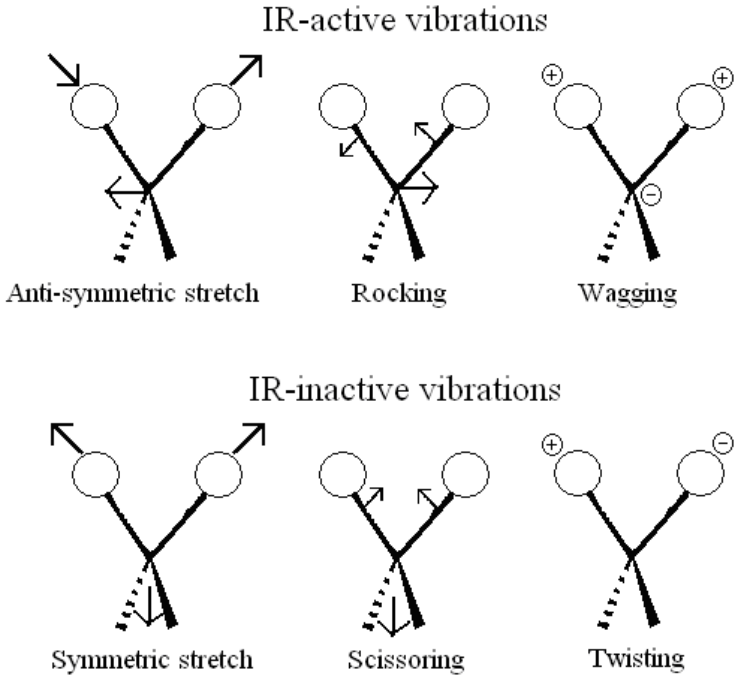

Figure 19: Diagrams showing the IR-active and inactive vibrations for a CH_2 group. Plus signs indicate that the atom is moving towards the reader, minus signs mean the atom is moving away from the reader.[48]

For Fourier Transform IR, a beam of light containing many different frequencies is shone on a sample. This allows the spectrometer to work out what absorptions happen at different wavelengths of radiation. FTIR is a popular choice for spectrometry because of its advances in speed and the sensitivity of the analysis. As Fellgett showed back in 1949, by observing all known frequencies, the signal-to-noise ratio is reduced.[48, 49]

Sampling can be made better if Attenuated Total Reflectance (ATR) is used. The sample is placed onto the spectrometer, on top of a crystal with a high refractive index. The infra-red beam is then shone through the crystal, at such an angle that it undergoes total reflections. This produces an evanescent wave, which extends beyond the dimensions of the crystal and into the sample. Where the sample absorbs infra-red radiation, the evanescent wave is altered or attenuated. The energy from this attenuation is passed back into the IR beam, which then makes its way to the detector (see Figure 20). This method requires that the sample be in close contact with the ATR crystal. The technique itself provides faster analysis of samples, and little pre-preparation of samples for analysis, since the sample can just sit directly on top of the ATR crystal.

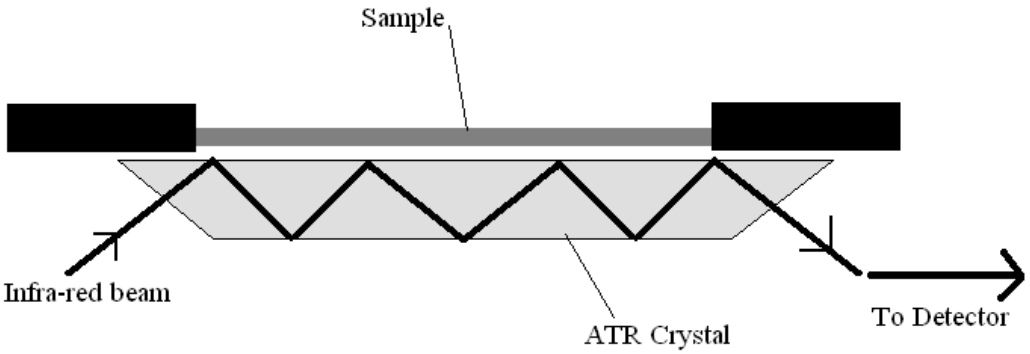

Figure 20: Diagram showing the process of Attenuated Total Reflectance (ATR) in an IR spectrometer.

A Nicolet Nexus Spectrometer was used for all FTIR analysis. A HgCdTe crystal detector was used, which was cooled using liquid nitrogen, and the samples were mounted onto a germanium crystal platform. Solid samples were dried at room temperature or in an oven before analysis. Before sample analysis, a background spectrum was taken, collecting 128 separate scans over a range of 600 – 4000 cm^{-1}. The sample was then placed directly on the germanium platform, and the crystal detector lowered so that it was in contact with the sample. As before, 128 scans were performed over the same range of wavenumbers. The background spectrum was then subtracted to give a final spectrum for the sample.

2.2.2 X-Ray Powder Diffraction

X-ray powder diffraction analysis, XRPD, can be used to obtain information on the crystal structure of materials. It works by firing a monochromatic beam at a solid sample. Upon hitting the sample, the beam will be scattered and a detector may pick up some of the scattered radiation. The idea of using electromagnetic waves to determine crystal structure was put forward by Ewald and von Laue in 1912. They hypothesised that crystals could act as a diffraction grating for electromagnetic waves, but only X-Rays could be used. Following on from that discovery, in 1913 William Henry Bragg and William Laurence Bragg found that if certain wavelengths of radiation interacted with a crystal at certain angles, the crystals would emit intense peaks of reflected radiation.[50] They were able to explain this occurrence by modelling the crystal as a series of planes with a discrete separation, termed d. They also hypothesised that the reflected waves interacted constructively, giving rise to the intense peak, but only when the phase shift was a multiple of 2π, thus giving rise to Bragg's Law $n\lambda = 2d\sin\theta$ (where θ is the angle of incidence, d is the spacing between

the crystal planes, *n* is an integer and λ is the wavelength of the X-rays - see Figure 21). In time this law would enable the scientific community to confirm the existence of particles at the atomic scale.

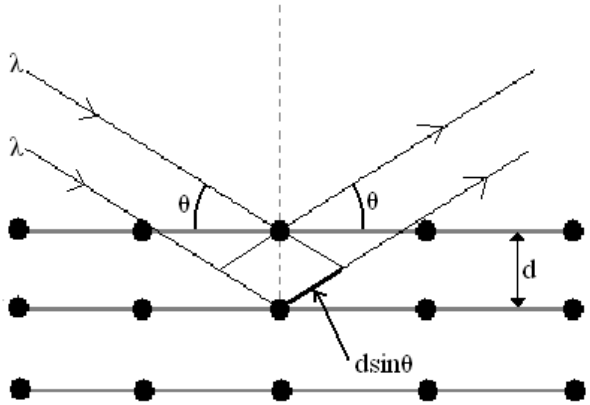

Figure 21: Diagram showing the hypothetical travel of X-Rays and their interaction with the crystal.

XRPD was primarily performed on the Bruker AXS D8, using GADDS (General Area Detector Diffraction System) software to analyse the resultant scattering data. Samples were ground up and placed onto a silicon wafer. The wafer was then manually loaded onto the sample stage. The incident beam (CuKα radiation) was set at an angle 15°, and the detector at an angle of 10° for all experiments, with the experiment timelength being 1200 seconds.

2.2.3 Transmission electron Microscopy (TEM)

In 1925, Davisson *et al*. found that when electrons were fired at a nickel crystal, they were scattered at different angles, and subsequent experiments observed specific beams of diffracted electrons, similar to X-Ray diffraction. This meant that electrons, despite having a defined mass, could exhibit wave-like properties. The subsequent publication of the de Broglie hypothesis led to the realisation that the wavelengths of the diffracted electrons were much smaller than that of light, meaning that they could be used as an analysis technique at the atomic scale.[51] In TEM analysis, the electron beam hits a sample and the scattered electrons pass through an objective lens, where they are then focussed into points which form a diffraction pattern. The extent of diffraction, like X-Ray diffraction, is determined by Bragg's Law and the structure factor F_{hkl}. By using apertures, scattered rays can be blocked and the unscattered electrons can be detected to form bright field images. Using the same apparatus,

High Resolution Electron Microscopy (HREM) can be performed. This works by focussing many beams onto a sample, which gives an image which is a reflection of the crystal structure, though not the actual structure. A large aperture is needed to obtain a high-resolution image.

The material to be analysed was deposited onto a copper-carbon grid and left for at least 24 hours to dry before analysis. A JEOL 2100F field emission gun TEM (FEG TEM) operating at 200 kV was used to examine the sample. Phase contrast HREM was used to image crystals of sizes 2 – 7 nm. Energy-Dispersive X-Ray spectroscopy (EDX) was also utilised to provide an elemental analysis of the sample. The structure of an individual nanocrystal was determined by indexing the Fast Fourier Transform and selected area diffraction patterns.

2.2.4 Small-Angle X-Ray Scattering (SAXS)

SAXS analysis can be used to determine other information about samples that techniques like powder XRD analysis cannot obtain, such as the size and shape of ~ nm sized particles in solution. Other advantages of SAXS analysis are that samples comprised of multiple phases can be analysed, and in addition to particles, it can be used to study other structures like lamellae and the internal structure of colloidal particles. This means that they can analyse microemulsions without the need to physically or chemically change the state of the microemulsion.

SAXS experiments were carried out using a Bruker Nanostar machine to determine the droplet size of the confined phase within the microemulsion. Experiments were carried out at 106 cm from the detector. An X-ray source was operated at 40 kV and 35 mA to give CuKα radiation of wavelength 1.54 Å. Analysis of the droplet size was determined from use of the Generalised Indirect Fourier Transform (GIFT) package, which is largely considered model-independent.

With reference to microemulsions, because the concentration of surfactant is high, both intraparticle and interparticle scattering need to be taken into consideration. The intensity of the scattered particles at any one angle is denoted as I(q), where q is the length of the scattering vector. I(q) is approximated as the product of the form factor P(q) and the structure factor S(q). The form factor deals with intraparticle scattering i.e. the interference between X-rays scattered from different regions of the same

particle. Hence the form factor is related to the size and shape of particles. The structure factor describes the effect of interparticle scattering of the X-rays, i.e. the interference between X-rays scattered from different particles. Consequently, the structure factor depends upon the concentration and relative positioning of the different particles. When the concentration of the microemulsion droplets in solution is sufficiently low, the scattering is dominated by the form factor, and so the structure factor has a value of 1. In the GIFT analysis, a hard sphere model was used to calculate $S(q)$. Before submitting the data for analysis, the residual background is subtracted from $I(q)$. This ensures that the pair-distance distribution function (p(r)) will be equal to zero at $r = 0$. Some estimates of values are then inputted for the calculation of the structure factor, including the volume fraction of the disperse phase, the approximate particle radius and the polydispersity of the sample. As a result, the analysis cannot be considered entirely model-free. Nevertheless, provided the inputted values incorporate a wide range, the GIFT analysis solutions should be valid. From the GIFT analysis, a pair-distance distribution curve, p(r), is obtained, which shows the mean distribution of distances within the particles at a constant volume, Hence, this enables the mean radius of the microemulsion droplets to be calculated.[52]

2.2.5 Laser Diffraction Analysis

Laser diffraction analysis has its basis in the theory of Fraunhofer diffraction, which states that the intensity of light scattered by a particle is directly proportional to the size of the particle.[53] It works by using a broadened beam of laser light on a group of particles. The light is scattered onto a Fourier lens, which re-focuses the light onto a detector array, from which a particle size distribution can be formed. The technique is made more accurate by utilising Polarisation Intensity Differential Scattering (PIDS). This uses three wavelengths of light fired along two planes of polarisation to improve the resolution of the particle sizes.[54]

For obtaining a distribution of crystal sizes > 40 nm, a Beckman Coulter LS 13 320 Laser Diffraction Particle Size Analyser was used, in conjunction with the Beckman Coulter LS Program. Firstly, the solvent to be used was chosen. For aqueous samples (water-in-oil microemulsions), isopropanol was used (to prevent diffraction from multiple phases). For solid samples, water was used. The analyser was then rinsed

three times, then filled with the relevant solvent. The solvent was then de-bubbled to eliminate any droplets which would show up in the final analysis. After this, a background state was analysed. Garnet crystals of diameter 35 μm were then loaded into the analyser, using a glass rod to push the crystals into the machine. Three runs of 60 seconds each were taken to ensure that the machine was calibrated properly. Once done, the solvent was emptied, the analyser rinsed with more solvent, and the process repeated, this time with the sample. Particles of sizes from 10 – 2000 μm could be analysed.

2.2.6 Optical Microscopy

Optical microscopy was used to check on occasion whether a microemulsion, rather than a lyotropic liquid crystalline phase or emulsion, had formed - and also to view extracted crystals to determine size and shape. An Olympus Optical Microscope was used, which was equipped with 10 x and 50 x lenses. An Olympus Camedia 2.1 megapixel digital camera was used in conjunction with the microscope to allow images to be viewed on a connected computer. Linkam Linksys software was used to take and analyse pictures. Samples were loaded onto glass slides. If a lyotropic liquid crystalline phase, such as the lamella phase, had formed the sample would show birefringence. If an emulsion had formed, two distinct phases could be discerned under the microscope – whilst very little would be seen if a microemulsion was present.

3. Control of Polymorphism of Glycine I

3.1 Introduction

3.1.1 Glycine and its polymorphs

Glycine (chemical formula NH_2CH_2COOH) is well known as one of the twenty amino acids present in proteins. As it has the simplest structure, it is also the only amino acid that is achiral. It was discovered in 1820 by Henri Braconnot, who reacted gelatine with sulphuric acid.[55] Currently, industrial synthesis of glycine is carried out by reacting chloroacetic acid with ammonia.

The first known appearance of a second form of glycine was reported in 1905 by Fischer, but it wasn't until 1931 when Bernal first produced both visual and analytical proof of the existence of two different polymorphs of glycine (now known as α- and β-glycine), via X-ray crystallography studies.[56-58]

γ-glycine was first found in 1954 by Iitaka, whilst crystallising glycine from an extremely basic solution.[59] It was found that unlike α-glycine, γ-glycine gives a large response to piezoelectric tests. When he summarised his findings a few years later, he believed that the new polymorph was more stable than either of the two polymorphs already known, and further studies have since confirmed this. However, the stabilisation energies of α- and γ-glycine are very similar, creating a problem as to which polymorph forms at room temperature. The respective heat capacities of α- and γ-glycine are 99.2 and 96.0 J K^{-1} mol^{-1}. The resulting difference in heat capacity increases at low temperatures, while at higher temperatures the α-form becomes the most stable.[60] Further proof of γ-glycine being the stable polymorph was found by Boldyreva et al. by calculating the Gibbs' free energy of the transition γ → α.[61] The resulting value was +160 J mol^{-1} when measured at 298 K, meaning the transformation would theoretically be disallowed, while the reverse reaction would be allowed.[62] Further work suggested that the γ-glycine polymorph is only ~0.2 kJ mol^{-1} more stable than α-glycine at 298 K, but it has been found that α-glycine crystallises 500 times faster than γ-glycine from aqueous solution and many times faster than β-glycine.[63-65] Hence it is likely the α-form will crystallise at room temperature (see Figure 22). It is hoped that with the use of microemulsions, an

environment can be set up where stability can be enforced, even with the small difference in relative energies.

The original reasoning for this was that in a supersaturated glycine solution, the glycine molecules form dimers, in a similar manner to the way α-glycine molecules are arranged in a crystal.[66-68] Recent work has cast doubt on this, instead saying that glycine molecules exist predominantly as monomers.[64]

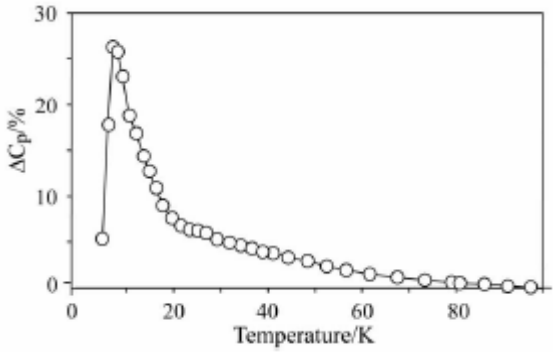

Figure 22: Graph showing the percentage change in the heat capacity difference between α- and γ-glycine. Even at 80K, the difference is minimal, showing why it is so difficult to enforce the transformation α→γ at room temperature.

Both α- and β-glycine are related in that they are monoclinic, whereas γ-glycine adopts a trigonal structure.[69] The main difference in each structure is how the glycine zwitterions ($^{+}NH_3$-CH_2-COO^{-}) are linked by hydrogen bonds.[60] In α-glycine, the zwitterions are linked in layers by hydrogen bonds, and the layers themselves are antiparallel to each other. In β-glycine, the layers themselves are linked by hydrogen bonds and are parallel to each other. Pairs of glycine molecules are in a polar organisation.[63] In γ-glycine, the zwitterions form a helix-type structure, and the structures then link to each other (see Figures 23, 24 and 25). In effect, α-glycine has a centrosymmetric structure, while the other two polymorphs are polar. The unit cells of α-, β-, and γ-glycine are listed below in Table 1:

		Unit cell dimensions / Å			Angles / °		
Polymorph	Space Group	a	b	c	α	β	γ
α	$P2_1/c$	5.107	12.040	5.460	90.00	111.82	90.00
β	$P2_1/c$	5.077	6.267	5.379	90.00	113.20	90.00
γ	$P3_2$	7.035	7.035	5.481	90.00	90.00	120.00

Table 1: Data showing the unit cell parameters of the three polymorphs of glycine.

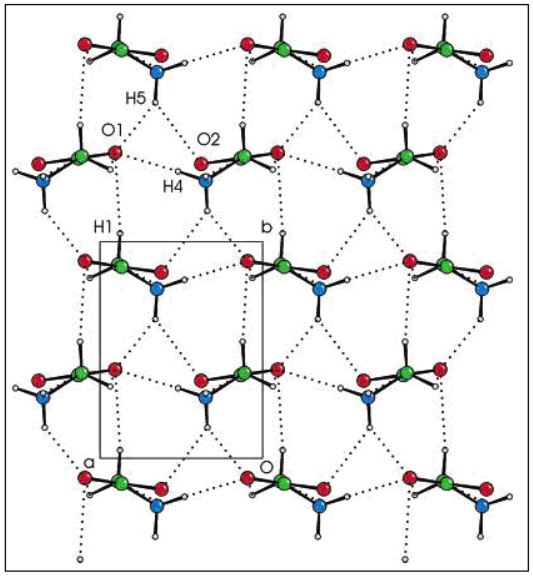

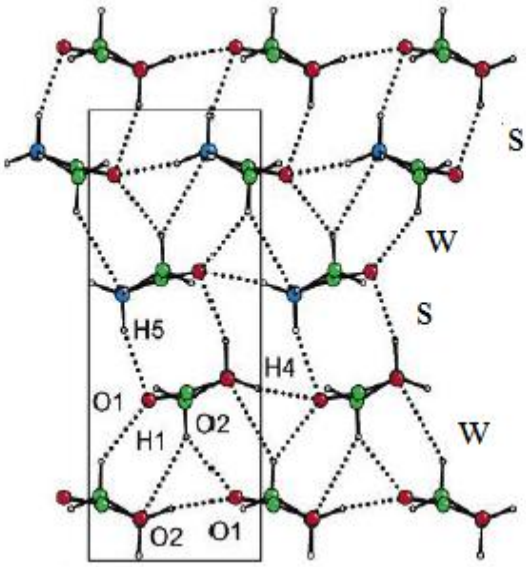

Figures 23 & 24: Packing drawings of the molecular layers of glycine looking along the c-axis. (23) = β-glycine, (24) = α-glycine (diagrams from Dawson *et al.*)[57, 70] The letters S and W in Figure 24 indicate the stronger and weaker hydrogen bonds in the structure.

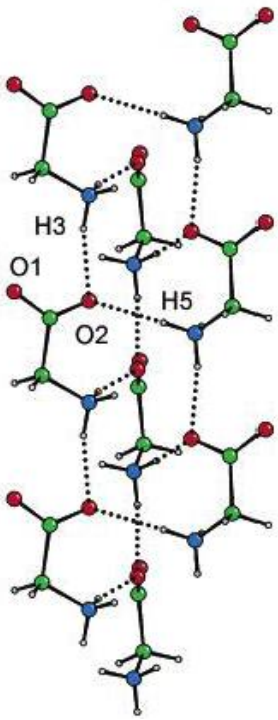

Figure 25: Packing drawing of the molecular layers of glycine looking along the c-axis for γ-glycine[57, 70, 71]

In recent years, There have been reports of two more polymorphs of glycine being formed, termed δ- and ζ- glycine.[61, 72] These were formed by applying hydrostatic pressure of up to 8.0 GPa onto γ-glycine. This formed the δ- polymorph. Rapid decompression then forced another change to the ζ-polymorph. These polymorphs

will not be considered, since they do not exist naturally (and therefore are unlikely to appear in the experiments which follow, as ambient conditions are used).

The glycine polymorphs have also been studied with regards to their pharmaceutical properties. It was found by Markel *et al.* that γ-glycine was better at relieving the symptoms of catalepsy in rats than α-glycine.[73] α-glycine has also been used in combination with other drugs to successfully treat the symptoms of schizophrenia.[74, 75]

3.1.2 Past and current work on polymorphism in glycine

As shown by Garti *et al.* and Davey *et al.*, γ-glycine can be made by using microemulsions and temperature variations, and using pH studies respectively.[32, 76] Further work by Dowling *et* al. was able to crystallise γ-glycine through the use of additives.[77] One of the main aims of this PhD was to attempt to crystallise out the three polymorphs of glycine under room temperature and standard conditions (i.e. no special pressure, acidity/basicity or atmosphere are required) by using microemulsions. The work by Davey *et al.* used AOT in the microemulsions to crystallise the stable γ-polymorph, with the γ-polymorph thought to arise solely because AOT could heterogeneously nucleate this polymorph in bulk solution.[76] We aim to show that the glycine γ-polymorph can also be crystallised from microemulsions that use surfactants that do not aid γ-polymorph crystallisation in bulk systems. In particular, it has also been shown that a combination of Span, Brij and Tween-type surfactants aid crystallisation of the metastable α- and β-glycine polymorphs, and so γ-glycine has never been observed in the presence of these surfactants. Glycine solution has never been utilised in these non-ionic surfactant microemulsions, so a further challenge will be to obtain stable microemulsions and then to produce the three polymorphs of glycine using the techniques and constraints (standard temperature and pressure) in these systems.

3.2 Experimental details

3.2.1 The materials

Glycine (99 % purity) and Span 80 were obtained from Sigma. Brij 30, Tween 80 and AOT-100 (sodium salt, 98 % purity) were purchased from Aldrich. Heptane was purchased from Fluka. All water used in the glycine solutions was obtained from a USFelga Purelab Ultra High Quality water dispenser.

The experimental section will often refer to the concentration of the glycine solutions with respect to the percentage of the mass of glycine present. The solubility of α-glycine in water at 20 °C is 204.1g/L as measured by Davey *et al.*[76] This is equivalent to a concentration of 20.4 % by mass glycine, and it is this value that was used for all experiments. The solubility of α-glycine is used rather than the γ-form, because it is easier to crystallise, and hence is less likely to be contaminated with other forms.

3.2.2 Preliminary experiments

Iitaka was able to isolate γ-glycine by crystallising glycine out of a solution mixture with ammonium hydroxide. Knowing that the stabilisation energy of γ-glycine is very similar to the α-form, it was felt that this experiment should be carried out to prove that γ-glycine could be made and extracted without too much trouble.

A simple test was set up by taking a glycine solution of concentration 18.3 % by mass glycine, and adding an excess of sodium hydroxide. The solution was then left open to air until sufficient crystallisation via water evaporation had occurred. Analysis of the crystals was then carried out, using IR spectroscopy. The peaks found in the spectrum corresponded well to those which were found in γ-glycine as described by Chernobai.[78]

3.2.3 The AOT microemulsion and emulsion systems

A stock solution of AOT and heptane was made up. To this was added glycine solution of varying concentrations. This mixture was shaken by hand again, and then placed on a vortex mixture set at 1500 rpm for 15-20 seconds. A clear, colourless solution indicated the formation of a water-in-oil microemulsion.

To make nanoemulsions using AOT, less surfactant was used. The method proceeded as before. After addition of glycine solution, a slightly cloudy, blue-coloured solution showed formation of a nanoemulsion.

All experiments were left to stand for a few minutes after the addition of glycine solution, to check for the stability of the microemulsion or nanoemulsion types. Once stability had been confirmed, recrystallisation of the glycine was obtained by adding methanol dropwise at various rates, ranging from 1.0 g s^{-1} to 0.02 g min^{-1}. after which the system was placed in a Hettich centrifuge, and spun at 4000 rpm for 3 minutes. This separated the solid glycine from the various solvents and other liquids, making for easier extraction. The extracted glycine was then dried in an oven set at 25 °C to gently remove excess solvents, after which the sample could be analysed.

3.2.4 The Span 80/Tween 80 microemulsion systems

Span 80 and Tween 80 were mixed together in the ratio 50 : 50 (kept constant for all experiments involving these two surfactants). Heptane was added, and the mixture stirred using a magnetic stirrer bar to form the stock solution. Measurements taken by Porras et al. were used as the basis for deciding some of the compositions.[34] The process then continued as for the AOT systems, with glycine solution being added to form the emulsion/micro-/nanoemulsion, followed by the addition of methanol, extraction, drying and analysis.

3.2.5 Temperature Studies

A Span 80/Tween 80/heptane stock solution was made up and 12.0 g aliquots taken as before. The aliquots were then placed in a sonicator set at the relevant temperature, and left for a period of time. A Hanna HI 8757 Microprocessor

Thermometer was used to check the temperature of the water bath and the samples, since the temperature gauge present in the sonicator was judged to be unreliable. Once at the correct temperature, glycine solution was added quickly to the samples. The samples were then shaken vigorously by hand, as it was found that the mixing ability provided by the sonicator was not sufficient to obtain a microemulsion from the components in the system. Once micro/nanoemulsion had been obtained, the samples were placed in a fridge cooled to 5 °C, to attempt to crystallise out the glycine. If crystallisation did not occur or took a long time, 0.05 g aliquots of methanol were added to encourage the glycine crystals to crystallise from the micro/nanoemulsion.

3.3 Analysis of the samples

3.3.1 Analytical Instruments

After each sample was dried in the oven, it was analysed by two different methods. The main piece of apparatus used was a Nicolet FTIR ATR spectrometer with a germanium crystal. For almost all of the experiments involving AOT as the surfactant, a D8 X-Ray Diffractometer was also used to corroborate the readings obtained using IR spectroscopy.

3.3.2 Deducing the polymorphs

FTIR

Since glycine is always the end product, the shape of the spectrum will change very little, so at first it seems tricky to work out the spectra given by different polymorphs. However, the packing of the molecules in the crystal will lead to distortions in the vibrations and the intermolecular interactions. For the experiments, the IR spectra of the polymorphs obtained by the Chernobai, Ferrari and Lee groups were used as a reference to determine which polymorph had been obtained (see Table 2).[78-80] Once the spectra were obtained, observation by eye could determine the polymorph.

Vibration Type	α-glycine / cm^{-1}	β-glycine / cm^{-1}	γ-glycine / cm^{-1}
NH_3^+ antisym stretch	3162	3176	
COO^- antisym stretch	1609	1662	
	1576	1590	1577
NH_3^+ deformation	1500	1515	1495
CH_2 bend	1443	1446	1437
COO^- sym stretch	1410	1409	1393
CH_2 wag	1331	1334	1335
NH_3^+ rock	1132	1134	1155
	1112	1117	1129
C-N stretch	1034	1042	1044
CH_2 rock	910	915	930
C-C stretch	892	893	892
O-C=O bend	694	701	

Table 2: Major peaks in IR spectra of the α- and β-forms of glycine.[79, 80]

As shown in Table 2, the difference in the peaks between polymorphs at times can be relatively large, for example the difference of ~ 50 cm^{-1} for the CO_2^- anti-symmetric stretch. By contrast, the COO^- symmetric stretch for instance varies by less than one unit between the α- and β-polymorphs. Taking into consideration the error margin on the IR spectrometer, the decision was made to ignore this peak when determining whether a sample was comprised of α- or β-glycine.

As well as using the values above, the spectra for each polymorph obtained by Chernobai et al. will be used, mainly for comparing the shape of the peaks themselves.[78]

It must be stressed that the listed values in Table 2 may vary from the values obtained in our ATR-FTIR measurements. Since the environments are different, then it is inevitable that some of the values will differ. However, since the experiments of Ferrari and Chernobai were carried out at room temperature, then the peaks in the IR spectrum are unlikely to differ too much. As a useful reference point, the IR spectrum of the stock glycine was taken. Since it is distributed as the α-form, this could now be used to compare against the spectra obtained from the experiments.

X-Ray Diffraction

IR spectroscopy would be used for the bulk of the analysis, since it could detect very small amounts of material. Where there was more abundant final product, it could then be analysed by X-Ray diffraction to give more proof and guidelines on what should be found for future experiments. Garti *et al.* found peaks in diffraction patterns for α-glycine, Liu *et al.* for β-glycine and Bhat *et al.* for γ-glycine.[31, 32, 81, 82] This information will be used as a guideline for polymorph deduction. Table 3 shows the characteristic peaks for α-, β- and γ-glycine:

Glycine polymorph	Major peaks in order / °
α	19, 20, 24, 28, 30, 35, 37
β	18, 19, 24, 29, 31, 37
γ	18, 22, 25, 28, 36, 39

Table 3: The characteristic peaks found for XRD patterns of each glycine polymorph.

It is important to note that a different orientation of the sample which undergoes analysis will alter the relative peak intensities. However, it will not affect the peak positions.

The characteristic peaks can also be deduced from the simulated powder patterns obtained using Cerius software (Molecular Simulations) of the α-, β- and γ-glycine structures (see Table 4):

Polymorph	h	k	l	d-spacing / Å	2-theta	Intensity / %
	0	4	0	3.010	29.68	100.00
	1	2	0	3.725	23.89	64.87
	0	1	1	4.672	19.00	59.85
α	1	2	-2	2.455	36.60	52.32
	1	3	0	3.063	29.15	36.70
	0	3	1	3.147	28.36	29.44
	1	0	1	2.957	30.22	21.47
	1	4	0	2.541	35.32	21.00
	0	2	0	3.134	28.48	100.00
	1	1	0	3.743	23.77	81.68
	0	0	1	4.944	17.94	55.73
β	1	1	-2	2.449	36.69	38.62
	0	2	1	2.647	33.87	19.66
	1	2	0	2.601	34.48	16.56
	1	0	1	2.875	31.11	16.54
	0	1	2	2.300	39.17	11.52
	1	1	0	3.518	25.32	100.00
	1	0	1	4.075	21.81	45.35
γ	1	0	2	2.499	35.93	41.55
	2	1	0	2.303	39.12	27.21
	2	0	0	3.046	29.32	16.50
	2	0	2	2.037	44.47	9.49

Table 4: Data from the simulated powder diffraction patterns of α-, β- and γ-glycine, showing the most intense peaks.

3.4 Results and Discussion

3.4.1 AOT systems

	Masses of surfactant, oil and aqueous phases used / g						
System	**AOT**	**Heptane**	**Glycine / g**	**Water volume / cm^3**	**Micro/nano-emulsion?**	**Methanol addition speed[(a)]**	**Polymorph of glycine obtained**
Test 1	0.12	1.6	0	0.4	Nanoemulsion		
Test 2	0.18	1.6	0	0.4	Microemulsion		
Test 3	0.5	4.5	0	0.5	Microemulsion		
Test 4	0.5	4.5	0	1.5	Nanoemulsion		
1	0.12	1.6	0.07	0.4	Emulsion	-	-
2	0.25	2.25	0.04	0.2	Microemulsion	Slow	α
3	0.25	2.25	0.04	0.2	Microemulsion	Fast	β
4	0.5	4.5	0.28	1.5	Nanoemulsion	Fast	β
5	0.5	4.5	0.28	1.5	Nanoemulsion	Slow	α
6	1	3	0.09	0.5	Microemulsion	Slow	γ

Table 5: The original tests and experiments involving the system AOT / heptane / glycine solution. The glycine was added as a glycine solution with the water volume stated. (a) Methanol Addition Speed: Fast = Methanol added quickly in one go. The amount added was variable between 0.7 and 1.5 g. Slow = Methanol was added at a rate of 0.04g every 20 seconds, followed by thorough mixing of the system.

The test experiments denoted in Table 5 were carried out first to see roughly what proportions of the system components gave which type of emulsions. From there the experiments could be repeated with glycine solution, or modified as needed. System 1 gave an emulsion and therefore was of no use for the later stage, since phase separation occurred and therefore the Winsor type IV system was broken.

FTIR analysis

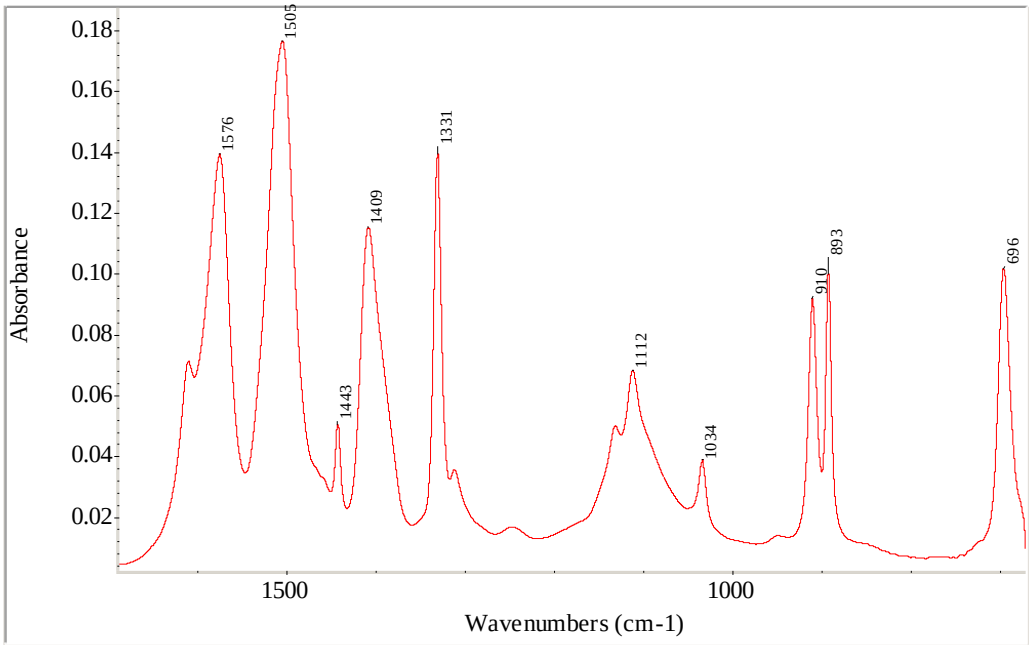

Figure 26: Fourier transform infra-red (attenuated total reflection) (FTIR ATR) spectrum obtained from system 2 with major peaks marked.

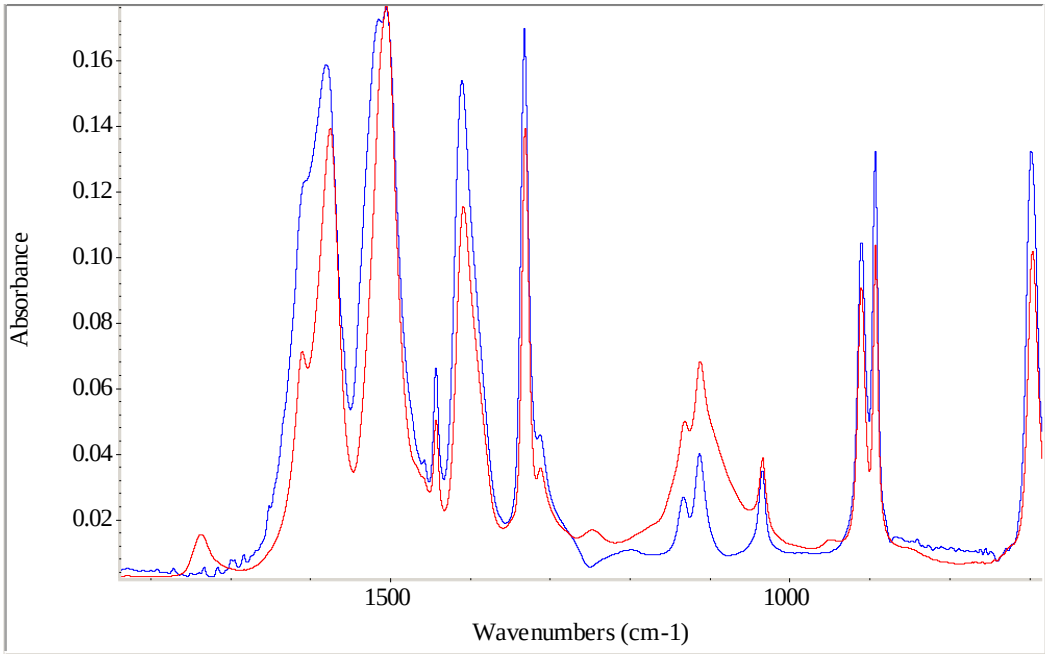

Figure 27: FTIR ATR spectrum of system 5 (red spectrum) overlaid with the spectrum obtained from as-received α-glycine (blue spectrum) for comparison

Both systems 2 and 5 crystallised glycine as the α-phase (see Figures 26 and 27). The IR spectra show almost no change compared to the as-received α-glycine (see Figure 27). Systems 3 and 4 show a marked change in the spectra (see Figures 28 and 29):

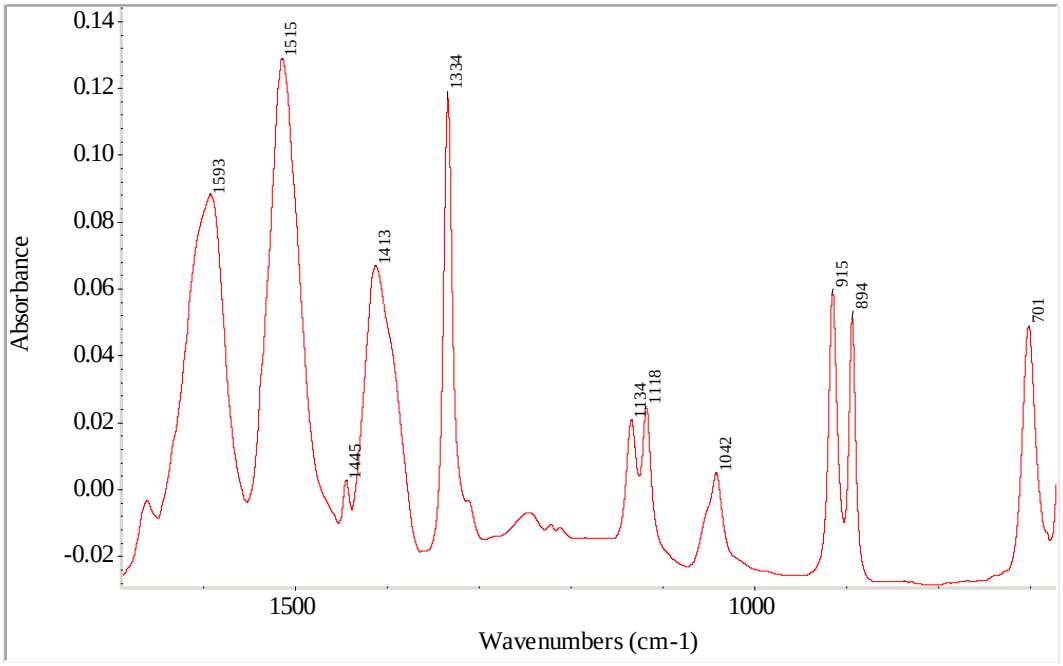

Figure 28: FTIR ATR spectrum obtained from system 3.

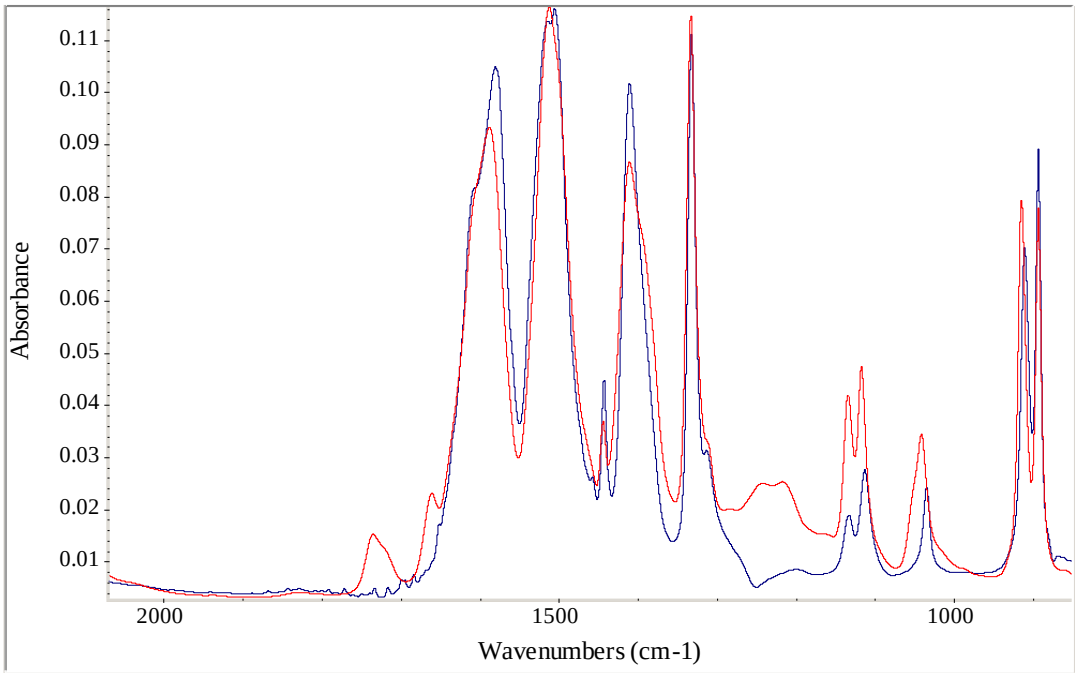

Figure 29: FTIR ATR spectra showing a comparison between as-received α-glycine (blue spectrum) and the spectrum obtained from system 4 (red spectrum).

The shifting of the peaks can be clearly seen in Figures 28 and 29. The peak at 701 cm^{-1} has been shifted to larger wavenumbers, as have the peaks at 1592, 1118 and 1041 cm^{-1}. The two peaks at 915 and 893 cm^{-1}, as well as being shifted, also have a different shape.

The spectra from systems 3 and 4 show more similarities to the β-glycine spectrum obtained by Chernobai et al., and so it can be said that these experiments have made β-glycine.[78]

What can also be seen is that when methanol addition is fast, the β-phase is crystallised, whereas when methanol is added slowly, the α-phase forms more readily. Whether a microemulsion or nanoemulsion is present, no change in the polymorph occurs – it is the rate of addition that is important.

System 6 was the first AOT-containing system to show signs of the γ-polymorph. The original IR spectrum is shown below in Figure 30:

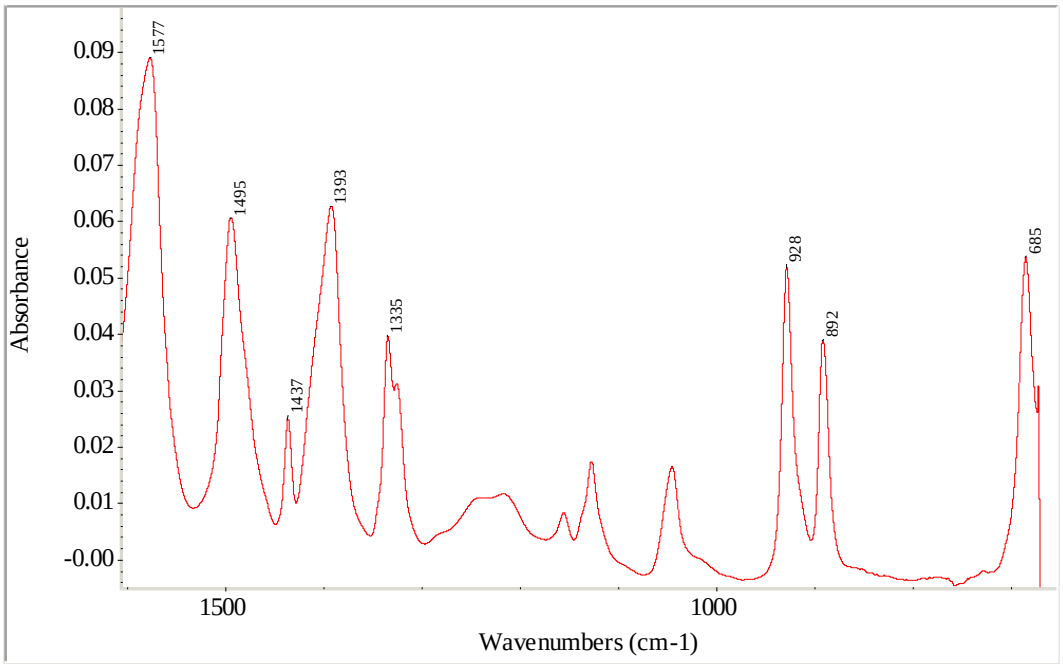

Figure 30: FTIR ATR spectrum of glycine crystals obtained from system 6

The separation of the peaks at 928 and 891 cm^{-1} is larger than that found in α- and β- glycine. A comparison with the as-received α-glycine is shown in Figure 31:

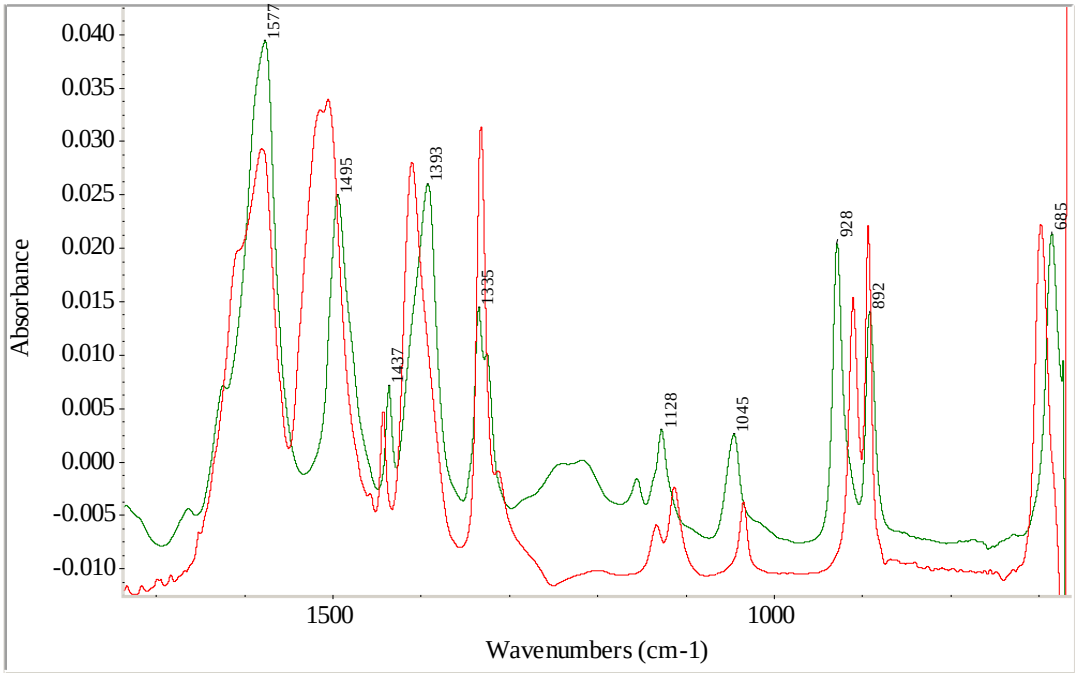

Figure 31: FTIR ATR spectrum from system 6 (green spectrum) overlaid with the spectrum obtained from as-received α-glycine (red spectrum).

Many peaks have shifted, or have a completely different shape to the α-glycine spectrum. This is enough evidence to state that the sample obtained is not α-glycine. The γ-glycine spectrum has a few more similarities to the spectrum for β-glycine (see Figures 32 and 33):

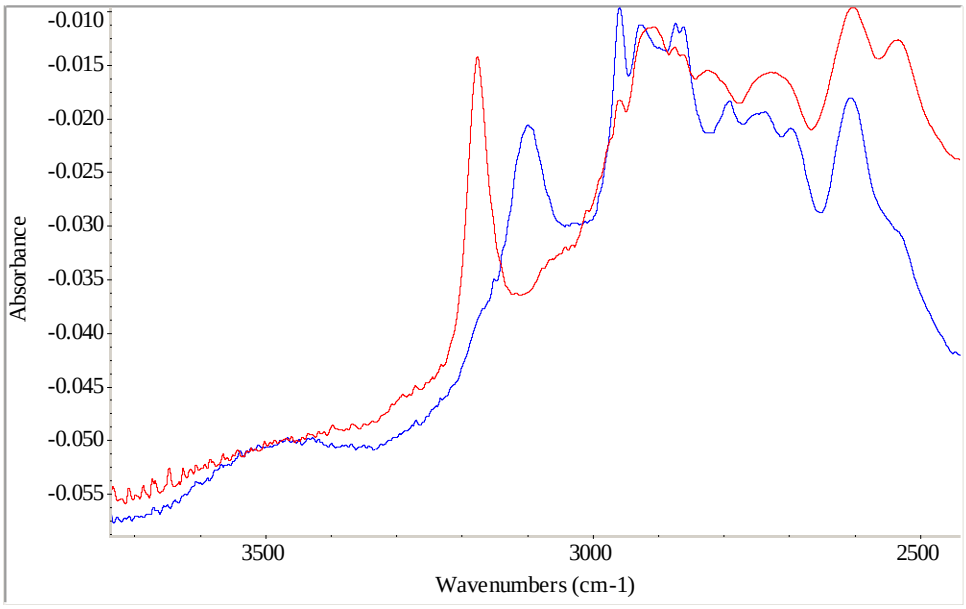

Figure 32: FTIR ATR spectra showing the comparison between the results obtained for system 6 (blue spectrum) against a typical spectrum obtained for β-glycine (red spectrum). Range is from 2750-3750 cm^{-1}.

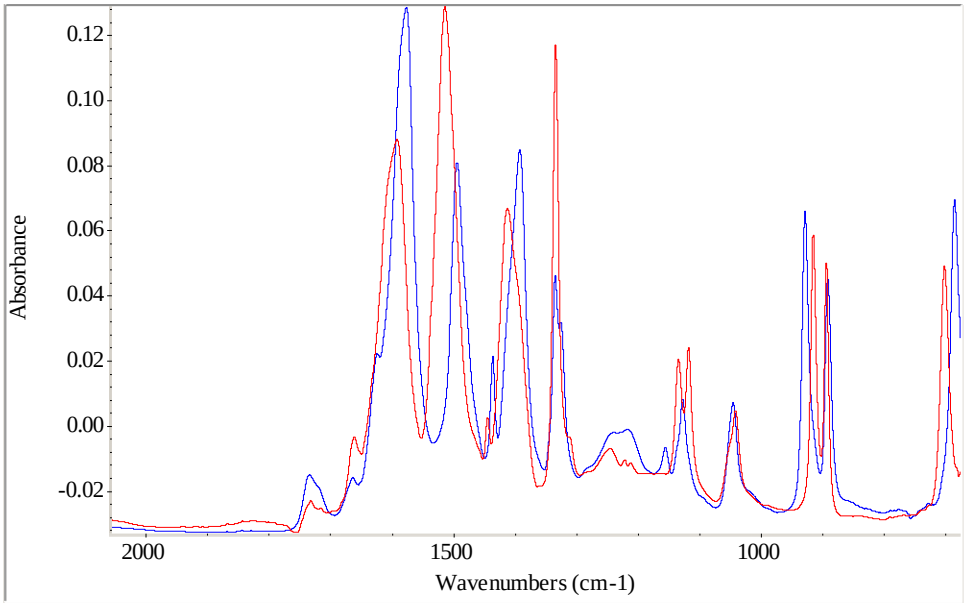

Figure 33: FTIR ATR spectra showing the comparison between the results obtained for Experiment 6 (blue spectrum) against a typical spectrum obtained for β-glycine (red spectrum). Range is from 650-2050 cm^{-1}.

The overall shapes of the graphs are fairly similar, but a few crucial differences point to the appearance of different polymorphs. For β-glycine, a clear peak at about 3175 cm^{-1} has been shifted to 3150 cm^{-1} in the case of γ-glycine. And the peak at ~700 cm^{-1} in β-glycine has shifted to 685 cm^{-1} in the γ-form. Since the peak shifts between α- and β-glycine are almost always far less than those found here, then it can be said with confidence that the glycine polymorph obtained is not either of these two, and therefore the γ-form has been crystallised. Figure 34 shows the FTIR spectra of α-, β- and γ-glycine and the differences between each of the spectra in the region 850 – 950 wavenumbers:

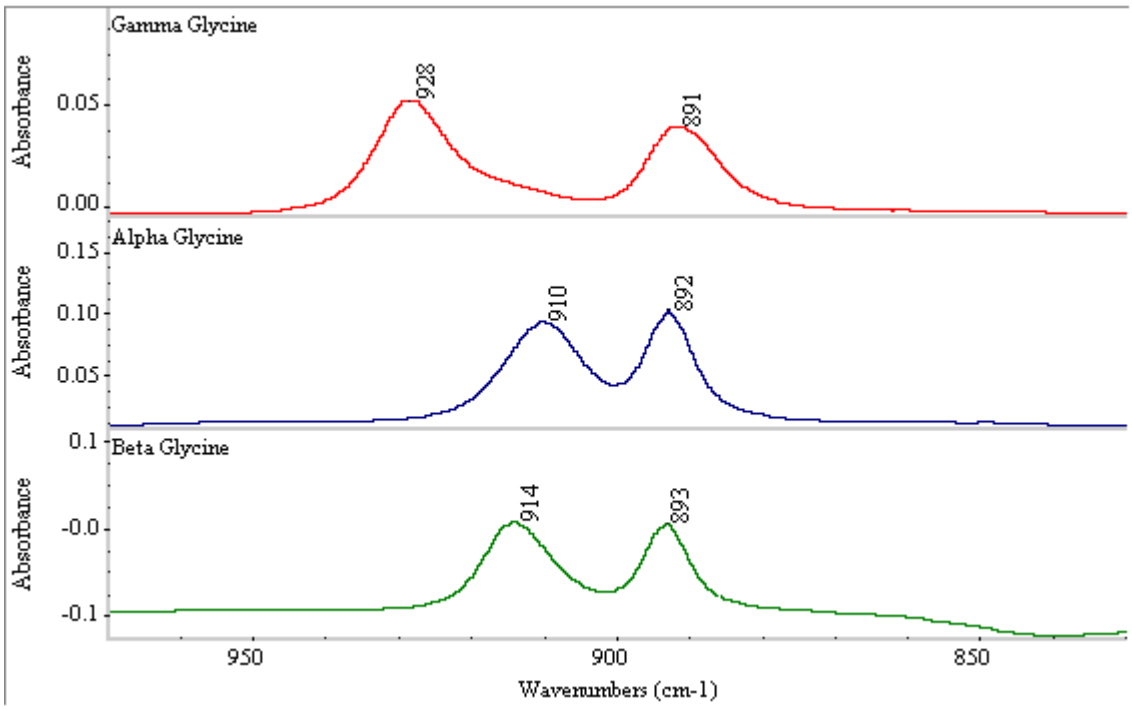

Figure 34: FTIR ATR spectra comparison of the IR spectra of the three polymorphs of glycine in the region 850-950 wavenumbers. α-glycine = blue spectrum, β-glycine = green spectrum, γ-glycine = red spectrum.

It is important to note that spectra obtained using ATR methods can vary in peak height and shape due to two variables. Firstly, the force with which the sample is pressed into the ATR crystal can vary the peak heights greatly. If no force is applied, the crystals to be analysed have poor contact with the ATR crystal and the peak heights are reduced. Secondly, the orientation of crystals on an ATR crystal may also affect peak heights and shapes greatly. To minimise force effects, the crystal detector which pressed the samples onto the ATR crystal would lock into place once tightened, ensuring that the pressure on the sample was always the same. To combat orientation effects, the samples were crushed up after extraction and drying. This meant that the sample surface orientation was random, therefore producing more consistency with regards to peak shapes.

XRD analysis

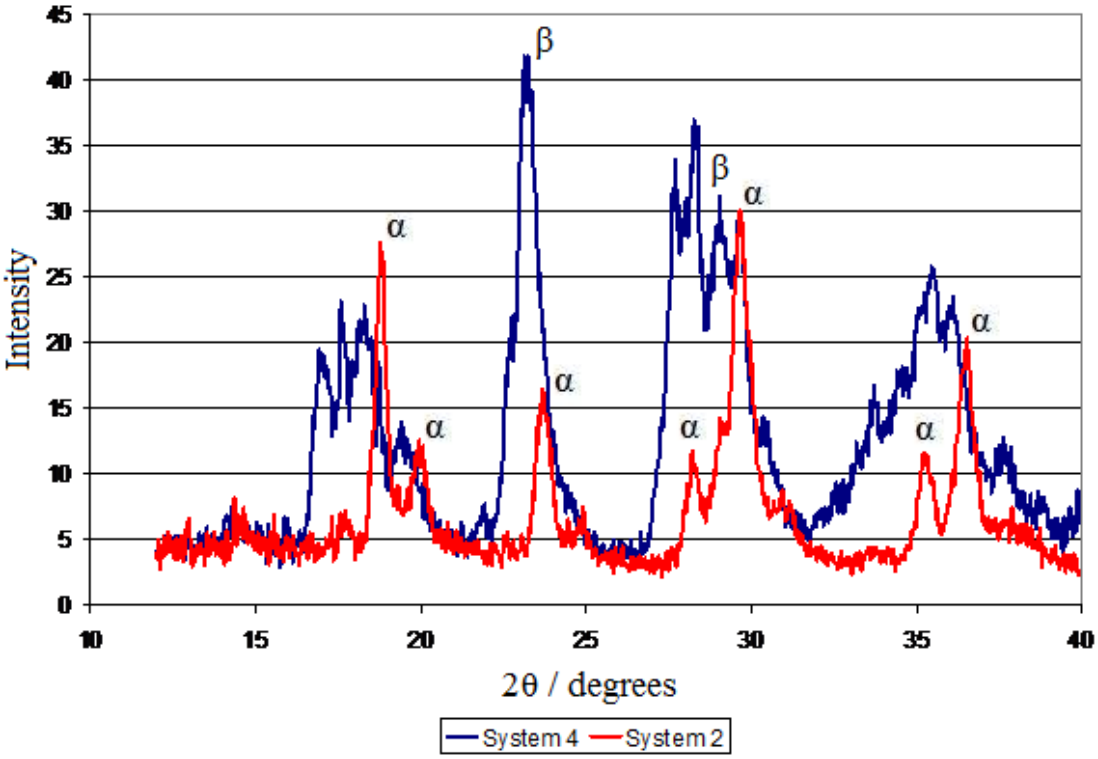

Figure 35: Comparison of the X-Ray diffraction patterns of Systems 2 (red) and 4 (blue).

Though the XRD patterns in Figure 35 look noisy due to the limited amount of sample available for analysis, results can be defined. The two major peaks in System 2 (α-glycine according to FTIR data) appear at ≈ 18.5°, where no peak appears in System 4 (β-glycine according to FTIR data), and ≈ 29.5° where a peak can be found in System 4. The peak at ≈ 20° in system 2 is also unique to that polymorph. The peak at ≈ 24° does raise some issues though, as both peaks appear in the two graphs, though this peak does appear in both the simulated diffraction patterns for α- and β-glycine. Hence there are enough differences in the graphs to suggest that different polymorphs have been found.

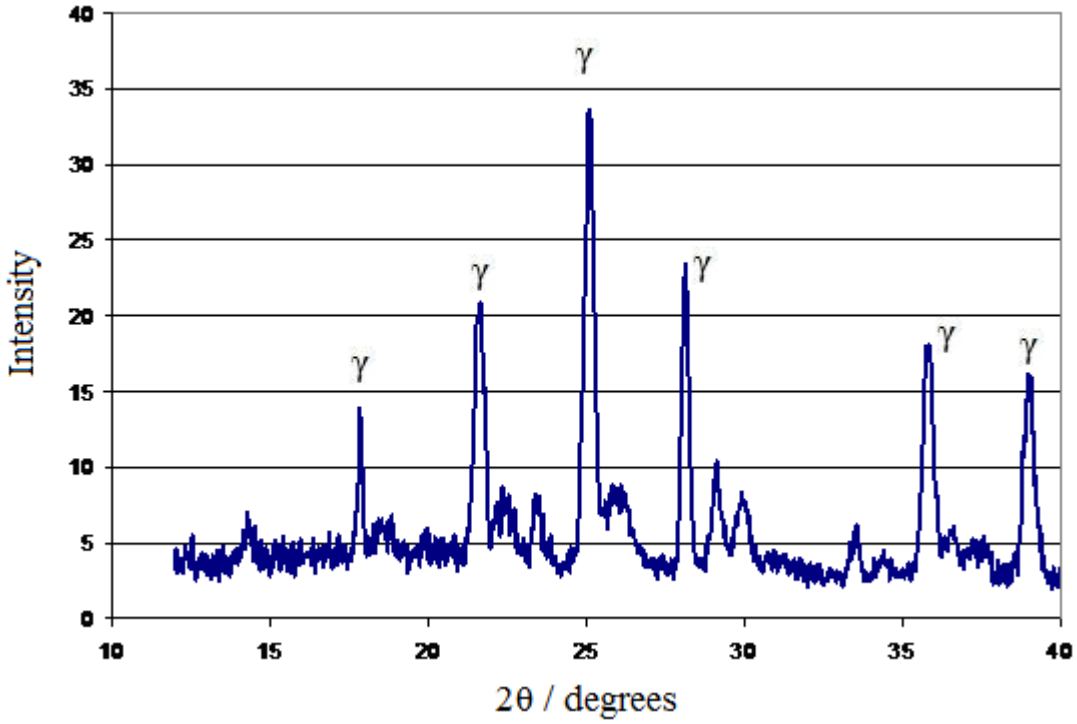

Figure 36: XRD pattern for System 6 – γ-glycine according to FTIR data.

The differences in the XRD trace shown in Figure 36 obtained from system 6, and from those shown in Figure 31 are apparent. Large peaks at ≈ 25°, ≈ 22°, ≈ 36° and ≈ 39° do not appear in any other XRD traces, and the peak at ≈ 30° is far smaller than those found in both α- and β-glycine. The presence of three large peaks with no similarity position-wise to previous data suggests that γ-glycine is indeed the main polymorph formed in System 6.

The AOT system was therefore found to be very good at nucleating each of the polymorphs under different rates of methanol addition.

Optical Microscopy

α- and γ-glycine were also studied by optical microscopy to show differences in the crystal shape and morphology (see Figures 37 and 38):

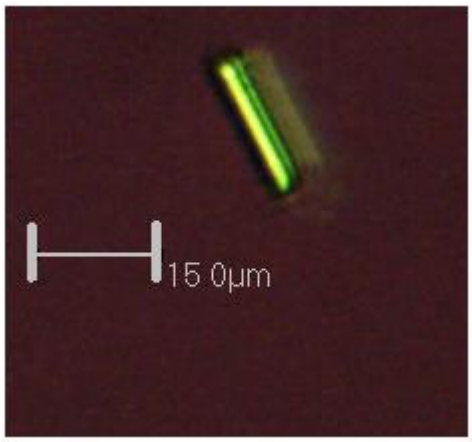

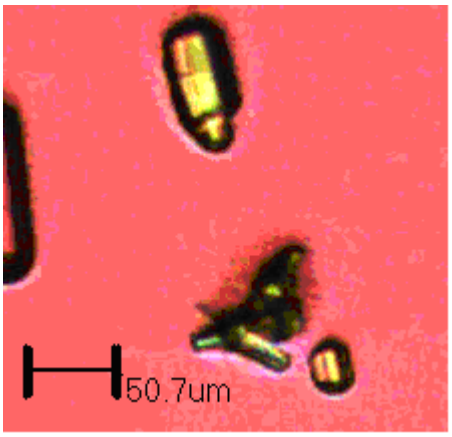

Figures 37 and 38: Microscopy pictures for α-glycine (Fig. 37) and γ-glycine (Fig. 38)(relevant crystal at top centre). Both sets of crystals were still in solution and had not been extracted

The images clearly show a pencil-like crystal present in γ-glycine, whilst the crystals are far more prism-like in α-glycine. Similar shapes of the polymorphs were obtained by Garti for the α-form, Davey for the γ-form and Torbeev et al. for both types.[32, 67, 76]

3.4.2 Span 80/Tween 80 systems

Stock solution setup and FTIR analysis

Large batches of mixtures of Span 80, Tween 80 and heptane were made up with the compositions listed in Table 6 (for structures of Span 80 and Tween 80, see Figures 42 and 43). Thorough mixing was needed to ensure that all aliquots taken would have the same composition.

% surfactant in stock solution (by mass)	Mass of stock solution / g	Span 80 / g	Tween 80 / g	Heptane / g
20	4	0.4	0.4	3.2
20	8	0.8	0.8	6.4
20	12	1.2	1.2	9.6
25	4	0.5	0.5	3
25	8	1	1	6
25	12	1.5	1.5	9
50	4	1	1	2
50	8	2	2	4
50	12	3	3	6

Table 6: The components of each Span/Tween stock solution used

The first experiments using these surfactants (systems 7 and 8 in Table 7) used 0.8 g Span/Tween mixture in a 50:50 ratio, 3.2 g heptane and 0.3 g glycine solution (90% saturated). An emulsion was formed, and when heated to ~ 45 °C, a nanoemulsion was formed, characterised by a blue-tinged, but clear solution. When methanol quantities of 1.0 to 2.5g were added in one go, immediate nucleation and crystallisation occurred. After drying, the crystals were analysed by IR spectroscopy and found to be the β-form of glycine (see Table 7 and Figure 39).

Experiment No.	Mass of surfactant solution / g	% surfactant by mass	Glycine solution/g	Glycine solution conc. / mass %	Methanol addition speed[(a)]	Polymorph obtained
7	4	20	0.2	18.4	Fast	β
8	4	20	0.3	18.4	Fast	β
9	4	20	0.3	10.2	Slow	α
10	12	20	0.9	10.2	Slow	α
11	12	20	0.8	10.2	Slow	α
12	8	20	0.6	8.2	Slow	α
13	8	20	0.6	8.2	Very Slow	α
14	8	20	0.5	8.2	Fast	β
15	8	20	0.5	8.2	Slow	α
16	8	25	0.5	8.2	Slow	α
17	8	25	0.4	10.2	Slow	α
18	12	20	0.6	5.1	Slow	α

Table 7: Various microemulsion systems involving Span 80 and Tween 80 as the surfactants. A microemulsion was formed in every experiment except for experiments 8 and 10, where a nanoemulsion formed. (a) Methanol addition speed: Fast = Methanol added quickly in one go. The amount added was variable between 0.7 and 1.5 g. Slow = Methanol was added at a rate of 0.04 g every 20 seconds, followed by thorough mixing of the system. Very slow methanol addition = 0.02 g methanol added every minute, with vigorous shaking in between additions.

Experiment No.	Glycine solution/g	Methanol addition speed	Polymorph
19	1.25	1g in 0.15g increments	α
20	1.5	1g in 0.15g increments	α
21	1.25	1g in 0.20g increments	α
22	1.5	1g in 0.20g increments	α
23	1.25	0.5g in one go, then 0.2g increments	α
24	1.5	0.5g in one go, then 0.2g increments	α
25	1.5	0.6g in layer on top	α
26	1.5	0.7g in layer on top	α
27	1.5	0.8g in layer on top	α
28	0.6	0.6g in 0.05g amounts per minute	α

Table 8: More microemulsions using Span 80/Tween 80 surfactants. For this set of experiments, the mass of the surfactant stock solution was 12.0 g – 50 % of which was Span 80 and Tween 80. The glycine solution concentration was 3.0 % by mass glycine. These values were held constant for all experiments, and a microemulsion was formed every time.

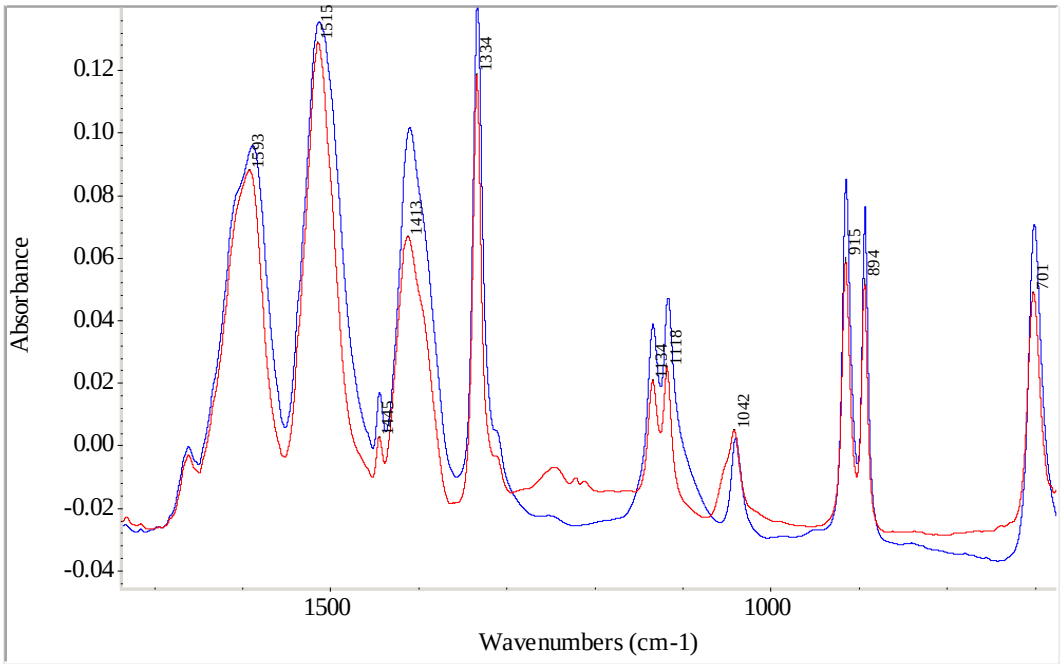

Figure 39: FTIR ATR spectra comparison of similar results in different systems. Red spectrum = AOT system, blue spectrum = Span 80/Tween 80 system (Experiment 14).

It is interesting to compare one of the spectra – obtained from Experiment 14 (see Table 7) - with that of an AOT system which also produced β-glycine (see Figure 28). Despite the variation of the systems in which glycine is present, overall β-glycine is still the dominant polymorph.

This first experiment using Span/Tween surfactants was probably less valid than other experiments, as significant heating was required to obtain a nanoemulsion. Once again, this result has shown that fast addition of methanol causes immediate nucleation and growth of the crystals, which will likely end up being the least stable polymorph (i.e. the β-form).

XRD analysis of Span/Tween systems

Most of experiments 7-18 (see Table 7) gave enough crystalline material for them to be studied by XRD. Experiment 13, which gave α-glycine according to the IR data, can be compared with experiment 2 (an AOT system), which also gave α-glycine (see Figure 40):

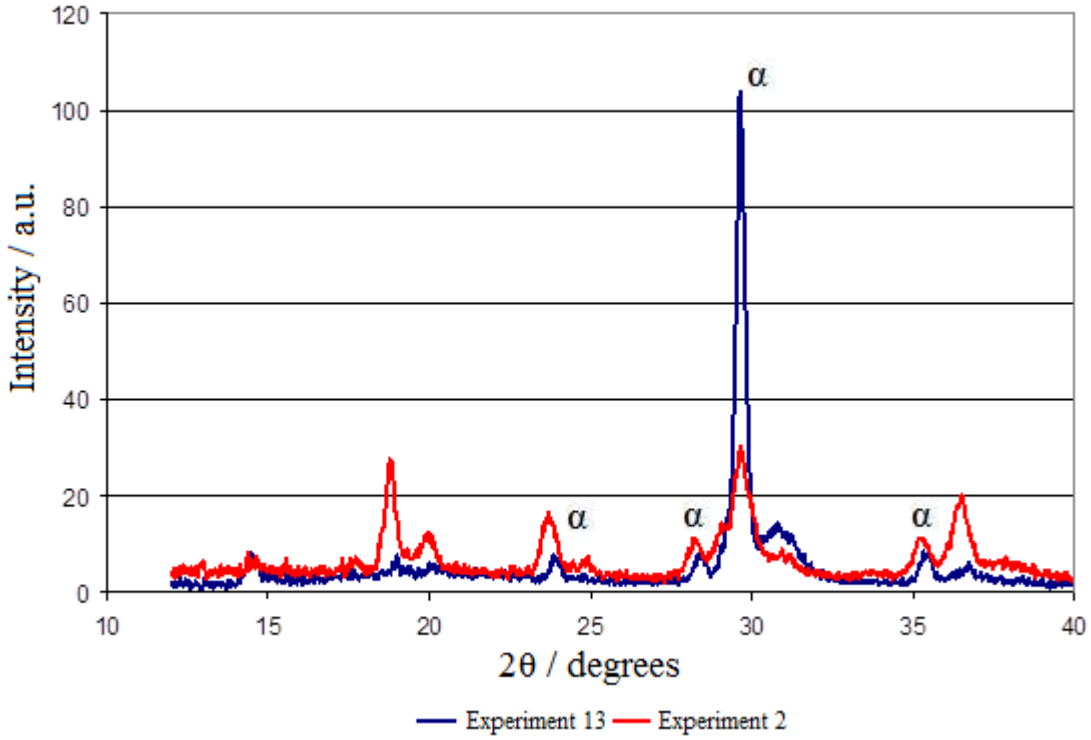

Figure 40: X-Ray diffraction patterns for experiments 2 and 13.

Though some peaks in the experiment 13 (the Span/Tween system) are not apparent due to the limited amount of product compared to experiment 2, some major peaks still stand out, most notably the peak at 29.6°, which was also found in experiment 2. The peaks at 24°, 28.5° and 35.5° also compare favourably. With this in mind, it can be said with confidence that experiment 13 has crystallised α-glycine.

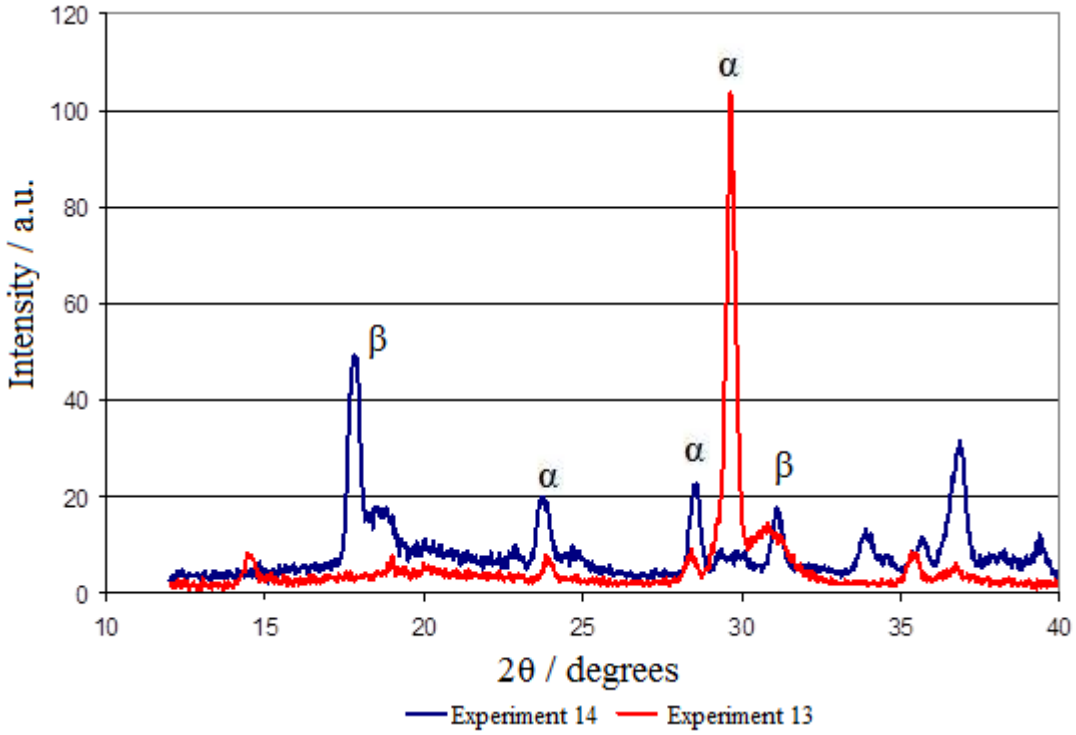

Figure 41: Comparison of X-Ray diffraction patterns between experiments 13 and 14.

By FTIR data, it was thought that Experiment 14 had made β-glycine (see Figure 39). The X-Ray data shows many discrepancies between the spectra of Experiments 13 and 14 (see Figure 41) – the peaks at ≈ 15° and ≈ 30° are far more visible in Experiment 13, whilst the peaks at ≈ 18° and ≈ 37° which appear in Experiment 14 are almost non-existent in Experiment 13. The peaks at ≈ 24° and ≈ 28° appear in both patterns – and both can indicate the formation of α- or β-glycine. But differences in the first four peaks previously mentioned gives proof that experiment 14 gave β-glycine.

In attempting to crystallise the γ-form, it was realised that this could not be achieved if a nanoemulsion, rather than a microemulsion was formed. This would not give the thermodynamic control required to force glycine to not crystallise in its usual α-form. As described above, significant heating was required just to obtain a nanoemulsion.

It may seem surprising that even at glycine solution concentrations of 10 % by mass glycine, glycine crystallisation can occur with ~ 1.0 g methanol addition, whereas in the bulk solution, no crystallisation would be observed. This was attributed to the fact that each of the functional groups present on Span 80 and Tween 80 molecules can form hydrogen bonds with water molecules present in the glycine solution which is added (see Figures 42 and 43). In doing so, the water content of the nanoconfined glycine solution is reduced, as water becomes bound to the surfactant and the interfacial boundary, effectively increasing the concentration and saturation of the solution. Indeed, research suggests that ~ 2.5 water molecules are bound per ethylene oxide group in non-ionic surfactants. Therefore, adding methanol will induce crystallisation much faster compared to the analogous bulk system, and will thereby be far more likely to give the less stable polymorphs.

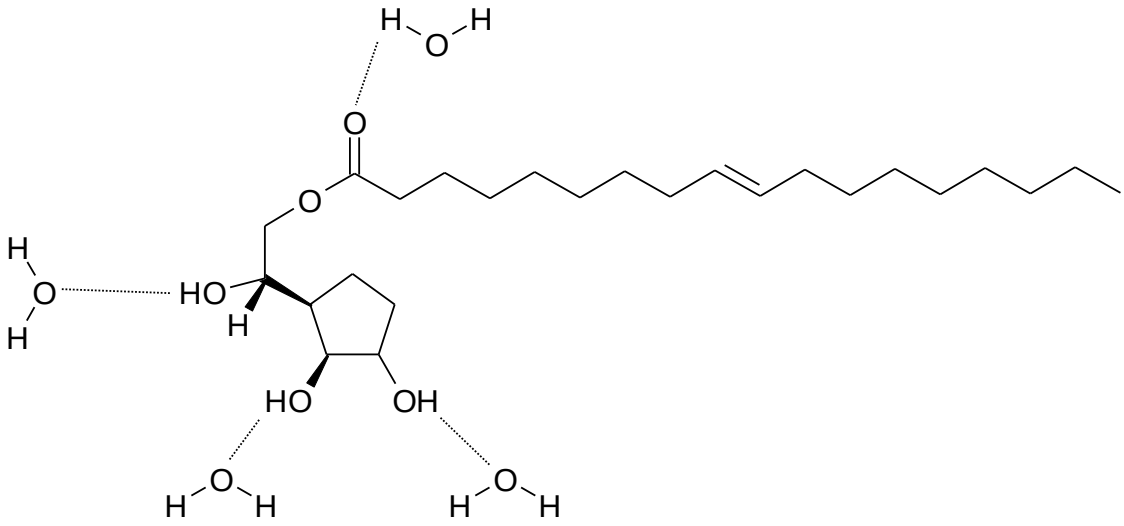

Figure 42: Structure of Sorbitan Monooleate (Span 80), showing possible hydrogen bonding with water molecules

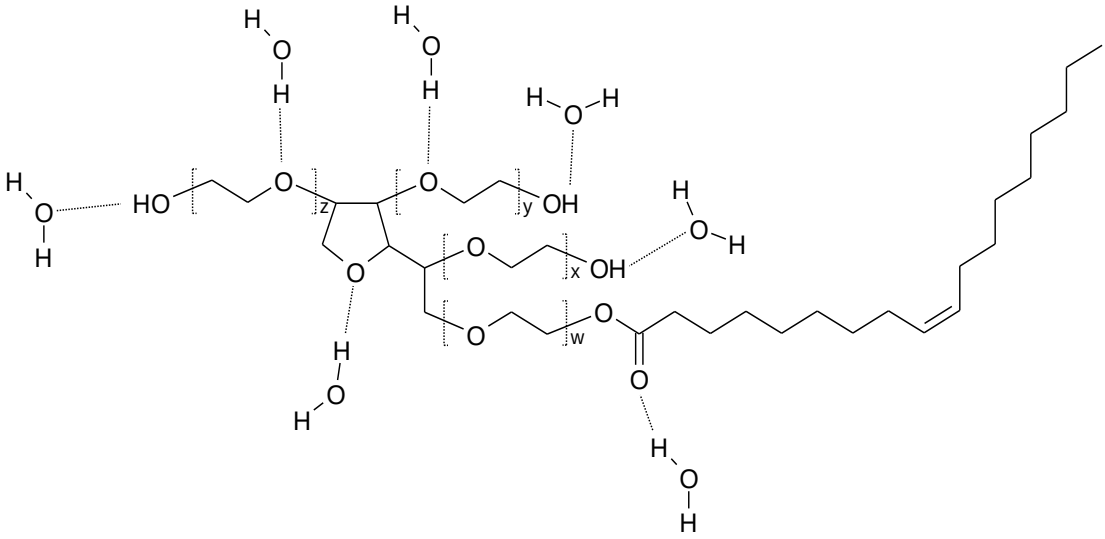

Figure 43: Structure of Polysorbate 80 (Tween 80), showing some of the possible hydrogen bonds that can be formed with water

It was therefore decided to increase the amount of glycine solution added and reduce the saturation of it. This though would make it harder to make the microemulsions, so the overall proportion of surfactant/heptane was increased to 50:50 to accommodate this change. Through solubility tests, it was found that the optimal saturation for the glycine solution was about 14.5 %, which corresponded to 0.30 g glycine in 1.0 g water (3 % by mass glycine – see Table 8). Despite these attempts, every sample showed up as the α-form. For the cases where methanol was added as a layer, the crystals formed were large and needle-like, immediately suggesting that α- glycine had formed.

As a further test, bulk crystallisation experiments were conducted using 0.25 g samples of glycine solution (90 % saturated). Dilute solutions of AOT, Span 80, Tween 80 and Brij 30 in heptane were then added in a layer above the glycine solution. Methanol was then added dropwise, and the samples analysed for any signs of crystallisation. After 0.04 g was added, the system containing Tween 80 had crystals at the glycine/stock solution interface. Crystals did not appear in any other system until 0.10 g of methanol had been added. By the time 0.14 g of methanol had been added, all systems had an appreciable amount of glycine crystals. Each systems' crystals were analysed by FTIR ATR and were found to be α-glycine, except for the AOT system which had crystallised γ-glycine. This showed that it can promote nucleation of this form, as found previously by Davey *et al.*, so the γ-

glycine crystallisation in AOT microemulsions is aided by the AOT and so might not be just due to 3D-nanoconfinement.

The early crystallisation with the Tween 80 surfactant seemed to show why α-glycine was continually crystallised. The Tween 80 surfactant is very good at nucleating the α-form. This suggests that heterogeneous nucleation of the α-glycine polymorph, caused primarily by the Tween surfactant, could have been occurring in the Tween 80-containing microemulsions, rather than homogeneous nucleation, preventing the crystallisation of the thermodynamically favoured γ-glycine polymorph.

3.4.3 Span/Tween temperature-based experiments

Original attempts at obtaining the three polymorphs via a temperature change did not work because obtaining a full microemulsion at higher temperature proved difficult, and upon cooling, no crystals came out of solution. As stated in the experimental methods, vigorous shaking was required to mix the requisite components. To solve the problem of crystallisation, methanol was added in 0.05 g aliquots at hourly intervals, whilst the microemulsion was kept at a constant temperature of 5 °C.

Tests at 45 °C, using water instead of glycine solution, showed that an emulsion formed after 0.15 g of water had been added. If this was substituted for a low saturation glycine solution, not enough crystals would be obtained for analysis. The temperature was therefore dropped to 35° C. The same tests were carried out, and this time up to 0.6 g of water could be added.

Two experiments were carried out. Again, 12.0 g of stock solution was used, with a surfactant : heptane ratio of 75:25 and a 50:50 ratio of Span 80 to Tween 80. Therefore, stock contained 1.5 g Span 80, 1.5 g Tween 80 and 9.0 g heptane (see Table 9):

Experiment No.	Mass of surfactant solution/g	% surfactant	Glycine solution/g	Glycine solution concentration / mass %
29	12.00	25.00	0.60	5.00
30	12.00	25.00	0.60	8.10
Experiment No.	**Micro/nano-emulsion?**	**Methanol addition speed**	**Polymorph obtained**	
29	Microemulsion	None needed	α	
30	Nanoemulsion	Fast	β	

Table 9: The tabulated results of the two temperature studies carried out

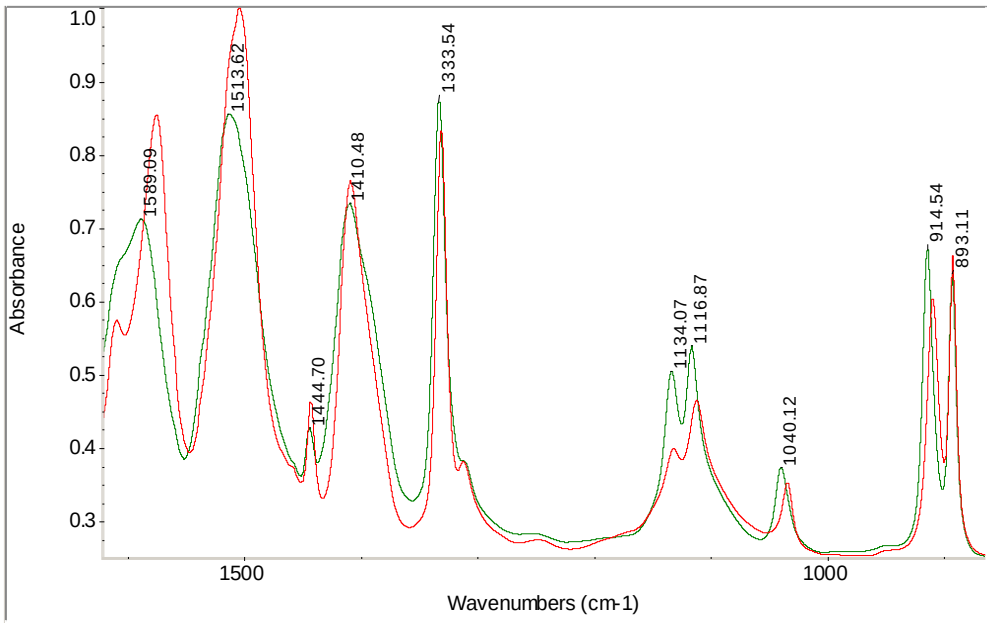

Figure 44: FTIR ATR spectra of experiments 29 and 30, showing the area from 850-1625cm^{-1}. Experiment 28 = red spectrum, experiment 29 = green spectrum.

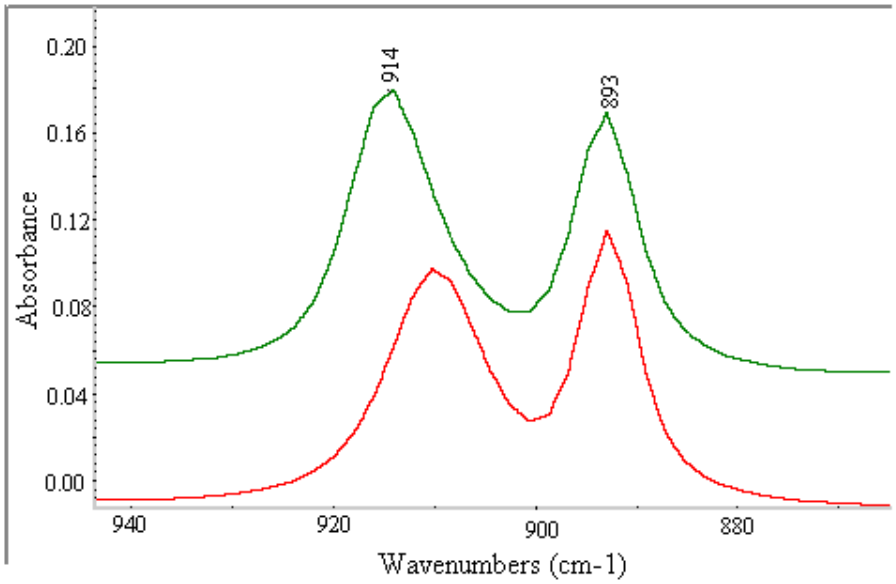

Figure 45: FTIR ATR spectra of systems 29 and 30, showing the area from 850-950cm^{-1}. Experiment 28 = red spectrum, experiment 29 = green spectrum.

What can be noticed in Figures 44 and 45 is that the peaks at 914 and 893 cm^{-1} for β-glycine are almost the same height, compared to other spectra for β-glycine where the peak at 914 cm^{-1} was usually higher. This suggests that α-glycine has been also been formed. Further evidence is seen at the peak at 1589 cm^{-1}. It contains a step in the peak, similar to that found in α-glycine. Despite this, the majority of peaks have been shifted by the correct amounts, meaning that mostly β-glycine has been produced from Experiment 30.

As with previous Span/Tween experiments, obtaining α- and β-glycine was fairly easy. However the experiments were unsuccessful in obtaining γ-glycine. The same reasons can be used here – the fact that the presence of Tween promotes α-glycine formation. The other problem was that despite attempting to perform the experiment in more varied conditions, the actual temperature range was just a few degrees from room temperature, in order to preserve a stable microemulsion state.

3.4.4 Discussion

The aim of obtaining the three polymorphs of glycine – α-, β-, and γ-glycine - was achieved when using AOT as the surfactant. The XRD data show peaks at different 2θ values for each of the polymorphs, though for β-glycine, there were many cases where certain peaks overlapped well with peaks normally found in α- and γ-glycine. This though can be used to show more evidence of β-glycine being the least stable of the three polymorphs. It must be stated though that there was no evidence of samples of β-glycine changing to α-glycine when the samples were left open to the atmosphere for some time, so the presence of any α-glycine in the mainly β-glycine systems could not be attributed to initial β-glycine crystallisation, followed by its transformation to the α-form once it was removed from solution. We cannot rule out a solvent-mediated β- to α-glycine transformation though, as this can occur more quickly.

When methanol was added at a rapid speed to each sample, the same polymorph emerged (β-glycine) regardless of whether a microemulsion or nanoemulsion was used.

There was less success with trying to obtain the three polymorphs in Span/Tween and Span/Brij systems. As already stated, Tween 80 was found to take up a lot of water from the aqueous phase, which increased the saturation of the glycine and destabilised the system somewhat. Indeed, attempts to make a Tween-only microemulsion failed very quickly, lending more proof to the thought that it is unsuitable for these experiments. Consequently, most of the further experiments did not use the Tween surfactant but a Span 80/Brij 30 surfactant mixture, in an attempt to obtain better stability.

3.5 Methanol vapour diffusion experiments

So far, the only method of adding methanol to the microemulsions was to pipette it directly into the microemulsion. In the experiments where Span 80 and Tween 80 were used as surfactants, the rate of addition of methanol could not be reduced enough to induce crystallisation of γ-glycine. It was suggested that instead of using methanol solution, methanol vapour could be used, so that locally high concentrations of methanol could be avoided. In this way, the rate of addition could be reduced yet still maintained at a relatively constant rate. Since thermodynamic control of crystallisation in microemulsions occurs at the point when crystallisation is only just possible, the methanol addition needs to be added slowly and accurately. Hopefully, methanol vapour addition could fulfil these requirements.

3.5.1 Materials and Composition of Microemulsions

Tween 80 and Glycine (99 % purity) were obtained from Sigma-Aldrich. Span 80, Brij 30, Heptane (≥99.9 % purity) and Methanol (LC-CHROMASOLV, ≥99.9 %) were purchased from Fluka.

To make all microemulsions, a combination of surfactants (Span 80 / Tween 80 or Span 80 / Brij 30) was mixed with heptane to form the stock solution. Glycine solution was added to the stock solution, shaken by hand, and then placed on a vortex mixer at 2000 rpm for 5-10 seconds to form the microemulsion. Methanol vapour was then added as an anti-solvent to induce crystallisation.

3.5.2 Methods and Results

Nine experiments were set up, with the stock solution being 16.0 g in each experiment (see Table 10). The mass ratio of surfactant : heptane phase was kept constant (25 : 75). Microemulsions were prepared as before, and placed in a large glass tray filled with methanol. These were then left, allowing the methanol to evaporate, diffuse and enter the microemulsion. Once sufficient crystals were found, they were extracted via centrifuging and analysed by FTIR spectroscopy.

Experiment Name	Surfactants used	Glycine Solution / g	Glycine concentration / % mass
1	Span 80 / Tween 80	0.40	3.00
2	Span 80 / Tween 80	0.40	5.00
3	Span 80 / Brij 30	0.40	5.00
4	Span 80 / Brij 30	0.40	3.00
5	Span 80 / Tween 80	0.40	1.00
6	Span 80 / Tween 80	0.40	2.00
7	Span 80 / Tween 80	0.60	2.00
8	Span 80 / Tween 80	0.60	2.50
9	Span 80 / Tween 80	0.60	3.00

Table 10: Table showing the contents of the nine microemulsions used for the vapour diffusion experiments. Each microemulsion had a surfactant to heptane mass ratio of 1 : 3.

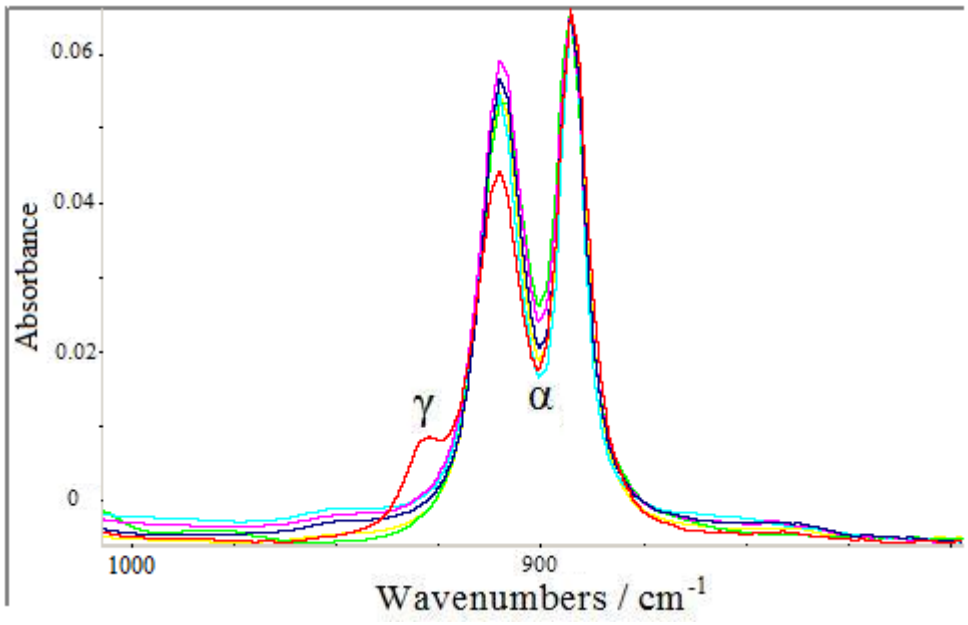

Figure 46: FTIR ATR spectra of the nine methanol vapour diffusion experiments. Not all the experiments are shown, because the mass of crystals extracted in some experiments was too small to analyse.

The spectra obtained (see Figure 46) show that one of the experiments –case experiment 4, gave a small proportion of γ-glycine. This experiment used Span 80 and Brij 30 as the surfactants with 0.40 g of 3 % by mass glycine solution (see Table 10). Measuring the height proportions of the peaks found that about 15 % of the extracted crystals were γ-glycine. It showed that the most stable polymorph could be

grown under confined conditions for a non-ionic surfactant system known not to promote the crystallisation of the stable polymorph in bulk solution.

Variations of Experiment 4 were then set up. The stock solution mass was kept at 16.0 g, while the mass and concentration of the glycine solution added was varied (see Figure 47 and Table 11). The exact conditions used in Experiment 4 are denoted in Table 11 as sample name 4(a):

Sample name	Glycine solution / g	Glycine Solution Conc. / % mass	Microemulsion Formed?	Polymorph (at bottom)	Polymorph (on sides)
4(p)	0.35	2.0	Y	-	-
4(k)	0.40	2.0	Y	-	-
4(n)	0.43	2.5	Y	α	-
4(d)	0.30	3.0	N	-	-
4(h)	0.33	3.0	Y	α, γ	β
4(b)	0.35	3.0	Y	α, γ	-
4(a)	0.40	3.0	Y	α, γ	β
4(c)	0.45	3.0	Y	α, γ	α
4(i)	0.48	3.0	N	-	-
4(e)	0.50	3.0	N	-	-
4(j)	0.40	4.0	Y	α, γ	α, β, γ
4(o)	0.45	4.0	Y	γ, α	-
4(z)	0.30	5.0	N	-	-
4(g)	0.35	5.0	N	-	-
4(f)	0.40	5.0	Y	α, γ	α, γ
4(t)	0.45	5.0	N	-	-
4(m)	0.40	5.5	Y	α	-
4(l)	0.40	6.0	Y	α	-
4(u)	0.47	6.0	N	-	-
4(x)	0.30	7.0	N	-	-
4(y)	0.50	7.0	N	-	-
4(w)	0.35	8.0	N	-	-
4(q)	0.40	8.0	Y	α, γ	-
4(r)	0.45	8.0	Y	α	-
4(v)	0.47	8.0	N	-	-
4(s)	0.40	10.0	Y	α	-

Table 11: Table showing the make-up of the experiments based on Experiment 4 which first gave γ-glycine (see Table 10). Dashes in the last two columns indicate either that there were too few crystals for analysis, or that the microemulsion failed.

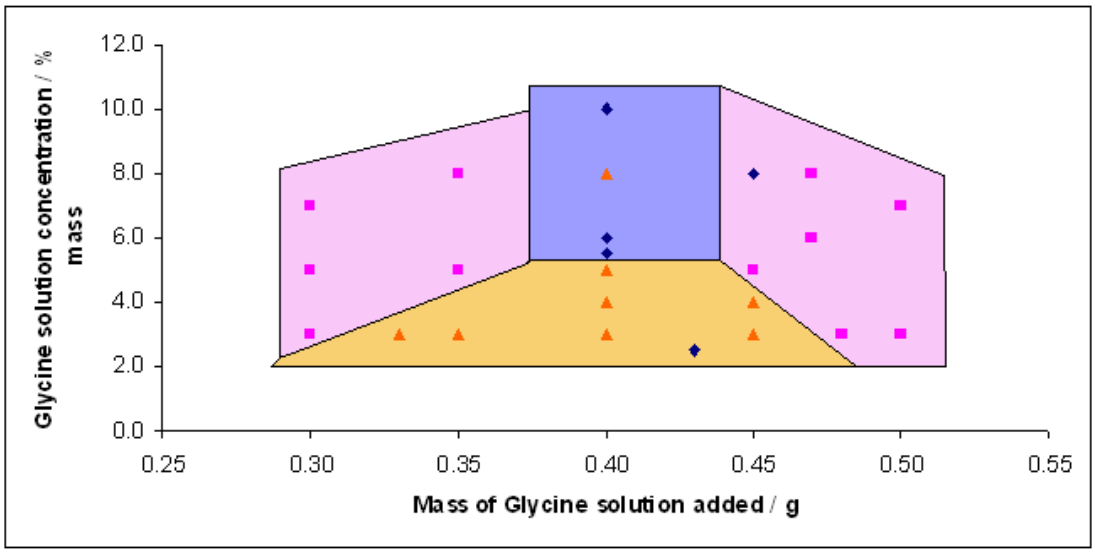

Figure 47: Graph showing the various solutions tested where the mass and concentration of glycine solution was varied for Span 80/Brij 30 experiments. Pink squares indicate that a microemulsion was not formed. Blue diamonds indicate that a microemulsion was formed and the crystals which were subsequently extracted were found to be α-glycine. Orange triangles indicate experiments where a microemulsion was formed and γ-glycine was found in the subsequent crystals. General areas in the graph have been highlighted in the same colour. For table of results, see Table 11.

Figure 47 shows that the margin for error in obtaining microemulsions is relatively small. For consistent microemulsion formation, the mass of glycine solution needs to be between 0.35 g and 0.45 g. In addition, obtaining a significant amount of γ-glycine requires that the concentration of the glycine solution is generally no more than 5 % by mass of glycine.

Note that experiments where a microemulsion was not formed (when the solution phase separated or an emulsion was formed) were immediately discarded, since confinement of the aqueous phase was not achieved.

Though γ-glycine had been obtained, it was noted that glycine crystals were often appearing along the side of the reaction vessel. The crystals may have been formed through evaporation, due to the microemulsions themselves losing material. To counter this, the entire reaction area was covered by a glass tray (see Figure 48). Evaporation was greatly reduced, and the microemulsions did not lose any significant volume.

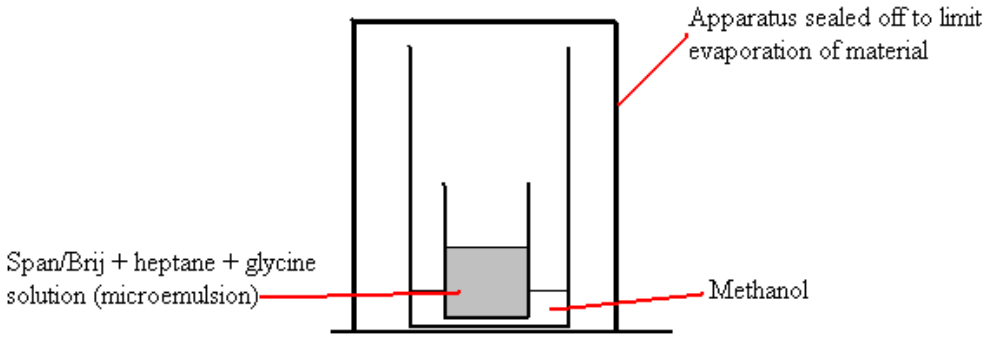

Figure 48: Diagram showing the setup of the apparatus for the methanol diffusion experiments.

3.5.3 Discussion of initial vapour diffusion experiments

The initial variations of a partially-successful experiment gave rise to some important observations. Though microemulsions could be made easily, the confinement required to produce γ-glycine was tricky to pin down. Many of the experiments were found to have crystals growing on the side of the vials due to evaporation of the microemulsion. This meant that those crystals were probably growing via a heterogeneous nucleation mechanism (crystallisation upon a substrate), most likely in pits and/or defects in the glass surface. In addition to this not being valid for this investigation, the rate of crystallisation has changed.

The equation for heterogeneous nucleation rate is similar to that for homogeneous nucleation:

$$J_{het} = \Omega_{het} \exp\left[-\frac{\Delta G^*_{het}}{k_B T} \right] \qquad (15)$$

The main difference is that the values for both ΔG_{het}^{*} and for Ω_{het} are smaller – typical values for the latter are in the range of $10^{17} – 10^{22}$ cm^{-2} s^{-1}. The shape of the graph produced is the same, but the Ostwald metastable limit occurs at much lower supersaturations due to the lower value for ΔG_{het}^{*}. As a result, the crystallisation is much faster.

The extent of evaporation of the microemulsion was tested by repeating experiments 4(f) and 4(j). After 40 hours, crystals were found in abundance, but roughly 8-10 % of the volume of the microemulsions was lost. The extracted crystals were analysed and most were of the γ-form. It was unsure whether these crystals were formed at the air/liquid or vial/liquid interfaces, or whether they had been formed by homogeneous nucleation, but from this point on, the microemulsions were regularly checked to ensure that evaporation was kept to an absolute minimum.

The surfactant mixture of Span 80 and Tween 80 had not produced any sign of γ-glycine in any of the experiments that had been carried out, and so this mixture was discontinued permanently. Previously, it had been found that both surfactants take up a large amount of water from the glycine solution, increasing its supersaturation and therefore making crystallisation faster when the anti-solvent is added. Tween 80 was therefore swapped with Brij 30. Brij 30 contains less heteroatoms, therefore less hydrogen bonding takes place, and more water molecules stay as part of the water droplets in the microemulsion. More importantly, as detailed earlier, Tween 80 is a powerful α-glycine nucleator, making heterogeneous nucleation of this form in the microemulsions more likely. This prevents the homogeneous nucleation of the thermodynamic product γ-glycine. Both Span 80 and Brij 30 are less potent α-glycine nucleators though. It is interesting to note that with respect to geometric considerations, Brij 30 readily forms oil-in-water microemulsions, whilst Span 80 is more suited to forming water-in-oil microemulsions. In practice however, utilising Span 80 as the only surfactant will not form microemulsions, and will instead only form an emulsion. It is therefore necessary to utilise Brij 30 as the second surfactant, in order to fit more surfactant molecules around the water droplets, and therefore achieve better stability.

3.5.4 Repeated vapour diffusion experiments - results

From the set of variations shown in Table 11, three experiments stood out – 4(j), 4(o) and 4(f) - due to two reasons. Firstly, a high proportion of γ-glycine crystallised from each of the microemulsions. Secondly, because of the concentrations of the glycine solutions, these would hopefully give the most amount of glycine out of a single experiment. Repeats were then taken of each of these three variations.

IMPORTANT NOTE

From now on, referrals to the glycine solutions (j), (f) and (o) will be made. This is to indicate what glycine solution was used in which specific amount:

(j) = 0.40 g glycine solution (4 % by mass)

(o) = 0.45 g glycine solution (4 % by mass)

(f) = 0.40 g glycine solution (5 % by mass)

Experiment Name	Description of Experiment	T = 25 degrees C?	Polymorph	Polymorph (on sides)
4(o).1	Undetermined time under methanol	-	γ, α	β
4(o).2	Undetermined time under methanol	-	α, γ	β
4(o).3	Undetermined time under methanol	-	γ, α	α
4(o).4	Undetermined time under methanol	-	γ, α	γ, α
4(o).5	Undetermined time under methanol	-	γ	γ
4(o).6	Undetermined time under methanol	-	α, γ	n/a
4(o).13	24 hours under methanol	Y	α	n/a
4(o).14	90 hours under methanol	Y	α, γ	n/a

Table 12 a): Descriptions of experiments carried out using glycine solution (o) (0.45g, 4.0% by mass of glycine).

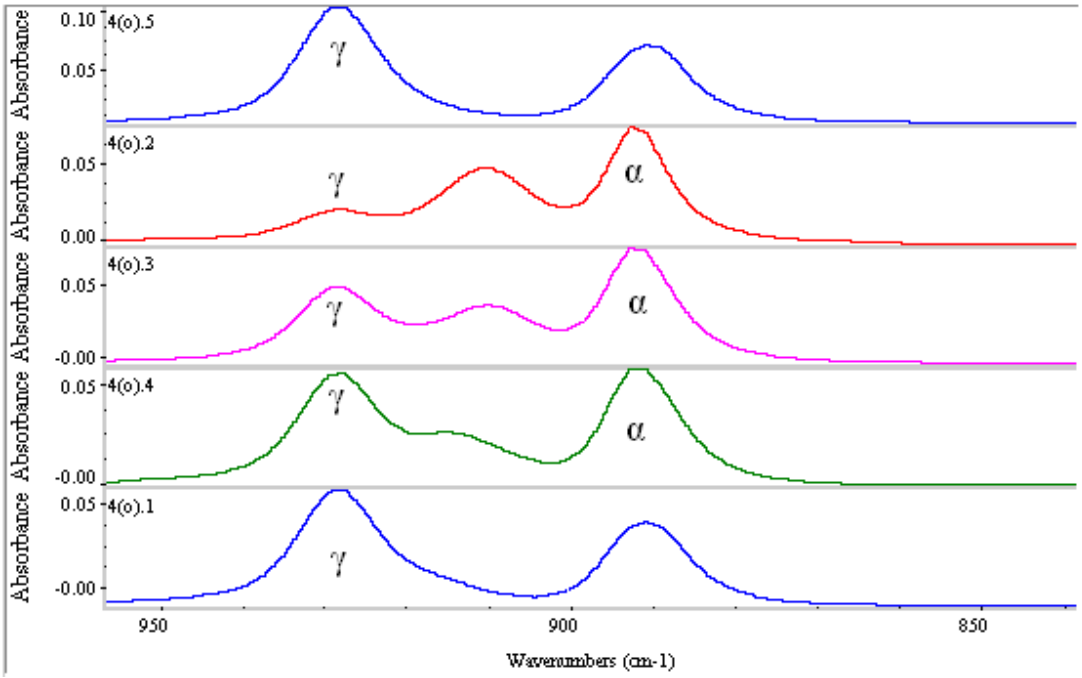

Figure 49: FTIR ATR spectra of five repeats of experiment 4(o). The crystals were taken from the bottom of the vial, and were therefore formed via homogeneous nucleation.

The first repeats of experiment 4(o) (details shown in Table 12 a)) were promising, with γ-glycine obtained in most of the samples (see Figure 49). However, evaporation continued to be a problem, with many crystals appearing at the liquid/vial interface, which gave a mixture of all three polymorphs (see Figure 50):

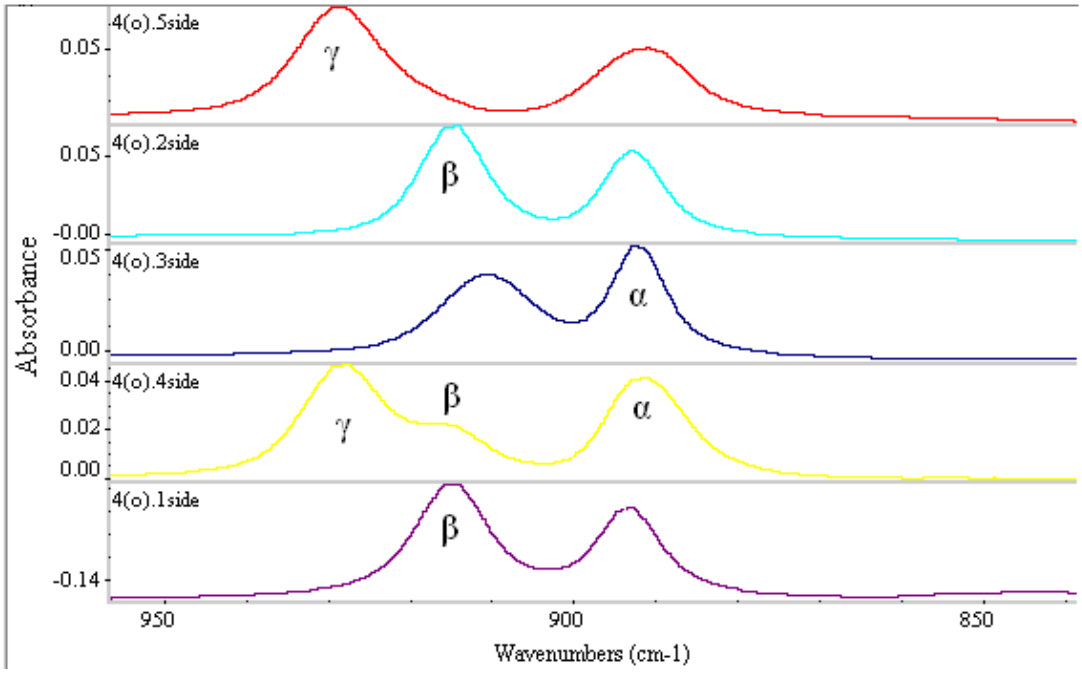

Figure 50: FTIR ATR spectra of the same five repeated experiments, but with the crystals taken from the sides of the vial.

From the spectra in Figures 49 and 50, all three polymorphs can be identified in varying proportions. The problem was that the experiments up till now had been under methanol vapour for up to 90 hours and even longer periods. Not only did this inevitably result in some evaporation, it also meant that the methanol concentration in the microemulsions continued to increase, well past the point at which crystallisation was first favourable. Thermodynamic control of crystallisation will only operate close to conditions where crystallisation can only just occur, because if the crystallisation rate is too fast, kinetic control dominates.

To limit both problems, the time spent under the methanol vapour would have to decrease dramatically. A maximum time for the microemulsions to be exposed to methanol vapour was set at 72 hours. Other durations used were 48, 24, 7 and 4 hours. In addition, experiments would be carried out at a standard temperature of 298 K to limit variations in the methanol vapour diffusion rate. The experiment details are shown in Table 12 b), and the spectra in Figure 51:

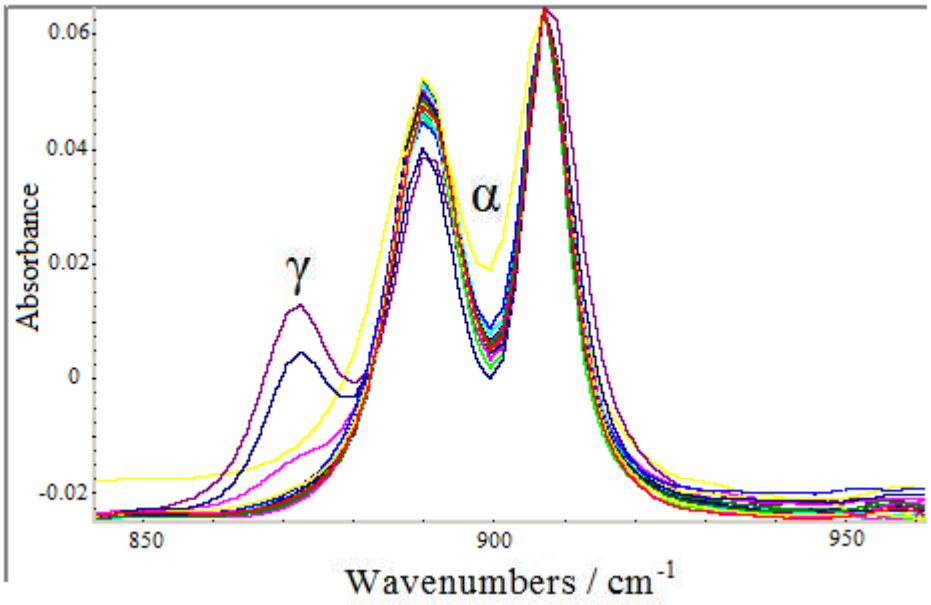

Figure 51: FTIR ATR spectra of experiments 4(o).15-33.

Experiment Name	Hours under methanol	T = 298K?	Methanol used / cm^3	Polymorph
4(o).15	48	Y		α, γ
4(o).16	24	Y	30.0 → 17.1	α
4(o).17	24	Y	30.0 → 17.1	α
4(o).18	24	Y	30.0 → 17.1	α
4(o).19	24	Y	30.0 → 17.1	α
4(o).20	24	Y	30.0 → 17.1	α, γ
4(o).21	24	Y	30.0 → 17.1	α
4(o).22	72	Y		α
4(o).23	72	Y		α
4(o).24	72	Y		α
4(o).25	72	Y		α
4(o).26	72	Y		α
4(o).27	72	Y		α
4(o).28	48	Y		α
4(o).29	48	Y		α, γ
4(o).30	48	Y		α
4(o).31	48	Y		α
4(o).32	48	Y		α, γ
4(o).33	48	Y		α, γ

Table 12 b): Further experiments carried out using glycine solution (o) (0.45g, 4.0% by mass of glycine).

Despite the standardisation of the conditions, the end results are still inconsistent. The three spectra which show traces of γ-glycine (experiments 4(o).29,32,33 – see Table 12 (b)) all came when the microemulsions were exposed to methanol vapour for 48 hours. However the same amount of experiments also gave α-glycine only. A similar trend is found when glycine solution (j) is used – there are some experiments where traces of γ-glycine are found, but they are in a minority when compared to the number of experiments which fully crystallised α-glycine (see Table 13 and Figure 52):

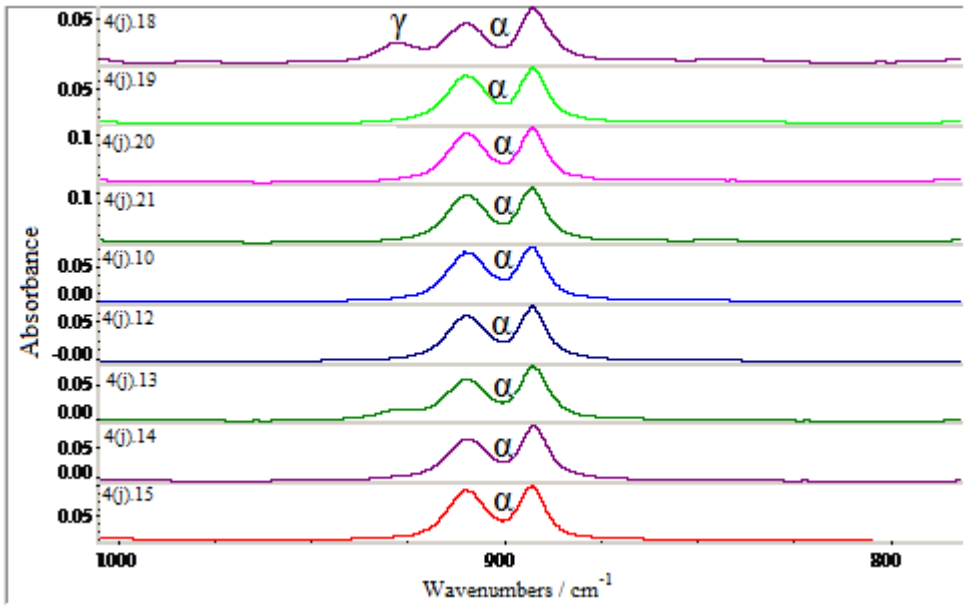

Figure 52: FTIR ATR spectra of experiments 4(j).10-21.

Experiment Name	Description of Experiment	Polymorph
4(j).1	24 hours under methanol	α
4(j).2	24 hours under methanol	α
4(j).3	48 hours under methanol	α
4(j).4	48 hours under methanol	α, γ
4(j).5	48 hours under methanol	α
4(j).6	48 hours under methanol	γ
4(j).7	48 hours under methanol	α
4(j).8	48 hours under methanol	α
4(j).9	48 hours under methanol	α
4(j).10	7 hours under methanol	NA
4(j).11	7 hours under methanol	α
4(j).12	7 hours under methanol	α, γ
4(j).13	7 hours under methanol	α, γ
4(j).14	7 hours under methanol	α, γ
4(j).15	7 hours under methanol	α
4(j).16	72 hours under methanol	α, γ
4(j).17	72 hours under methanol	α, γ
4(j).18	72 hours under methanol	α, γ
4(j).19	72 hours under methanol	α
4(j).20	72 hours under methanol	α
4(j).21	72 hours under methanol	α
4(j).22	48 hours under methanol	NA
4(j).23	48 hours under methanol	NA
4(j).24	48 hours under methanol	NA
4(j).25	48 hours under methanol	NA
4(j).26	48 hours under methanol	NA
4(j).27	48 hours under methanol	NA
4(j).28	4 hours under methanol	NA
4(j).29	4 hours under methanol	α
4(j).30	4 hours under methanol	α
4(j).31	4 hours under methanol	α, γ

Table 13: Details of the methanol vapour diffusion experiments where glycine solution (j) was used (0.4 g, 4.0 % by mass glycine). NA = No Analysis.

3.5.5 Discussion of vapour diffusion experiments

Possible reasons for the failure of many vapour diffusion experiments include:

1) The amount of methanol present: In earlier experiments, the amount of methanol put in the outer vessel was not accurately measured. Subsequent tests found that if a large amount of methanol was placed in the outer vessel, a high proportion of it would evaporate and therefore come into contact with the experiment vessels containing the microemulsion. Experiments 4(j).44-49 were carried out in conditions where 50 cm^3 of methanol was put in the outer vessel. After just 5 hours, the volume of methanol left was roughly 38 cm^3. Even allowing for methanol vapour which does not interact with the samples, nearly 2 cm^3 of methanol entered each sample over a period of 17 hours. This was a faster rate than what was needed to ensure crystallisation was only just favourable and therefore could occur under thermodynamic control.
2) The amount of glycine solution added to the microemulsions: The variations of experiment 4(a) did give γ-glycine, but it is possible that these were isolated cases, and that the overall inconsistency of the results may be due to the supersaturation of the glycine solution being too high.

To test point 2), a long-running set of solubility tests were set up to investigate how much glycine powder was needed to saturate the microemulsions. Stock solutions of volume 16.0 cm^3 were made up at room temperature as before. 0.40 g of water was then added to form a stable microemulsion. Then glycine powder was added of various masses to each microemulsion. The microemulsions were then left to stand and when all the glycine powder had dissolved, the time taken was noted (see Table 14).

Glycine powder added / mg	Time taken to fully dissolve
5	2 days
10	2 days
12	9 days
15	30 days
17	31 days
18	-
19	-
20	-

Table 14: The results of the long-running solubility tests

The table partially shows why some experiments gave crystallisation very quickly. In the case of glycine solution (j), 16 mg of glycine is contained in 0.4 g of water. For glycine solution (o), 18mg of glycine is present and for glycine solution (f), 20 mg of glycine is in the aliquot added to the microemulsion. The solubility tests show that under normal conditions, it is unlikely that more than 18 mg of glycine will dissolve within a suitable time period. This may explain partially why so many experiments involving glycine solutions (f) and (o) gave α-glycine only.

A fourth problem was that extracting the crystals from the vials proved difficult at times. In some of the experiments, only a single crystal was extractable for analysis. This could lead to misleading results, because the polymorph could not be determined on the analysis of one crystal only (given that in a theoretical example, if two crystals are extracted, one could be purely α-glycine and one could be γ-glycine – if one was picked for analysis, the other polymorph wouldn't be detected). Hence if some crystals couldn't be extracted, this could provide a false indicator of the majority polymorph obtained.

3.5.6 Vapour diffusion experiments with monitoring of methanol amounts

No monitoring of the methanol masses, combined with the inconsistent results, meant it was likely that an excess of methanol was used. It was decided firstly to reduce the amount of methanol in the outer vessel to 12.5 cm^3. Secondly, the experiments denoted with letters (o) and (f) (experiments using 0.45 g glycine solution (4 % by mass) and 0.40 g glycine solution (5 % by mass)), were discontinued, and the glycine solution (a) (0.40 g glycine solution (3 % by mass)) was brought back to use in further studies. This was to totally ensure that the microemulsions formed would be fully stable, and that the number of glycine molecules encased in the microemulsion droplets would be minimised to help ensure thermodynamic control.

For the new set of experiments (4(a).1 onwards – see Tables 15 a) and b)), the amount of methanol put into the outer vessel was noted, as was the approximate amount of methanol left afterwards.

Experiment Name	Hours under methanol	Time Length of experiment	Polymorph	Volume of methanol used / cm^3
4(a).1	72	13 days	α	12.5 → 0
4(a).2	72	13 days	α	12.5 → 0
4(a).3	72	13 days	γ, α	12.5 → 0
4(a).4	72	13 days	α	12.5 → 0
4(a).5	72	13 days	α, γ	12.5 → 0
4(a).6	72	13 days	α, γ	12.5 → 0
4(a).7	24	10 days	α, γ	12.5 → 0
4(a).8	24	10 days	α	12.5 → 0
4(a).9	24	10 days	α, γ	12.5 → 0
4(a).10	48	10 days	α	12.5 → 0
4(a).11	48	10 days	α, γ	12.5 → 0
4(a).12	48	10 days	α	12.5 → 0
4(a).13	7	7 days	α, γ	20.0 → 15.0
4(a).14	7	7 days	α, γ	20.0 → 15.0
4(a).15	7	7 days	α, γ	20.0 → 15.0
4(a).16	7	7 days	α, γ	20.0 → 15.0
4(a).17	7	7 days	α, γ	20.0 → 15.0
4(a).18	7	7 days	α	20.0 → 15.0
4(a).19	4	8 days	α	12.5 → 8.0
4(a).20	4	8 days	α	12.5 → 8.0
4(a).21	4	8 days	α	12.5 → 8.0
4(a).22	5	8 days	α	12.5 → 8.0
4(a).23	5	8 days	α	12.5 → 8.0
4(a).24	5	8 days	α	12.5 → 8.0

Table 15 a): Descriptions of vapour diffusion experiments involving glycine solution (a) (0.40g, 3% by mass glycine).

Experiment Name	Hours under methanol	Time Length of experiment	Polymorph	Volume of methanol used / cm^3
4(a).37	7	3 weeks	NA	12.5 → 8.5
4(a).38	7	3 weeks	NA	12.5 → 8.5
4(a).39	7	3 weeks	NA	12.5 → 8.5
4(a).40	7	3 weeks	NA	12.5 → 8.5
4(a).41	7	3 weeks	NA	12.5 → 8.5
4(a).42	7	3 weeks	NA	12.5 → 8.5
4(a).25	3	6 weeks	NA	12.5 → 9.5
4(a).26	3	6 weeks	NA	12.5 → 9.5
4(a).27	3	6 weeks	NA	12.5 → 9.5
4(a).28	3	6 weeks	NA	12.5 → 9.5
4(a).29	3	6 weeks	NA	12.5 → 9.5
4(a).30	3	6 weeks	NA	12.5 → 9.5
4(a).31	2	6 weeks	NA	12.5 → 10.0
4(a).32	2	6 weeks	NA	12.5 → 10.0
4(a).33	2	6 weeks	NA	12.5 → 10.0
4(a).34	2	6 weeks	NA	12.5 → 10.0
4(a).35	2	6 weeks	NA	12.5 → 10.0
4(a).36	2	6 weeks	NA	12.5 → 10.0
4(a).19R	4	3 weeks	α	12.5 → 8.0
4(a).20R	4	3 weeks	α	12.5 → 8.0
4(a).21R	4	3 weeks	α	12.5 → 8.0
4(a).22R	5	3 weeks	α	12.5 → 8.0
4(a).23R	5	3 weeks	α	12.5 → 8.0
4(a).24R	5	3 weeks	α	12.5 → 8.0

Table 15 b): Further vapour diffusion experiments using glycine solution (a) (0.40g, 3% by mass glycine). The last 6 experiments are repeats of experiments 4(a).19 – 24. NA = Not Analysed – usually due to lack of crystals required for analyses.

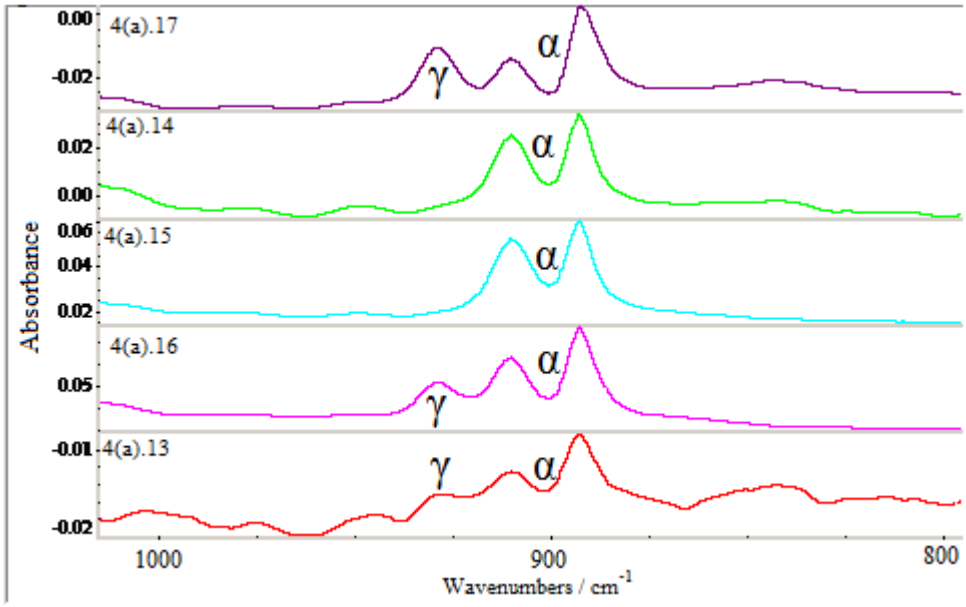

Figure 53: FTIR ATR spectra of the experiments 4(a).13-19.

Compared to previous experiments, and with respect to whether γ-glycine is obtained in any amount, the experiments are far more consistent in their outcomes. Figure 53 shows that three of the five experiments show a significant proportion of γ-glycine in the crystallised product.

The reduction in methanol showed that larger amounts would, over time, lead to more methanol vapour entering the microemulsions. This had the effect of increasing the rate of crystallisation, thereby producing the metastable forms of glycine. Reducing the amount of methanol and the time in which the microemulsions are exposed to methanol has worked with γ-glycine now often being crystallised, but the rate is at times still too fast, and inconsistencies still appear in certain sets of experiments. With this in mind, future experiments should look at ways to limit the rate of methanol addition. A simple idea would be to close off part of the vial holding the microemulsion. Other experiments should look into the diffusion processes and rates of the methanol vapour in the overall experimental system. The later experiments could only give a rough estimate as to how much methanol entered the microemulsion, and there was no way of checking whether the rate of diffusion was constant throughout, or whether the top surface of the microemulsion always had an increased methanol concentration.

3.6 Temperature studies

Experiments involving microemulsions containing a Span 80/Tween 80 mixture of surfactants failed to produce γ-glycine due a large uptake of water by the surfactants, and the α-glycine nucleating power of the Tween 80 surfactant, pushing the system towards crystallisation of this polymorph. The Span 80/Brij 30 system is better, but the predominance of α-glycine in almost all the samples shows that the supersaturation still increases too much in many systems, thereby also causing a predominance of the α-glycine phase under kinetic, rather than thermodynamic control.

It was also found that temperature changes as small as 5 °C from room temperature (22 °C /295 K) could cause phase separation when the microemulsion was being made. Therefore, the theory was put forward that a temperature change after formation would destabilise the system and cause crystallisation. In thermodynamic terms, as the temperature decreases, the value of the entity $\exp(-\Delta F/kT)$ increases. If the increase of the entity is slow enough, there will be a period of time where $\Delta F_{min,A}^{*} \leq kT < \Delta F_{min,B}^{*}$, and the most stable polymorph could be formed preferentially (see Figure 54):

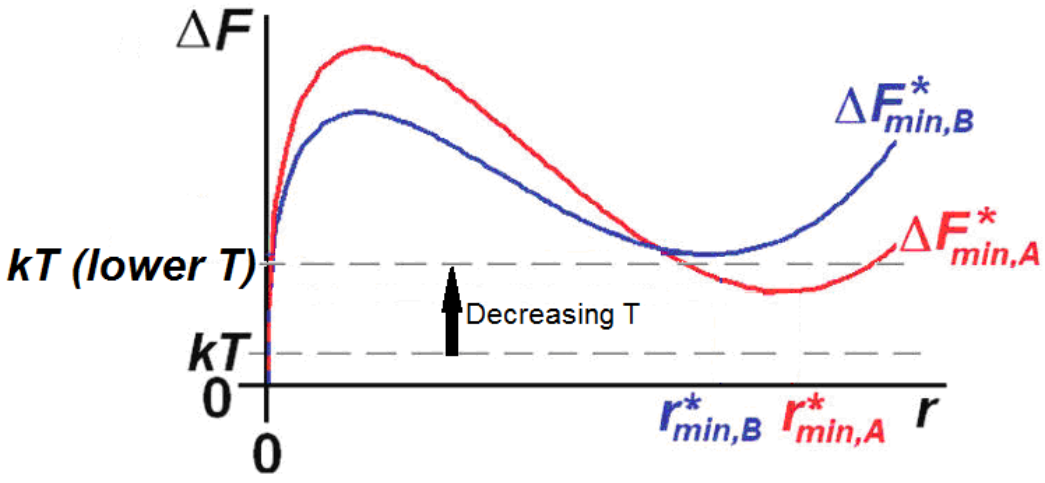

Figure 54: Graph showing theoretical thermodynamic changes and results when the temperature of the system is decreased.

3.6.1 Preliminary tests

As a preliminary test, to determine whether temperature could be used effectively to elicit thermodynamic control of crystallisation in the microemulsions, one microemulsion of each composition 4(f), 4(j), and 4(o) was made up at room temperature (295 K). The microemulsions were then put in a fridge without addition of methanol. The fridge was found to cool the samples from 25.0 - 5.0 °C in 10 minutes. After two hours, some crystallisation was found in sample 4(f). After 72 hours, all samples showed some crystallisation. The samples were left in the fridge for 3 weeks in order to obtain enough crystals to analyse by IR spectroscopy. Analysis showed that all the crystals were α-glycine.

Further tests were also carried out to see whether the timescale of the experiments could be reduced and still produce results. Again, a microemulsion of each composition was made up at room temperature (295 K). 0.10 g methanol was added to each microemulsion, and mixed by hand. The microemulsions were then placed in the fridge again and checked periodically. Crystallisation occurred after 17 hours, and again the samples were left at fridge temperature (278 K, 5 °C) for a number of weeks to allow for full crystallisation. The samples were analysed by IR spectroscopy and each sample was found to be of the form α-glycine.

The fridge tests showed that crystallisation from microemulsions could be induced by temperature changes. Though the fridge could give adequate cooling for the above experiments, there was no way of controlling the rate of temperature decrease or reducing the temperature any further. The cooling apparatus was therefore changed to a Lauda RE306 water bath filled with ethylene glycol (Melting point = -13 °C (260 K)). This was connected to a computer using Wintherm_Plus software, which could program a temperature profile for the water bath to follow.

3.6.2 Methods and Results

For a second preliminary test, repeats of each of the three microemulsions, with no added methanol, were placed in a water bath at an initial temperature of 20 °C. The temperature was lowered until the microemulsions destabilised. At -14 °C, all the microemulsions showed total phase separation and at -20 °C, the microemulsions

solidified. No glycine crystals were found, suggesting that the addition of a small amount of methanol would be required for all further experiments.

To ensure that methanol would not be responsible for crystallisation in these experiments, four test microemulsions of the same proportions (i.e. surfactants, heptane and glycine solutions (j) and (o) – two of each glycine solution) were made up.

Microemulsions containing glycine solutions (f) and (j) were immersed in a water bath at room temperature and left for an hour to ensure the correct starting temperature. The temperature was then decreased at a rate of 1.0 °C per hour and the temperature at which crystals formed was noted. When the temperature had reached 1.0 °C, it was kept constant until sufficient crystals were found in the sample. Table 16 and Figure 55 document the results:

Experiment Name	**Temperature decrease rate**	**Temperature Range / °C**	**Polymorph**
TS(j).1	1 °C/hour	25 → 1	α
TS(j).2	1 °C/hour	25 → 1	α
TS(j).3	1 °C/hour	25 → 1	α
TS(f).1	1 °C/hour	25 → 1	α
TS(f).2	1 °C/hour	25 → 1	α
TS(f).3	1 °C/hour	25 → 1	α

Table 16: Description of experiments where temperature variations were carried out without addition of methanol.

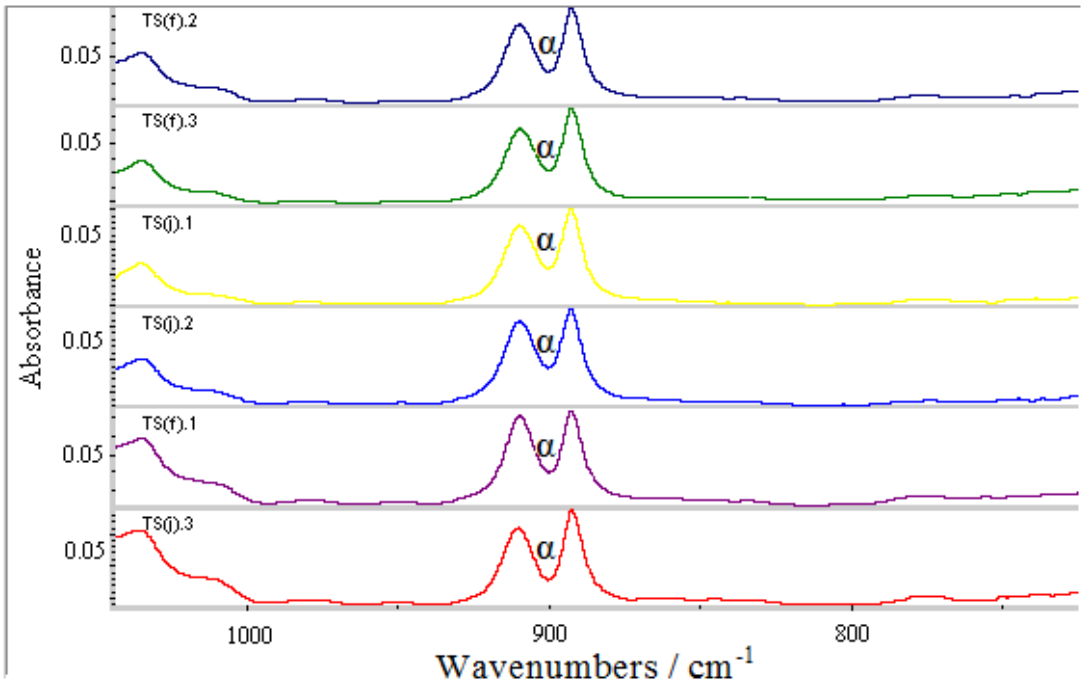

Figure 55: FTIR ATR spectra of experiments TS(j).1-3 and TS(f).1-3. None of the spectra show the characteristic γ-glycine peak at 928 cm^{-1}, and all the spectra have the same shape, proving that all the crystals are of the α-form.

Isolated crystals were first seen in the microemulsions at a temperature of 7.0 °C. No additional crystals were found when the temperature was decreased further. At 1.0 °C, the temperature was kept constant and the microemulsions left in the bath indefinitely. Further crystals were found after 48 hours. Sufficient crystals appeared in samples containing glycine solutions (f) and (j) only. Analysis by FTIR spectroscopy found that all crystal samples were of the α-glycine form (see Figure 54).

In an effort to decrease the timescale of the experiments, Span 80/Brij 30 microemulsions were made by the methods defined in Chapter 2. Before going into the water bath, 0.15g of methanol was added. Stability studies showed that this would not be enough on its own to cause crystallisation. The experiments were then placed in the water bath and cooled to 1.0 °C as before at the same rate of cooling.

The results were very similar to those shown in Figure 54, with crystallisation first occurring at a temperature of 7 °C, and many crystals appearing after the temperature was held at 1 °C for 48 hours. Some phase separation was seen in the experiment TS(o).12. The results obtained are shown in Figure 56 and Table 17:

Experiment Name	Temperature decrease rate	Temperature Range / °C	Polymorph	Methanol used? / g
TS(o).12	1 °C/hour	25 → 1	α	0.15
TS(j).10	1 °C/hour	25 → 1	α	0.15
TS(j).11	1 °C/hour	25 → 1	α	0.15
TS(j).12	1 °C/hour	25 → 1	α	0.15

Table 17: Description of experiments where temperature variations were carried out with the addition of 0.15g methanol.

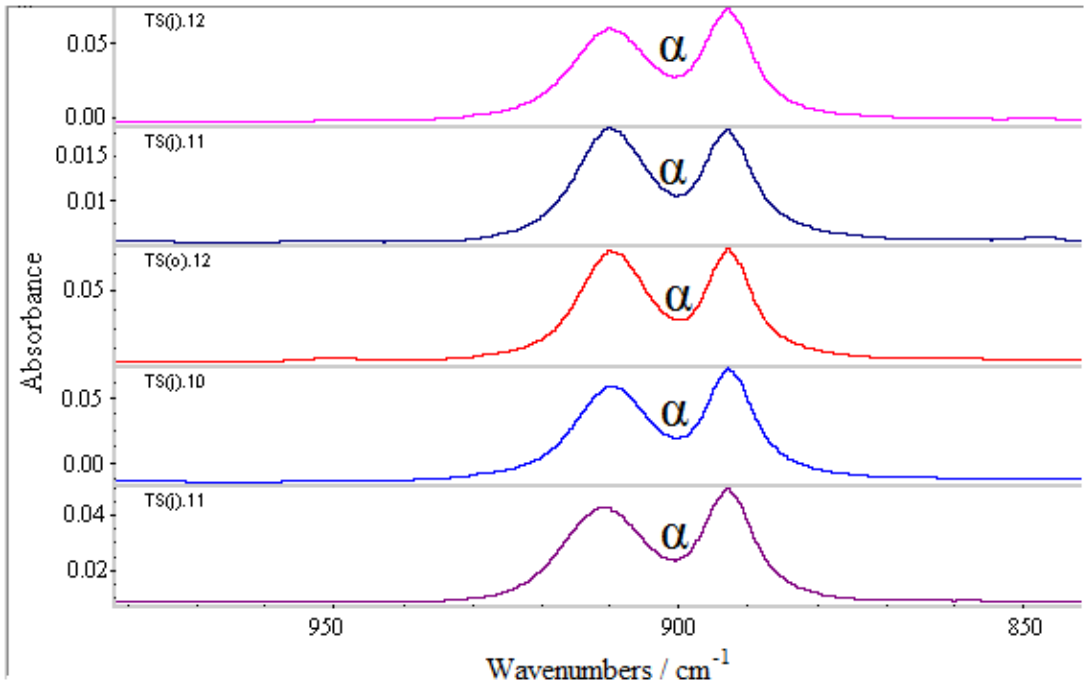

Figure 56: FTIR ATR spectra showing the results of the experiments TS(j).10-12 (with TS(j).11 being repeated)) and TS(o).12. All graphs show the same characteristics as previous temperature-varied experiments. In all cases, α-glycine has crystallised, since no peak at 928 cm^{-1} is observed.

For the next set of experiments, 0.10 g of methanol was added to each microemulsion and the temperature cooling was done at a rate of 0.5 °C per hour, in an attempt to slow the rate of cooling and possibly obtain crystallisation at a higher temperature. In the event, crystals were again not seen until the temperature reached 1.0 °C, and had been at that temperature for some time. FTIR spectra were taken, and each of the experiments was found to have formed α-glycine (see Table 18 and Figure 57):

Experiment Name	Temperature decrease rate	Temperature Range / °C	Polymorph	Methanol used? / g
TS(j).13	0.5 °C/hour	25 → 1	α	0.1
TS(j).14	0.5 °C/hour	25 → 1	α	0.1
TS(j).15	0.5 °C/hour	25 → 1	α	0.1

Table 18: Description of experiments where temperature variations were carried out with the addition of 0.15g methanol.

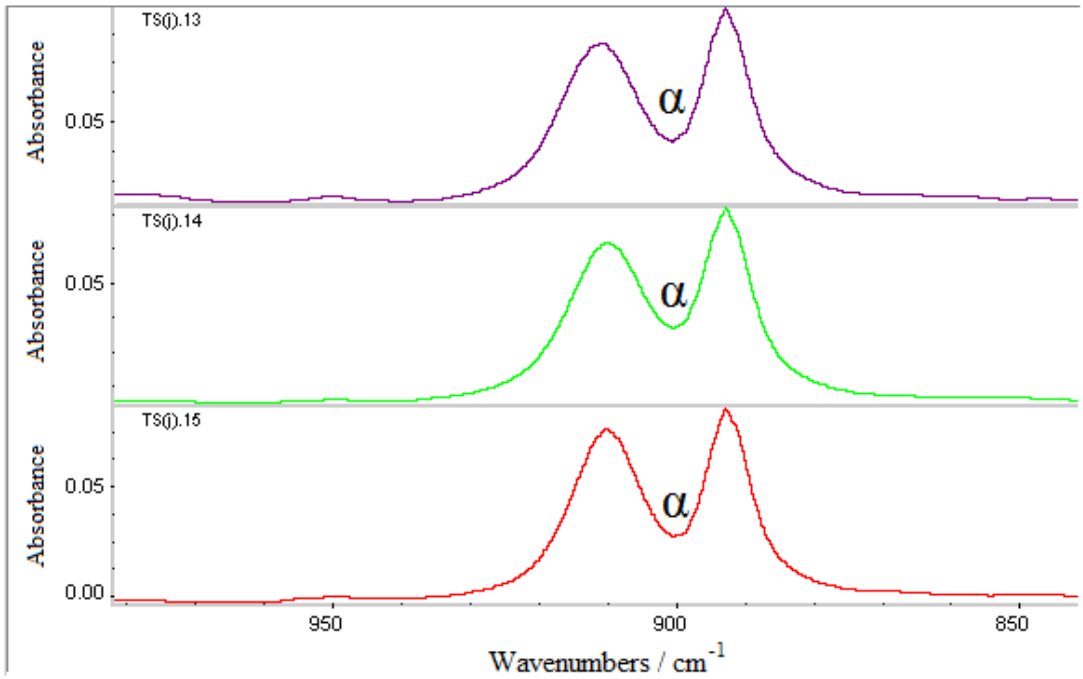

Figure 57: FTIR ATR spectra of experiments TS(j).13-15. As before, no peak at 928 cm^{-1} exists. This would denote the presence of γ-glycine. Therefore, all the crystals extracted are α-glycine.

3.6.3 Discussion

The temperature studies were able to crystallise glycine, but only α-glycine was able to form. It is possible that when during a large temperature change, the microemulsions may have phase separated, though to a very small degree. A very small degree of phase separation might not be easily observable, but even so, this would be enough to destroy the confinement that the microemulsions previously offered. Phase separation can be checked by shaking the vials and looking for any cloudiness due to emulsion droplet formation.

Work by Chen *et al.* has found that all components of the microemulsion are integral to the crystallisation process – changing one component can affect both

microemulsion stability and crystallisation time. The results found that at 5 °C, using de-ionised water speeds up the crystallisation process, and that an increase in surfactant (weight fraction of surfactant from 8 – 15 %) greatly reduced the stability of the microemulsions. In the experiments carried out for this investigation, the surfactant proportion was 25 %. There is certainly scope for reducing the proportion of surfactant to organic phase, which may reduce the possibility for phase separation.

Even without any phase separation it is possible that the temperature changes were not slow enough to pass through conditions under which crystallisation was only just favourable - hence the γ-glycine polymorph was not formed. The rate of cooling could be reduced to 0.1 °C / hour, meaning that the cooling process would take 10 days. This is still faster than the bulk of the methanol vapour diffusion experiments (see Tables 15 a) and b) – where the experiment runtimes were of the order of a few weeks), and could promote the growth of γ-glycine to a higher degree.

3.7 Conclusions

Three different micro-/nanoemulsion systems were employed to test whether by changing conditions, the three polymorphs of glycine could be made under mild conditions. Each product was analysed by infra-red spectroscopy, and where possible, by powder X-ray diffraction.

With a system containing AOT/heptane/glycine solution, all three glycine polymorphs were made upon addition of drops of methanol anti-solvent under ambient conditions, with additional proof provided by optical microscopy. When the ratio of surfactant : oil phase was 1:3 and the methanol addition rate was 0.1 g per minute, γ-glycine was formed as the single polymorph. Smaller ratios meant that α-glycine was formed, and when the rate of methanol addition was increased to 1.0 g per second, β-glycine was formed. This showed that the degree of confinement is a major determining factor in obtaining the desired polymorph, and that a stable microemulsion is needed if the most thermodynamically stable polymorph is to be formed.

In a Span 80/Tween 80/heptane system, α- and β-glycine were both formed made upon addition of drops of methanol anti-solvent under ambient conditions, yet γ-glycine could not be crystallised. It was suggested that water molecules form hydrogen bonds with the Span and Tween molecules, effectively increasing the concentration of the glycine solution contained in the droplets. Further experiments where the concentration of glycine was reduced to 3.0 % by mass continued to crystallise α-glycine. It was suggested that methanol, used to crystallise the glycine, was added too quickly to the systems, causing fast nucleation. Alternative methods to induce nucleation at the correct rate were attempted, including cooling the system down, and exposing the system to methanol vapours only - again α-glycine was made. Tween 80 was then abandoned in favour of Brij 30, since it was considered that Tween 80 was too potent an α-glycine polymorph nucleator

Methanol vapour diffusion experiments were carried out using microemulsions with Span 80 and Brij 30 as the surfactant mixture. γ-glycine could be obtained, but repeatability was difficult to achieve. In many cases this was due to the aqueous phase in the microemulsion being too supersaturated, forcing quick crystallisation and leading to α-glycine being formed. The addition of methanol vapour being added past the point at which crystallisation was just favourable was also thought to be a major reason for the limited amount of γ-glycine crystallised. The AOT system and methanol vapour diffusion experiments showed that in some cases Ostwald's Rule of Stages could be circumvented to produce γ-glycine, and that thermodynamics can be the defining factor for polymorph formation.

4. Control of Polymorphism of Glycine II

4.1 Introduction and Theory

Following on from the experiments using AOT as the surfactant, the Span 80/Tween 80 surfactant microemulsion experiments, the vapour diffusion experiments and the temperature variation experiments were all inconsistent in obtaining γ-glycine. In the case of Span 80 and Tween 80 surfactants, many water molecules formed hydrogen bonds with the surfactants, greatly increasing the supersaturation (sees Figures 42 and 43). The methanol vapour diffusion experiments were subject to variations of the rate and the amount of methanol entering the microemulsions, which meant one could never determine when a sufficient amount of methanol to just cause crystallisation had been added. An alternative method for the addition of methanol was proposed – separate microemulsions, one containing glycine solution and the other containing methanol would be combined to form a single microemulsion with all components from every part of the process present (see Figure 58). Two advantages of the technique are that the amount of methanol in the system is now known precisely, compared to the methanol vapour diffusion experiments where the only way to get a rough estimate was to weigh the aqueous methanol at the base of the reaction vessel before and after crystallisation. Secondly, the methanol addition is now controlled – methanol can only interact with glycine via inter-micellar interactions, compared to the vapour diffusion experiments, where methanol was continuously being added to the system. It was impossible to know with any accuracy what the methanol concentration in the microemulsions was at any time. This also meant that the rate of methanol addition was higher – this increased the supersaturation of the droplets more rapidly, which also increased the formation of near-stable nuclei to such an extent that thermodynamic control of the system was lost.

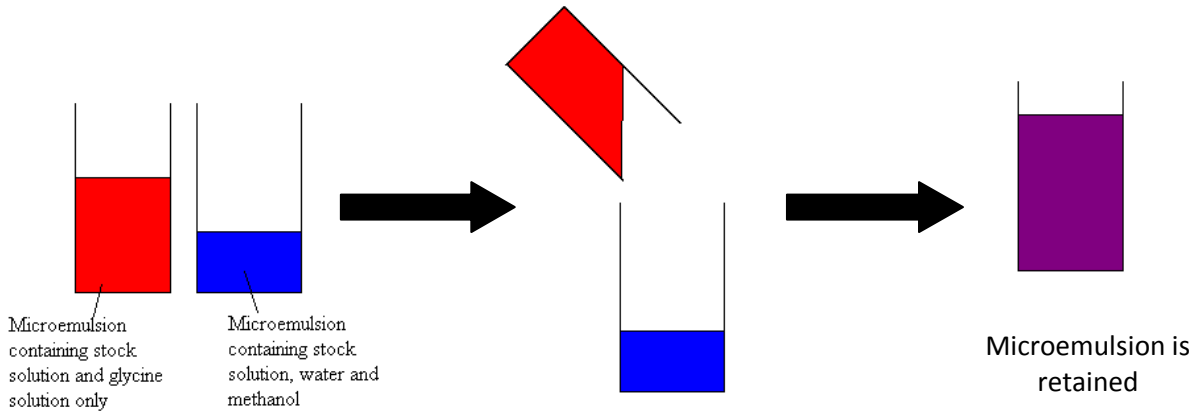

Figure 58: Pictorial description of how the mixed microemulsions method works. In colour terms, two colours have been mixed, but the final result is a definitive colour. In actual terms, two microemulsions have been mixed, where the result is a third mixture, which crucially is still a microemulsion, thereby retaining confinement.

4.2 Methods and initial experiments

IMPORTANT NOTE

When referring to the glycine solutions by letters, the mass of those solutions no longer apply to these experiments. Therefore, the letter refers to the concentration only (the concentration still in the form of percentage by mass of glycine in water). Therefore, (f) = 5 % by mass glycine, (j) = 4 % by mass glycine and (a) = 3 % by mass glycine.

As a test, the standard experimental setup of 16.0 g of stock (Span 80/Brij 30/heptane), 0.4 g of glycine solution (j) was used. To make this up, two stock solutions of 8.0 g were prepared – containing 25 % by mass of surfactant as before. To the first (Microemulsion 1) was added 0.2 g of glycine solution (j). In order to keep the same proportions as previous experiments, a halving of the stock solution

meant halving the amount of glycine solution used. To the other (Microemulsion 2), 0.1 g of methanol was added. Microemulsion 1 was then added to Microemulsion 2 and shaken by hand and by vortex mixing. The resulting combination showed phase separation and crystallisation within a few minutes. This was due to the lack of water phase (glycine solution) when attempting to create a microemulsion – previous experiments had had at least 0.4 g of aqueous solution.

To rectify this, the microemulsion was split in a 12.0 : 4.0 g ratio. 0.30 g of glycine solution (j) was added to Microemulsion 1. 0.1 g of water, plus the specified amount of methanol was added to Microemulsion 2. No phase separation was observed upon addition of the extra compounds, and when mixed, a stable microemulsion was maintained. A set of experiments with these specific amounts of microemulsion/water/glycine solution were carried out, with the only varying component being the mass of methanol added. All the experiments took place over a period of 7 days. The details and results of the experiments are shown in Table 19 and Figure 59:

Solution Name	Methanol added to 2nd microemulsion / g	Crystal Formation?	Polymorph(s)
M(j).3,4	0.10	-	-
M(j).5,6	0.20	-	-
M(j).7,8	0.30	-	-
M(j).9,10	0.40	-	-
M(j).11,12	0.50	-	-
M(j).13,14	0.60	Y	α, γ
M(j).15,16	0.70	Y	α
M(j).17,18	1.00	Y	α

Table 19: Table showing the initial mixed microemulsion experiments. Dashes indicate that crystals did not appear, or that there were not enough crystals for confidence in analysis. For both reasons, analysis was impossible.

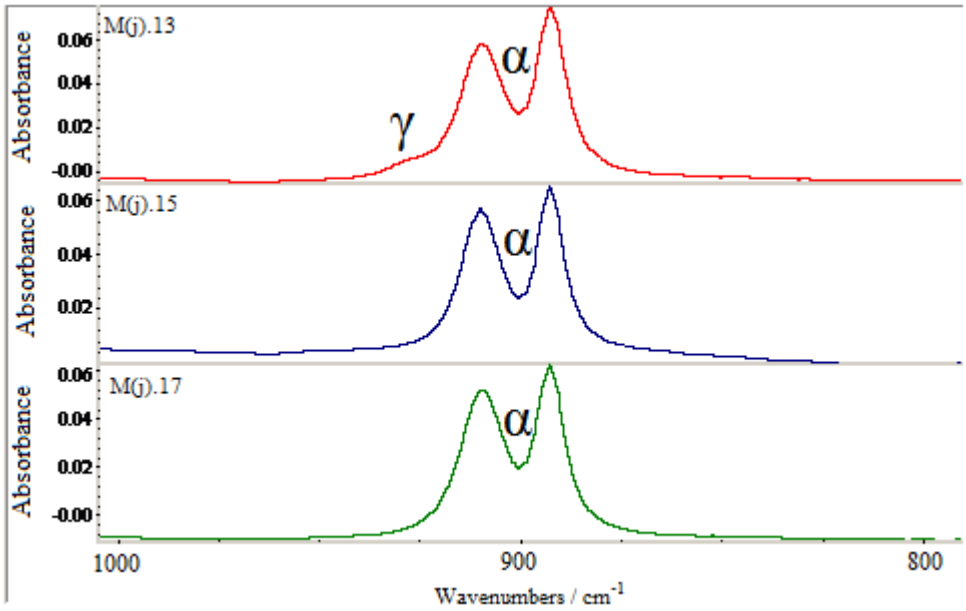

Figure 59: FTIR ATR spectra showing the three mixed microemulsion experiments which gave crystals. M(j).13,14 = red spectrum, M(j).15,16 = blue spectrum, M(j).17,18 = green spectrum.

From the spectra in Figure 59, it can be seen that one of the experiments (M(j).13,14) gave a small amount of γ-glycine. The amount of γ-glycine obtained is also similar to many experiments using vapour diffusion techniques which also gave γ-glycine. This gave an indication that the new technique did not compromise the yield of crystals. Experiment M(j).17,18 gave crystals after 48 hours, whilst M(j).13,14 and M(j).15,16 gave crystals after 72 hours. These final three experiments show that the

technique is viable – since the timescale is not significantly lengthened, yet γ-glycine can still be obtained, if in a small amount.

A change in surfactant concentration

All experiments so far had used a surfactant : heptane ratio of 25:75. However, work by Chen *et al.* on similar systems showed that γ-glycine was obtained more readily when the ratio was 40:60.[83] This ratio of surfactant : heptane had not been used previously because previous experiments involving Span 80/Tween 80 surfactant mixtures where the ratio was 50:50 required much larger amounts of methanol to obtain crystals.

Therefore, the amount of surfactant in the stock solution was increased from 25 % by mass to 40 % by mass. Test experiments were set up to see how the microemulsions should be made up. It was found that if using 0.4 g of glycine solution (4 % by mass as before), 12.0 g of stock solution would be needed to produce a microemulsion. The experiments were left for three weeks before extraction and analysis could take place. In some cases, a longer period of time (5 weeks) was required to obtain sufficient crystals

In some experiments, glycine growth was so slow that very few glycine crystals were present after an extended period of time. When this was the case, the experiments were repeated, but scaled up, with the stock solution increasing to 16.0 g in mass, meaning that the glycine solution and the overall aqueous phase would be raised by 33 %.

Apart from the change in surfactant concentration, the method for making the mixed microemulsion experiments was unchanged.

4.3 Results

FTIR analysis

The experiments where the glycine solution concentration was 5 % by mass glycine are shown in Table 20 and Figure 60:

	Microemulsion 1		Microemulsion 2				
Solution Name	**Stock Solution / g**	**Glycine Solution / g**	**Stock Solution / g**	**Water / g**	**Methanol / g**	**Crystal Formation / hours**	**Polymorph**
MC(f).1	6	0.2	6	0.2	0.5	18	α
MC(f).2	8	0.27	4	0.13	0.5	18	α
MC(f).3	9	0.3	3	0.1	0.5	18	α
MC(f).4	8	0.27	4	0.14	0.3	7	NA
MC(f).5	8	0.27	4	0.13	0.4	7	NA
MC(f).6	8	0.27	4	0.13	0.45	7	NA
MC(f).7	8	0.27	4	0.13	0	No crystals	NA
MC(f).8	8	0.27	4	0.13	0.1	No crystals	NA
MC(f).9	8	0.27	4	0.13	0.2	24	NA
MC(f).10	8	0.27	8	0.27	0.65	72	NA
MC(f).11	8	0.27	8	0.27	0.8	72	NA
MC(f).12	8	0.27	8	0.27	1	72	NA

Table 20: Descriptions of the mixed microemulsions experiments where the concentration of glycine solution was 5.0 % by mass glycine. NA = No Analysis, where crystals could be seen, but not enough could be extracted for analysis.

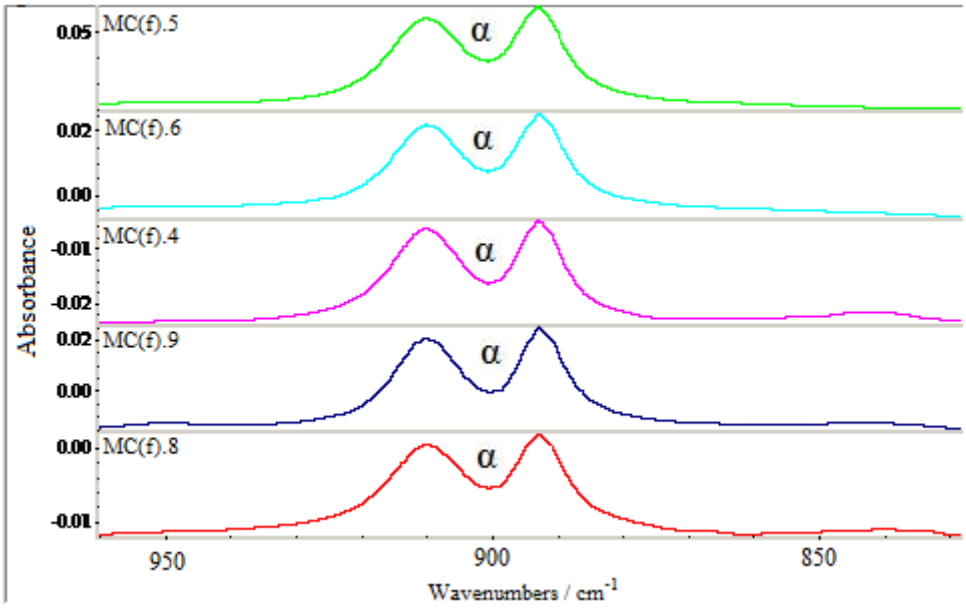

Figure 60: FTIR ATR spectra of glycine crystals obtained from experiments detailed in Table 18.

All spectra in Figure 59 show no peak at the value of 928 cm^{-1}, and therefore every experiment has crystallised out α-glycine, regardless of how much methanol was used and how the microemulsions were initially split. This is as expected, because most of the methanol vapour diffusion experiments also gave α-glycine when glycine solution (f) was used. This technique though has given greater consistency than previous methods so far.

The concentration of the glycine solution was reduced from 5.0 % to 4.0 % by mass of glycine. The method of experiment preparation, extraction and analysis of the crystals remained unchanged. These experiments are detailed in Table 21 and the resulting FTIR spectra are shown in Figure 61:

	Microemulsion 1		**Microemulsion 2**				
Solution Name	**Stock Solution / g**	**Glycine Solution / g**	**Stock Solution / g**	**Water / g**	**Methanol / g**	**Crystal Formation / hours**	**Polymorph(s)**
MC(j).1	6	0.2	6	0.2	0.5	100	NA
MC(j).2	8	0.27	4	0.13	0.5	68	NA
MC(j).3	9	0.3	3	0.1	0.5	68	NA
MC(j).4	7	0.23	5	0.17	0.5	24	NA
MC(j).5	8	0.27	4	0.13	0.4	24	α , γ (1%)
MC(j).6	8	0.27	4	0.13	0.55	24	α , γ (1%)
MC(j).7	6	0.2	6	0.2	0.6	72	NA
MC(j).8	6	0.2	6	0.2	0.8	72	NA
MC(j).9	6	0.2	6	0.2	1	20	α , γ (<1%)
MC(j).10	8	0.27	4	0.13	0.45	60	NA
MC(j).11	8	0.27	4	0.13	0.8	60	α
MC(j).12	8	0.27	4	0.13	1	2	α

Table 21: Descriptions of the mixed microemulsions experiments where the concentration of glycine solution was 4.0% by mass glycine. NA = No Analysis.

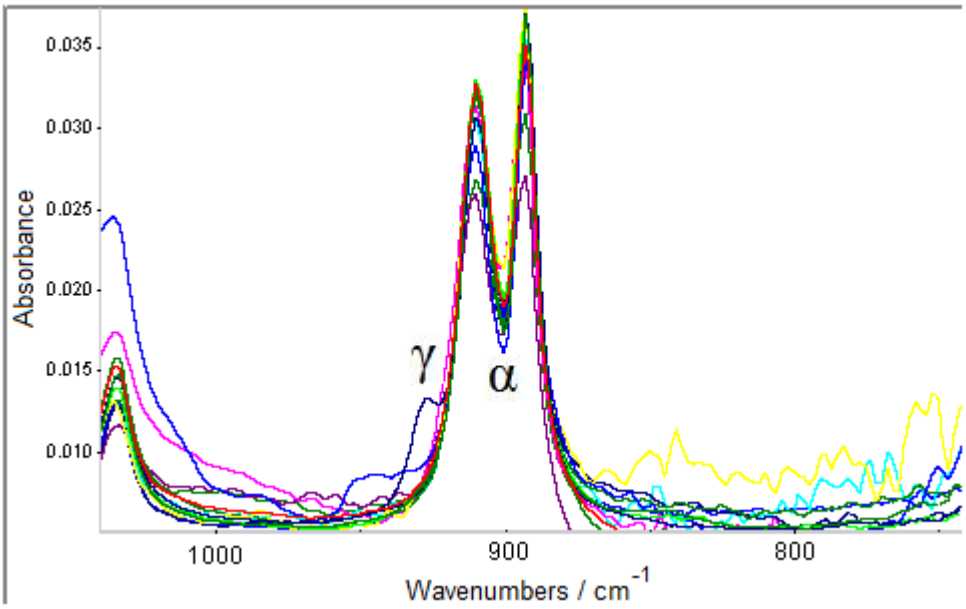

Figure 61: FTIR ATR spectra of mixed microemulsions experiments involving glycine solution (j), and where the two microemulsions before mixing were not split evenly.

Figure 61 shows that bar one experiment, all the experiments have crystallised α-glycine only.

The first experiments kept the mass of methanol constant and changed the proportions of the two microemulsions. Some of the experiments were observed for 5 months and did not produce crystals in that time period. However, the slow experiments were found to be those where the proportions of the two microemulsions were more equal. This meant that less glycine solution could be feasibly added to the first unmixed microemulsion. Therefore, a set of new experiments were made up with the two microemulsions containing 8.0 g of stock solution before mixing. Because of the overall increase in stock solution (from 12.0 to 16.0 g), the total aqueous phase had to rise by the same proportion from 0.40 to 0.54 cm^3 (see Table 22 and Figure 62).

	Microemulsion 1		Microemulsion 2				
Solution Name	**Stock Solution / g**	**Glycine Solution / g**	**Stock Solution / g**	**Water / g**	**Methanol / g**	**Crystal Formation / hours**	**Polymorph(s)**
MC(j).13	8.00	0.27	8.00	0.27	0.50	No crystals	NA
MC(j).14	8.00	0.27	8.00	0.27	0.67	No crystals	NA
MC(j).15	8.00	0.27	8.00	0.27	0.80	17	NA
MC(j).16	10.70	0.36	5.33	0.18	0.50	20	α
MC(j).17	10.70	0.36	5.33	0.18	0.67	20	α, γ (12%)
MC(j).18	10.70	0.36	5.33	0.18	0.80	20	α
MC(j).19	8.00	0.27	8.00	0.27	1.00	20	α, γ (35%)
MC(j).20	8.00	0.27	8.00	0.27	1.20	20	α
MC(j).21	8.00	0.27	8.00	0.27	1.33	20	α
MC(j).22	10.70	0.36	5.33	0.18	0.42	70	α
MC(j).23	10.70	0.36	5.33	0.18	0.50	48	α
MC(j).24	10.70	0.36	5.33	0.18	0.60	No crystals	NA
MC(j).2R	8.00	0.27	4.00	0.13	0.50	28	α
MC(j).2R	8.00	0.27	4.00	0.13	0.50	28	α, γ (10%)
MC(j).2R	8.00	0.27	4.00	0.13	0.50	28	α

Table 22: Descriptions of the mixed microemulsions experiments where the concentration of glycine solution was 4.0 % by mass glycine and the ratio of mass of stock solutions was 2:1. NA = No Analysis.

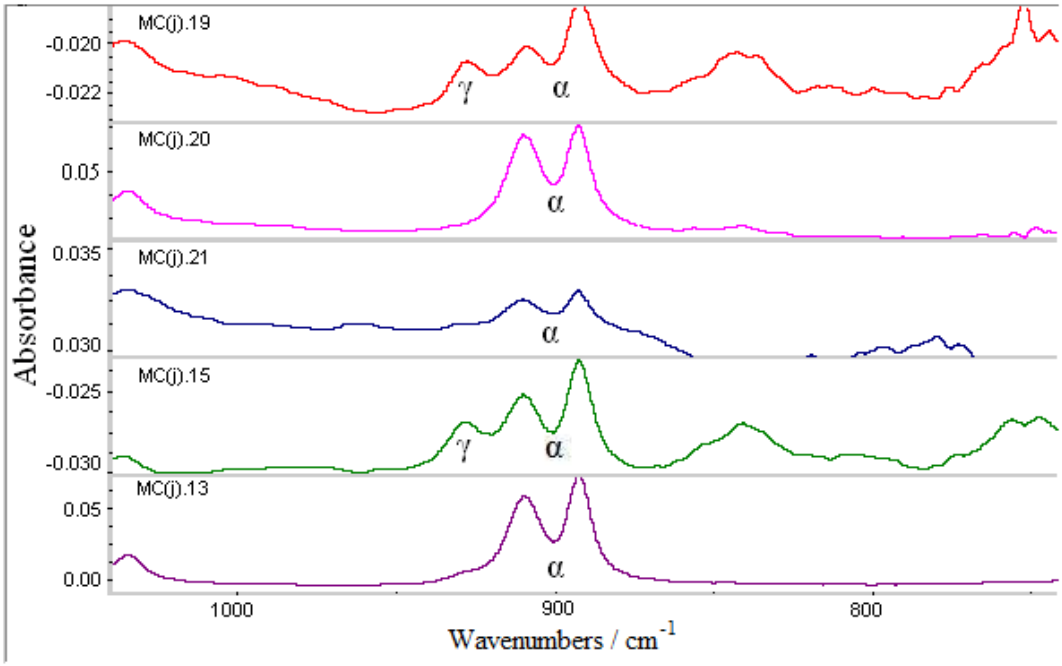

Figure 62: FTIR ATR spectra of mixed microemulsions experiments involving glycine solution (j), and where the two microemulsions before mixing each contained 8.0 g of stock solution.

The change can immediately be seen in Figures 61 and 62 (detailing experiments in Table 20), with almost all of the experiments showing some sign of γ-glycine formation (Only experiment MC(j).20 failed to show any sign of γ-glycine). There is no sign of a correlation between the amount of methanol used and the relative amount of γ-glycine crystallised.

4 % glycine solution was producing γ-glycine to an appreciable degree, but it was still accompanied by a large amount of α-glycine. The glycine solution was therefore diluted further – down to 3 % by mass glycine, and the experiments continued as before. The details of the experiments are shown in Table 23 and Figure 63:

	Microemulsion 1		Microemulsion 2				
Solution Name	**Stock Solution / g**	**Glycine Solution / g**	**Stock Solution / g**	**Water / g**	**Methanol / g**	**Crystal Formation / hours**	**Polymorph(s)**
MC(a).1	8.00	0.27	4.00	0.13	0.50	168	NA
MC(a).2	8.00	0.27	4.00	0.13	0.60	168	NA
MC(a).3	8.00	0.27	4.00	0.13	0.80	168	NA
MC(a).4	8.00	0.27	4.00	0.13	1.00	120	γ
MC(a).5	8.00	0.27	4.00	0.13	1.20	100	γ
MC(a).6	8.00	0.27	4.00	0.13	1.33	100	α, γ

Table 23: Descriptions of the mixed microemulsions experiments where the concentration of glycine solution was 3.0 % by mass glycine and the ratio of mass of stock solutions was 2:1. NA = No Analysis

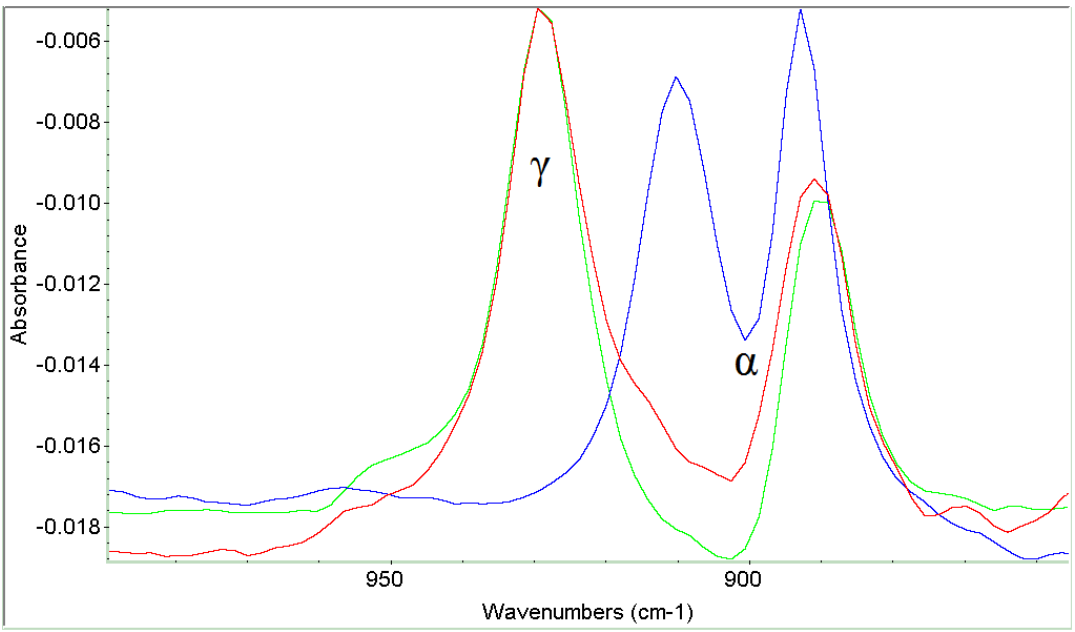

Figure 63: FTIR ATR spectra of two of the mixed microemulsion experiments involving glycine solution (a) – MC4(a).5 (red spectrum) and MC4(a).4 (green spectrum). For comparison, the spectrum of α-glycine is shown.

γ-glycine has been found in the highest proportion seen yet (see Figure 63). As with many of the experiments involving glycine solution (a), the crystallisation process was very slow, with the two experiments taking 15 weeks to give enough crystals for analysis. But the slow timescale has enabled the formation of γ-glycine with very few impurities. Further analysis was carried out on experiments MC4(a).4, including TEM and SAXS analysis.

SAXS Analysis

Using the Bruker Nanostar machine, SAXS analysis was carried out by the technician Helen Riggs on sample MC(a).4 to determine whether a microemulsion had formed and if so, the droplet size in the microemulsion. Using the GIFT analysis pack, the mean size of the hydrophilic core of the microemulsion droplets was calculated at 2.34 nm – the location of the first maxima on the p(*r*) curve gives this value. This proves that a microemulsion had formed and maintained its stability, thereby giving proper confinement to the disperse phase. The SAXS curve and the p(*r*) curve obtained from this experiment are shown in Figures 64 and 65:

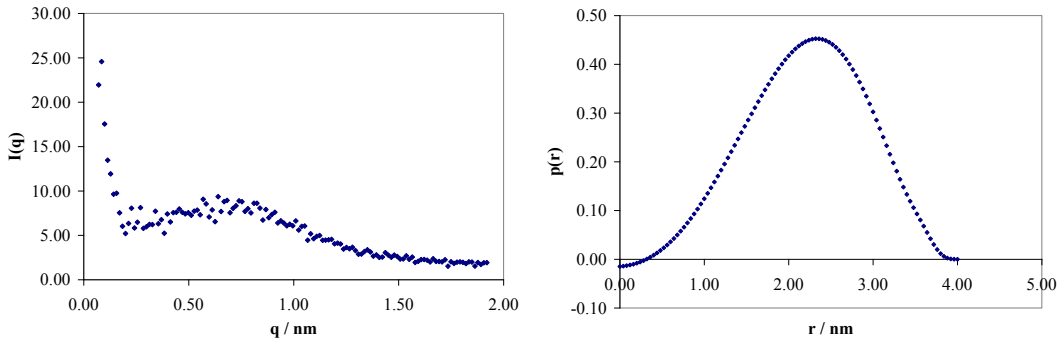

Figures 64 and 65: SAXS curve and p(*r*) curve for experiment MC(a).4.

TEM analysis

Using the simulated powder XRD data for each glycine polymorph in Table 3, and the bright field image and electron diffraction pattern in Figures 66 (a) and (b), the polymorph of the observed crystals can be determined.

a) 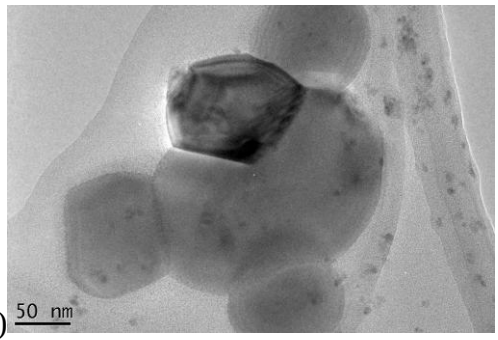

b) 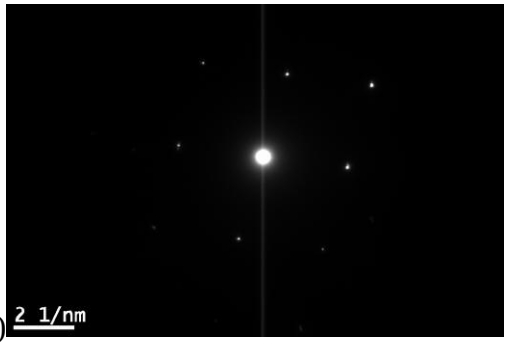

Figures 66 a) and b): a): TEM bright field image of glycine crystals found from experiment MC(a).4. b): Electron diffraction pattern from the same crystals.

From the diffraction pattern in Figure 66 (b), diffraction spots were found at d-spacings of 3.55 Å and 2.34 Å. These values correspond well to the [110] and [210] planes for γ-glycine.

A comparison can now be shown where the concentration of glycine solution is varied (see Figure 67):

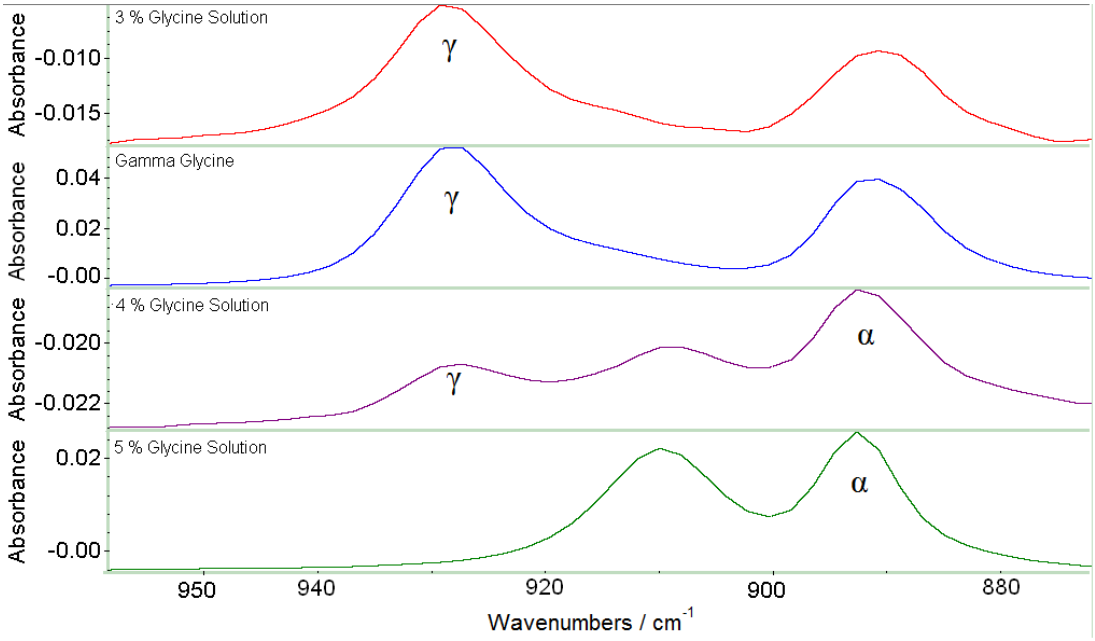

Figure 67: FTIR ATR spectra showing the change in proportions of the polymorphs of glycine formed, when the concentration of glycine solution is varied. The γ-glycine spectrum was that of experiment 6 from the AOT-based experiments.

A clear trend can now be seen – with experiments using 3.0 % by mass glycine solution producing γ-glycine with almost 100 % of polymorphic product. 4.0 % by mass glycine solution gives about 45 – 50 % γ-glycine, and 5.0 % by mass glycine solution giving 100 % α-glycine.

4.4 Discussion and Future Work

Results using the mixed microemulsions were more consistent than those obtained from methanol vapour diffusion experiments, and better trends could be seen from the various sets of experiments. XRD analysis was not carried out on any of the samples, due to the small amount of product obtained – all of which would be used for IR analysis

Having shown from the Span 80/Tween 80 experiments that α-glycine is preferentially formed the main challenge was to show that despite this, thermodynamic control of crystallisation could be enforced. This was done successfully with the Span 80 / Brij 30 combination, with γ-glycine being formed primarily from the 3.0 % by mass glycine microemulsions.

The test experiments where surfactants were added in a layer above a glycine solution (see page 55) gave valuable confirmations about subsequent experiments. Since both the Span 80 and Brij 30-containing tests produced α-glycine, the success of experiments MC(a).4 and MC(a).5 proved that the surfactants did not enforce a templating effect on the system, and that the production of γ-glycine as the sole polymorph was down to nanoconfinement.

Another test that was carried out was to check whether the crystal was pure, or whether traces of surfactant had been incorporated into the crystal. FTIR analysis was carried out on a mixture of Span 80, Brij 30 and heptane and compared with γ-glycine made from experiment MC(a).5 (see Figure 68):

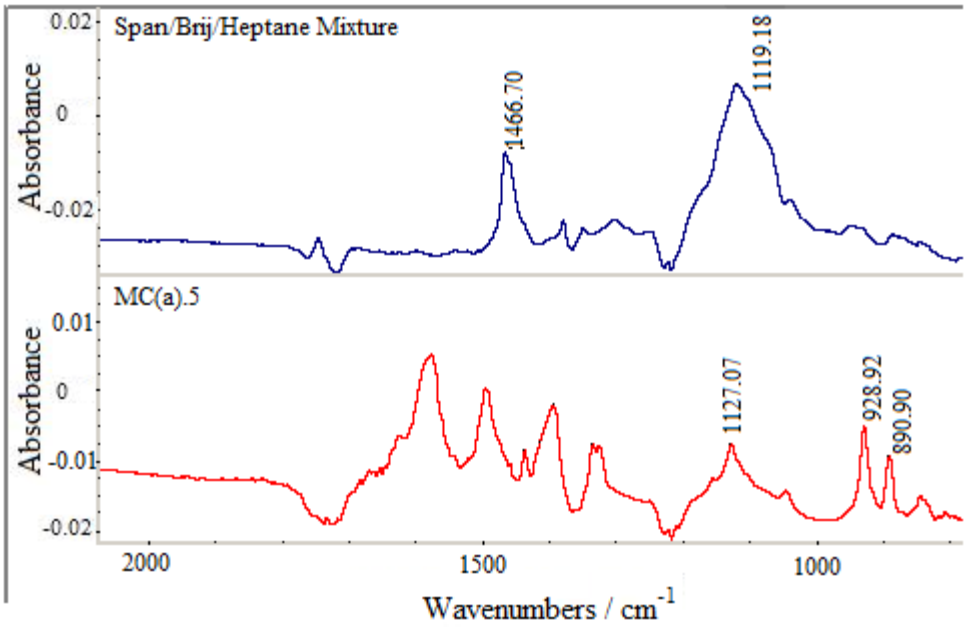

Figure 68: FTIR ATR spectra comparing the spectra obtained from Experiment MC(a).5 and a stock solution mixture of Span 80, Brij 30 and heptane.

The two peaks present in the surfactant mixture do not correspond to any peak present in the γ-glycine sample.

This work compares favourably with recent work into the crystallisation of glycine. Much work has looked into the crystallisation of glycine on engineered surfaces.[80, 84, 85] Though good control of the size of crystals was achieved, control of polymorphism was not. Kim *et al*. used slow cooling to induce crystallisation. Only when the cooling rate was 0.001 °C per minute did α-glycine form, and at no point did γ-glycine crystals appear. When solvent evaporation techniques were used, a mixture of all three polymorphs appeared. This is consistent with the results found here. Temperature studies were only able to crystallise the α- and β-forms, while certain vapour diffusion experiments (4(o), 4(f) and 4(j) in particular) crystallised all three polymorphs where crystals were found on the side of the reaction vessels due to evaporation.

Using microemulsions for polymorph control has become even more important following research by the Han group into the effect of additives on polymorph formation.[77, 86] The group found that both acidic and basic solutions, which before then were believed to inhibit the formation of α-glycine, actually promoted the growth of α-glycine. Furthermore, in basic environments the α-glycine growth rate

was higher – the findings being contrary to what many groups had explored previously.

4.5 Conclusions

Mixed microemulsion techniques were used to attempt to obtain the most stable polymorph of glycine (γ-glycine). Span 80 and Brij 30 were used as the surfactants, and heptane as the oil phase. Taking two stock solutions, glycine solution was added to one, and a water/methanol mixture to the other. These microemulsions were then mixed and left at room temperature (298K). When the glycine solution concentration was fixed at 3.0% by mass, γ-glycine was predominately crystallised. The subsequent success suggests that this point should be applied to future experiments, in order that a higher proportion of the required polymorph is crystallised. Overall, the experiments showed that by using the mixed microemulsion technique, Ostwald's Rule could be circumvented.

Two changes to the methods carried out using AOT as the surfactant for microemulsion formation were critical in achieving sole growth of γ-glycine:

1) The reduction of the concentration of the glycine solution used. This had the effect of reducing the number of near-stable nuclei present in the microemulsion, thereby ensuring that the system was totally stable due to nanoconfinement before anti-solvent was added.

2) The confining of the methanol to droplets within the microemulsion, which slowed the rate of decrease of supersaturation within the microemulsion. With regards to the free energy curves in Figure 10, this meant that the minimum points of the curves did not drop too quickly below the value of *kT*, thereby maintaining thermodynamic control.

Instead of kinetics determining the polymorph of crystals, thermodynamics were now the defining factor for polymorph formation, and so the most stable γ-glycine polymorph could be obtained, even though it is only ~0.2 kJ mol^{-1} more stable than the α-glycine polymorph, and grows 500 times slower in aqueous solution.[61]

5. Synthesis of Hydroxyapatite

5.1 Introduction and Theory

5.1.1 Hydroxyapatite

Because of various injuries, it sometimes becomes necessary to replace bone fragments or material to a patient via surgery. Endogenous bone material (bone that has come from the patient itself) is usually the best method, but there is limited material to work with.[87-89] Exogenous bone material (from other humans) can be used, but there is a chance that the host body may reject the implants, and that diseases may be transmitted to the body during the processes. The same problems occur with xenografts – replacement material that originates from another species.[90] With these problems with naturally-occurring implants, the search shifted to finding suitable artificial replacements. Metallic replacements were suggested due to their excellence at load-bearing applications, but this brought a new series of problems, including corrosion, rusting and the increase of toxicity levels in the human body.[91, 92]

In the early 20th century, it was discovered that calcium phosphate phases were an abundant inorganic component of bones, teeth and some hard tissues.[93] Therefore, work became focused on artificially creating these phases as a possible solution to repairing bone defects. Albee is credited as the first person to demonstrate the effects of using a tricalcium phosphate material to increase osteogenesis and repair bone material.[94] Half a century later, Nery *et al.* carried out experiments using porous tricalcium phosphate to repair infrabony defects in dogs and found that no adverse reactions were present.[95] Future groups looked to find other materials with increased biocompatibility.

Hydroxyapatite (abbreviated to HAp) is a naturally occurring material with the formula $Ca_{10}(PO_4)_6(OH)_2$. It belongs to the apatite family of minerals, which also include fluorapatite and chlorapatite. As a result, HAp has become the main focus for many as a useful material for *in vivo* scaffolds used for tissue engineering.[93, 96-98] HAp is often used as the main material because of its excellent osteoconductivity (the ability of bone cells and bone minerals to grow on a material used as a scaffold)

and biocompatibility. Because of this, HAp is often denoted as a second-generation biomaterial, since first-generation materials were only picked based on their ability to give a bioinert tissue response once in the body. Second-generation materials are defined as those that can also "generate a controlled action and reaction in the physiological environment".[99]

One thing to note, and what is often confused with respect to hydroxyapatite, is that while HAp is osteoconductive, it is not osteoinductive or osteogenic. Osteoinductivity refers to the ability to convert tissue cells into tissue formers, whilst osteogenesis refers to the formation of mineralised bone tissue.

5.1.2 Physical and chemical properties of hydroxyapatite

Bone mineral is not solely made up of HAp – rather it is a combination of calcium phosphate materials that contribute to the overall makeup. The ratio of calcium to phosphorous is usually between 1.5 and 1.7. HAp itself has a ratio of 1.61. Other calcium salts which are present include brushite ($CaHPO_4 \cdot 2H_2O$) and octacalcium phosphate [$Ca_8H_2(PO_4)_6 \cdot 5H_2O$].

HAp can decompose according to the equation:[100-103]

$$Ca_{10}(PO_4)_6(OH)_2 \rightarrow 2Ca_3(PO_4)_2 + Ca_4P_2O_9 + H_2O\,. \qquad (16)$$

This, however, does not occur in the human body, after Skinner *et al.* (and subsequently Mostafa) proved that at atmospheric pressure, hydroxyapatite can survive heating up to 1000 °C.[101, 104] In a vacuum, pyrolysis can occur at temperatures of around 850 °C, resulting in the loss of hydroxyl groups and structural changes.[101]

Apatite-type compounds found naturally are often coloured with faint hues of brown and green. This can be often attributed to fluorine degradation of the compounds, similar to how teeth colour may become mottled through over-exposure to fluorine.[105] Pure hydroxyapatite is white, and this can be used as a general estimate of purity.

5.1.3 Why synthesise nanoparticles of hydroxyapatite?

The early studies into the decomposition of HAp in the human body found that the rate of decomposition of HAp was faster when the sample of HAp was microporous or macroporous.[106] This degradation rate eventually slows over time, with most of the material being lost after the first 72 hours. But if the HAp molecules and crystals are densely packed i.e. increasing the overall density of the construct, the overall material is very nearly inert.

As mentioned before, HAp can provide a scaffold for new cells and tissue to grow on. On its own, HAp is not at all like natural bone, since that is a composite of apatite and collagen fibres.[107, 108] The apatite material in natural bone is present in the form of nanoparticles. Therefore, the synthesis of HAp nanoparticles is essential as one of the main steps to make a bone scaffold/substitute that is more comparable to natural bone. In addition, ceramic replacements of apatite were found to not be structurally sound compared to composite scaffolds.[90, 109] Therefore, HAp nanoparticles bound by, for example, a polymer scaffold base will make for a biocompatible implant, whilst retaining good load-bearing properties.

Hydroxyapatite has been synthesised via microemulsions by previous groups.[110-114] Yamada *et al.* used a combination of calcium chloride, ammonium hydroxide and calcium hydrogen phosphate – using ultrasound techniques to obtain microparticles.[113] Koumoulidis *et al*. reacted monocalcium phosphate with ammonium hydroxide and calcium chloride to produce hydroxyapatite, using dispersing apparatus to drive the reaction.[115] Guo *et* al. used a combination of calcium nitrate and ammonium phosphate with additional ammonia and ethanol.[116] From these previous works, the popular method involves combining a calcium salt with a phosphate-containing material. Presented here are two syntheses which give hydroxyapatite particles, firstly by a "direct addition" method, where the reactants are added to a microemulsion containing an initial reactant. The second method involves the technique of mixing microemulsions to give slower, but more structured growth of HAp crystals.

5.2 Synthesis by direct addition of reagents

5.2.1 Materials and Methods

Triton X-100, 1-hexanol, ammonium hydroxide (ACS reagent 28 – 30 % NH_3 basis) calcium chloride dehydrate (ACS reagent ≥ 99 %) and ammonium phosphate dibasic (ACS reagent ≥ 98 %) were all obtained from Sigma-Aldrich. Cyclohexane (analytical standard) was obtained from Fluka.

A surfactant stock solution was made up, using Triton X-100 as the surfactant, 1-hexanol as the co-surfactant and cyclohexane as the oil phase. The proportions by mass were 1.8 : 1.2: 7.0 (Triton X-100 : hexanol : cyclohexane). 10.0 cm^3 samples of the stock solution were taken, and calcium chloride solution of varying amounts was added to form an emulsion or microemulsion, depending on the amount added.

A magnetic stirrer bar was added, then the sample was placed in a water bath at 30°C - the mixture was constantly stirred. Ammonium hydroxide solution of concentration 0.08 M was added dropwise to the microemulsion until roughly 1.0 cm^3 had been added over a period of 30 minutes. Ammonium phosphate solution of concentration 0.06 M was then added dropwise until a white suspension had formed. This indicated the formation and presence of hydroxyapatite crystals (see Figures 68 a)-c)). The crystals were separated from the rest of the emulsion by centrifuge, washed with ethanol and water and then dried in an oven at 30 °C.

Experiments were carried out where the volume of calcium chloride solution was varied between 1.0 and 5.0 cm^3. The details of four of these initial experiments are shown in Table 24:

Sample Name	$CaCl_2$ / cm^3	Emulsion Type	NH_4OH added / g	$(NH_4)_2HPO_4$ added / g
HAP1	5.0	Nanoemulsion	1.23	0.80
HAP4	4.0	Nanoemulsion	1.45	1.51
HAP6	2.0	Microemulsion at 30°C	1.73	1.63
HAP7	1.0	Microemulsion at rtp	0.85	0.85

Table 24: Table of four initial experiments carried out using direct addition methods.

a) 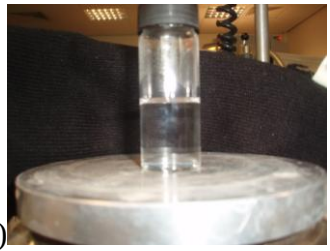 b) 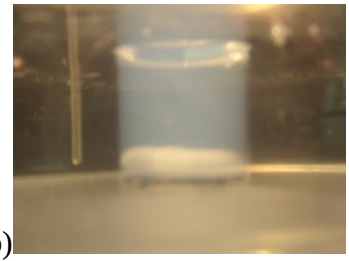 c) 

Figures 68 a), b) and c): Pictures showing how the experiments progress from the view of the naked eye. Picture a) shows the calcium chloride microemulsion before addition of any other reactants. Picture b) is taken after the ammonium hydroxide and 0.3 ml of ammonium phosphate have been added. Picture c) is taken after the reaction is completed (1.0 – 1.5 ml of ammonium phosphate have been added at this point).

5.2.2 Results

It was found that if the ratio of the aqueous to oil phase was more than 3:10 (by volume), a nanoemulsion was formed, characterised by its blue colour. When the ratio was less, a microemulsion was formed, though this was occasionally dependant on the temperature. At 25 °C, a ratio of 2:10 would stay as a nanoemulsion, whilst anything less would end up as a microemulsion. At 30 °C, the same ratio of phases always gave a microemulsion.

Addition of ammonium hydroxide caused little change to the emulsions, because there is no reaction with the calcium chloride. The addition is still necessary though, since it has been discovered that the pH of the microemulsion affects the rate of reaction. The reaction proceeds at a quicker rate if the pH is alkaline.[117] Some turbidity was observed upon addition of ammonium hydroxide. Initial addition of ammonium phosphate also caused very little change. Once ~ 1.0-1.5 g of phosphate was added, the emulsion turned white, indicating that crystals had been formed. The crystals obtained were white in colour, initially suggesting that the purity of the product was relatively high.

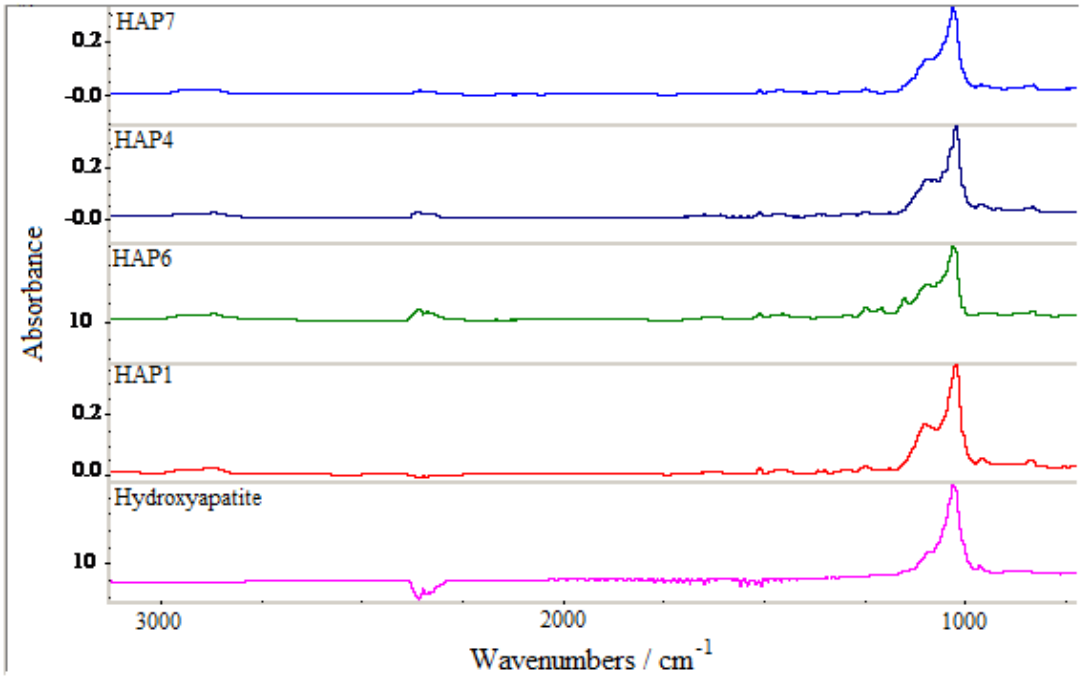

Figure 69: Stacked FTIR ATR spectra of the experiments HAP 1, 4, 6 and 7 between 500 and 2000 cm^{-1}. Bottom spectrum shows in-bought hydroxyapatite for comparison.

Comparison with in-bought hydroxyapatite showed that there were only two major peaks between 1000 and 1500 cm^{-1} (see Figure 69). The main peak at ~ 1036 cm^{-1} is prominent in every spectrum – this corresponds to the P-O stretching vibration (the v3 mode) in the PO_4^{3-} group in hydroxyapatite.[112, 114] A small peak at ~ 970 cm^{-1} can also be seen – this also is caused by the phosphate group in the form of the v1 mode.[118] In addition to these important peaks, many small peaks can be found. It was realised that surfactant could still be present in the final product. Therefore, the FT-IR ATR spectrum of Triton X-100 was taken and compared with previous spectra (see Figure 70):

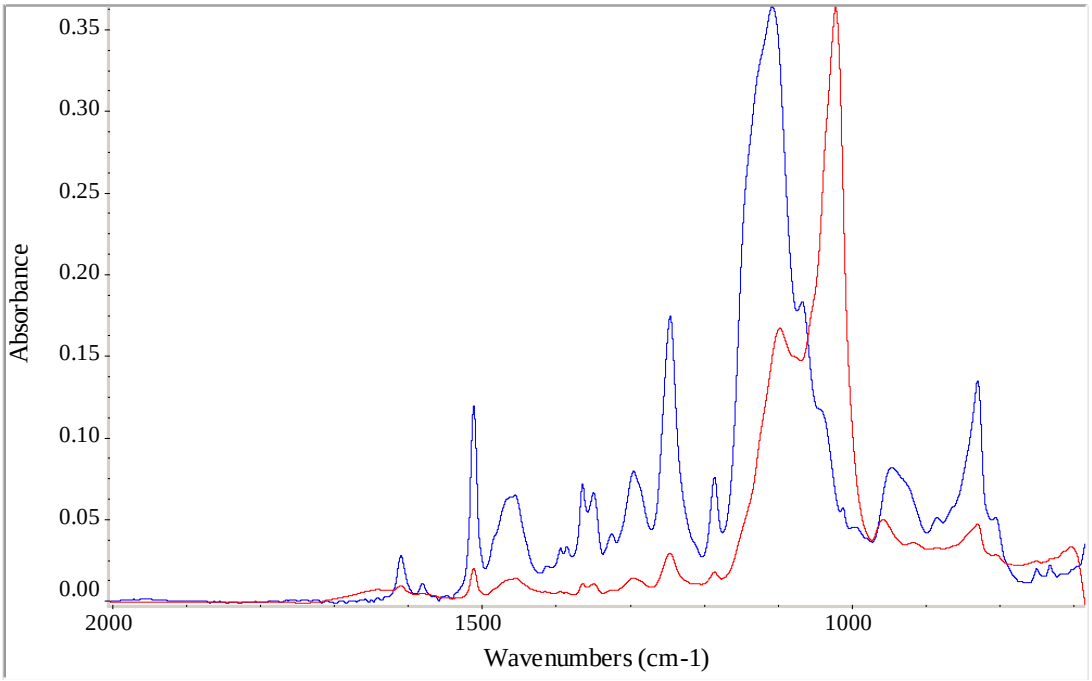

Figure 70: Comparison of FTIR ATR spectra between experiment HAP1 (red spectrum) and Triton X-100 (blue spectrum).

Many of the small peaks in the 1150-1500 cm^{-1} region correlate with the Triton X-100 peaks. More specifically, the peak at 1100 cm^{-1} is shown to be the major peak to show up in the Triton X-100 spectrum and as such has the largest presence in the HAp spectrum. Therefore, washing of samples must take place after extraction. The optimum washing process was eventually designated as successive washings of the sample with cyclohexane, water, ethanol and water again. This eliminated the minor peaks, and correlation with the in-bought hydroxyapatite was far better. This also showed why an optical estimation of purity would be flawed, since even before washing, the crystals were white in colour.

It was also noted that the reaction may not have gone to completion, and that calcium chloride and ammonium phosphate were being recrystallised. To check, this, FT-IR ATR spectra of both of these compounds were also taken, and then compared with a previous result (see Figure 71):

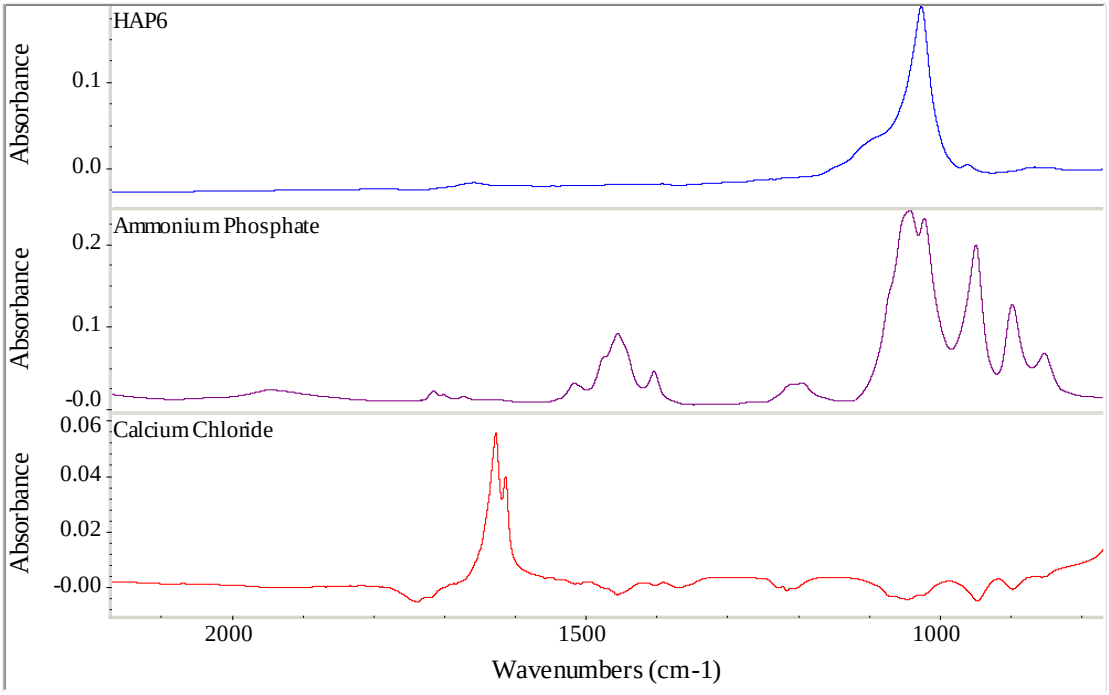

Figure 71: Comparison of FTIR ATR spectra: Ammonium phosphate (purple spectrum), calcium chloride (red spectrum) and experiment HAP6 (blue spectrum) between 500 and 4000cm^{-1}.

Large differences in the spectra shown in Figure 71 can be found, with no peaks in the hydroxyapatite spectrum corresponding to any other peak in the calcium chloride and ammonium phosphate spectra. This suggests that a reaction has taken place and has gone to completion, with very little of the original reactants left in the final product. The one area where the peaks are of similar value and height is between the sample and the ammonium phosphate spectra at ~1050 cm^{-1}. Mainly this is because both compounds contain the PO_4^{3-} ion. However, the environments that the phosphate ions exist in the two compounds are slightly different, therefore a slight shifting of the peaks can be detected. This was confirmed by Adler, who wrote a comprehensive treatment on the IR spectra of phosphate materials and specifically, the shapes and values of phosphate ligand peaks.[119]

X-Ray diffraction

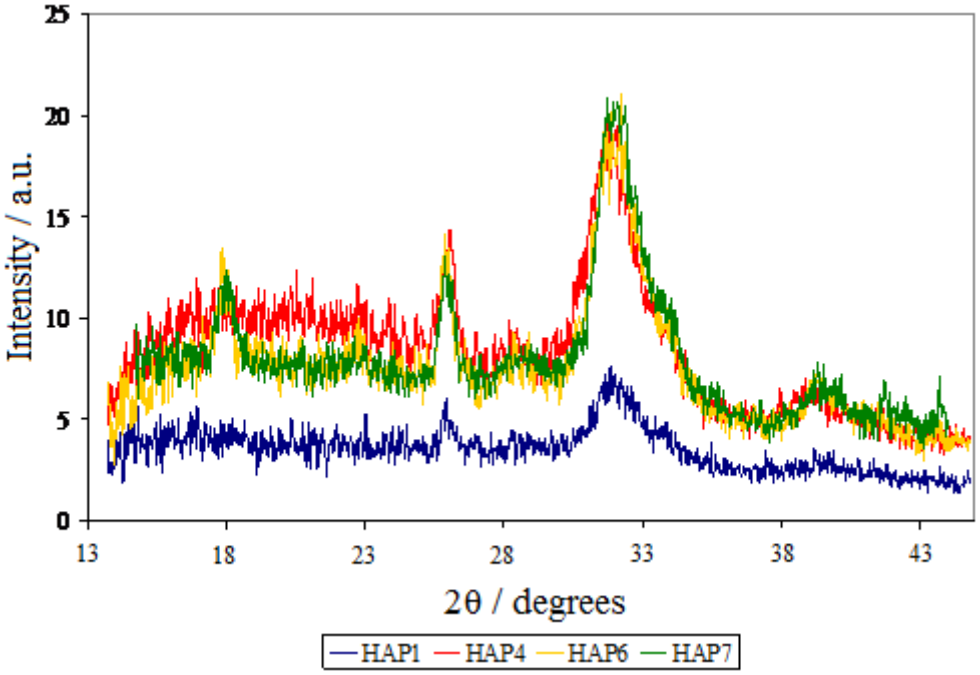

Figure 72: X-Ray diffraction patterns of the four experiments documented in Table 22.

The diffraction patterns are similar to one another (see Figure 72). The main peaks at 26°, 32° and 39° attributed to hydroxyapatite are clear in all experiments.[112, 120] The peaks made using experiment HAP1 are only a ¼ of the height of the other experiments – suggesting that the product is less crystalline.

Particle sizing

Using a LS13320 Laser Diffraction Particle Size Analyser, the size of the HAP particles could be probed at various points in the process. The initial four experiments detailed in Table 24 were set up again. This time, the masses of ammonium hydroxide and ammonium phosphate were standardised for all experiments, the details of which are shown in Table 25. The crystals were extracted, dried and then analysed:

Sample Name	$CaCl_2$ / cm^3	Emulsion Type	NH_4OH added / g	$(NH_4)_2HPO_4$ added / g
HAP1	5.0	Nanoemulsion	1.40	1.40
HAP4	4.0	Nanoemulsion	1.40	1.40
HAP6	2.0	Microemulsion at 30°C	1.40	1.40
HAP7	1.0	Microemulsion at 23°C	1.40	1.40

Table 25: The four experiments to which laser diffraction analysis was applied.

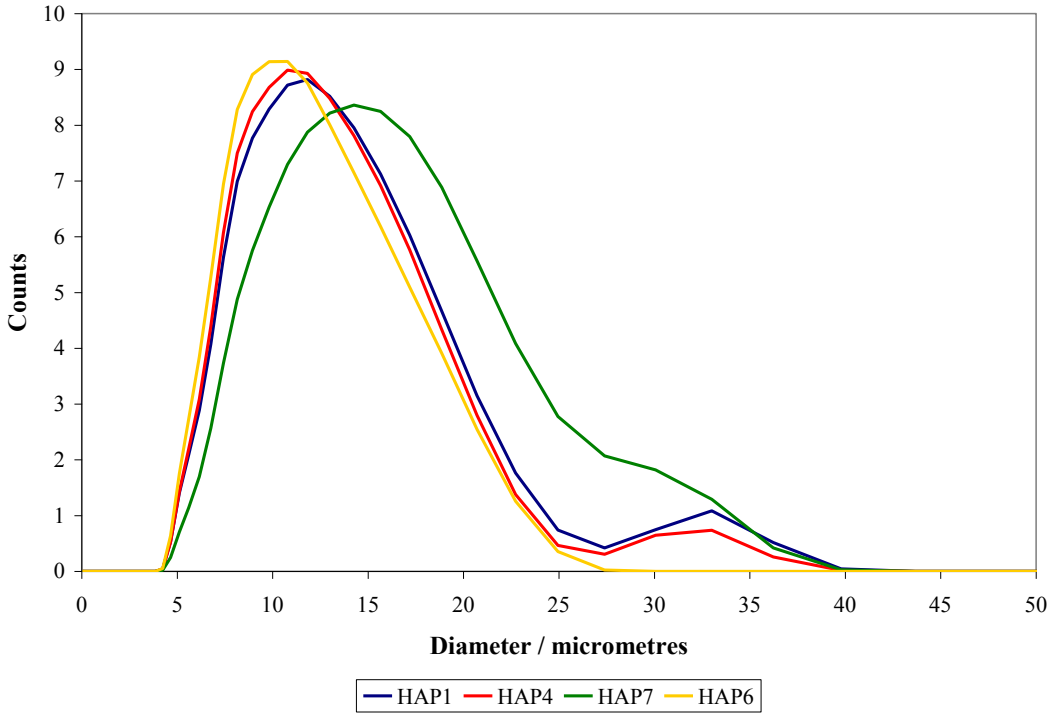

Figure 73: Particle size distribution of three of the direct addition experiments. 1.4 g each of ammonium hydroxide and ammonium phosphate was added to the experiments. Crystals were analysed after 24 hours.

Despite the change in proportions – with the amount of ammonium hydroxide and ammonium phosphate increased in experiments HAP1 and HAP7 and the amounts reduced in HAP4 and HAP5, the size of the hydroxyapatite crystals obtained are relatively similar (see Figure 73). This is possibly due to limiting the amount of ammonium hydroxide and ammonium phosphate added. But an alternative explanation is that because the reactants were added directly to the $CaCl_2$ - containing microemulsion, the process of destabilising the microemulsion has led to a similar crystallisation environment for each experiment. As a result, the crystal growth ends up being similar in each experiment. The distribution for experiment HAP7 is has a small shift towards larger particle sizes, possibly indicating that an excess of reactants has already been added.

Another set of experiments was carried out in a similar vein. To this set, an excess of ammonium phosphate was added (to totally ensure that a reaction would occur and crystals would form). These experiments are detailed in Table 24:

Sample Name	$CaCl_2$ / cm^3	Emulsion Type	NH_4OH added / g	$(NH_4)_2HPO_4$ added / g
HAP1	5.0	Nanoemulsion	1.40	2.50
HAP4	4.0	Nanoemulsion	1.40	2.50
HAP6	2.0	Microemulsion at 30°C	1.40	2.50
HAP7	1.0	Microemulsion at 23°C	1.40	2.50

Table 26: The four experiments to which an excess of ammonium phosphate had been added.

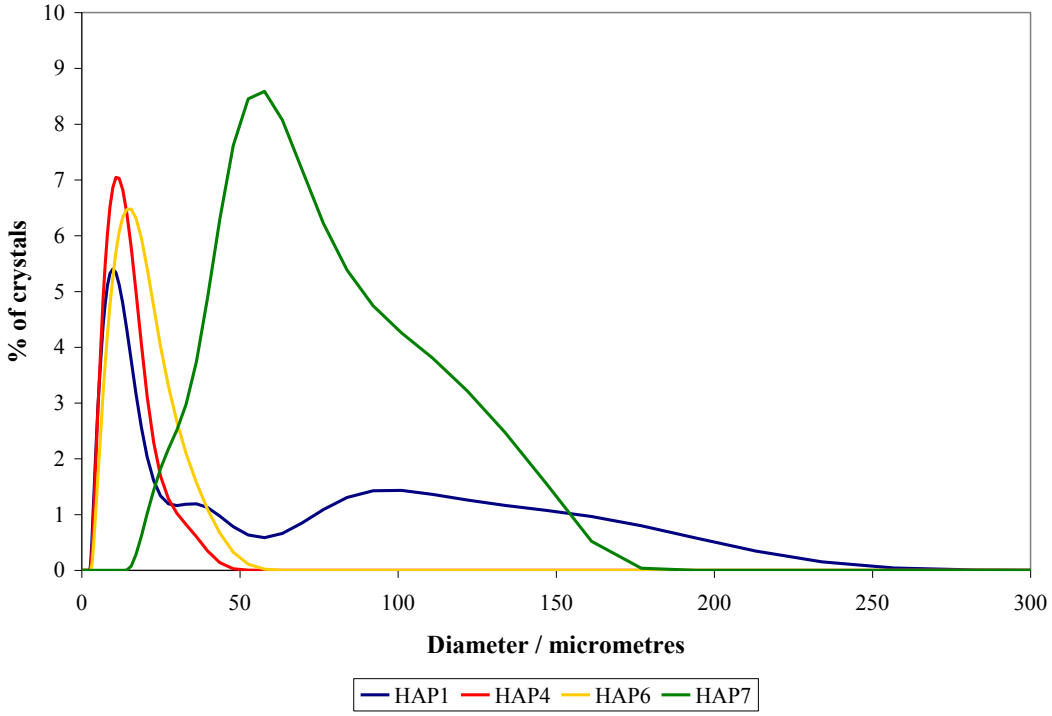

Figure 74: Laser diffraction analysis of the same four experiments – this time an excess of ammonium phosphate has been added. Crystals were analysed after 24 hours.

With the excess ammonium phosphate added, differences can now be seen in Figure 74. The larger droplets present in experiment HAP1 mean that range of crystal size is much larger. When excess ammonium phosphate was added, the crystal sizes ranged from 5 – 250 μm, compared to the range 5 - 40 μm when the amount of ammonium phosphate added was controlled. The anomalous curve found for HAP7 could be due to a lower nucleation rate so that fewer, but larger HAp crystals were formed. Alternatively, it could be the result of the analysis machine detecting particles of unreacted ammonium phosphate. In the original direct addition experiments, less ammonium phosphate was required to create crystals for that experiment. To check this possibility, FTIR ATR spectra of experiment HAP7 and ammonium phosphate were compared (see Figure 75):

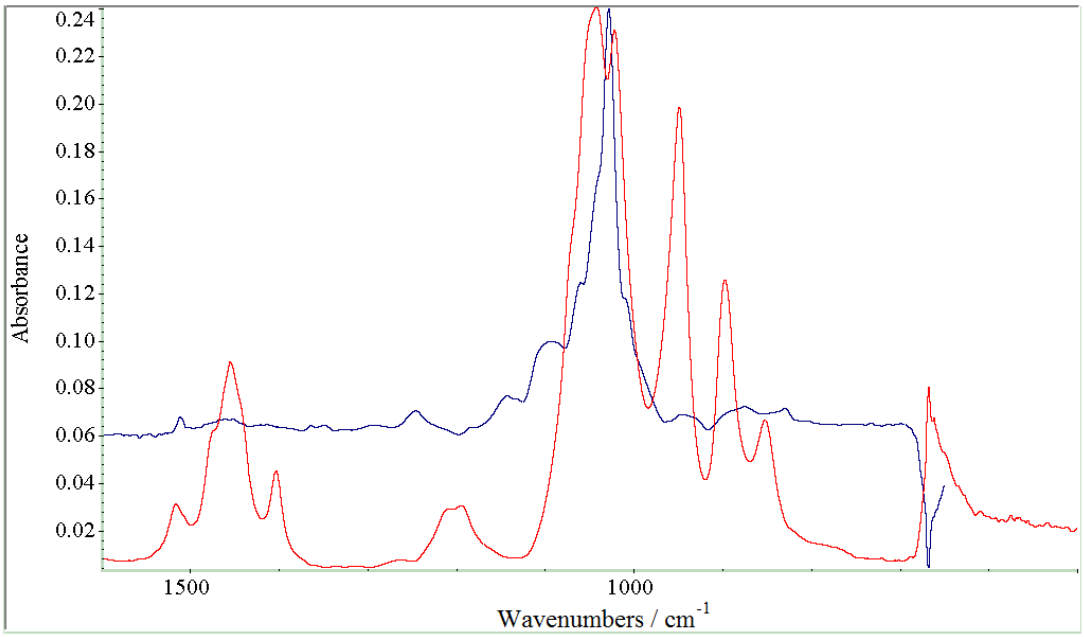

Figure 75: FTIR ATR spectra of experiment HAP7 (blue spectrum) and ammonium phosphate (red spectrum).

Small similarities can be seen between the spectra in Figure 74. The two peaks in the ammonium phosphate spectrum at 1025 cm^{-1} and 1050-1070 cm^{-1} also appear as small 'shoulders' on the main peak at 1040 cm^{-1} in the hydroxyapatite spectrum. Another small peak appears at 1450 cm^{-1} which matches up to the middle peak in the triplet group between 1400 and 1510 cm^{-1} in the ammonium phosphate spectrum. This suggests that there has been some ammonium phosphate present in the synthesised hydroxyapatite, and this may have contributed to the difference in particle sizes found in Figure 74.

TEM analysis

Using a JEOL 2100F FEG Transmission Electron Microscope, small particulates of diameters less than 100 nm could be studied. Two experiments were analysed – HAP1 and HAP7. These were chosen as they were the two extremes of the amount of reactants added:

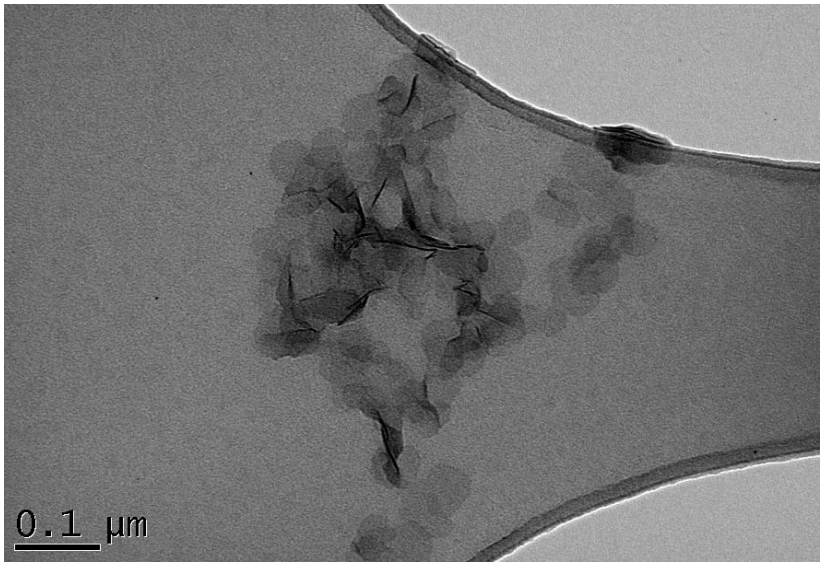

Figure 76 a): TEM picture of experiment HAP1.

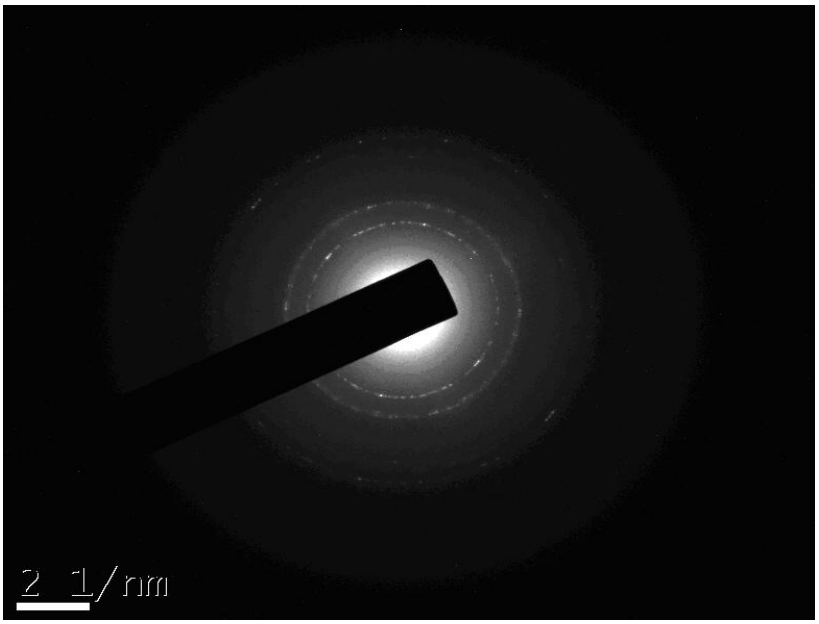

Figure 76 b): Electron diffraction pattern obtained from the bright field image in Figure 76. Experiment is HAP1.

The picture in Figure 76 a) shows that some spherical crystals have grown. The sizes of the spherical crystals vary from 36 – 60 nm There are also some more needle-like crystals with sizes between 30 – 75 nm.

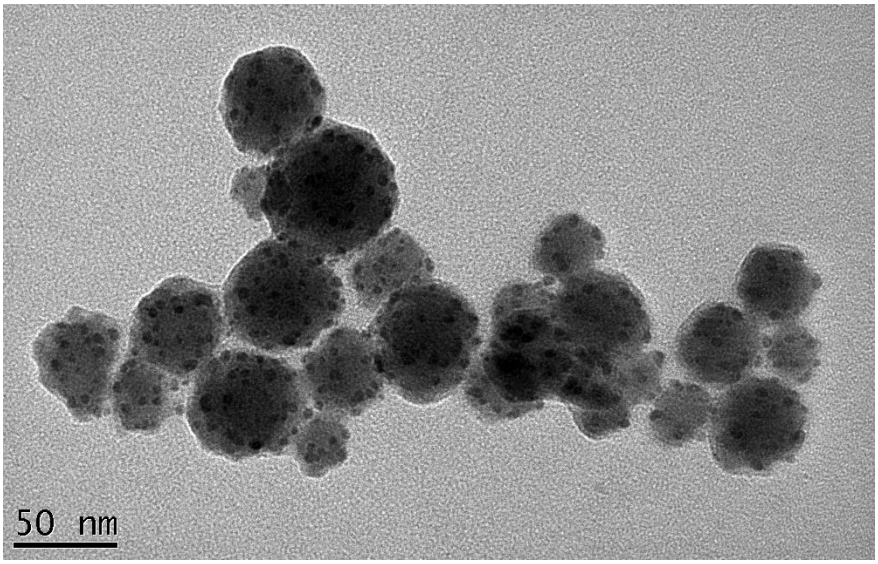

Figure 77 a): TEM picture taken of experiment HAP7.

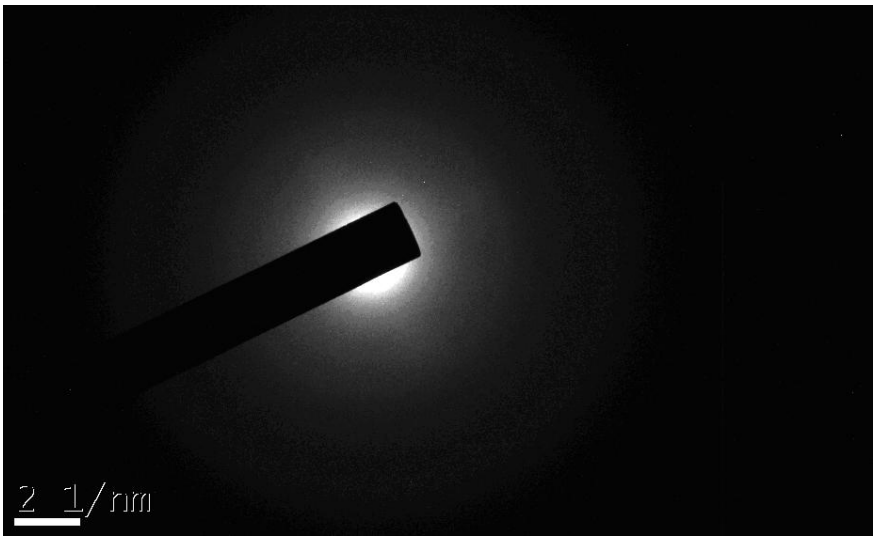

Figure 77 b): Electron Diffraction pattern of experiment HAP7.

The pictures show how the proportions of each compound in the microemulsion affect the crystals produced (see Figures 76 a) and b) & Figures 77 a) and b)). In the case with experiment HAP1, the crystals grown from the nanoemulsion are vaguely spherical, but are not particularly regular in their growth. The selected diffraction pattern in Figure 76 a) shows three rings, which corresponds to d-spacings of 4.03 Å, 3.15 Å and 1.88 Å.[121] These correspond relatively well to the [200], [102] and [312] planes of hydroxyapatite respectively. By contrast, the crystals from experiment HAP7 are much smaller but are also more spherical, showing that they have been confined to the microemulsion droplets. The sizes of the crystals are between 3 – 6

nm (see Figure 77 a)). The larger globules are likely due to excess surfactant on the copper grid, enveloping the newly-formed nanoparticles. This is borne out by Figure 77 b) showing very little information, because the crystallinity of the HAp crystals is not evident above the amorphous halo of the surfactant

5.3 Synthesis by mixing of microemulsions

The "mixed microemulsions" method to produce crystals follows the same principals as those carried out in the experiments involving glycine. The reactants are originally trapped within the water droplets, and cannot enter the oil phase. Through Brownian motion the droplets will collide, and any energetically favourable collisions will result in a transient dimer being formed. Only when this occurs, can reactant transfer and reaction take place, leading to the formation of hydroxyapatite crystals (see Figure 78).

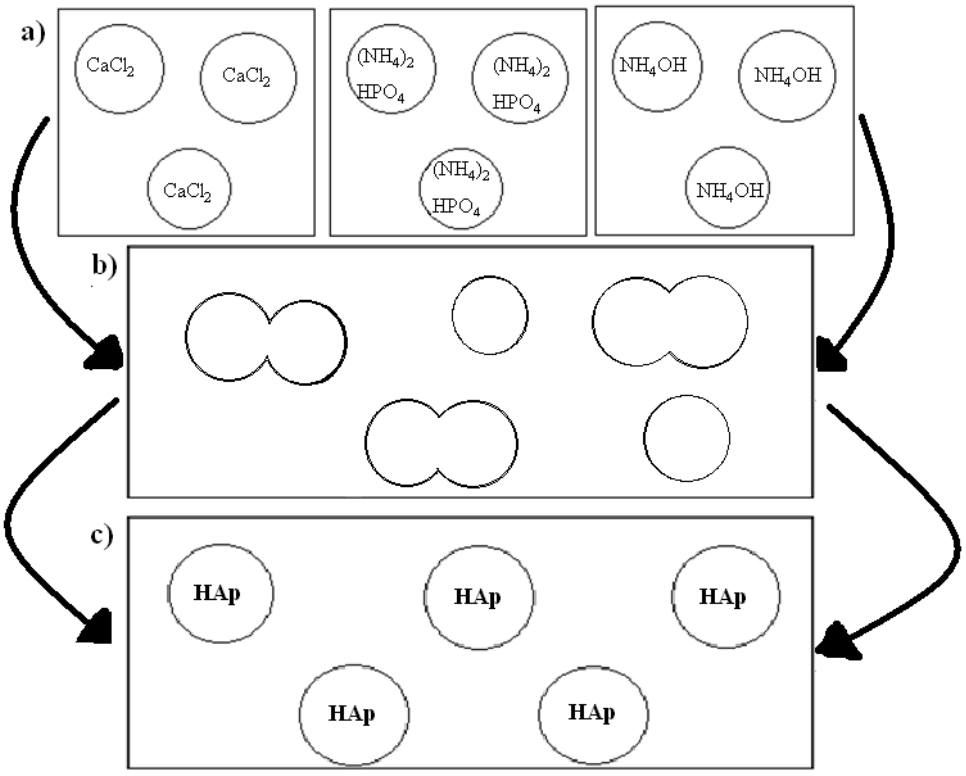

Figure 78: Diagram showing the general path of the reaction. In picture a), the reactants are in three separate microemulsions. Picture b) shows a point where transient dimers have formed, allowing reactant transfer and reaction. By picture c), enough reactions have occurred for hydroxyapatite to form within the droplets. These crystals will slowly expand (due to further droplet interactions) and finally break the microemulsion to settle at the bottom of the reaction vessel.

5.3.1 Methods

The same stock solution was used as before. Groups of three 5.0 cm^3 (3.8 g) aliquots (and occasionally volumes of 7.0 - 10.0 cm^3) were made, and to each stock solution calcium chloride, ammonium hydroxide and ammonium phosphate was added to form three emulsions/microemulsions. The samples were then mixed in the following order: the ammonium hydroxide microemulsion was added in one go to the calcium chloride microemulsion, followed by the ammonium phosphate microemulsion. This was to ensure that the emulsion/microemulsion mixture was basic before ammonium phosphate was added, which would allow the reaction to proceed. After all the mixing had been carried out, the overall microemulsion was shaken by hand, then left at 25 °C and observed at regular intervals. The experiments carried out are detailed in Tables 27 a) and b):

	Microemulsion 1		**Microemulsion 2**		**Microemulsion 3**	
Sample Name	**Surfactant Stock Solution / cm^3**	**Calcium Chloride / cm^3**	**Surfactant Stock Solution / cm^3**	**Ammonium Hydroxide / cm^3**	**Surfactant Stock Solution / cm^3**	**Ammonium Phosphate / cm^3**
HMM1	5	0.5 (0.1M)	5	0.5 (0.08M)	5	0.5 (0.06M)
HMM2	5	0.5 (0.5M)	5	0.5 (0.08M)	10	1.0 (0.06M)
HMM3	5	0.5 (0.5M)	5	0.5 (0.08M)	5	1.0 (0.06M)
HMM4	5	0.5 (0.5M)	5	0.5 (0.08M)	10	0.5 (0.40M)
HMM5	5	0.5 (0.5M)	0	0.5 (0.08M)	5	0.5 (0.06M)
HMM6	5	0.5 (0.5M)	0	1.0 (0.08M)	5	0.5 (0.20M)
HMM7	5	0.5 (0.1M)	5	1.0 (0.08M)	5	1.0 (0.06M)
HMM8	5	0.5 (0.1M)	5	1.0 (0.08M)	5	1.5 (0.06M)
HMM9	5	1.0 (0.1M)	5	1.0 (0.08M)	5	1.5 (0.06M)
HMM10	5	0.5 (0.1M)	5	0.8 (0.08M)	5	1.0 (0.2M)
HMM11	5	0.5 (0.1M)	5	0.8 (0.08M)	5	1.0 (0.4M)
HMM12	5	0.5 (0.1M)	5	0.6 (0.08M)	5	0.8 (0.06M)
HMM13	5	0.5 (0.5M)	5	0.6 (0.08M)	5	0.8 (0.2M)
HMM14	5	0.5 (0.1M)	5	0.6 (0.08M)	5	0.8 (0.2M)
HMM15	5	0.5 (0.1M)	5	0.4 (0.08M)	5	0.4 (0.06M)

Table 27 a): The "mixed microemulsions" experiments, showing the amounts and concentrations of each aqueous phase, if applicable. Experiments HMM5 and HMM6 involved the addition of ammonium hydroxide directly to the calcium chloride microemulsion.

	Microemulsion 1		Microemulsion 2		Microemulsion 3	
Sample Name	**Surfactant Stock Solution / cm^3**	**Calcium Chloride / cm^3**	**Surfactant Stock Solution / cm^3**	**Ammonium Hydroxide / cm^3**	**Surfactant Stock Solution / cm^3**	**Ammonium Phosphate / cm^3**
HMM16	5.0	0.5 (0.1M)	5.0	0.2 (0.08M)	5.0	0.5 (0.06M)
HMM17	5.0	0.5 (0.1M)	5.0	0.3 (0.08M)	5.0	0.5 (0.06M)
HMM18	5.0	0.5 (0.1M)	5.0	0.6 (0.08M)	7.0	0.8 (0.06M)
HMM19	5.0	0.5 (0.5M)	5.0	0.5 (0.40M)	5.0	0.5 (0.4M)
HMM20	5.0	0.5 (0.5M)	5.0	0.5 (0.40M)	5.0	0.5 (0.2M)
HMM21	5.0	0.5 (0.5M)	5.0	0.6 (0.40M)	5.0	0.5 (0.4M)
HMM22	5.0	0.5 (0.5M)	5.0	0.6 (0.40M)	5.0	0.8 (0.4M)
HMM23	5.0	0.5 (0.1M)	8.0	0.8 (0.08M)	7.0	0.8 (0.06M)
HMM24	5.0	0.5 (0.08M)	5.0	0.5 (0.064M)	5.0	0.5 (0.048M)
HMM25	5.0	0.5 (0.08M)	5.0	0.4 (0.064M)	5.0	0.4 (0.048M)
HMM26	5.0	0.5 (0.08M)	5.0	0.6 (0.064M)	5.0	0.8 (0.048M)
HMM27	5.0	0.4 (0.08M)	5.0	0.5 (0.064M)	5.0	0.5 (0.06M)
HMM28	5.0	0.4 (0.08M)	5.0	0.5 (0.08M)	5.0	0.5 (0.06M)
HMM29	5.0	0.4 (0.08M)	5.0	0.5 (0.04M)	5.0	0.5 (0.06M)
HMM30	5.0	1.0 (0.1M)	5.0	1.0 (0.08M)	5.0	1.0 (0.06M)

Table 27 b): More details of the “mixed microemulsions” experiments.

5.3.2 Results

In almost all experiments, a blue layer of varying thickness was found at the bottom of the vial after 18 hours, suggesting the formation of HAp crystals of sizes ≥ 50 nm. When the various aqueous phases were more concentrated, definite crystals could be seen, and could be extracted and analysed:

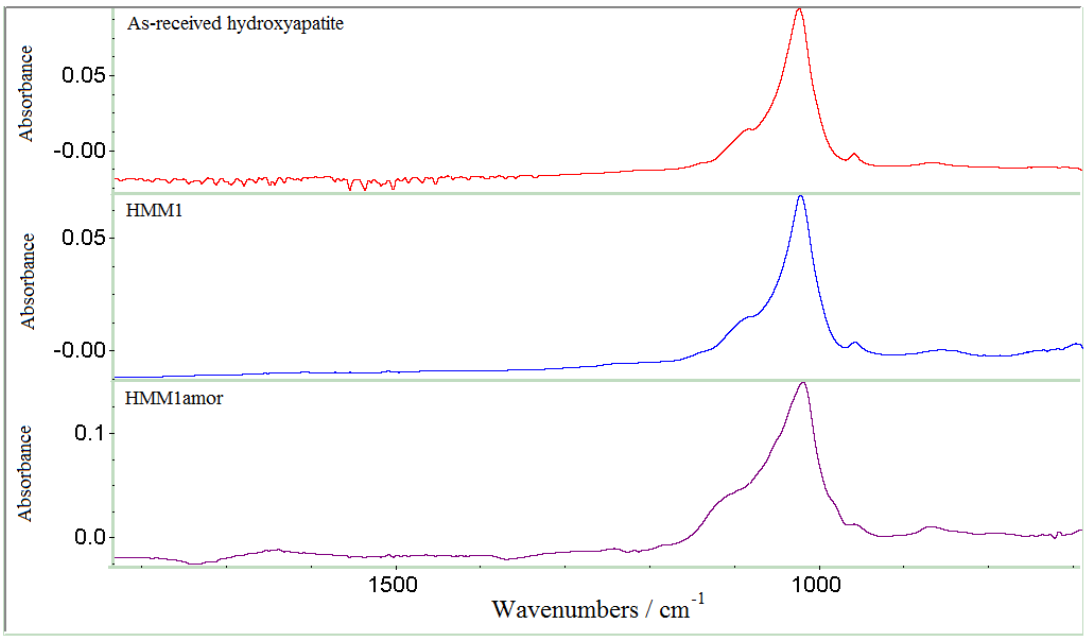

Figure 79: FTIR ATR spectra of two "mixed microemulsions" experiments – HMM1(blue spectrum) and HMM1amor (purple spectrum – using 1.0 M reactants. For composition, see Table 31). Bought-in hydroxyapatite (reagent grade - red spectrum) is shown for comparison.

From Figure 79, it can be seen that Experiment HMM1 shows good correlation with the bought-in hydroxyapatite (Aldrich – reagent grade). Again, successive washings with cyclohexane, ethanol and water (x2) were needed to remove impurities from the final product. But overall the main peaks in the region 950 – 1150 cm^{-1} are all present.

X-Ray diffraction spectra were also taken of samples HMM1 and HMM1amor (see Figure 80):

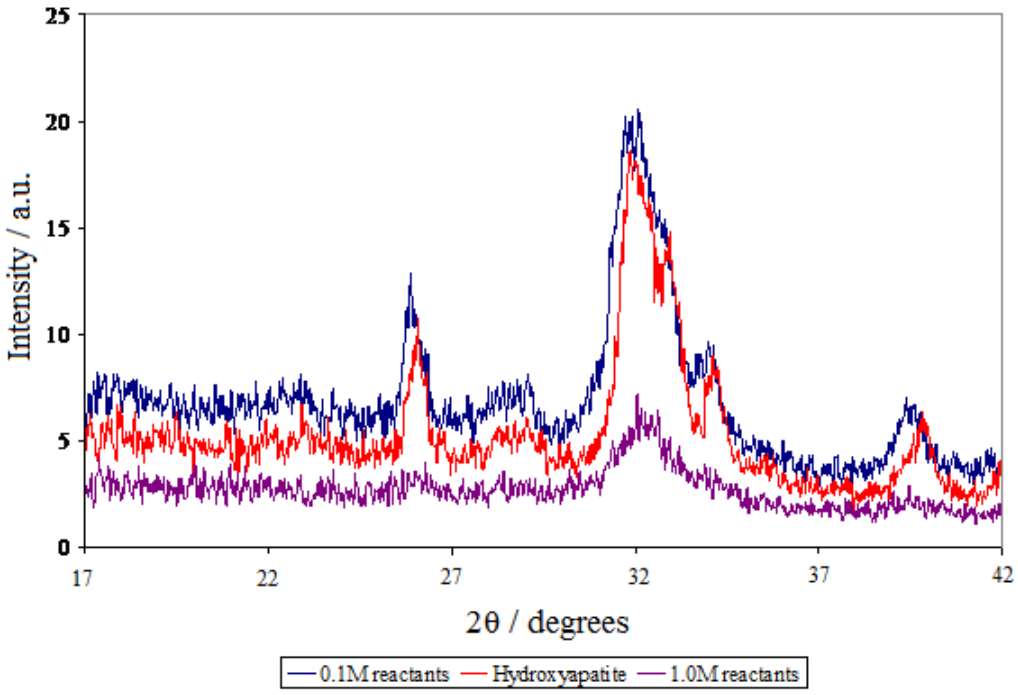

Figure 80: Powder X-Ray diffraction patterns of the same experiments shown in Figure 79. Colours have been kept the same for ease of comparison.

Good correlation between the patterns for in-bought hydroxyapatite (reagent grade) and experiment HMM1Sc can be seen. And as before in the IR-spectra comparison, when using 1.0 M reactants, the peaks are broader and in the diffraction pattern, the weaker peaks at 29° and at 40° both disappear, suggesting a less crystalline product when using 1.0 M reactants instead of 0.1 M.

Laser Diffraction analysis

Two experiments – HMM1 and HMM30 - were used for laser diffraction analysis to show the differences in particle size when the volume of reactants added is increased. The concentration of reactants and the volume of the organic phases were kept constant – the volume of reactants was the only variable for the experiment (see Table 26):

	Microemulsion 1		Microemulsion 2		Microemulsion 3	
Sample Name	**Surfactant Stock Solution / cm^3**	**Calcium Chloride / cm^3**	**Surfactant Stock Solution / cm^3**	**Ammonium Hydroxide / cm^3**	**Surfactant Stock Solution / cm^3**	**Ammonium Phosphate / cm^3**
HMM1	5.0	0.5 (0.1M)	5.0	0.5 (0.08M)	5.0	0.5 (0.06M)
HMM30	5.0	1.0 (0.1M)	5.0	1.0 (0.08M)	5.0	1.0 (0.06M)

Table 28: The two mixed microemulsion experiments used for laser diffraction analysis.

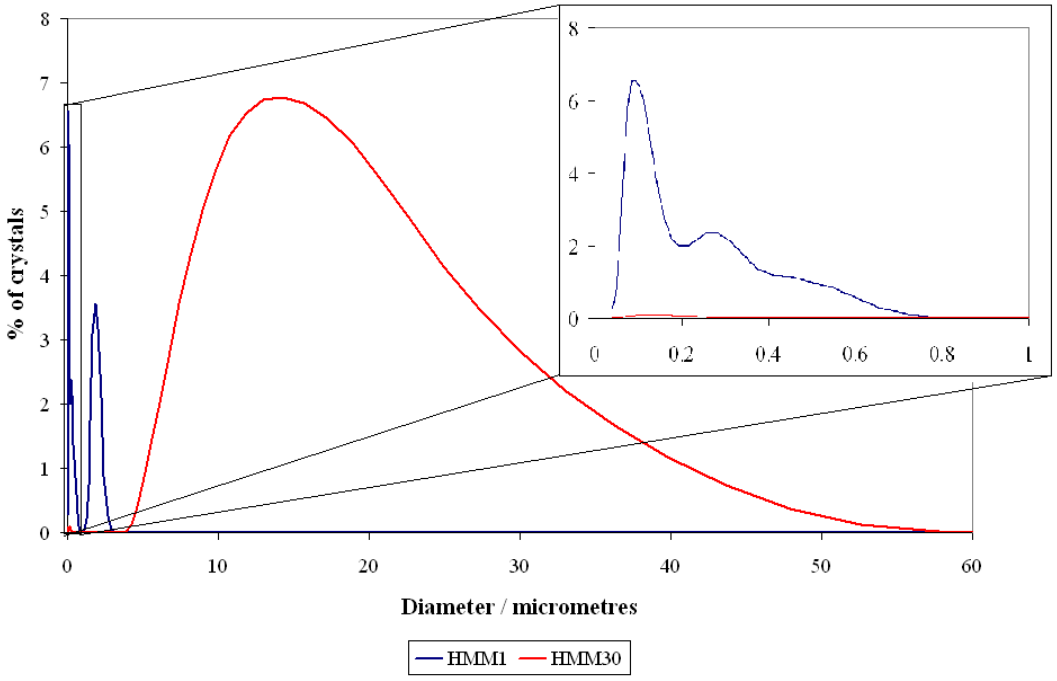

Figure 81: Graph showing the laser diffraction results from experiments HMM1 and HMM30 – taken 20 hours after mixing the microemulsions. A magnification of the portion of the graph from 0 – 1 μm is shown as well.

The laser diffraction results in Figure 81 show the importance of confinement when comparing microemulsions and nanoemulsions. Experiment HMM30 used twice the mass of reactants that HMM1 did. As a result, the droplet size was much larger, forming a nanoemulsion. The range of crystal sizes detected then is much greater in

experiment HMM30 – from 5-55 μm compared to 0.05-3.0 μm in experiment HMM1.

It should be noted that despite the large standard deviation, the range of particle sizes is still smaller when compared to the direct addition experiments which also had an excess of reactants added. Therefore, mixed microemulsions are the better way to obtain a more uniform crystallite size.

SAXS analysis

Using the Bruker Nanostar machine, GIFT analysis was carried out by the technician Helen Riggs on both the group of separate microemulsions (which contained only one reactant each) and the final microemulsions formed after mixing to find the droplet sizes 18 hours after microemulsion formation. As an example, the graphs obtained from SAXS analysis and GIFT analysis for the experiment with reactant concentrations of 0.1 M are shown in Figure 82 and 83:

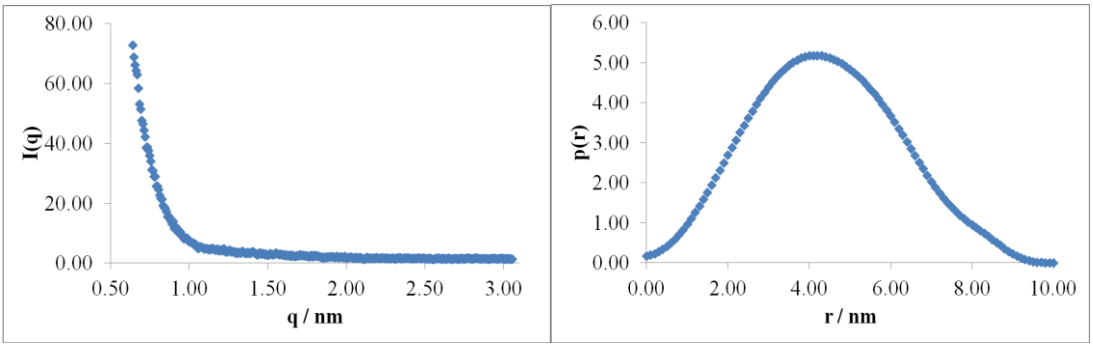

Figures 82 and 83: SAXS curve (fig. 82) and p(*r*) curve (fig. 83) for the hydroxyapatite synthesis experiment involving 0.1 M reactants.

The particle size was calculated from the graphs and GIFT analysis to be 4.34 nm.

The SAXS results from the microemulsions containing the separate reactants are shown in Table 29:

Reactant contained in microemulsion	**Droplet size / nm**
$CaCl_2$	1.89
NH_4OH	1.99
$(NH_4)_2HPO_4$	2.10

Table 29: SAXS data showing the droplet sizes of the microemulsions containing the separate reactants.

The differences in size are very small. Perhaps more importantly, all the samples produced a positive result for a particle size. This means that droplet microemulsions are formed, rather than bicontinuous solutions or simple solutions and are maintained throughout the process, and that nanoconfinement of materials is achieved.

TEM analysis

Using the JEOL 2100F FEG Transmission Electron Microscope, bright field images of the crystals could be taken and studied. Figures 84 a) and b) & Figures 85 a) and b) show images taken from mixed microemulsions using 0.1 M and 0.08 M reactants respectively:

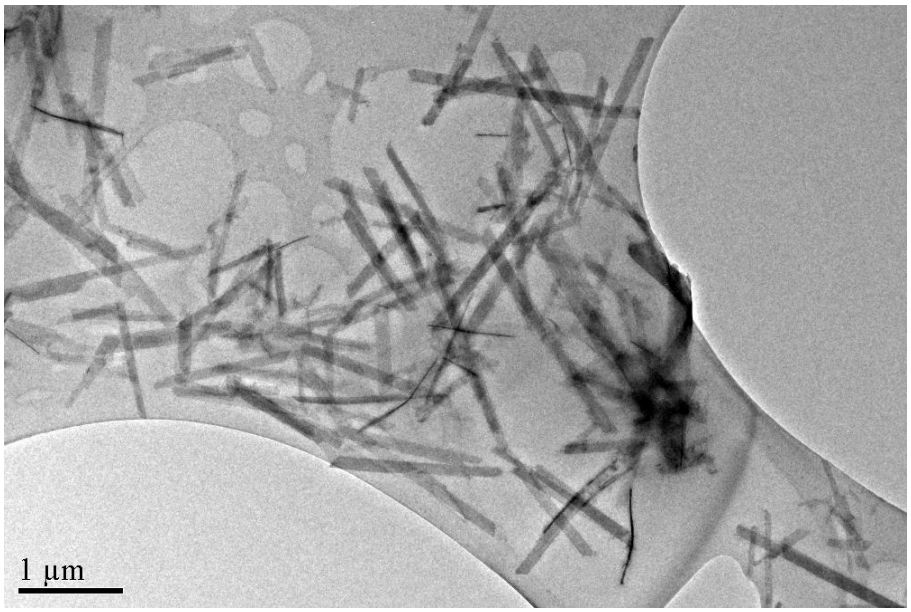

Figure 84 a): TEM bright field image of HAP crystals grown from microemulsions after 1 week. Concentration of reactants were 0.1 M $CaCl_2$, 0.1 M NH_4OH and 0.1 M $(NH_4)_2HPO_4$.

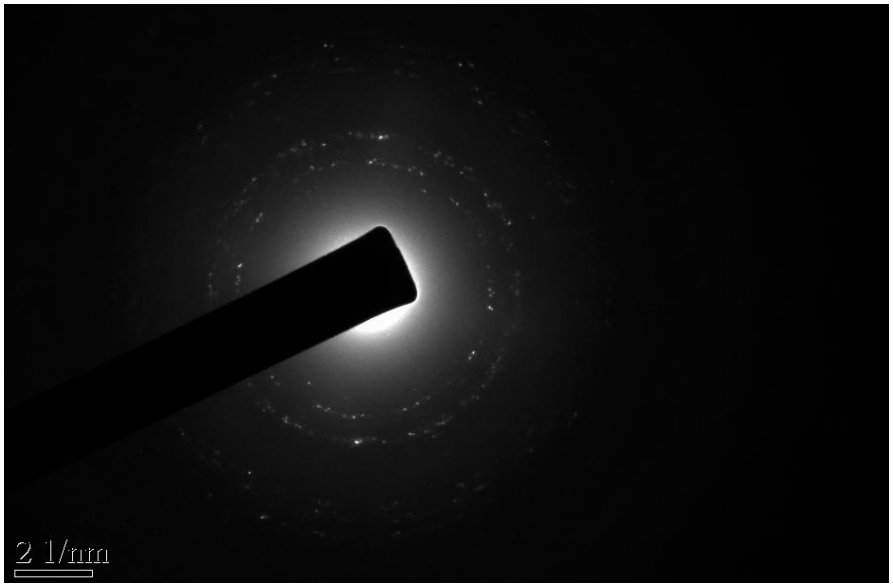

Figure 84 b): Electron diffraction pattern obtained from the bright field image in Figure 84 a).

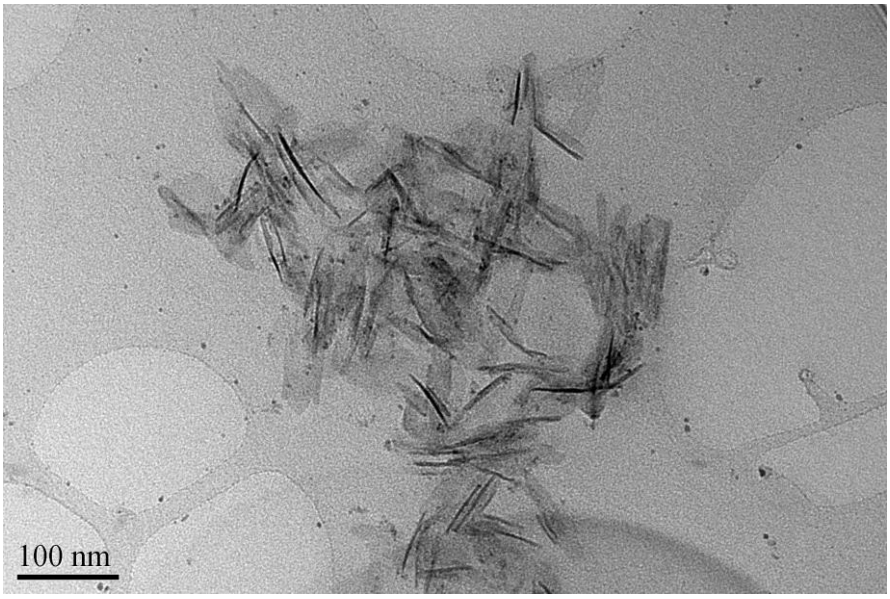

Figure 85 a): TEM bright field image of HAP crystals grown from microemulsions after 1 week. The concentration of all reactants was 0.08 M.

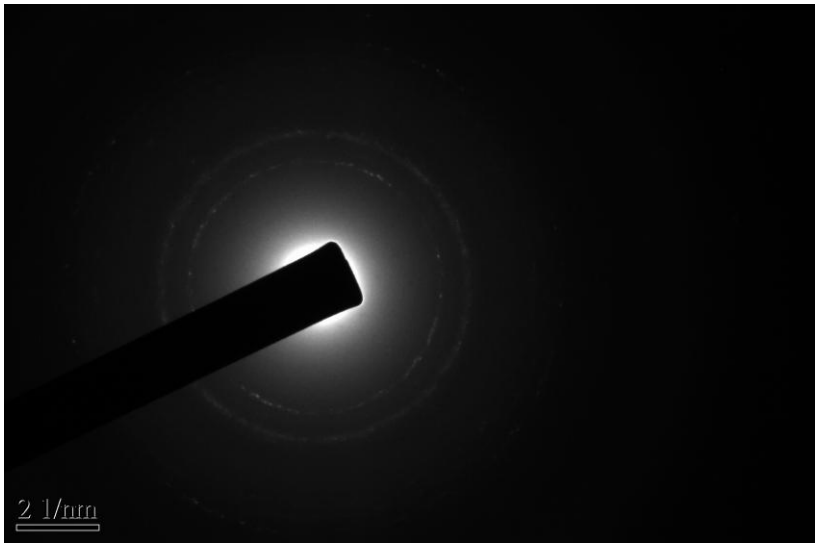

Figure 85 b): Electron diffraction pattern obtained from the bright field image in Figure 85 a).

Both experiments were analysed after 1 week, and the crystals seen in Figures 84 a) and 85 a) are needle-like. In both Figures 84 b) and 85 b), the two inner rings give d-spacings of 3.18 Å and 2.62 Å, showing that the same product is produced. In addition, these values correspond well to the values obtained by Koutsopoulos for the [102] and [202] planes of hydroxyapatite.[121] There is still a good correlation between concentration of reactants and the particle size, with the crystals produced in Figure 83 a) being between 1 – 2 µm and the crystals in Figure 85 a) having lengths of 100 nm.

In addition to the images obtained by TEM, elemental analyses were performed on the experiments involving the 0.1 M reactants (see Figure 86):

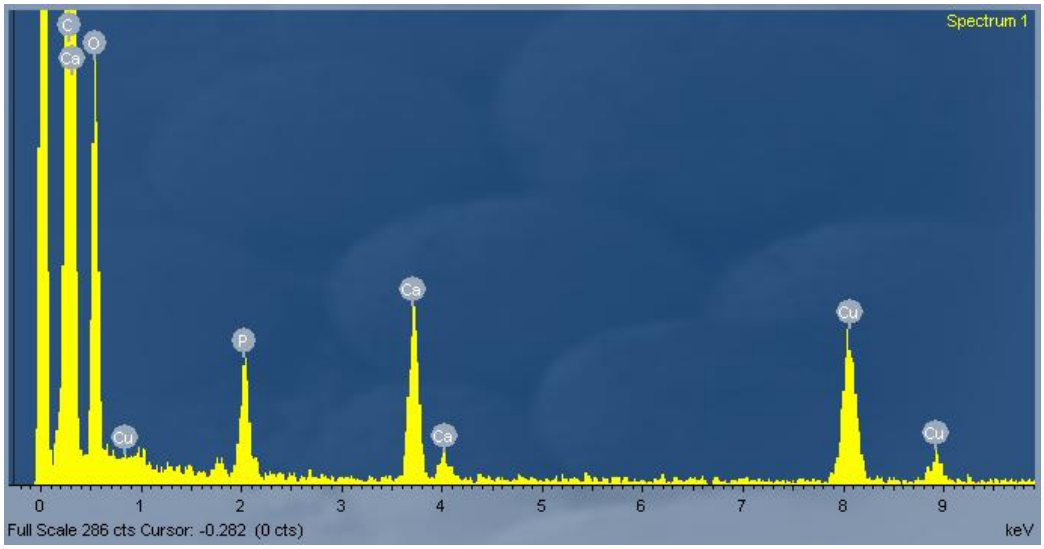

Figure 86: Energy-dispersive X-Ray spectrum of the mixed microemulsion experiment HMM1 (0.1M reactants).

From Figure 86, all the peaks can be defined and explained. The copper peaks at 0.8, 8.0 and 8.9 keV are due to the copper grid used to hold the samples. The carbon peak at 0.3 keV is due to the carbon film on the copper grid. The oxygen, phosphorous and calcium peaks correspond possibly to hydroxyapatite. To fully confirm that hydroxyapatite is present, the height proportions of the phosphorous and calcium peaks between 2 and 4.5 keV should be analysed. Adding the heights of the two calcium peaks, and dividing by the height of the phosphorous peak gives an answer of 1.61 – very close to the given Ca/P ratio of 1.615. Therefore, it can be said that hydroxyapatite has been formed in the microemulsion, and that it is the dominant product.

5.4 Obtaining amorphous hydroxyapatite

Both direct addition and mixed microemulsion methods were used, with some modifications, for the purpose of obtaining amorphous hydroxyapatite. This was to show that the rate of addition of reactants is important when determining the degree of crystallinity. The modified methods are described below.

5.4.1 Methods

For the direct addition method, the concentrations of the reactants were increased to values in the range 1.0 - 4.0 M. The experiments were carried out at 30 °C as before, with 0.9 – 1.1 g of ammonium hydroxide and 1.1 – 1.5 g of ammonium phosphate added to each sample. Instead of adding small amounts over a period of time, each reactant was added in one addition, with just 20 seconds mixing between each addition. A white precipitate was formed immediately, and was extracted by centrifuge. Drying and washing processes then took place as before. The details of each experiment are shown in Table 30.

Utilising the mixed microemulsions technique, again the concentrations of the reactants was increased to values in the range 1.0 – 4.0 M. Because of the higher concentrations, formation of a white compound (assumed to be hydroxyapatite) formed over a period of roughly 2 hours, compared to 24 hours in previous mixed

microemulsion experiments. Extraction, washing and drying of samples took place as before. Details of the experiments are shown in Table 31:

Sample Name	Rate of $(NH_4)_2HPO_4$ addition	$CaCl_2$ conc.	NH_4OH Added / cm^3	$(NH_4)_2HPO_4$ Added / g
HAP1fast	0.5cm^3 / min	0.1M	0.9 - 1.1 (0.1M)	1.1 - 1.5 (0.1M)
HAP1vfast	One addition	0.1M	0.9 - 1.1 (0.1M)	1.1 - 1.5 (0.1M)
HAP1-1Mreag	One addition	1.0M	0.9 - 1.1 (1.0M)	1.1 - 1.5 (1.0M)
HAP1-2Mreag	One addition	2.0M	0.9 - 1.1 (2.0M)	1.1 - 1.5 (2.0M)
HAP1-4Mreag	One addition	4.0M	0.9 - 1.1 (2.0M)	1.1 - 1.5 (4.0M)
HAP1-4Mreag(4)	One addition	4.0M	0.9 - 1.1 (4.0M)	1.0 - 1.2 (4.0M)

Table 30: Direct addition experiments designed to obtain amorphous hydroxyapatite. In all cases, the volume of the surfactant stock solution was 10.0 cm^3, the volume of calcium chloride solution was 5.0cm^3, and the ammonium hydroxide and the ammonium phosphate were added in one addition. Since all the experiments were based on Experiment HAP1 with regards to the volumes of the stock solution and the calcium chloride solution, a nanoemulsion was formed every time when the two solutions were mixed.

	Microemulsion 1		Microemulsion 2		Microemulsion 3	
Sample Name	Surfactant Stock Solution / cm^3	$CaCl_2$ / cm^3	Surfactant Stock Solution / cm^3	NH_4OH / cm^3	Surfactant Stock Solution / cm^3	$(NH_4)_2HPO_4$ / cm^3
HMM1amor	3.0	0.3 (1.0M)	3.0	0.3 (1.0M)	3.0	0.3 (1.0M)
HMM2amor	3.0	0.3 (1.0M)	3.0	0.3 (1.0M)	3.0	0.3 (0.2M)
HMM3amor	3.0	0.3 (2.0M)	3.0	0.3 (2.0M)	3.0	0.3 (2.0M)
HMM4amor	3.0	0.3 (4.0M)	3.0	0.3 (2.0M)	3.0	0.3 (4.0M)
HMM5amor	3.0	0.3 (4.0M)	3.0	0.3 (4.0M)	3.0	0.3 (4.0M)

Table 31: Mixed microemulsion experiments designed in an attempt to obtain amorphous hydroxyapatite.

5.4.2 Results

Direct Addition Experiments

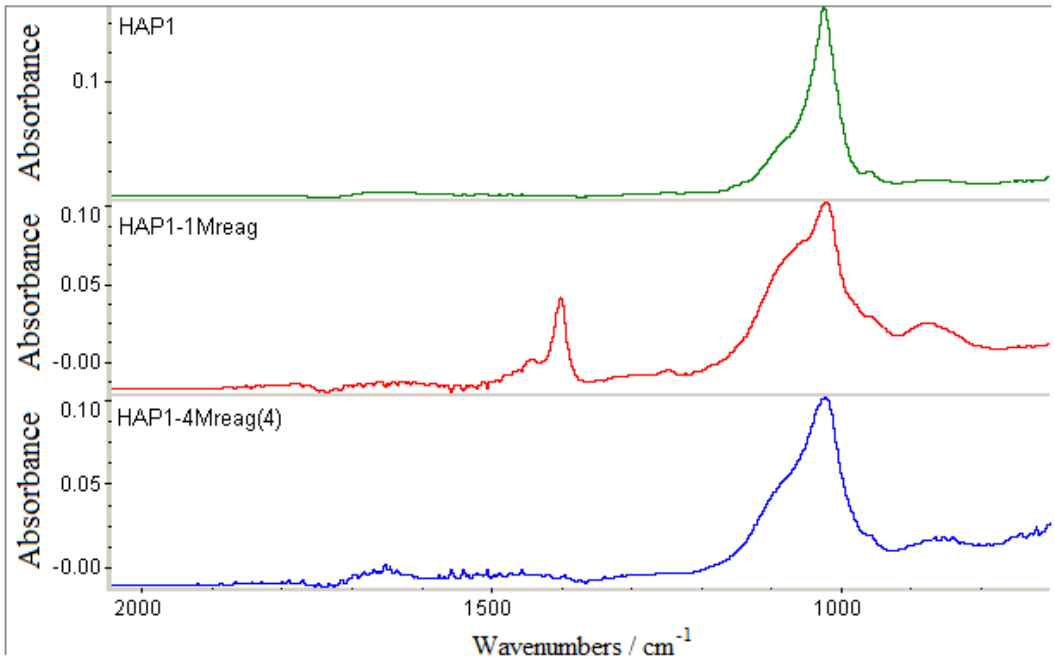

Figure 87: FTIR ATR spectra of experiments where the concentrations of reactants have been varied. The top spectrum used the normal concentrations (0.1 M calcium chloride, 0.08 M ammonium hydroxide, 0.06 M ammonium phosphate), the middle spectrum used 1.0 M reactants, and the bottom spectrum used 4.0 M reactants.

The IR spectra in Figure 87 show a trend in decreasing crystallinity for the 1.0M and 4.0 M reactants compared to the 0.1 M reactants – indicated by the peak at ~ 1040 cm^{-1} broadening. The anomalous peaks found with the 1.0 M reactants are likely due to an excess of ammonium phosphate – given the peak at ~1400 cm^{-1} is prominent in both spectra.

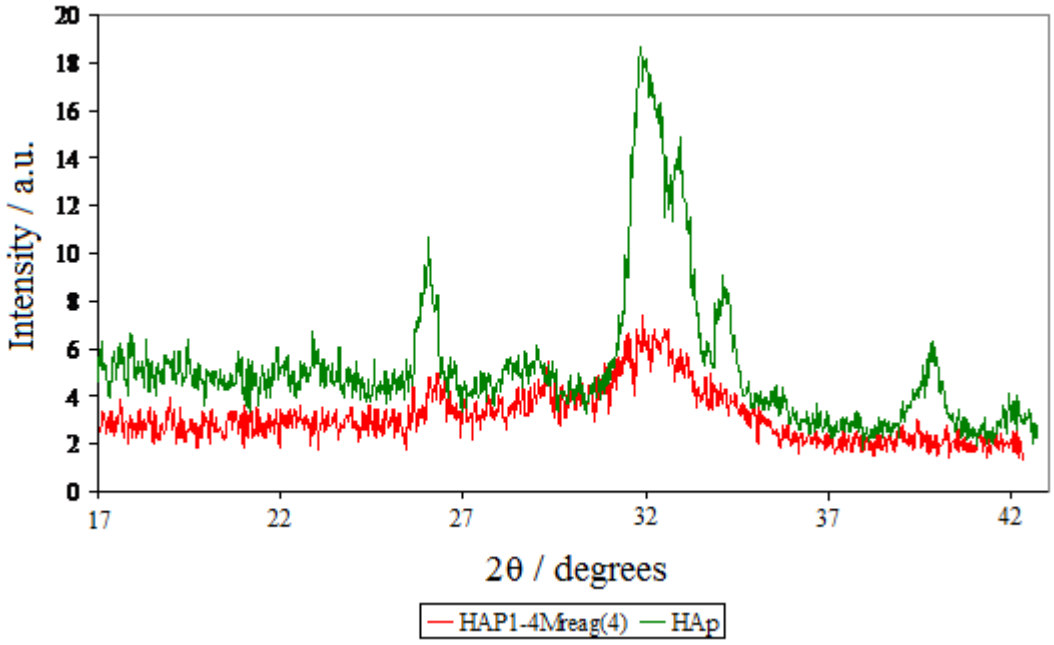

Figure 88: XRD patterns for experiment HAP1-4Mreag(4) and as-received HAP.

The effect of amorphous HAp (spectrum HAP1-4Mreag(4)) on the diffraction patterns can be seen in Figure 88. Just two weak and broad peaks can be seen – and the large set of peaks at ~ 29° has become one broad peak.

Mixed Microemulsion Experiments

With the large increase in reactant concentrations, it was difficult to maintain microemulsions. Often a precipitate would crystallise out immediately after all the reactants had mixed. However, two experiments produced crystals for analysis – HMM3amor and HMM4amor (see Table 29). The XRD patterns obtained are shown in Figure 89:

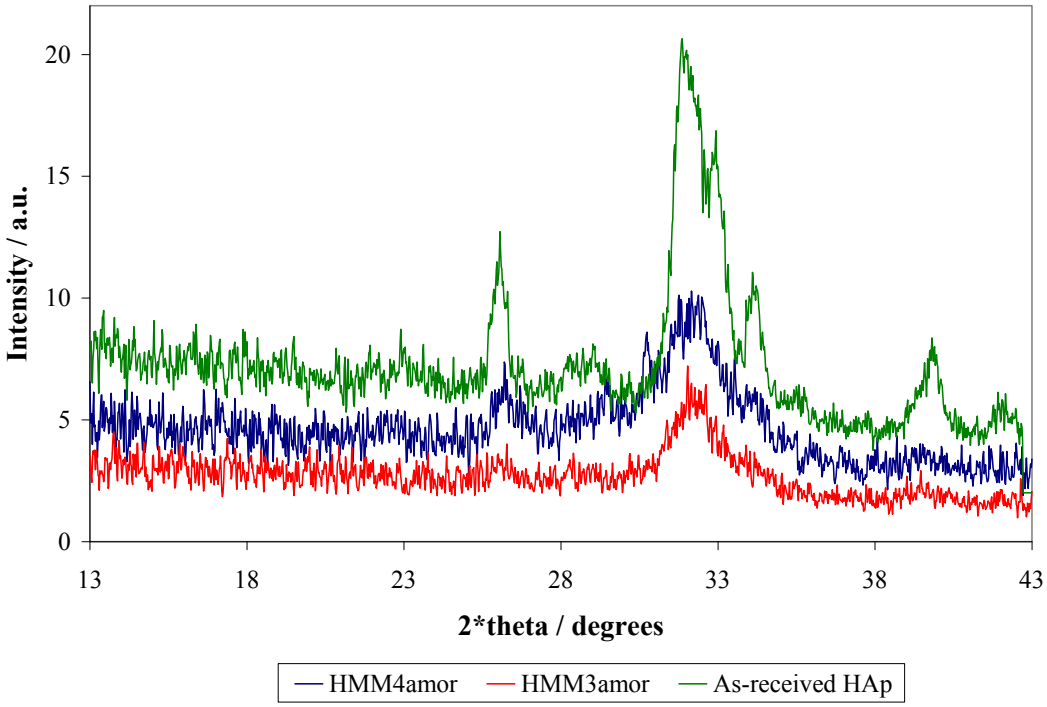

Figure 89: XRD patterns of two of the mixed microemulsion experiments designed to obtain amorphous HAp. As-received HAp (reagent grade) is shown for comparison.

The two experiments are very similar with regards to peak heights and widths. The large peak at 32° is still visible and the small, but broad peak can be seen at 26°. Importantly, both are missing many peaks that the as-received HAp shows. This shows that the solid product made is relatively amorphous in nature, but slightly less so than the fastest reactions carried out using direct addition methods.

5.5 Discussion

Despite the huge numbers of compounds associated with the apatite family of minerals, both direct addition and mixed microemulsion methods produced crystals with the correct molecular formulas. This shows that the proportions of each reactant used were more than adequate for the experiments, and that the addition of ammonium hydroxide does aid the synthesis of HAp by increasing the pH. All the different types of experiment carried out correspond well to pre-synthesised hydroxyapatite (reagent grade). But more than the others, the mixed microemulsion experiments give the best correlation.

The final set of experiments (obtaining amorphous hydroxyapatite) were carried out to show that despite the simple synthesis of HAp, the right concentration of reactants and the microemulsion environment must be used to ensure a degree of crystallinity within the final sample. This is harder to quantify when nanosized particles are synthesised, because in such a small crystal, a much higher proportion of molecules will be at the exposed surfaces so broadening of XRD peaks will occur.

The results of this chapter highlight that in order to produce uniformly-sized HAp crystals with good crystallinity, a mixed microemulsion method using low reactant concentrations is required. More amorphous product is produced with fast, direct addition of higher concentration reactants or with high concentration reactants in the mixed microemulsion experiments. This shows again that a more crystalline product is obtained when working under conditions closer to those at which crystallisation is just possible. This chapter improved on the studies of Li *et al.* who used only direct addition methods to obtain hydroxyapatite, and required calcinations to obtain crystalline product.[112] The direct addition experiments were able to determine numerical values for the amounts of ammonium hydroxide (0.9 – 1.1 g) and ammonium phosphate added (1.0 – 1.5 g), thereby giving some clarity as to how much needed to be added to produce hydroxyapatite with good crystallinity. Laser diffraction analysis was able to determine particle sizes of $50 \leq d \leq 200$nm, which other analyses such as TEM would be more time-consuming in working out. For the mixed microemulsion experiments, nanoparticles were picked up via TEM analysis, and found to be of a comparable size to previous results. Through the mixed microemulsion results, the crystals produced were very similar when analysed alongside bought-in hydroxyapatite. The results compare even more favourably with the work of Koumoulidis *et al.* The untreated hydroxyapatite that the group produced was of poor crystallinity – as evidenced by the X-Ray diffraction patterns obtained, which had just one wide peak visible in the region 30 - 33° (2θ value).[115] Throughout, the crystallinity of our samples was excellent, and there was little need to calcine the finished products to give a product similar to in-bought hydroxyapatite.

Overall, a good comparison relating speed of reaction to the degree of crystallinity can be drawn (see Figure 90). The nanoconfinement afforded by mixing the microemulsions gives a product similar to in-bought HAp:

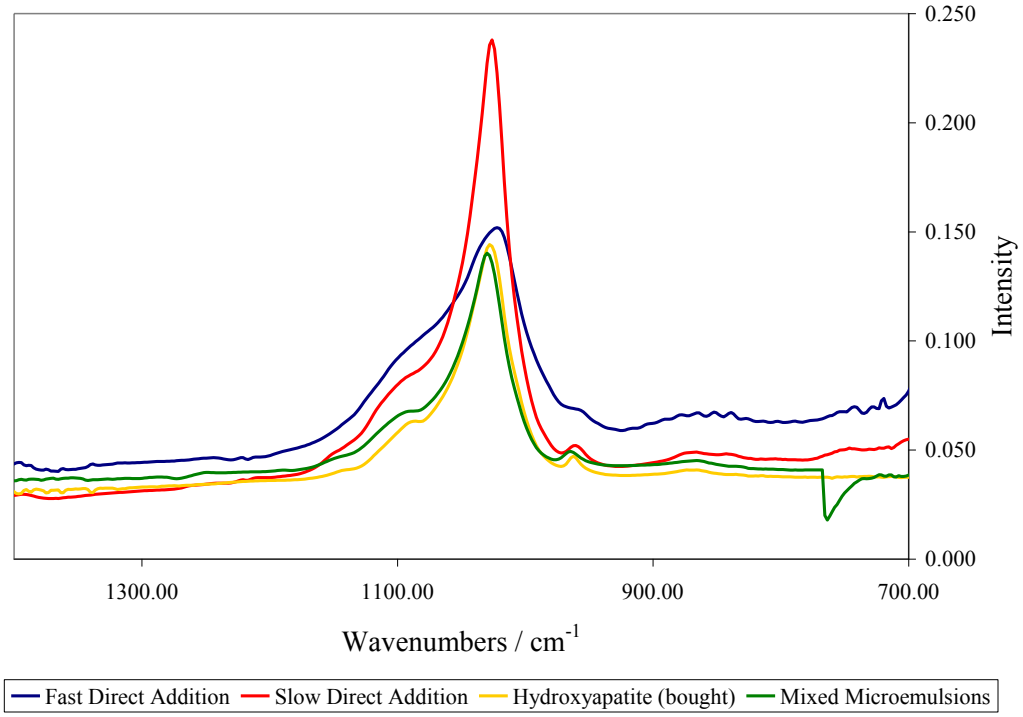

Figure 90: Comparison of FTIR ATR spectra from one of each type of experiment. 'Bought hydroxyapatite' is of reagent-grade purity.

5.6 Conclusions

Hydroxyapatite crystals were made via two different methods with the same reactants. In the first, ammonium hydroxide and ammonium phosphate solutions were added to nanoemulsions and microemulsions containing calcium chloride as the dispersed phase. The crystals precipitated out within an hour, and subsequent analysis showed that the right form of apatite was synthesised, and that the final product was crystalline. Subsequent experiments performed at a faster rate gave the amorphous form.

The second method utilised a "mixed microemulsion" method, where three microemulsions, each containing one of the reactants, were mixed to form a single microemulsion. Crystals of 0.1 – 3.0 nm formed after 24 hours, and after washing, were found to be of excellent crystallinity and purity, with results corresponding well with bought-in hydroxyapatite (reagent grade). Laser diffraction analysis showed that not only were the crystals smaller (in comparison to the sizes of 5.0 – 40.0 nm for the direct addition methods), but also that the range of crystal sizes was much smaller. This method is therefore more preferable when trying to synthesise HAp nanocrystals.

6. Synthesis of Titanium Dioxide Through the Use of Microemulsions

6.1 Introduction and Theory

Titanium dioxide, also referred to as titania, has for many years been crucial to many parts of research and industry. For the last 50 years, it has been studied with reference to its photocatalytic properties, and its subsequent use in photoelectrochemical (PEC) solar cells. One of the most important experiments which utilised titanium dioxide was the splitting of water.[122-124] This involves a process in which water is broken down into hydrogen and oxygen. The equation for the reaction is $2H_2O \rightarrow 2H_2 + O_2$. With hydrogen-based fuels becoming a major discussion point in recent years, much research has gone into finding efficient ways to carrying out the process on a large scale to deliver sufficient amounts of fuel for a small cost. Fujishima *et al*. discovered that the water splitting reaction could be catalysed if a titanium dioxide surface was present to act as the catalyst.[122] Further work by Khan *et al.* used the techniques of flame pyrolysis on a titanium sheet in an attempt to increase the absorption of photons.[125] Alternative methods have included using nitrogen doping of titanium dioxide to improve photon absorption[126] and doping using metal ions.[127]

Many other uses of titanium dioxide have been suggested in the last 20 years. Ferroni *et al.* tested the ability of thin films of titania to act as a gas sensor.[128] Using nitrogen dioxide as a test gas, a concentration as small as 1 part per million (ppm) could be detected, and at higher temperatures, the amount required for detection shrank to 0.02 ppm. This led to subsequent work by Baraton *et al.*, who combined titania with poly(p-phenylenevinylene) to make a device to detect oxygen, and also Savage *et al.*, who combined titania with lanthanum and copper oxides to make a carbon monoxide sensor.[129, 130]

Using electrochemical techniques, titanium dioxide can be reduced to obtain titanium metal via the FFC Cambridge Process.[131] This is a favourable alternative to using titanium tetrachloride in methods such as the Kroll Process, where partial

reduction can take place.[132] Also, a purification process is not needed, compared to the Kroll process, where purification and extra solidifying and re-melting processes are carried out. Further chemical processes using titanium dioxide include the synthesis of titanium carbide – which has found a widespread use as a material for tool bits.[133]

6.1.1 Properties and polymorphism of titanium dioxide

Titanium dioxide has three well-known polymorphs which can be made without specialist techniques such as doping and ball milling.[134, 135] These are brookite, anatase and rutile, in order of increasing stability. All three polymorphs are based on arrangements of TiO_6 octahedra (see Figures 91 a), b) and c)).[136] The relative stability of each polymorph can be related to the volume of the unit cell – since rutile takes up the least amount of space, its stability is greater. Rutile and anatase are both related by their unit cells being tetragonal, while brookite has an orthorhombic unit cell (see Table 32). A fourth polymorph can be obtained under high pressures, which has a lead oxide-type structure.[135, 137-139] Rutile is widely used as a pigment in white paints and other white-coloured materials. In fact, this is the single greatest use of titanium in any commercial avenue.

All the polymorphs occur naturally, and can therefore be mined relatively simply. They can also be produced through the alteration of other naturally-occurring minerals, such as ilmenite and leucoxene.[140, 141]

		Unit cell dimensions / Å			Angles / °		
Polymorph	Space Group	a	b	c	α	β	γ
Brookite	Pbca	9.184	5.447	5.145	90	90	90
Anatase	$I4_1/amd$	3.784	3.784	9.515	90	90	90
Rutile	$P4_2/mnm$	4.593	4.593	2.959	90	90	90

Table 32: Details of the unit cells of the three main polymorphs of titanium dioxide.[142, 143]

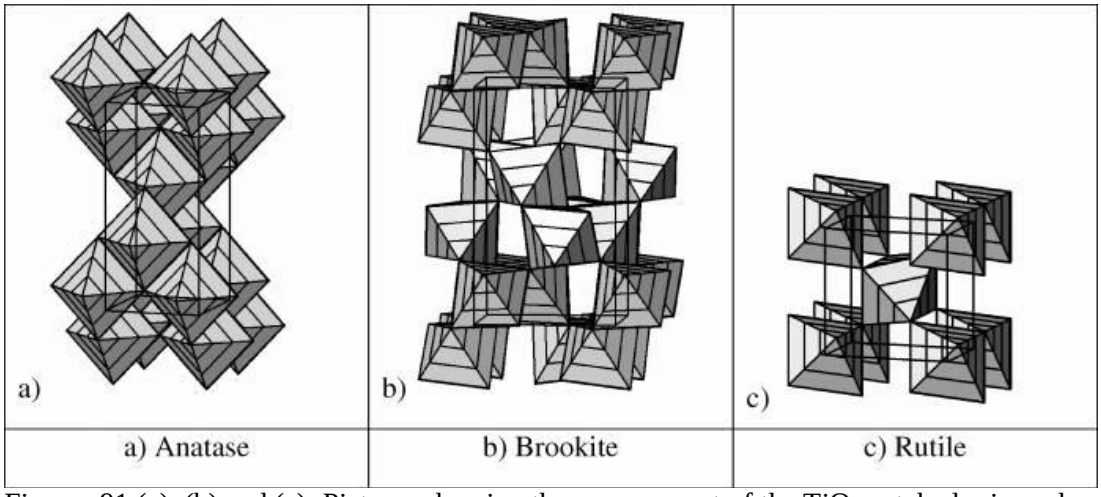

Figures 91 (a), (b) and (c): Pictures showing the arrangement of the TiO_6 octahedra in each of the main polymorphs of titanium dioxide.[136]

Using the techniques described previously, both the synthesis and the control of polymorphism of TiO2 can be carried out.

6.1.2 Titanium dioxide nanoparticle synthesis in the literature

Many methods for synthesising titania nanoparticles have been suggested. Kolen'ko *et al.* were able to make titanium dioxide quickly using a mixture of titanium chloride and hydrochloric acid.[144] The final product, however, was amorphous in character and a further step was required to make nanostructures.[145] While Berger was able to synthesise titanium carbide from titanium dioxide, Li *et al.* were able to carry out the reverse reaction, using thermal plasma oxidation to synthesise titanium dioxide spheres.[146] Though control of size was achieved after a sedimentation separation of the primary product, X-Ray diffraction showed that a mixture of polymorphs (rutile and anatase) was formed. Also, very high temperatures (up to 10,000 °C) are needed to make spheres of the products. Furthermore, the polymorph of the product was not specified. Diffusion flame reactors have also been utilised to make nanoparticles.[147, 148] The experiments of Jang *et al.* were able to give particle sizes between 10 and 30 nm using temperatures of ~ 1000 °C but again, a mixture of anatase and rutile was also formed – the percentage of anatase being between 41 and 80 %.[148] Hydrothermal techniques have also been used to make titanium dioxide, but relatively high temperatures (100 °C)

and volatile reactants (hydrogen peroxide) are required.[149] Consequently, high temperatures and/or pressures are typically needed to crystallise the titanium dioxide polymorphs. In contrast, this thesis will show that titanium dioxide can be synthesised in microemulsions at room temperature. Furthermore, the most stable polymorph of titanium dioxide, namely rutile, can be produced and the final product is crystalline without the need for further calcination.

The experiments carried out in this thesis use titanium isopropoxide (TIPO) as a starting material, which reacts with water to form titanium dioxide. The overall equation for the reaction is as follows:

$$Ti(OCH(CH_3)_2)_4 + 2H_2O \rightarrow TiO_2 + 4(CH_3)_2CHOH \qquad (17)$$

The reaction is similar to that of sol-gel syntheses of metal oxides, which have three distinct steps – a hydrolysis reaction, followed by polycondensation reactions and a dealcoholation step.[150-152] The general process is as follows: the first step involves the metal alkoxide reacting with water to form a metal hydroxide:

$$M-OR + H_2O \rightarrow M-OH + R-OH \qquad (18)$$

Polycondensation reactions then occur to transform the metal hydroxides and alkoxides into a metal-oxygen-metal network. Metal hydroxides may react with each other to form the same network via a dealcoholation step:

$$M-OH + M-OR \rightarrow M-O-M + R-OH \qquad (19)$$

$$M-OH + M-OH \rightarrow M-O-M + H_2O \qquad (20)$$

The pH of the reaction is very important as this can determine many factors including yield and morphology. Sugimoto *et al.* found that increasing the pH above 8.0 resulted in the yield of TiO_2 decreasing.[153] Indeed at a pH value of 11.6, the yield was close to 0 %. By contrast, Yue *et al.* found that ferrite networks were better synthesised when the pH was less acidic.[154] Other effects of pH on the process include the ability to incorporate other metal-containing compounds into the gel.[155] These findings can be applied to microemulsion synthesis of titanium dioxide to obtain the best results. Both the Sugimoto and Yue groups found that reducing the pH level to 2.0 – 6.0 reduced the particle size of metal oxides. Further work by

Engelhardt *et al.* and Yordas found the presence of an acid increases the rate of hydrolysis, but lowers the rate of the condensation reaction.[152, 156-158] This is favourable for nanoparticle formation as the low pH prevents gelling of the particles. Work carried out by Finnegan *et al.* has shown that rutile is more stable and likely to be synthesised if the pH of the system is highly acidic. Therefore, hydrochloric acid is used both as a reactant and as a buffer-type solution in our work to reduce the reaction rate and prevent an amorphous gel from forming. The crystallinity of titanium dioxide is also an important requirement in synthesis – with regards to photocatalytic activity. In particular, the ability of amorphous titanium dioxide to act as a photocatalyst was found to be negligible.[159]

6.2 Materials and Methods

Triton X-100 (laboratory grade), 1-hexanol (reagent grade 98%) and titanium isopropoxide (TIPO – 97%) were obtained from Sigma-Aldrich. Cyclohexane (analytical standard) was obtained from Fluka.

Stock solution of various concentrations were made up, according to the mass ratio of surfactants to cyclohexane phase – a 30 : 70 surfactant : oil ratio was used. 1.75 g aliquots were taken from this stock solution and separated into pairs. To one of the solutions was added 2.0 M hydrochloric acid of volumes between 20 and 200 µl, forming a microemulsion. To the other, titanium isopropoxide (TIPO) was added, again in volumes between 20 and 200 µl, to form a solution. The microemulsion and the solution were mixed together and left at room temperature (296 K). Crystals grew over a period of 4 - 6 days, and were subsequently extracted, washed and dried. This is known as the mixed or multiple microemulsion method.[160]

Various analyses were carried out on the dried samples, including TEM, FTIR ATR spectroscopy and powder X-Ray diffraction. Small-angle X-Ray scattering (SAXS) and laser diffraction particle sizing were used on the microemulsions themselves at various stages of the process.

The results of each experiment are shown in Figure 93, with further details about the experiments shown in Tables 33 a), 33 b) and 33 c).

IMPORTANT NOTE

All experiments will be referred to by the volumes of TIPO and hydrochloric acid added to the microemulsions. For example, experiment 180 + 200 will refer to an experiment where the number 180 refers to the volume of TIPO added (in microlitres). The second number is the volume of hydrochloric acid added (also in microlitres). Any following symbols, numbers or letters will be explained when the experiment is discussed.

6.3 Results

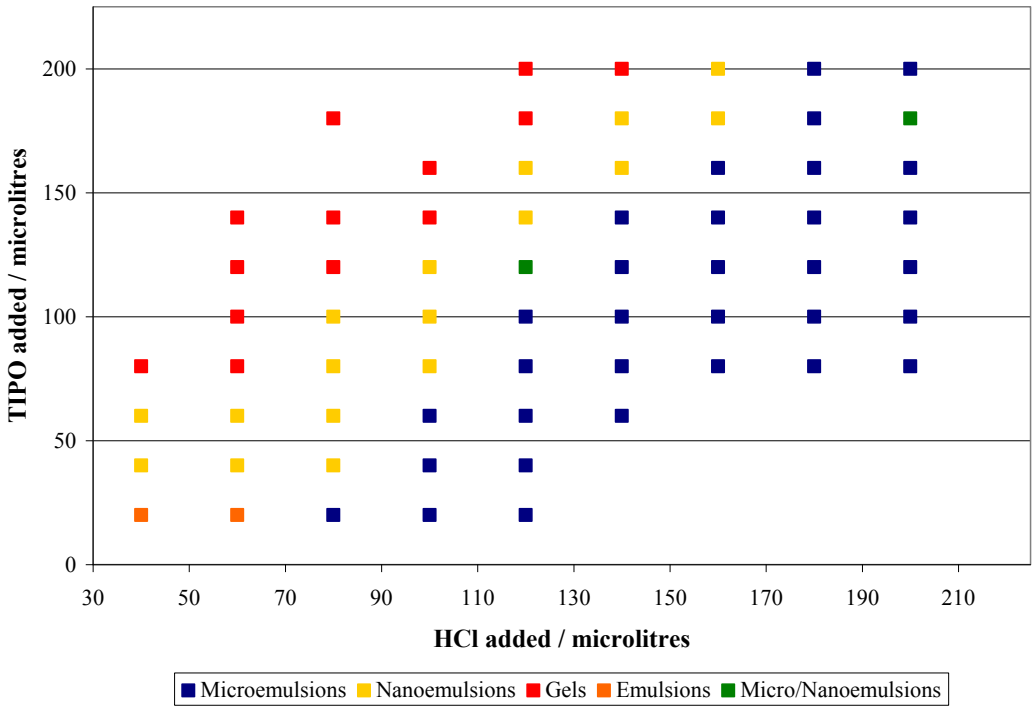

Figure 92: Graph showing the outcomes of mixing microemulsions when the volumes of HCl and TIPO are varied. Observations were noted 2 minutes after the microemulsions were mixed.

Overall, using a 1:1 ratio of HCl : TIPO or more gave a microemulsion, whilst lower levels of acid usually tended to give nanoemulsions, emulsions and gels (see Figure 92). Above additions of 100 µl, a 1 : 1 and greater ratio of TIPO to hydrochloric acid gave a microemulsion. Below 100 µl, the ratio required was 1 :

1.66. With fewer anomalies observed throughout the experiments, it became easier to determine the limits to what proportions of chemicals can be added to keep a microemulsion. The lower surfactant concentration had not affected the formation of microemulsions and as a result, the 30 % surfactant system was used throughout the rest of the investigation.

No changes in the appearance of the microemulsions were observed for 3 days. After 4 days, a blue colouration was observed, though the solution itself remained transparent. This blue colour could have been due to the replacement of water by $(CH_3)_2CHOH$, causing a nanoemulsion to form. However, laser diffraction analysis showed that the colouration was probably due to larger particles of the order 30-200 nm were also present, showing that new particles were indeed crystallising. These particles could have caused the blue colouration wholly, or in part (see Figure 93):

TIPO added / µL	HCl added / µL	OBSERVATIONS
20	20	Microemulsion
40	20	Microemulsion, WP after 5 hours, Gel after 3 days
60	20	Microemulsion, Gel after 2 days
80	20	Microemulsion, BC after 2 days, Gel after 9 days
20	40	Emulsion, Phase separation after 10 days
40	40	Nanoemulsion
60	40	Nanoemulsion, WP after 3 days
80	40	Gel
20	60	Microemulsion, Phase separation after 10 days
40	60	Nanoemulsion, WP after 3 days
60	60	Nanoemulsion, WP after 14 days
80	60	Gel
100	60	Gel
120	60	Gel
140	60	Gel
20	80	Microemulsion, BC after 10 days
40	80	Nanoemulsion, Microemulsion after 3 days, WP after 10 days
60	80	Nanoemulsion, WP after 3 days
80	80	Nanoemulsion, WP after 14 days
100	80	Nanoemulsion, WP after 14 days
120	80	Gel
140	80	Gel
180	80	Gel
20	100	Microemulsion, WP after 14 days
40	100	Microemulsion, BC after 7 days, WP after 14 days
60	100	Microemulsion, BC after 7 days, WP after 14 days

Table 33 a): Details of experiments shown in Figure 93. The letters BC in the observations column stand for Blue Colouration, which was often seen after a few days. Laser diffraction showed that these indicated the formation of new particles, rather than the formation of a nanoemulsion. The letters WP stand for White Precipitate – the larger crystals which formed after the blue colouration.

TIPO added / µL	HCl added / µL	OBSERVATIONS
80	100	Nanoemulsion, WP after 14 days
100	100	Nanoemulsion, WP after 14 days
120	100	Nanoemulsion, WP after 14 days
140	100	Gel, BC after 3 days, WP after 10 days
160	100	Gel, WP after 10 days
20	120	Microemulsion
40	120	Microemulsion, WP after 9 days
60	120	Microemulsion, BC after 6 days, WP after 13 days
80	120	Microemulsion
100	120	Microemulsion, BC after 4 days, WP after 14 days
120	120	Micro/Nano, BC after 4 days, WP after 14 days
140	120	Nanoemulsion, WP after 13 days
160	120	Nanoemulsion, WP after 13 days
180	120	Gel, Phase separation after 2 days (Temp. change?)
200	120	Gel
60	140	Microemulsion, WP after 6 days
80	140	Microemulsion, WP after 6 days
100	140	Microemulsion, BC after 3 days, WP after 10 days
120	140	Microemulsion, BC after 3 days, WP after 10 days
140	140	Microemulsion, BC after 4 days, WP after 7 days
160	140	Nanoemulsion, WP after 6 days
180	140	Nanoemulsion, WP after 10 days
200	140	Gel, WP after 9 days
80	160	Microemulsion, WP after 9 days
100	160	Microemulsion, BC after 3 days, WP after 10 days
120	160	Microemulsion, BC after 3 days, WP after 10 days

Table 33 b): Continuation of the details of the experiments from Figure 93. BC = Blue Colouration, WP = White Precipitate.

TIPO added / µL	HCl added / µL	OBSERVATIONS
140	160	Microemulsion, BC after 3 days, WP after 10 days
160	160	Microemulsion, BC after 4 days, WP after 7 days
180	160	Nanoemulsion, WP after 6 days
200	160	Nanoemulsion, WP after 6 days
80	180	Microemulsion, WP after 9 days
100	180	Microemulsion, WP after 9 days
120	180	Microemulsion, BC after 3 days, WP after 10 days
140	180	Microemulsion, BC after 3 days, WP after 10 days
160	180	Microemulsion, BC after 3 days, WP after 10 days
180	180	Microemulsion
200	180	Microemulsion, BC after 3 days, WP after 13 days
80	200	Microemulsion, WP after 9 days
100	200	Microemulsion, WP after 9 days
120	200	Microemulsion, BC after 3 days, WP after 10 days
140	200	Microemulsion, BC after 3 days, WP after 10 days
160	200	Microemulsion, BC after 3 days, WP after 6 days
180	200	Microemulsion, BC after 3 days, WP after 10 days
200	200	Microemulsion, BC after 4 days, WP after 7 days

Table 33 c): Continuation of the experiments in Figure 93. BC = Blue Colouration, WP = White Precipitate.

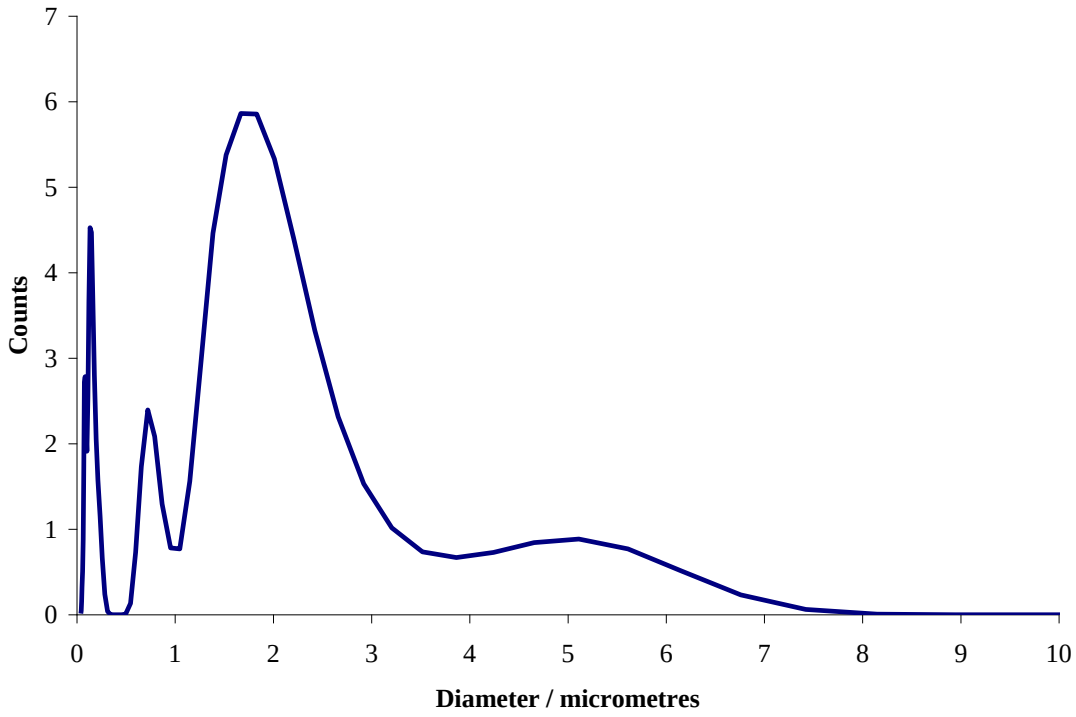

Figure 93: Graph showing the particle sizing of the microemulsion obtained through laser diffraction analysis, when the microemulsion had turned blue after four days (experiment added 200 µl TIPO to 200 µl hydrochloric acid).

As shown in Figure 93, one of the major peaks on the graph corresponds to diameters 30 – 200 nm. Further peaks at 800 nm, 2 µm and a wide peak at ~5 µm indicate that certain crystals are now larger than the droplets, and that they continue to grow by fusing or aggregating with other crystals which have broken out of the droplets. After a period of 1-2 weeks, the solution was mostly opaque, indicating that the bulk of the crystallisation had occurred. The solutions were centrifuged at 9000 rpm for 30-60 minutes, which separated the solid and liquid phases. It was noticed that after centrifuging, the liquid part remained as a single phase. This showed that the microemulsion was still stable, and therefore the blue colouration observed after 4 – 5 days could not be the formation of a nanoemulsion.

FTIR and XRD Analysis

Previous infra-red analyses had shown that the differences in spectra between the three polymorphs of titanium dioxide could be found in the region 500-800 cm^{-1}.[161, 162] In this region, the vibration modes of the O-Ti-O bonds appear. Because the IR spectrometer available could not accurately record spectra in that area, it could not be used solely to determine whether the polymorph rutile was formed. However, IR could still be used to determine whether titanium dioxide itself had been formed, since peaks in the region 1000-4000 cm^{-1} could be found and compared.[163] Four of the experiments were analysed – the details of each experiment are shown in Table 32 and the resulting FTIR spectra are shown in Figure 94:

TIPO added / µL	HCl added / µL	OBSERVATIONS
200	200	Microemulsion, BC after 4 days, White precipitate after 7 days
200	180	Microemulsion, BC after 3 days, White precipitate after 13 days
140	180	Microemulsion, BC after 3 days, White precipitate after 10 days
160	160	Microemulsion, BC after 4 days, White precipitate after 7 days

Table 34: Details of the four experiments which were analysed using FTIR-ATR spectroscopy. BC = Blue Colouration.

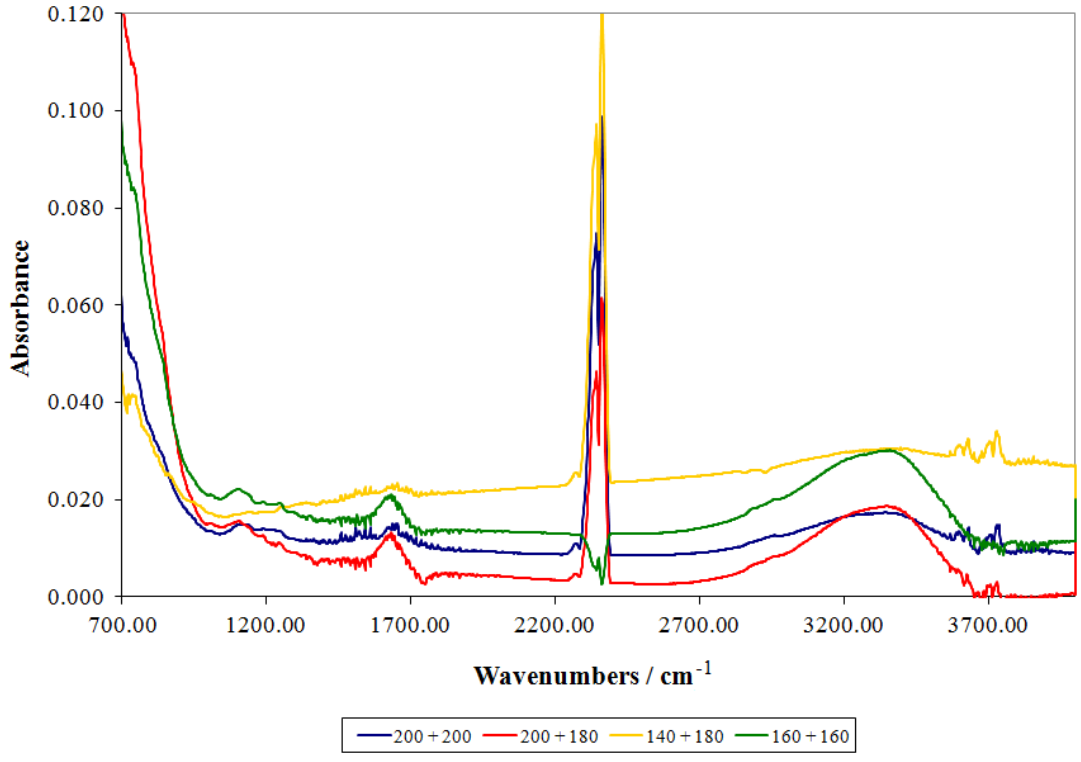

Figure 94: FTIR ATR spectra of four of the initial experiments (between 700 and 4000 cm^{-1}).

The main peak at ~ 2300 – 2400 cm^{-1} is due to the presence of CO_2 in the atmosphere, whilst the large, broad peak at 3000 – 3500 cm^{-1} corresponds to the presence of water. To find the proof, the area between 1000 and 2000 cm^{-1} needs to be magnified (see Figure 95):

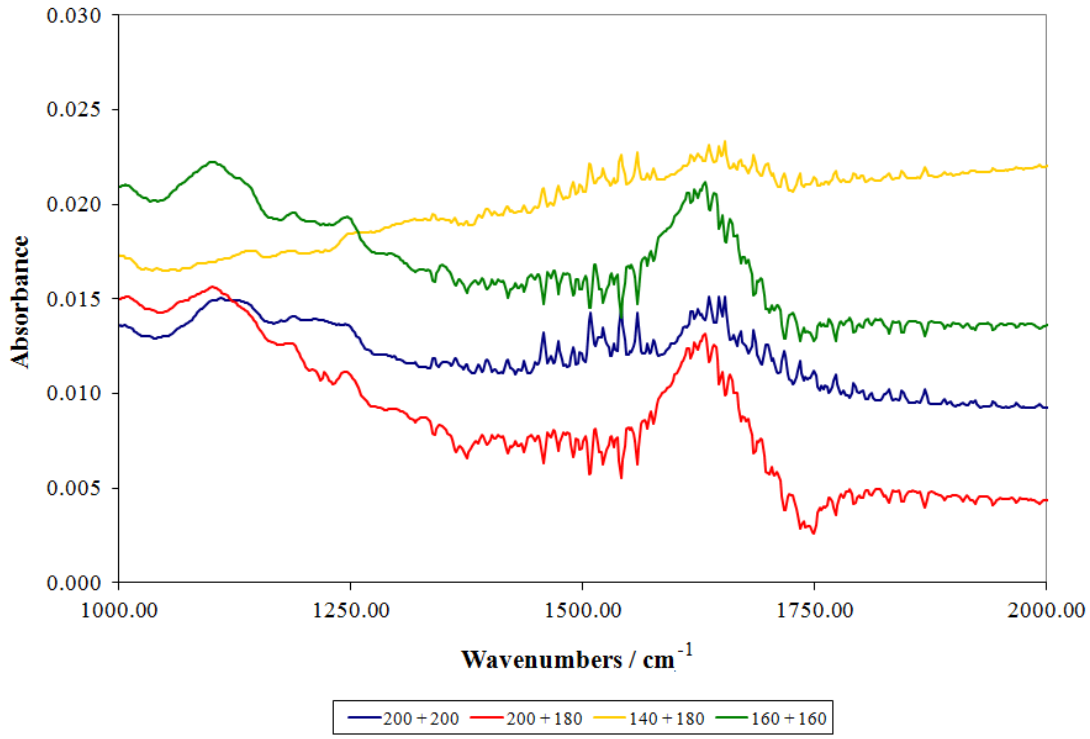

Figure 95: FTIR ATR spectra of four of the initial experiments. The spectra have been magnified to the range 1000-2000 cm^{-1}.

Having magnified part of the spectra, the defining peak at ~1630 cm^{-1} can now be seen clearly. This proves that titanium dioxide was synthesised, but it still does not confirm which polymorph (rutile, anatase or brookite) has been formed. X-Ray diffraction was used to verify the polymorph of titanium dioxide formed. The main peaks found when analysing anatase and rutile are detailed in Table 33:

TiO_2 Polymorph	Major Peaks (2θ / °)
Anatase	25, 38, 48
Rutile	27, 36, 41

Table 35: The major peaks found when performing X-Ray Diffraction on two polymorphs of titanium dioxide.[164]

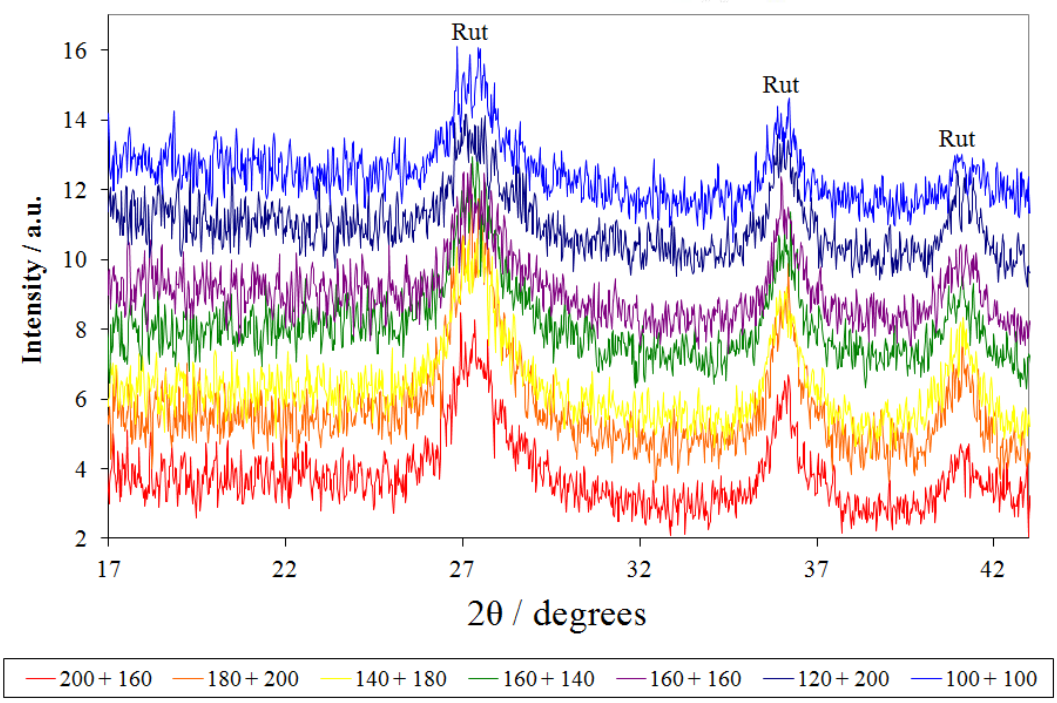

Figure 96: XRD results on 7 samples taken from the 30 % surfactant stock solution experiments. Rut = peak associated with the rutile polymorph.

Three peaks at 27, 36 and 41° can be easily defined in each pattern in Figure 96. These correspond well with peaks that rutile produces.[164-166] In all of the samples, no other peaks are present, suggesting that rutile is the only polymorph present in the final product.

Laser Diffraction Results

A LS13320 Laser Diffraction Particle Size Analyser was used to roughly determine the size of the particulates formed after a few days in the microemulsion. For these experiments, the volumes of the various reactants were scaled up in order to provide enough material for analysis. The details of these experiments are shown in Table 34 and the results are shown in Figures 97 and 97:

TIPO added / µL	HCl added / µL	OBSERVATIONS
500	500	Microemulsion, BC after 4 days
600	600	Microemulsion, BC after 4 days
700	700	Microemulsion, BC after 4 days
800	800	Microemulsion, BC after 4 days

Table 36: Details of the experiments used for laser diffraction analysis. 7.00 g stock was used for each microemulsion.

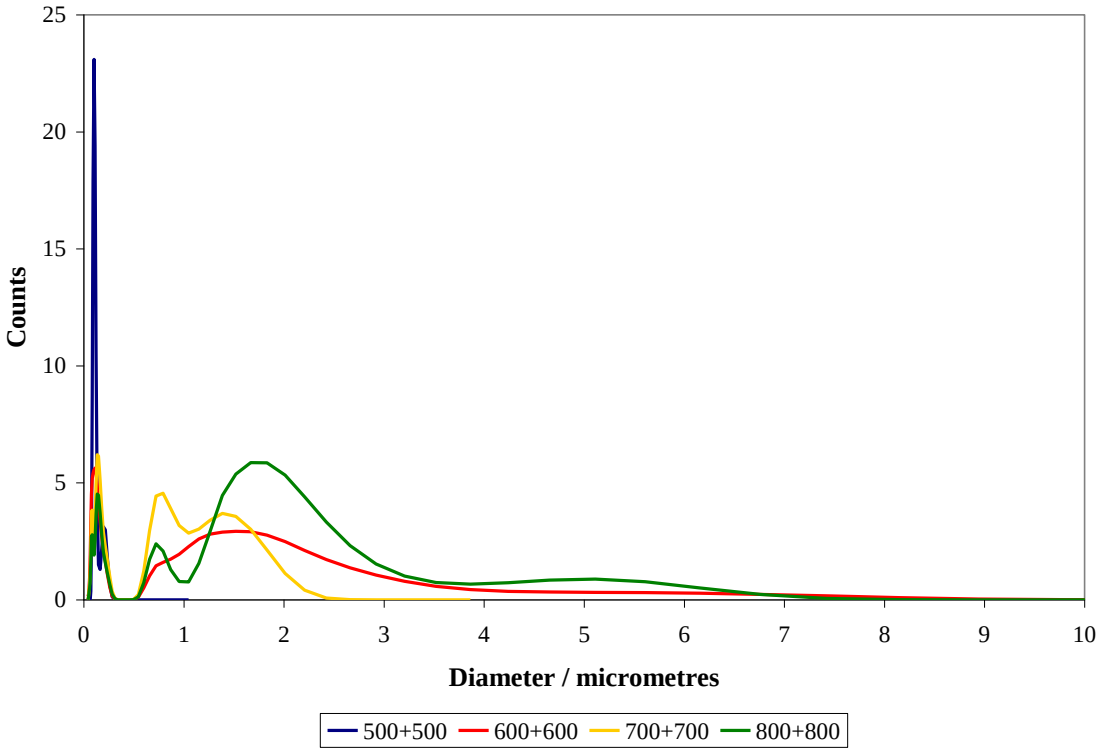

Figure 97: Laser diffraction results of the experiments detailed in Table 34. The numbers refer to how much (hydrochloric acid + TIPO) in microlitres was added.

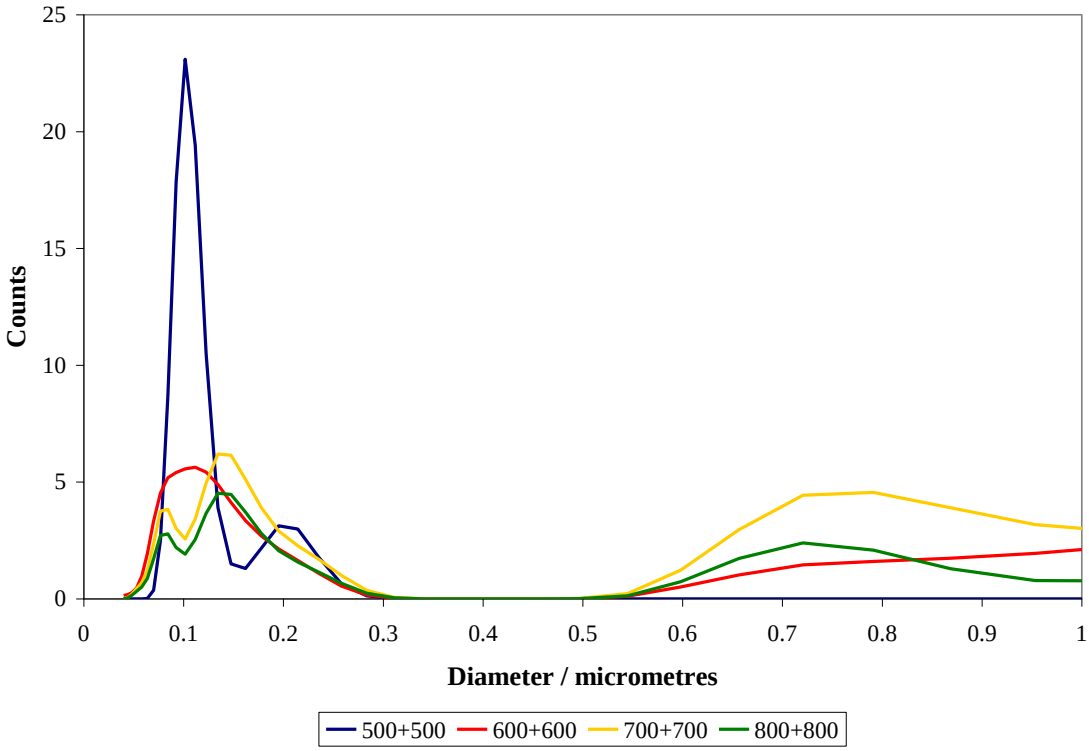

Figure 98: Laser diffraction results of the four experiments detailed in Table 34. The x-axis scale has been zoomed in to values up to a micrometre in diameter.

A good trend can be found from Figures 97 and 98, where increasing the volume of reactants tends to result in the growth of larger crystals. The range of particle sizes is also smaller when the volume of reactants is used. In the case of experiment 500 + 500, 24 % of the particles were 100 nm in diameter and the overall range only covered sizes between 60 and 300 nm. It is important to note that the rate of reaction is not necessarily increased – the smaller amounts of reactants mean that the overall confinement is much greater, giving smaller initial particulates. The increased counts at very low particle diameters can partially justify this.

SAXS and TEM Analysis

SAXS analysis was again carried out on the mixed microemulsions. The mixed microemulsions were made up – using 200 µl each of hydrochloric acid and TIPO and 1.74 g stock solution - and then left for 2 days. As observed previously, the blue colouration did not appear, meaning that larger crystals had not formed yet. Because of the ~50 nm size limitation of laser diffraction, SAXS and GIFT analysis was used to detect smaller particles and droplets, with the analysis being performed by the

technician Helen Riggs. An example SAXS curve and p(r) curve from the experiment are shown in Figures 99 and 100 respectively:

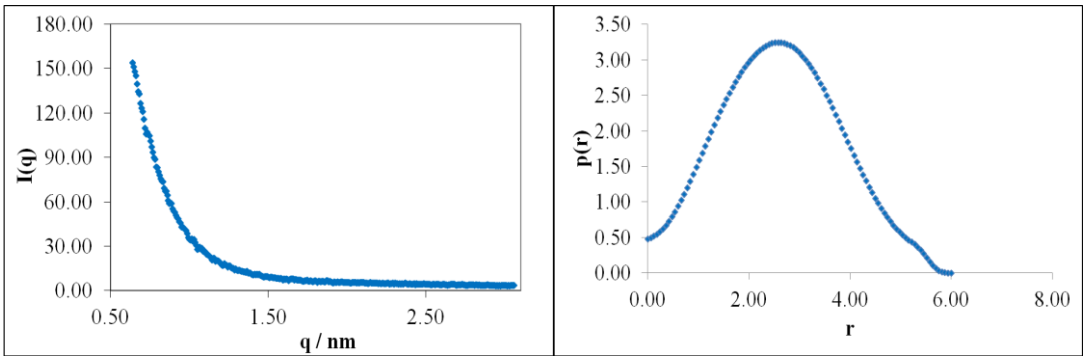

Figures 99 and 100: SAXS curve (fig. 100) and p(r) curve (fig. 101) for the titanium dioxide experiment.

The particle size calculated – assuming spherical, homogenous droplets – was 2.62 nm. As before with the hydroxyapatite experiments (see Table 27), the fact that a droplet size could be calculated at all proves that the microemulsion is retained throughout the experiment.

Using the JEOL 2100F FEG Transmission Electron Microscope, nanocrystals of titanium dioxide could be probed and analysed. Figures 101 a) and b) were taken from the experiment which utilised 200 µl of TIPO and 200 µl of hydrochloric acid:

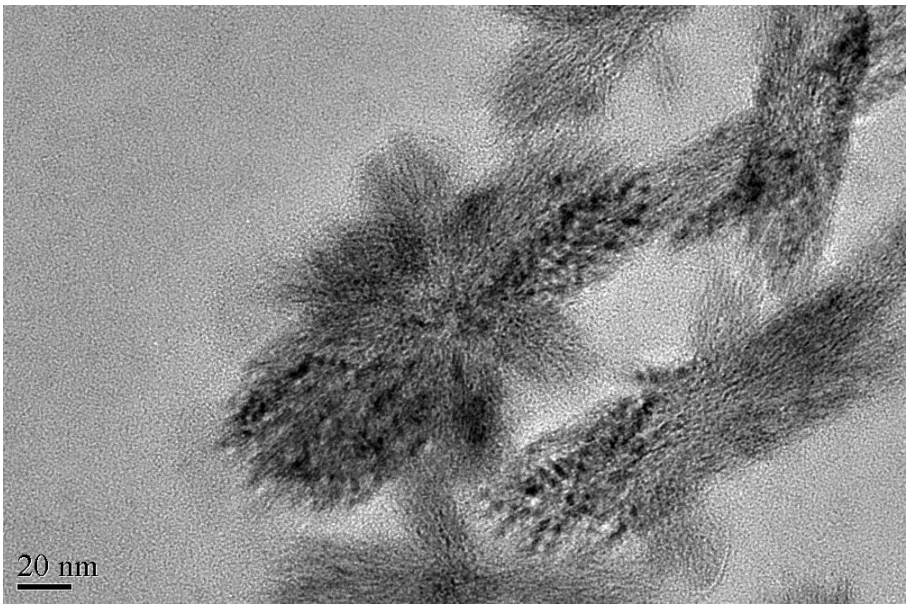

Figure 101 a): Bright field image obtained from TEM analysis showing the crystals obtained after 2 weeks.

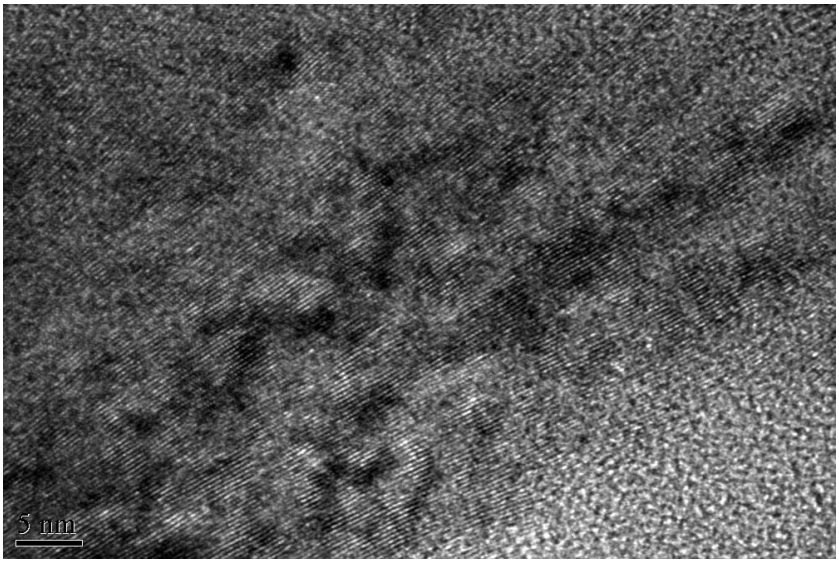

Figure 101 b): High-resolution electron microscopy image of the same crystals from figure 10.

After 14 days, the crystals found are all of a fairly regular size, being between 120 – 200 nm. This corresponds well with the results of the laser diffraction analyses, where the two particle sizes with the highest number of counts were 100 nm and 200 nm. This shows the advantage of using mixed microemulsion techniques, which reduce the range of the crystal sizes.

Electron diffraction patterns were also obtained from TEM analysis, and these could be used to work out the polymorph of titanium dioxide present. The pictures used are shown in Figures 102 a) and b), and were taken from the experiment 80 + 120:

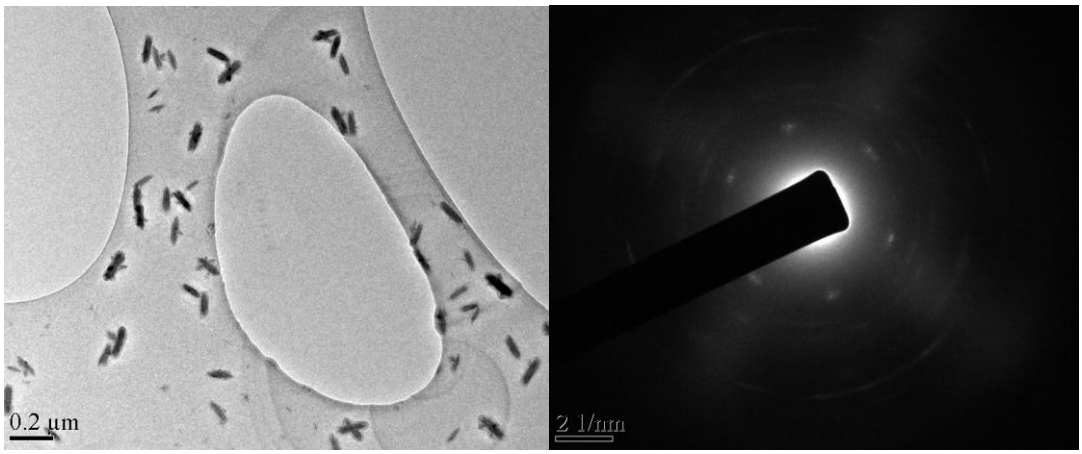

Figures 102 a) & b): Bright field image a) and electron diffraction pattern b) of sample 80 + 120. Crystals were analysed after 14 days.

By encompassing a number of crystals into the bright field image, a clear electron diffraction pattern can be seen. Comparing to TEM data obtained by Bakardjieva *et al.*, the polymorph of the crystals can be deduced.[167] The smallest ring present corresponds to a d-spacing of 3.26 Å, which compares well to the measured value of 3.25 Å for the [110] crystal plane for rutile. The next two outer rings give values of 2.54 Å and 2.22 Å, also in good agreement with the values of 2.49 Å and 2.19 Å for the [101] and [111] rutile crystal planes respectively. All these values do not correspond to d-spacing values found for anatase (3.50 Å for the [101] plane), and so it can be concluded that rutile has been formed.

In addition to the TEM images, Energy-Dispersive X-Ray spectroscopy (EDX) could be used as a form of elemental analysis to work out what elements the final product obtained. The results from this analysis are shown in Figure 103:

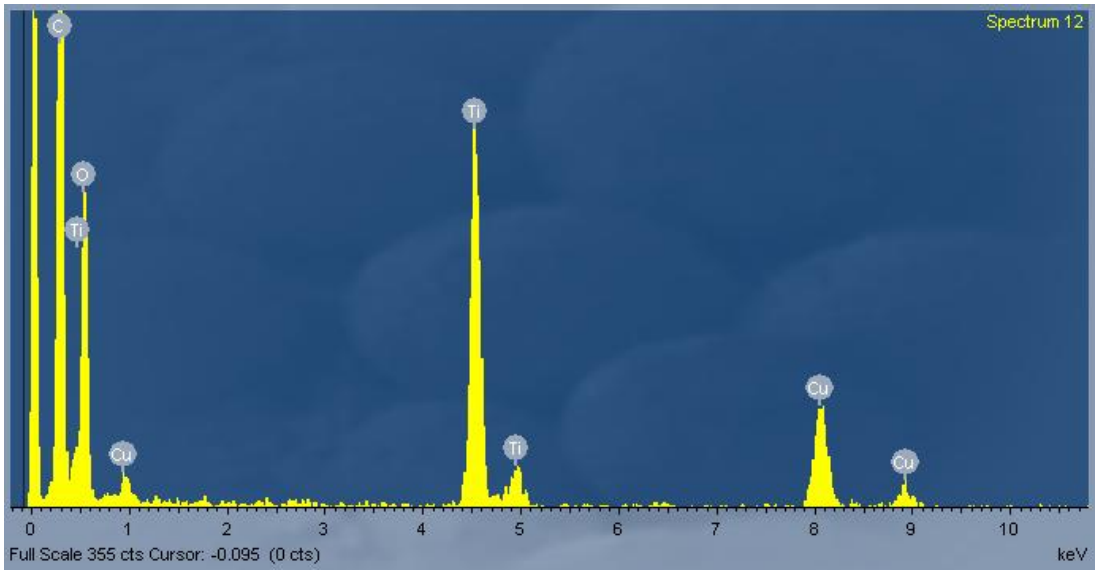

Figure 103: EDX pattern for titanium dioxide present on the copper grid used for holding samples for TEM analysis (again using the experiment 200 +200).

The patterns give a positive result for the presence of titanium dioxide. Apart from the titanium peaks present, the only other peaks are those which indicate the presence of copper metal and carbon, both of which are present on the TEM grid initially. The height ratio of titanium : oxygen peaks is also consistent with the formation of titanium dioxide, the ratio being roughly 6 : 4.

TEM analysis was also carried out on the microemulsion at specific time periods. Three mixed microemulsions were made containing 180 µl hydrochloric acid and 180 µl TIPO. After 8, 12 and 18 hours, samples were deposited onto a copper grid and left to dry for 36 hours. Figures 104, 105 and 106 show the pictures obtained at the respective times:

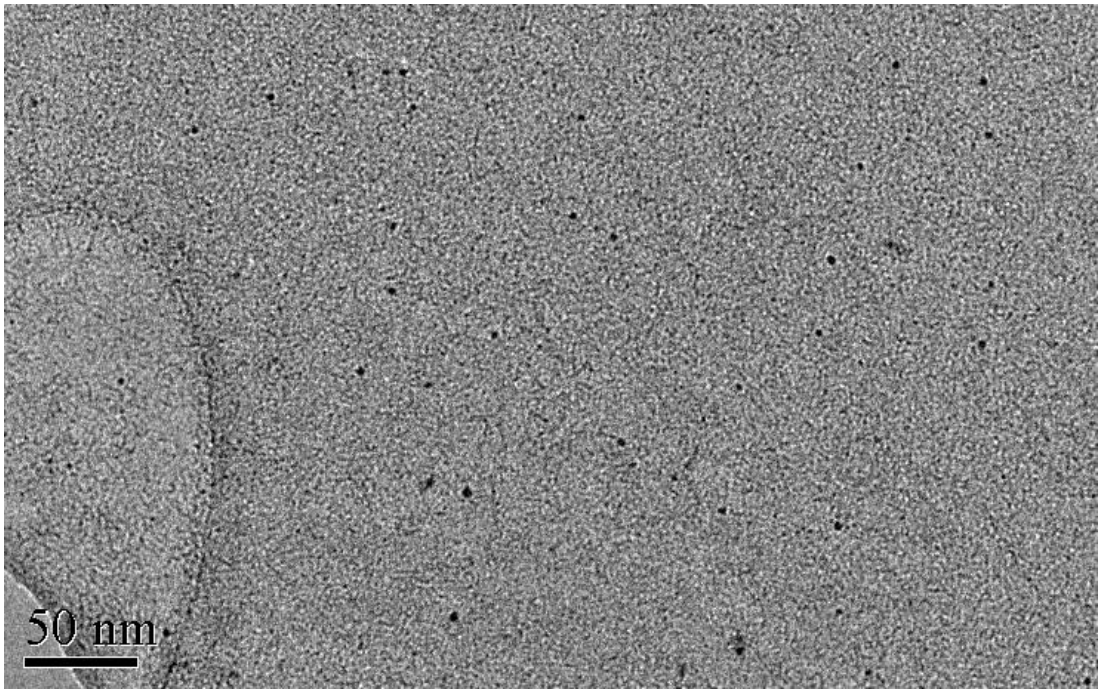

Figure 104: TEM bright field image of crystals obtained from the 180 + 180 experiment after 8 hours.

The crystals found were 2.0 – 3.0 nm in diameter after 8 hours. Gaps of at least 50 nm between each of the crystals suggests that they have not broken the droplets and that no fusing / aggregation of crystals has taken place yet.

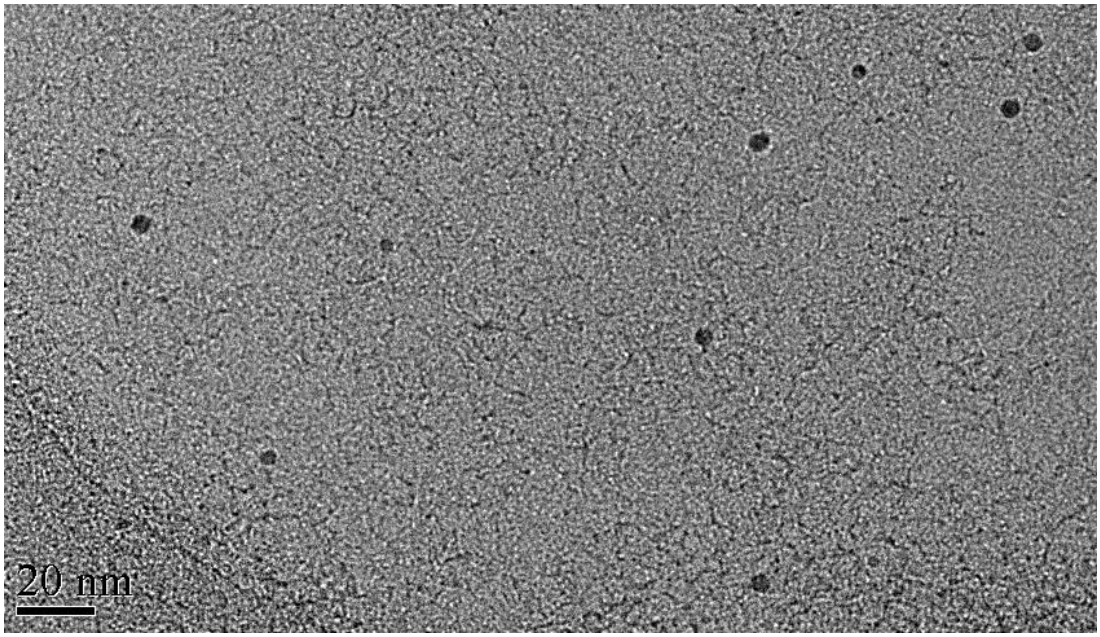

Figure 105: TEM bright field image of crystals obtained from the 180 + 180 experiment after 12 hours.

The crystal diameters have increased to a range of 2.5 – 5.0 nm after 12 hours. The distance between the droplets has closed to as little as 20 nm, but otherwise there is still no interaction between the crystals.

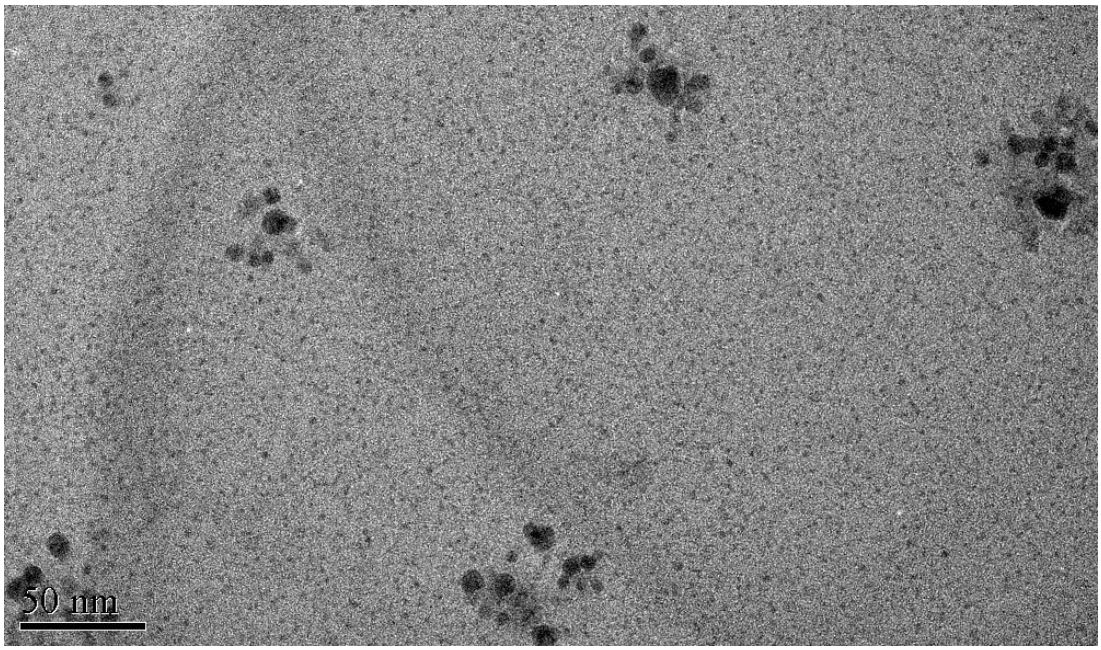

Figure 106: TEM bright field image of crystals obtained from the 180 + 180 experiment after 18 hours.

Crystal sizes range from 3.2 – 12.5 nm in diameter after 18 hours. At this point, the nanocrystals are starting to aggregate together. It is expected that throughout the next

few hours, the crystals would begin to fuse / aggregate together and form micron-sized crystals.

As a further test of polymorphism, a Fast Fourier Transform employed on Figure 96 obtained from the 12 hour sample was performed (see Figures 107 a) and b)):

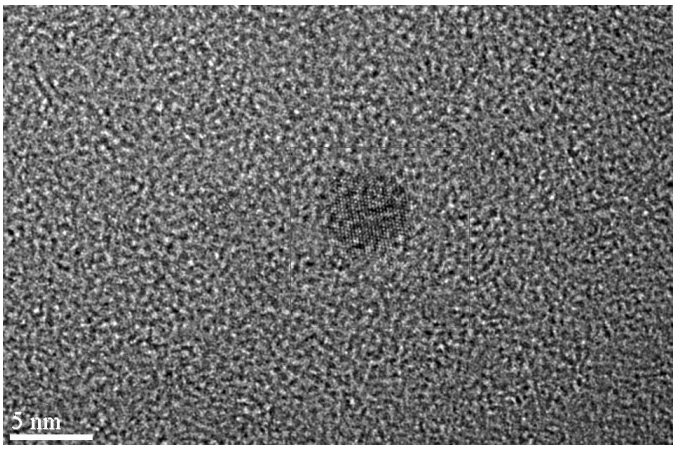

Figure 107 a): HREM image of a titanium dioxide crystal obtained from the 180 + 180 experiment after 12 hours.

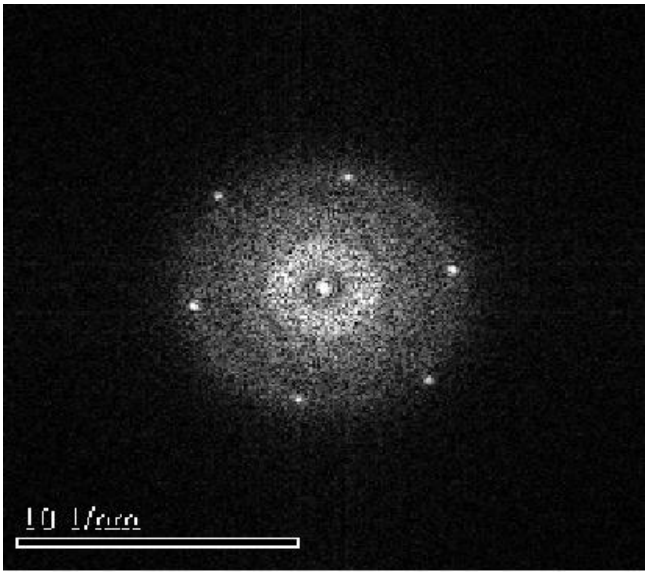

Figure 107 b): Fast Fourier Transform (FFT) image of a single crystal taken from the experiment 180 + 180 12 hours after the microemulsions were mixed.

Three values for the d-spacing can be calculated from Figure 107 b) – these values are 2.03 Å, 2.14 Å and 2.48 Å for respectively. These values compare very favourably with the rutile [210], [111] and [101] planes respectively, and unfavourably for anatase (see Tables 35 and 36). In particular, the values and angles between the spots are consistent with the [121] zone axis of rutile.

6.4 Water Addition Experiments

The initial experiments worked well when attempting to synthesise rutile; however the time taken before extracting the crystals was relatively long, with the bulk of experiments analysed needing at least two weeks before extraction and analysis took place.

In an attempt to speed up the production of rutile crystals, water was added through various techniques. The presence of more water was hoped to destabilise the microemulsion more quickly, enabling faster growth of crystals after the initial rutile nucleation. The water addition was carried out in different ways:

1) Water was added after mixing the HCl and TIPO-containing microemulsions. In all cases, a few minutes was allowed after the mixing of microemulsions to ensure that a microemulsion had been formed, was stable, and that titanium dioxide nucleation had occurred.
2) Before mixing the HCL and TIPO-containing microemulsions, water was added to the HCl microemulsion. This formed an emulsion, and was carried out to show that better crystallinity was obtained when all solutions were microemulsions, compared to combining a microemulsion and an emulsion.
3) In addition to 2), some experiments were carried out where water replaced some or all of the HCl present.

For all the experiments involving water addition, the mass of stock solution for each microemulsion was kept at 1.75 g.

6.4.1 Results

Water addition after microemulsion mixing

A full set of experiments was carried out, adding amounts of water between 50 and 800 µl. Table 35 shows the various results and changes in the microemulsions upon addition of the water. In all cases, the mixed microemulsion contained 3.48 g stock solution, 200 µl of HCl and 200 µl of TIPO:

Water added / µl	Observations
50 - 350	Microemulsion retained
400 - 500	Microemulsion retained, but viscosity increased after 17 hours
550 - 650	Microemulsion retained, viscosity increased, phase separation after 3 hours
700 - 800	Immediate phase separation

Table 37: Table detailing the changes in the mixed microemulsions when water was added.

Generally, the addition of smaller amounts of water (up to 500 µl) gave no real increase in the rate of crystallisation, with the appearance of a nanoemulsion-type solution occurring after 4 days, no quicker than the original experiments. Further experiments were carried out, where the volumes of TIPO and hydrochloric acid added were increased to values of 300, 350 and 400µl. These experiments are detailed in Table 36:

TIPO added / µL	HCl added / µL	Sub-letter	Water added / µl	Observations
300	300	a	300	Micro initially, Micro on H_2O addition, BC after 4 days
300	300	b	400	Micro initially, Micro on H_2O addition, BC after 4 days
300	300	c	500	Micro initially, Micro on H_2O addition, BC after 4 days
300	300	d	600	Micro initially, Emulsion on H_2O addition, BC after 4 days
300	300	e	700	Micro initially, Emulsion on H_2O addition, BC after 4 days
300	300	f	800	Micro initially, Emulsion on H_2O addition, BC after 4 days
300	300	g	900	Micro initially, Emulsion on H_2O addition, BC after 4 days
350	350	a	300	Micro initially, Micro on H_2O addition, BC after 4 days
350	350	b	400	Micro initially, Micro on H_2O addition, BC after 4 days
350	350	c	500	Micro initially, Micro on H_2O addition, BC after 4 days
350	350	d	600	Micro initially, Emulsion on H_2O addition, BC after 4 days
350	350	e	700	Micro initially, Emulsion on H_2O addition, BC after 4 days
400	400	a	300	Emulsion→Micro, Micro on H_2O addition, BC after 4 days
400	400	b	400	Emulsion→Micro, Micro on H_2O addition, BC after 4 days
400	400	c	500	Emulsion→Micro, Micro on H_2O addition, BC after 4 days
400	400	d	600	Emulsion→Micro, Emulsion on H_2O addition, BC after 4 days
400	400	e	700	Emulsion→Micro, Emulsion on H_2O addition, BC after 4 days
350	300	a	300	Nano initially, Micro on H_2O addition, BC after 4 days
350	300	b	400	Nano initially, Micro on H_2O addition, BC after 4 days
350	300	c	500	Nano initially, Micro on H_2O addition, BC after 4 days
350	300	d	600	Nano initially, Micro on H_2O addition, BC after 4 days
350	300	e	700	Nano initially, Micro on H_2O addition, BC after 4 days

Table 38: Descriptions of experiments where the volume of TIPO was increased. In the observations column, the state of the experiment was observed at three points – the state of the mixed microemulsion before adding water, the state after adding water and any changes in state afterwards.

The table shows that despite the changes in reactant volumes and initial observations, the appearance of the blue colouration indicating growth of crystals $\geq$ 30 nm always occurred after 4 days. This suggests that the addition of water, in whatever method, does not speed up the production of titanium dioxide macrocrystals.

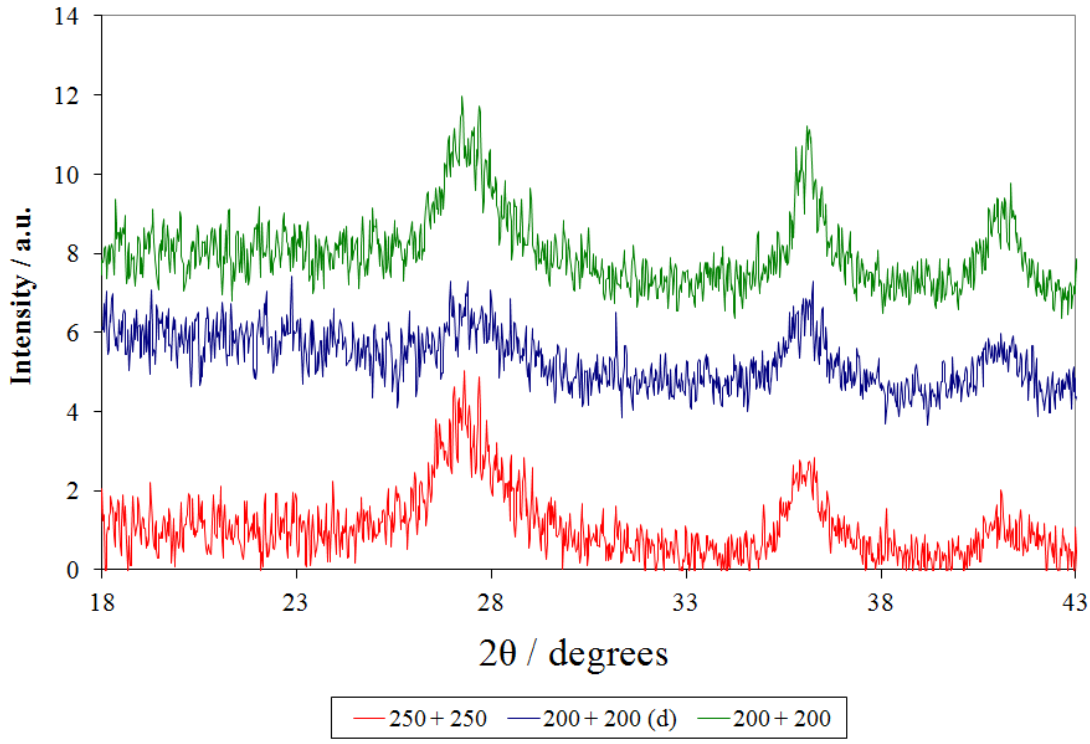

Figure 108: Comparison of XRD patterns of an experiment where 200 µl water was added to experiment (200 + 200)(blue graph), and an experiment where no water was added, and 250 µl of hydrochloric acid and TIPO were used (red graph). Experiment (200 + 200) is shown for comparison (green graph).

All XRD patterns in Figure 108 show peaks at 27°, 36° and 41°, indicating that rutile has been formed even when water is added, but that there is a reduction in crystallinity, even when compared to an experiment where more reactants have been added. This appears to show that the increase in water decreases the crystallinity of the final product.

Water addition before microemulsions mixing

Six experiments were carried out using this technique. The volume of TIPO added was either 200 or 300 µl, and the total amount of water and hydrochloric acid added was kept constant at 400 µl. The separate amounts of both aqueous liquids were varied. These experiments are detailed in Table 37:

TIPO added / µL	HCl added / µL	Water added / µL	OBSERVATIONS
200	100	300	Microemulsion initially, BC after 4 days
200	200	200	Microemulsion initially, BC after 4 days
200	300	100	Microemulsion initially, BC after 4 days
300	100	300	Gel
300	200	200	Phase separation, BC after 4 days
300	300	100	Phase separation, BC after 4 days

Table 39: Descriptions of experiments where water was added to the hydrochloric acid-containing microemulsion. BC = Blue Colouration.

Microemulsions still formed when water was added to the microemulsions when 200 µl of TIPO was present. This is consistent with the previous results – where up to 350 µl of water could be added without breaking the microemulsion. However, when the volume of TIPO was increased to 300 µl, the replacement of hydrochloric acid with water caused phase separation or formed a gel.

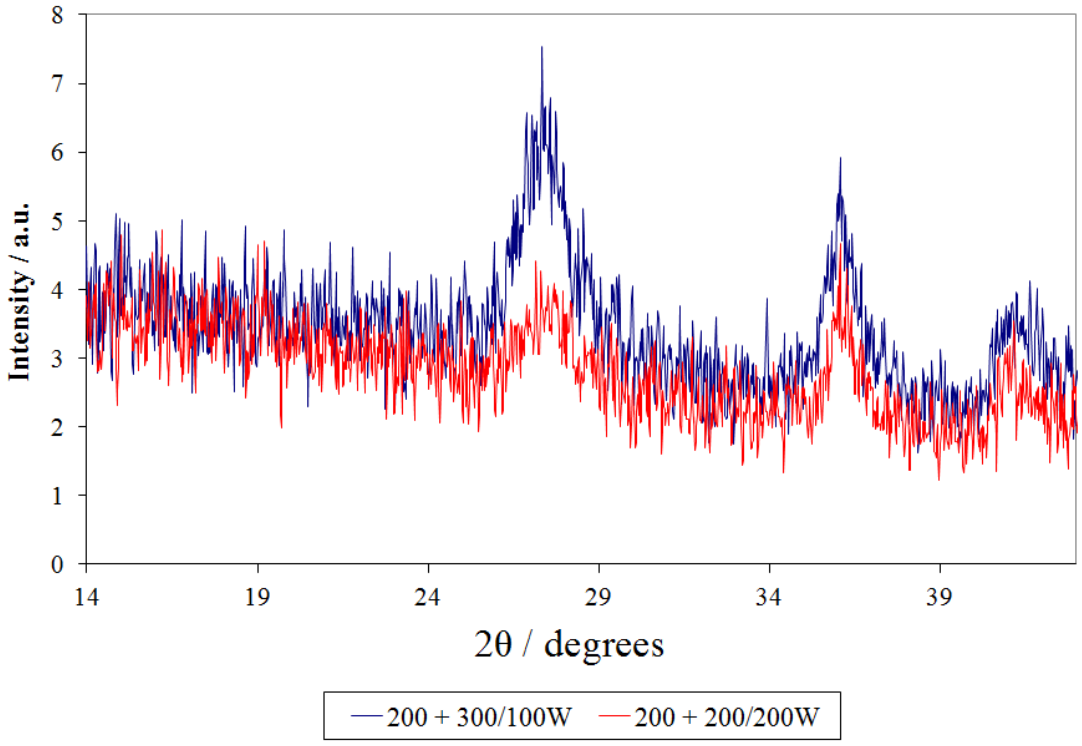

Figure 109: XRD pattern comparison of two experiments where water was added to the HCl-containing microemulsion before mixing. The total volume of hydrochloric acid and water was kept constant at 400µl. Blue graph had 100 µl water added, red graph had 200 µl water.

The main peak at 27° in Figure 109 has reduced in intensity from 4.5 (peak height in a.u.) to 2.0. The other peaks at 36°and 41° have also reduced in height. Similarly to Figure 109, this shows that the increase in the volume of water has decreased the crystallinity of the final product.

Water replacement of HCl

Three experiments were carried out. In place of hydrochloric acid, water was added to the 2nd microemulsion. Results and observations are shown in Table 40:

TIPO added / µL	Water added / µL	Observations
200	200	Gel
200	400	Gel
300	200	Gel

Table 40: Table showing the amounts of reactants added in the water replacement experiments.

Upon mixing, a gel formed immediately in all three experiments. Subsequent analysis by X-Ray diffraction gave no peaks, as shown in Figure 110:

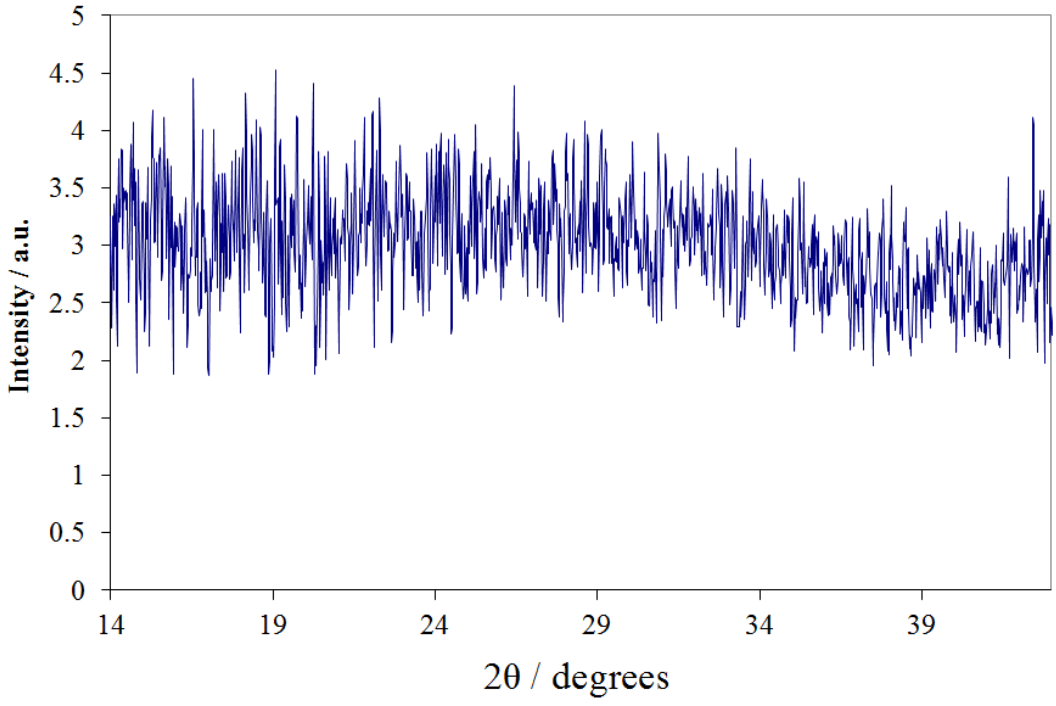

Figure 110: XRD pattern of product from mixed microemulsions containing 1.74 g stock solution for each microemulsion, 200 µl TIPO and 200 µl water.

With no definable peaks whatsoever, the product can confidently be described as amorphous. One further experiment was carried out where the stock solution in each of the unmixed microemulsions was doubled to 3.48 g. A similar result was obtained, with a gel forming immediately when the water-containing microemulsion was added.

6.5 Discussion of Results

Through the mixed microemulsion techniques, titanium dioxide was produced on a timescale of a few days, and relatively good crystallinity was achieved. Using the 30 % stock solution, all the experiments which produced microemulsions tended to give a blue colouration after 4 days, at which point the crystals could be extracted. The variation in volumes of hydrochloric acid and TIPO between 100 and 200 μl had little effect on the rate of formation of crystals. If microemulsions formed, a blue colouration appeared after 3-4 days, which became white and opaque upon full precipitation of TiO_2 forming after 10-14 days. There was also little variation in the crystallinity of the final products with variation of the reactant volumes.

Keswani *et al.* obtained similar results using similar microemulsion techniques.[168] In particular, he showed that titanium dioxide could be made via two different techniques – one similar to the process described here and one where the reactants were added directly to a microemulsion containing titanium tetrachloride ($TiCl_4$). However the process and results obtained from this investigation have several advantages over the experiments of Keswani *et al.*, namely:

1) The experiments carried out for this thesis use a mild concentration of hydrochloric acid (2.0M), compared to a highly concentrated solution of ammonium hydroxide used by said group. As a result, safety considerations are much more manageable
2) Also related to safety issues, the group used titanium tetrachloride which is known for its high volatility. It can react with the air to produce titanium dioxide and hydrogen chloride, and reacts explosively with water. Lal *et al.* also used $TiCl_4$ in their synthesis of TiO_2 nanoparticles.[169] Titanium isopropoxide, used in this investigation, is also volatile, but on a far smaller scale.
3) The concentration of surfactants in the stock solution is relatively low at 30 %, compared to 52 % used by Keswani *et al.*

The experiments involving the addition of water gave mixed results. At best, titanium dioxide could be made, though its rate of synthesis was unchanged. At worst, the final product was totally amorphous. It is clear that the complete

replacement of hydrochloric acid by water increases the rate of reaction hugely, presumably because the increased pH makes hydrolysis quicker. Consequently the reaction cannot be controlled thermodynamically to produce a crystalline product.

6.6 Conclusions

Titanium dioxide nanocrystals were synthesised by adding a titanium isopropoxide solution to an acidified aqueous microemulsion. A blue colouration which indicated the formation of crystals with sizes ≥ 30 nm was found between 5 -14 days. After extraction and washing, analyses were carried out on the crystals, including IR, X-Ray diffraction, laser diffraction particle sizing and TEM. The subsequent analysis showed that the rutile polymorph of titanium dioxide was formed with a good degree of crystallinity.

An exploration into whether the addition of water to the system could speed up the processes was also undertaken. Three different methods were undertaken – water was added after mixing the microemulsions, added to the hydrochloric acid-containing microemulsion before mixing and substituted in place of hydrochloric acid. In the first two cases, an overall microemulsion was maintained if less than 550 µl of water was added. But the crystallisation process was no faster, with crystals of size 200 µl appearing after 4 days – the same length of time as for previous experiments. In many cases, adding over 200 µl of water reduced the crystallinity of the final product. In the third case, a gel was immediately formed, leading to fully amorphous titanium dioxide being formed.

7. Overall Conclusions

Control of crystallisation has become increasingly important in the current age, where the demands for specific crystals in specific arrangements have become numerous and crucial. Within the pharmaceutical industry, the polymorph of a crystal must be defined and the compound itself checked to ensure that no other crystal forms exist. With the Ritonavir crisis showing that drugs may convert to new forms even in storage, a big challenge is to synthesise the correct polymorph and to ensure that in most cases, that it is the most stable polymorph present.

One problem is that many polymorphic compounds follow Ostwald's Rule of Stages, which states that upon crystallisation, a compound will crystallise as one of its metastable polymorphs, before transforming into the most stable polymorph – this can often take many weeks or months. By using microemulsions as a medium for crystallisation, the crystallisation process can take place under thermodynamic control – and therefore crystallise the most stable polymorph first. Microemulsions have also been suggested as a medium for chemical reactions. The droplets within a microemulsion offer excellent possibilities to speed up reactions, synthesise preferential products and overcome problems like solubility, which may otherwise stop reactions from ever starting.

Three compounds were studied using microemulsions to attempt to control the crystallisation of each of the compounds. Firstly, glycine was crystallised from various microemulsion systems. Methanol was added to the microemulsions to induce crystallisation. Using AOT as the sole surfactant and adding methanol dropwise, all three polymorphs of glycine could be crystallised singly, including γ-glycine – the most stable polymorph. Using a mixture of Span 80 / Tween 80 surfactants with dropwise addition of methanol, both α- and β-glycine were crystallised, but the γ-polymorph was not. This was due to the templating ability of the surfactants, which preferentially crystallised α-glycine. When Tween 80 was switched to Brij 30, and the method of methanol addition changed, γ-glycine was formed many times. In particular, when adding methanol vapour, γ-glycine was formed in addition to other polymorphs. When utilising a mixed microemulsions method, γ-glycine was crystallised as the sole polymorph. Analysis by FTIR, XRD

and TEM were used to confirm the polymorph. Consequently, we were able to show that the most stable form of glycine, γ-glycine, could be crystallised from microemulsions despite this form not typically crystallising from bulk aqueous solutions. This supported our hypothesis that microemulsions could be used to induce thermodynamic control of crystallisation, instead of the kinetic control that normally arises in bulk solutions.

The second compound studied was hydroxyapatite. It was known that using a combination of calcium chloride, ammonium hydroxide and ammonium phosphate would synthesise hydroxyapatite. The reaction was carried out in two ways – direct addition of reagents to a microemulsion and a mixed microemulsion method. In both cases, hydroxyapatite was formed and the crystallinity corresponded very well to as-received hydroxyapatite. Both TEM and laser diffraction analyses were used to work out the size of the particles formed. The mixed microemulsion method gave a slightly improved product compared to the direct addition of reagents to the microemulsions, in terms of crystallinity

The third compound studied was titanium dioxide. Using a mixed microemulsion method, the hydrolysis of TIPO to form titanium dioxide was carried out under thermodynamic control. Polymorphic control was a success, with rutile – the most stable polymorph – being formed. TEM analysis could detect particles as small as 2.0 nm – and further showed that full confinement within microemulsion droplets was realised.

The results obtained from the glycine and titanium dioxide experiments showed that the goal of obtaining the most stable polymorph was achieved. Furthermore, it was shown that thermodynamic control of crystallisation was achieved from conducting the crystallisation within 3D-nanoconfined solutions. This was proved through SAXS analysis, which was able to calculate droplet sizes in a microemulsion. This proved that the relevant microemulsions remain stable and continue to offer the required degree of confinement, even after a period of up to a week. In addition, both sets of experiments showed that Ostwald's Rule of Stages can be circumvented, meaning that direct crystallisation of the most stable polymorph can occur, rather than the crystallisation of a metastable polymorph, which then transforms into the most stable polymorph.

The hydroxyapatite and titanium dioxide experiments showed that synthesis of specific inorganic materials using microemulsions could be carried out. In particular, the experiments involving hydroxyapatite showed that, despite the huge number of compounds that the apatite family is composed of, the correct apatite-type compound could be made - the EDX results giving the correct calcium : phosphorous ratio of 1.61. The titanium dioxide experiments proved that nanoparticles of the most stable polymorph can be made over a large range of possible amounts of reactants for microemulsions – of the experiments that were analysed, values between 100 and 200 μl of TIPO and hydrochloric acid used could still produce crystals within the same timeframe and obtain the rutile polymorph – within certain constrictions of the ratio of TIPO : acid.

7.1 Future Work

Glycine

Despite the great success with obtaining γ-glycine from various microemulsions systems, there are still many possibilities of improving these experiments, as well as looking towards future experiments. One of the main issues still present is the matter of the timescale it requires to form visible crystals with the mixed microemulsion experiments – the two experiments MC(a).4 and MC(a).5 were both analysed after crystals had been left to grow for 15 weeks (compared to 3 weeks for all other experiments). Future experiments could try "seeding-type" techniques, which could improve the crystallisation rate from the microemulsions whilst still ensuring predominantly γ-glycine formation. For example, for the two glycine experiments MC(a).4 and MC(a).5 - another microemulsion of similar glycine composition could be added after ~ 1 day, by which time γ-glycine nanocrystals would have already grown. In theory, the presence of more glycine molecules will encourage faster growth of the existing glycine nanocrystals, but not form new nuclei, because crystal growth occurs at a faster rate than further nucleation.

Hydroxyapatite

As with the glycine experiments, the capacity to expand the range of further experiments is wide. Refinement of the experiments detailed is a necessity, with aspects to focus on including a detailed look at the initial nucleation and first steps of crystal growth. TEM analysis will be the important analysis technique in this. Future experiments can focus on what happens in the microemulsion for the first 24 hours of the experiment. To the naked eye, there are usually no optical changes in the experiment, but with crystals of length 100 nm grown after 24 hours, it is likely that crystal formation does occur after just a few hours. Comparisons of time and crystal size could then be drawn from the experiments. One property of the hydroxyapatite crystals that was not studied was the morphology of the crystal surfaces. Using a technique like scanning electron microscopy (SEM), this could give some insight into how the surface compares to other hydroxyapatite crystals synthesise via different methods. This type of information would be vital for further work combining HAp crystals with other materials, for example with polymers with the intention of creating biocompatible scaffolds for tissue engineering.

Titanium Dioxide

The experiments involved in synthesising titanium dioxide were successful in both making the most stable polymorph and making discrete nanoparticles between the sizes of 2 – 200 nm. Early future work could look at drawing up a comprehensive table of how the sizes of nanoparticles differ with time in the microemulsion, thereby enabling specific sizes to be made and extracted. Further TEM and SAXS analyses would be most useful in determining the particle sizes.

Future experiments involving the synthesised titanium dioxide nanoparticles could look into their photocatalytic activity, and see whether it is increased or decreased when titanium dioxide is made via microemulsions. Some photocatalytic operations are polymorph-specific, such as when using titanium dioxide as a base for self-cleaning glass, which anatase is more useful.[170,171] Other reactions, like the decomposition of crude oil and the conversion of carbon dioxide into hydrocarbons use rutile.[172] It will be of great importance to test whether the nanoparticles formed from these experiments can match or exceed the photocatalytic properties of other particles formed from different syntheses.

8.References

1. D. Kashchiev, G. M. van Rosmalen, *Crystal Research and Technology*, 2003, **38**, 555-574.
2. L. Farkas, *Z. phys. Chem*, 1927, **125**, 236-242.
3. R. Becker, W. Döring, *Annalen der Physik*, 1935, **416**, 719-752.
4. J. A. D. Wattis, C. D. Bolton, P. V. Coveney, *Journal of Physics A: Mathematical and General*, 2004, **37**, 2895.
5. J. A. D. Wattis, *Journal of Physics A: Mathematical and General*, 1999, **32**, 8755.
6. J. A. D. Wattis, P. V. Coveney, *Journal of Chemical Physics*, 1997, **106**, 9122-9140.
7. D. W. Oxtoby, R. Evans, *The Journal of chemical physics*, 1988, **89**, 7521.
8. I. V. Markov, *Crystal growth for beginners: fundamentals of nucleation, crystal growth and epitaxy*, World Scientific Pub Co Inc, 2003.
9. C. Pina, A. Putnis, *Geochimica et cosmochimica acta*, 2002, **66**, 185-192.
10. N. Blagden, R. Davey, G. Dent, M. Song, W. David, C. Pulham, K. Shankland, *Crystal Growth & Design*, 2005, **5**, 2218-2224.
11. S. Datta, D. J. W. Grant, *Nature Reviews Drug Discovery*, 2004, **3**, 42-57.
12. D. A. Snider, W. Addicks, W. Owens, *Advanced drug delivery reviews*, 2004, **56**, 391-395.
13. J. Bauer, S. Spanton, R. Henry, J. Quick, W. Dziki, W. Porter, J. Morris, *Pharmaceutical research*, 2001, **18**, 859-866.
14. B. C. Lippold, A. Ohm, *International journal of pharmaceutics*, 1986, **28**, 67-74.
15. S. Pinnamaneni, N. Das, S. Das, *Die Pharmazie*, 2002, **57**, 291.
16. J. C. Burley, M. J. Duer, R. S. Stein, R. M. Vrcelj, *European journal of pharmaceutical sciences*, 2007, **31**, 271-276.
17. M. Kitamura, *Journal of crystal growth*, 1989, **96**, 541-546.
18. R. Davey, N. Blagden, G. Potts, R. Docherty, *Journal of the American Chemical Society*, 1997, **119**, 1767-1772.
19. W. Ostwald, *Z. phys. Chem*, 1897, **22**, 306.
20. L. Addadi, S. Raz, S. Weiner, *Advanced Materials*, 2003, **15**, 959-970.
21. J. J. De Yoreo, P. G. Vekilov, *Reviews in mineralogy and geochemistry*, 2003, **54**, 57-93.
22. M. Kitamura, *CrystEngComm*, 2009, **11**, 949-964.
23. S. J. Cooper, C. E. Nicholson, J. Liu, *The Journal of chemical physics*, 2008, **129**, 124715.
24. C. Chen, O. Cook, C. E. Nicholson, S. J. Cooper, *Crystal Growth & Design*, 2011, **11**, 2228-2237.
25. M. Corti, C. Minero, V. Degiorgio, *The Journal of Physical Chemistry*, 1984, **88**, 309-317.
26. S. Kumar, D. Sharma, Kabir-ud-Din, *Langmuir*, 2000, **16**, 6821-6824.
27. K. Shinoda, H. Arai, *The Journal of Physical Chemistry*, 1964, **68**, 3485-3490.
28. E. Florin, R. Kjellander, J. C. Eriksson, *J. Chem. Soc., Faraday Trans. 1*, 1984, **80**, 2889-2910.
29. H. Kunieda, K. Shinoda, *The Journal of Physical Chemistry*, 1976, **80**, 2468-2470.

30. K. Krajnak, H. Kan, S. Waugh, G. R. Miller, C. Johnson, J. R. Roberts, W. T. Goldsmith, M. Jackson, W. McKinney, D. Frazer, *Journal of Toxicology and Environmental Health, Part A*, 2011, **74**, 1397-1404.
31. J. Yano, H. Füredi-Milhofer, E. Wachtel, N. Garti, *Langmuir*, 2000, **16**, 10005-10014.
32. J. Yano, H. Füredi-Milhofer, E. Wachtel, N. Garti, *Langmuir*, 2000, **16**, 9996-10004.
33. B. Jonson, B. Lindman, K. Holmberg, B. Kronberg, Wiley, New York, 1998.
34. M. Porras, C. Solans, C. Gonzalez, A. Martinez, A. Guinart, J. M. Gutiérrez, *Colloids and Surfaces A: Physicochemical and Engineering Aspects*, 2004, **249**, 115-118.
35. J. Esquena, C. Solans, *Trends in Colloid and Interface Science XII*, 1998, 235-239.
36. T. Lin, H. Kurihara, H. Ohta, *J. Soc. Cosmet. Chem*, 1975, **26**, 121-139.
37. A. J. Gotch, G. W. Loar, A. J. Reeder, E. E. Glista, *Langmuir*, 2008, **24**, 4485-4493.
38. P. Winsor, *Trans. Faraday Soc.*, 1948, **44**, 376-398.
39. W. Zhang, X. Qiao, J. Chen, *Materials Science and Engineering: B*, 2007, **142**, 1-15.
40. F. Candau, Y. S. Leong, G. Pouyet, S. Candau, *Journal of colloid and interface science*, 1984, **101**, 167-183.
41. A. Chhatre, R. Joshi, B. Kulkarni, *Journal of colloid and interface science*, 1993, **158**, 183-187.
42. F. Menger, A. Elrington, *Journal of the American Chemical Society*, 1991, **113**, 9621-9624.
43. C. M. Pechura, D. Rall, *Veterans at risk. National Academic Press, Washington DC*, 1993.
44. N. L. Klyachko, A. V. Levashov, *Current opinion in colloid & interface science*, 2003, **8**, 179-186.
45. M. Pileni, *The Journal of physical chemistry*, 1993, **97**, 6961-6973.
46. V. Pillai, P. Kumar, D. Shah, *Journal of magnetism and magnetic materials*, 1992, **116**, L299-L304.
47. D. H. Chen, S. H. Wu, *Chemistry of Materials*, 2000, **12**, 1354-1360.
48. C. P. S. Hsu, *Handbook of Instrumental Techniques for Analytical Chemistry, cap*, 2010, **15**.
49. P. Fellgett, *JOSA*, 1949, **39**, 970-976.
50. W. Bragg, W. Bragg, *Proceedings of the Royal Society of London. Series A*, 1913, **88**, 428-438.
51. C. Davisson, L. H. Germer, *Physical Review*, 1927, **30**, 705.
52. M. Tomšič, M. Bešter-Rogač, A. Jamnik, W. Kunz, D. Touraud, A. Bergmann, O. Glatter, *Journal of colloid and interface science*, 2006, **294**, 194-211.
53. G. B. J. de Boer, C. de Weerd, D. Thoenes, H. W. J. Goossens, *Particle & Particle Systems Characterization*, 1987, **4**, 14-19.
54. G. Levy, U. Mingelgrin, G. Eshel, M. Singer, *Soil Science Society of America Journal*, 2004, **68**, 736-743.
55. H. Braconnot, *Ann Chim Phys*, 1820, **13**, 113-126.
56. G. Perlovich, L. K. Hansen, A. Bauer-Brandl, *Journal of thermal analysis and calorimetry*, 2001, **66**, 699-715.

57. G. Albrecht, R. B. Corey, *Journal of the American Chemical Society*, 1939, **61**, 1087-1103.
58. J. Bernal, *Z. Kristallogr*, 1931, **78**, 363-369.
59. Y. Iitaka, *Proceedings of the Japan Academy*, 1954, **30**, 109-112.
60. E. Boldyreva, V. Drebushchak, T. Drebushchak, I. Paukov, Y. A. Kovalevskaya, E. Shutova, *Journal of thermal analysis and calorimetry*, 2003, **73**, 409-418.
61. V. Drebushchak, Y. A. Kovalevskaya, I. Paukov, E. Boldyreva, *Journal of thermal analysis and calorimetry*, 2003, **74**, 109-120.
62. H. Sakai, H. Hosogai, T. Kawakita, K. Onuma, K. Tsukamoto, *Journal of crystal growth*, 1992, **116**, 421-426.
63. I. S. Lee, K. T. Kim, A. Y. Lee, A. S. Myerson, *Crystal Growth and Design*, 2008, **8**, 108-113.
64. J. Huang, T. C. Stringfellow, L. Yu, *Journal of the American Chemical Society*, 2008, **130**, 13973-13980.
65. J. W. Chew, S. N. Black, P. S. Chow, R. B. H. Tan, K. J. Carpenter, *CrystEngComm*, 2007, **9**, 128-130.
66. I. Weissbuch, V. Y. Torbeev, L. Leiserowitz, M. Lahav, *Angewandte Chemie International Edition*, 2005, **44**, 3226-3229.
67. V. Y. Torbeev, E. Shavit, I. Weissbuch, L. Leiserowitz, M. Lahav, *Crystal Growth & Design*, 2005, **5**, 2190-2196.
68. I. Weissbuch, M. Lahav, L. Leiserowitz, *Crystal Growth & Design*, 2003, **3**, 125-150.
69. R. E. Marsh, *Acta Crystallographica*, 1958, **11**, 654-663.
70. A. Dawson, D. R. Allan, S. A. Belmonte, S. J. Clark, W. I. David, P. A. McGregor, S. Parsons, C. R. Pulham, L. Sawyer, *Crystal growth & design*, 2005, **5**, 1415-1427.
71. Y. Iitaka, *Acta Crystallographica*, 1961, **14**, 1-10.
72. E. V. Boldyreva, S. N. Ivashevskaya, H. Sowa, H. Ahsbahs, H. P. Weber, *Zeitschrift für Kristallographie/International journal for structural, physical, and chemical aspects of crystalline materials*, 2005, **220**, 50-57.
73. A. L. Markel, A. F. Achkasov, T. A. Alekhina, O. I. Prokudina, M. A. Ryazanova, T. N. Ukolova, V. M. Efimov, E. V. Boldyreva, V. V. Boldyrev, *Pharmacology Biochemistry and Behavior*, 2011.
74. R. Waziri, S. Baruah, *Schizophrenia research*, 1999, **37**, 205-215.
75. D. Babić, R. Babić, *Psychiatria Danubina*, 2009, **21**, 376-381.
76. C. S. Towler, R. J. Davey, R. W. Lancaster, C. J. Price, *Journal of the American Chemical Society*, 2004, **126**, 13347-13353.
77. R. Dowling, R. J. Davey, R. A. Curtis, G. Han, S. K. Poornachary, P. S. Chow, R. B. H. Tan, *Chemical Communications*, 2010, **46**, 5924-5926.
78. G. Chernobai, Y. A. Chesalov, E. Burgina, T. Drebushchak, E. Boldyreva, *Journal of Structural Chemistry*, 2007, **48**, 332-339.
79. E. S. Ferrari, R. J. Davey, I. Wendy, A. L. Gillon, C. S. Towler, *Crystal Growth & Design*, 2003, **3**, 53-60.
80. A. Y. Lee, I. S. Lee, A. S. Myerson, *Chemical engineering & technology*, 2006, **29**, 281-285.
81. Z. Liu, L. Zhong, P. Ying, Z. Feng, C. Li, *Biophysical chemistry*, 2008, **132**, 18-22.
82. M. N. Bhat, S. Dharmaprakash, *Journal of crystal growth*, 2002, **236**, 376-380.

83. C. E. Nicholson, C. Chen, B. Mendis, S. J. Cooper, *Crystal Growth & Design*, 2011, **11**, 363-366.
84. A. Y. Lee, I. S. Lee, S. S. Dette, J. Boerner, A. S. Myerson, *Journal of the American Chemical Society*, 2005, **127**, 14982-14983.
85. K. Kim, A. Centrone, T. A. Hatton, A. S. Myerson, *Cryst. Eng. Comm.*, 2011, **13**, 1127-1131.
86. G. Han, P. S. Chow, R. B. H. Tan, *Crystal Growth & Design*, 2012, **12**, 2213-2220.
87. J. R. Parsons, J. L. Ricci, H. Alexander, P. K. Bajpai, *Annals of the New York Academy of Sciences*, 1988, **523**, 190-207.
88. R. LeGeros, J. R. Parsons, G. Daculsi, F. Driessens, D. Lee, S. Liu, S. Metsger, D. Peterson, M. Walker, *Annals of the New York Academy of Sciences*, 1988, **523**, 268-271.
89. W. Suchanek, M. Yashima, M. Kakihana, M. Yoshimura, *Biomaterials*, 1997, **18**, 923-933.
90. G. Wei, P. X. Ma, *Biomaterials*, 2004, **25**, 4749-4757.
91. C. E. Wen, Y. Yamada, A. Nouri, P. D. Hodgson, *Acta Biomaterialia*, 2007, **3**, 403-410.
92. M. Boutonnet, J. Kizling, P. Stenius, G. Maire, *Colloids and Surfaces*, 1982, **5**, 209-225.
93. K. De Groot, *Biomaterials*, 1980, **1**, 47-50.
94. F. H. Albee, *Annals of surgery*, 1920, **71**, 32.
95. E. Nery, K. Lynch, W. Hirthe, K. Mueller, *Journal of periodontology*, 1975, **46**, 328.
96. D. Suárez-González, K. Barnhart, E. Saito, R. Vanderby Jr, S. J. Hollister, W. L. Murphy, *J. Biomed. Mater. Res. Part A*, 2010, **95**, 222-234.
97. J. S. Son, S. G. Kim, J. S. Oh, M. Appleford, S. Oh, J. L. Ong, K. B. Lee, *J. Biomed. Mater. Res. Part A*, 2011, **99A**, 638-647.
98. S. H. Li, J. R. De Wijn, P. Layrolle, K. De Groot, *Journal of biomedical materials research*, 2002, **61**, 109-120.
99. L. L. Hench, J. M. Polak, *Science*, 2002, **295**, 1014.
100. H. Newesely, *J. Oral Rehabil.*, 1977, **4**, 97-104.
101. H. C. W. Skinner, J. S. Kittelberger, R. A. Beebe, *J. Phys. Chem.*, 1975, **79**, 2017-2019.
102. G. Dewith, A. J. Corbijn, *Journal of materials science*, 1989, **24**, 3411-3415.
103. G. Dewith, H. J. A. Vandijk, N. Hattu, K. Prijs, *Journal of materials science*, 1981, **16**, 1592-1598.
104. N. Y. Mostafa, *Materials chemistry and physics*, 2005, **94**, 333-341.
105. G. Asgari, B. Roshani, G. Ghanizadeh, *Journal of Hazardous Materials*, 2012.
106. C. Klein, A. Driessen, K. De Groot, A. Van Den Hooff, *Journal of biomedical materials research*, 1983, **17**, 769-784.
107. W. F. Neuman, M. W. Neuman, *The chemical dynamics of bone mineral*, University of Chicago Press Chicago, 1958.
108. L. A. Evans, D. J. Macey, J. Webb, *Calcified tissue international*, 1992, **51**, 78-82.
109. S. I. Roohani-Esfahani, S. Nouri-Khorasani, Z. Lu, R. Appleyard, H. Zreiqat, *Biomaterials*, 2010, **31**, 5498-5509.
110. M. Murray, J. Wang, C. Ponton, P. Marquis, *Journal of materials science*, 1995, **30**, 3061-3074.

111. G. Lim, J. Wang, S. Ng, L. Gan, *Materials letters*, 1996, **28**, 431-436.
112. H. Li, M. Y. Zhu, L. H. Li, C. R. Zhou, *Journal of materials science*, 2008, **43**, 384-389.
113. Y. Yamada, K. I. Kurumada, K. Susa, N. Umeda, G. Pan, *Advanced Powder Technology*, 2007, **18**, 251-260.
114. F. Chen, Z. C. Wang, C. J. Lin, *Materials letters*, 2002, **57**, 858-861.
115. G. C. Koumoulidis, A. P. Katsoulidis, A. K. Ladavos, P. J. Pomonis, C. C. Trapalis, A. T. Sdoukos, T. C. Vaimakis, *Journal of colloid and interface science*, 2003, **259**, 254-260.
116. G. S. Guo, Y. X. Sun, Z. H. Wang, H. Y. Guo, *Ceram. Int.*, 2005, **31**, 869-872.
117. S. Bose, S. K. Saha, *Chemistry of Materials*, 2003, **15**, 4464-4469.
118. C. W. Chen, R. E. Riman, K. S. TenHuisen, K. Brown, *Journal of crystal growth*, 2004, **270**, 615-623.
119. H. H. Adler, *Amer. Mineralogist.–1964.–49.–P*, 1964, 1002-1015.
120. G. K. Hunter, H. A. Goldberg, *Proceedings of the National Academy of Sciences*, 1993, **90**, 8562.
121. S. Koutsopoulos, *Journal of biomedical materials research*, 2002, **62**, 600-612.
122. A. Fujishima, K. Honda, *Nature*, 1972, **238**, 37-+.
123. A. Fujishima, T. N. Rao, D. A. Tryk, *Journal of Photochemistry and Photobiology C: Photochemistry Reviews*, 2000, **1**, 1-21.
124. J. R. Bolton, *Solar Energy*, 1996, **57**, 37-50.
125. S. U. M. Khan, M. Al-Shahry, W. B. Ingler, *Science*, 2002, **297**, 2243.
126. R. Asahi, T. Morikawa, T. Ohwaki, K. Aoki and Y. Taga, *Science*, 2001, **293**, 269.
127. W. Choi, A. Termin, M. R. Hoffmann, *The Journal of Physical Chemistry*, 1994, **98**, 13669-13679.
128. M. Ferroni, V. Guidi, G. MartinelliG, P. Nelli, G. Sberveglieri, *Nanostructured materials*, 1996, **7**, 709-718.
129. M. I. Baraton, L. Merhari, J. Wang, K. E. Gonsalves, *Nanotechnology*, 1998, **9**, 356.
130. N. O. Savage, S. A. Akbar, P. K. Dutta, *Sensors and Actuators B: Chemical*, 2001, **72**, 239-248.
131. G. Z. Chen, D. J. Fray, T. W. Farthing, *Nature*, 2000, **407**, 361-364.
132. S. J. Gerdemann, *Advanced materials & processes*, 2001, **159**.
133. L. M. Berger, *Journal of Hard Materials(UK)*, 1992, **3**, 3-15.
134. X. Bokhimi, A. Morales, M. Aguilar, J. Toledo-Antonio, F. Pedraza, *International journal of hydrogen energy*, 2001, **26**, 1279-1287.
135. J. Chaudhuri, M. Ram, B. Sarkar, *Journal of materials science*, 1994, **29**, 3484-3488.
136. M. Gateshki, S. Yin, Y. Ren, V. Petkov, *Chemistry of Materials*, 2007, **19**, 2512-2518.
137. J. F. Banfield, D. R. Veblen, *The American mineralogist*, 1992, **77**, 545-557.
138. J. Huberty, H. Xu, *Journal of Solid State Chemistry*, 2008, **181**, 508-514.
139. F. Dachille, R. Roy, *Bull. Ceram. Soc. Amer*, 1962, **41**, 225.
140. D. Aphairaj, T. Wirunmongkol, S. Pavasupree, P. Limsuwan, *Procedia Engineering*, 2012, **32**, 1068-1072.
141. A. Mücke, J. Bhadra Chaudhuri, *Ore geology reviews*, 1991, **6**, 25-44.

142. D. T. Cromer, K. Herrington, *Journal of the American Chemical Society*, 1955, **77**, 4708-4709.
143. S. D. Mo, W. Ching, *Physical Review B*, 1995, **51**, 13023.
144. Y. V. Kolen'ko, K. A. Kovnir, A. I. Gavrilov, A. V. Garshev, J. Frantti, O. I. Lebedev, B. R. Churagulov, G. Van Tendeloo, M. Yoshimura, *The Journal of Physical Chemistry B*, 2006, **110**, 4030-4038.
145. T. Kasuga, M. Hiramatsu, A. Hoson, T. Sekino, K. Niihara, *Advanced Materials*, 1999, **11**, 1307-1311.
146. Y. L. Li, T. Ishigaki, *Chemistry of Materials*, 2001, **13**, 1577-1584.
147. M. Formenti, F. Juillet, P. Meriaudeau, S. Teichner, P. Vergnon, *Journal of colloid and interface science*, 1972, **39**, 79-89.
148. H. D. Jang, S. K. Kim, *Materials research bulletin*, 2001, **36**, 627-637.
149. J. Li, S. I. Seok, B. Chu, F. Dogan, Q. Zhang, Q. Wang, *Advanced Materials*, 2009, **21**, 217-221.
150. C. C. Wang, J. Y. Ying, *Chemistry of Materials*, 1999, **11**, 3113-3120.
151. C. Su, B. Y. Hong, C. M. Tseng, *Catalysis Today*, 2004, **96**, 119-126.
152. L. L. Hench, J. K. West, *Chemical Reviews*, 1990, **90**, 33-72.
153. T. Sugimoto, X. Zhou, A. Muramatsu, *Journal of colloid and interface science*, 2003, **259**, 43-52.
154. Z. Yue, W. Guo, J. Zhou, Z. Gui, L. Li, *Journal of magnetism and magnetic materials*, 2004, **270**, 216-223.
155. T. Lopez, R. Gomez, G. Pecci, P. Reyes, X. Bokhimi, O. Novaro, *Materials letters*, 1999, **40**, 59-65.
156. B. E. Yoldas, *Journal of Non-Crystalline Solids*, 1984, **63**, 145-154.
157. G. Engelhardt, W. Altenburg, D. Hoebbel, W. Wieker, *Zeitschrift für anorganische und allgemeine Chemie*, 1977, **428**, 43-52.
158. G. Engelhardt, W. Altenburg, D. Hoebbel, W. Wieker, *Zeitschrift für anorganische und allgemeine Chemie*, 1977, **437**, 249-252.
159. B. Ohtani, Y. Ogawa, S. Nishimoto, *The Journal of Physical Chemistry B*, 1997, **101**, 3746-3752.
160. A. Ramesh Kumar, G. Hota, A. Mehra, K. C. Khilar, *AIChE Journal*, 2004, **50**, 1556-1567.
161. U. Balachandran, N. Eror, *Journal of Solid State Chemistry*, 1982, **42**, 276-282.
162. D. Dvoranova, V. Brezova, M. Mazur, M. A. Malati, *Applied Catalysis B: Environmental*, 2002, **37**, 91-105.
163. A. Bobrova, I. Zhigun, M. Bragina, A. Fotiev, *Journal of Applied Spectroscopy*, 1968, **8**, 59-63.
164. Y. Wang, J. Li, L. Wang, T. Xue, T. Qi, *Industrial & Engineering Chemistry Research*, 2010.
165. K. Thamaphat, P. Limsuwan, B. Ngotawornchai, *Kasetsart J.(Nat. Sci.)*, 2008, **42**, 357-361.
166. M. Rehan, X. Lai, G. M. Kale, *CrystEngComm*, 2011, **13**, 3725-3732.
167. R. K. Keswani, H. Ghodke, D. Sarkar, K. C. Khilar, R. S. Srinivasa, *Colloids and Surfaces A: Physicochemical and Engineering Aspects*, 2010, **369**, 75-81.
168. M. Lal, V. Chhabra, P. Ayyub, A. Maitra, *Journal of Materials Research*, 1998, **13**, 1249-1254.
169. A. Nazari, M. Montazer, M. Moghadam, M. Anary-Abbasinejad, *Carbohydrate Polymers*, 2011, **83**, 1119-1127.

170. Y. Paz, Z. Luo, L. Rabenberg, A. Heller, *Journal of Materials Research*, 1995, **10**, 2842-2848.
171. S. S. Tan, L. Zou, E. Hu, *Catalysis Today*, 2006, **115**, 269-273.